UNCLASSIFIED

AD NUMBER: AD0818490

LIMITATION CHANGES

TO:

Approved for public release; distribution is unlimited.

FROM:

Distribution authorized to U.S. Government agencies and their contractors; Administrative or operational use; 01 Mar 1967. Other requests shall be referred to Federal Aviation Agency, Washington, DC, 20591.

AUTHORITY

ST-A FAA NOTICE, 2 JUL 1973

THIS PAGE IS UNCLASSIFIED

HIGH STRENGTH STEEL EVALUATION FOR SUPERSONIC AIRCRAFT

AD No. 818490
DDC FILE COPY

COMMERCIAL
SUPERSONIC TRANSPORT
PROGRAM

PHASE II-C REPORT

D6A10093-2

HIGH STRENGTH STEEL EVALUATION FOR SUPERSONIC AIRCRAFT.

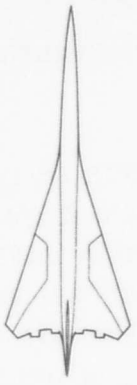

(9) Rept. for 1 Nov 65 - 31 Dec 66,

(10) James L. Guthrie

(6) COMMERCIAL SUPERSONIC TRANSPORT PROGRAM.

PHASE II-C REPORT.

[redacted] FA-SS-66-5

(15)

(14) D6A10093-2

(11) March 1967 (12) 246p.

Prepared for
FEDERAL AVIATION AGENCY

DDC
AUG 17 1967
E

Prepared by J. L. Guthrie
Supervised by John R. Baisch
Approved by M. G. Bartell
Approved by H. J. Hayden

THE BOEING COMPANY
SUPERSONIC TRANSPORT DIVISION
SEATTLE, WASHINGTON

ISSUE 38

FAA

(402 097)

NOTICES

When Government drawings, specifications, or other data are used for any purpose other than in connection with a definitely related Government procurement operation, the United States Government thereby incurs no responsibility nor any obligation whatsoever; and the fact that the Government may have formulated, furnished, or in any way supplied the said drawings, specifications, or other data, is not to be regarded by implication or otherwise as in any manner licensing the holder or any other person or corporation, or conveying any rights or permission to manufacture, use, or sell any patented invention that may in any way be related thereto.

Copies have been placed in the DDC collection. U.S. Government agencies may obtain copies from DDC. Other qualified DDC users may request, by submission of a DDC Form 1, through:

Director of Supersonic Transport Development
Federal Aviation Agency
Washington, D.C. 20553

Defense Documentation Center release to the Clearinghouse for Federal, Scientific, and Technical Information (CFSTI) and foreign announcement and dissemination are not authorized. The distribution of this report is limited because it contains technology identifiable with items excluded from export by the Department of State (U.S. Export Control Act of 1949 as amended).

FOREWORD

This report describes part of the work accomplished by The Boeing Company under contract FA-SS-66-5, which supports Phase II-C of the FAA Supersonic Transport Program.

The work was conducted under the direction of John F. Baisch of the Materials Technology Unit, Program Manager. Douglas F. Bulloch was the Technical Director and James L. Guthrie was the Principal Project Leader.

Significant contributions to this program were made by the following personnel: Wilfred C. Larson, Charles S. Martin and Walter O. Swift of the Structures Laboratory; Dave E. Austin, Donald A. Bolstad, and Rodney Boyer of the Materials Technology Laboratory.

The contract time period covered by this program was November 1, 1965 through December 31, 1966.

ABSTRACT

Forged billets of three vacuum melt heats of 4330 V-Modified, H-11 Modified, 9Ni-4Co-0.30C, 9Ni-4Co-0.45, and Maraging (18 percent Ni) 250 and two heats of 300M were evaluated to provide high strength steel alloy selection data for heavy section aircraft components. The evaluation included the following types of tests: tensile, precracked charpy impact, plane strain fracture toughness, stress corrosion, hydrogen embrittlement susceptibility, elevated temperature stability, and fatigue. The results of the testing are discussed and are related to alloy selection considerations.

TABLE OF CONTENTS

TABLE OF CONTENTS (Continued)

LIST OF ILLUSTRATIONS

LIST OF ILLUSTRATIONS (Continued)

LIST OF ILLUSTRATIONS (Continued)

LIST OF ILLUSTRATIONS (Continued)

LIST OF ILLUSTRATIONS (Continued)

LIST OF ILLUSTRATIONS (Continued)

LIST OF ILLUSTRATIONS (Concluded)

LIST OF ILLUSTRATIONS
APPENDIX A

LIST OF ILLUSTRATIONS (Concluded)

APPENDIX A

LIST OF TABLES

LIST OF TABLES (Concluded)

LIST OF SYMBOLS

A_{net}	Net section area
A_{gross}	Gross section area
a	Dimension of crack or flaw
	Notched bend specimen: average crack depth
	Surface-flawed specimen: crack depth
E	Young's modulus of elasticity
G_{IC}	Plane strain fracture toughness
K_{IC}	Plane strain critical stress intensity or plane strain fracture-toughness parameter
K_{Ii}	Initial applied plane strain stress intensity
L	Moment arm length
l	Length dimension
M_s	Martensite start temperature
NF	No failure
P_{DL}	Load at deviation from linearity
P_{max}	Maximum load
Q&T	Quench and temper heat treatment
R	Ratio of minimum to maximum fatigue stress
RA	Reduction of area
UTS	Ultimate tensile stress
W	Specimen width
WA	Precracked charpy energy divided by fracture face area
σ_g	Gross area stress
σ_n	Notched bend specimen: nominal stress at tip of crack
σ_{net}	Net section stress
σ_{ys} or YS	Yield stress
μ	Poisson's Ratio

SUMMARY

Billets of three vacuum melt heats each of 4330 V-Modified, H-11 Modified, 9Ni-4Co-0.30C, 9Ni-4Co-0.45C, and Maraging (18 percent Ni) 250 and billets of two vacuum melt heats of 300M were evaluated to provide alloy selection data for the supersonic transport program. The evaluation included the following types of testing: tensile, precracked charpy impact, plane strain fracture toughness, stress corrosion, hydrogen embrittlement susceptibility, metal-lurgical stability, and fatigue.

Initially, a heat treatment study was conducted with one heat of each alloy to establish strength-fracture toughness relationships. From these relationships, optimum heat treatments were selected to determine other material properties. Three heats of each alloy were used for the remainder of the program to determine the effect of chemistry variations on fracture toughness, stress corrosion and strength.

Within the 220-240 ksi ultimete strength range, 9Ni-4Co-0.30C had higher fracture roughness than 4330 V-Modified or H-11 Modified. At strength levels above 250 ksi, the Maraging 250 and bainitically treated 9Ni-4Co-0.45C alloys and had higher fracture toughness than 300M. However 300M had the highest strength properties.

Two types of stress corrosion testing were performed. Statically stressed smooth bend specimens were tested by alternate immersion in salt water and precracked notched bend specimens were sustain-loaded in salt water. Both tests indicated that the 9Ni-4Co-0.30C, 9Ni-4Co-0.45C (Bainitic), and Maraging 250 steels were the least susceptible to stress corrosion.

Specimens of 4330 V-Modified, 300M, 9Ni-4Co-0.45C, and Maraging 250 steel were exposed to 300°F and specimens of 9Ni-4Co-0.30C and H-11 Modified were exposed at 450°F and 550°F, respectively. With the exception of 4330 V-Modified, 5,000 hours of exposure at a sustained stress level of 40 ksi had no significant effect on room temperature strength or fracture toughness.

Stress-rupture tests of notched specimens charged with hydrogen indicated that the 300M and 9Ni-4Co-0.45 steels were severely embrittled at strength levels higher than 260 ksi. Limited tests of notched fatigue specimens ($K_t = 2.5$) indicated that there were no major differences in axial fatigue properties between the alloys.

1.0 INTRODUCTION

Structural components forged from the high strength steels 4330 V-Modified and 300M and heat treated to ultimate strengths of 220-240 and 270-300 ksi, respectively, have performed well in service on Boeing aircraft (Ref. 1). Because successful service experience has been acquired, 4330 V-Modified and 300M are prime alloy candidates for the supersonic transport. However, the Maraging and 9Ni-4Co alloys appear to be more reliable. To provide alloy selection data, the Federal Aviation Agency authorized a high strength steel evaluation program. The objective of the program was to compare and evaluate high strength steels in terms of strength, fracture toughness, metallurgical stability, susceptibility to stress corrosion, fatigue, and resistance to hydrogen embrittlement.

Alloys selected for evaluation were 4330 V-Modified, 300M, 9Ni-4Co-0.30C, 9Ni-4Co-0.45C, Maraging 250, and H-11 Modified. 4330 V-Modified and 300M were included to provide a basis for comparison. The H-11 Modified alloy was selected because of its potential for elevated temperature applications. All of the materials obtained for the program were produced by the consumable electrode vacuum melting process and several vacuum melt heats of each alloy were evaluated.

2.0 MATERIALS

This section describes the materials of the program in terms of their process history and chemical composition.

The six high strength steels selected for evaluation were as follows:

4330 V-Modified

300M

H-11 Modified

9Ni-4Co-0.45C

9Ni-4Co-0.30C

Maraging (18 percent Ni) 250

4330 V-Modified and 300M are modifications of the standard aircraft alloys, AISI 4330 and 4340 steels. The main landing gears of the Boeing Model 727 are forged from 4330 V-Modified. 300M was developed by the International Nickel Corporation under the trade name "Tricent". The main landing gears of both the Models 720 and 737 aircraft are forged from 300M. The H-11 Modified material evaluated had the trade name "Vascojet 1000" and is a modification of H-11 tool steel. The 9Ni-4Co alloys were developed by the Republic Steel Corporation. The 9Ni-4Co-0.30C alloy contains less carbon and a higher percentage of chromium and molybdenum than the 9Ni-4Co-0.45C alloy. Maraging (18 percent Ni) 250, which contains less than 0.03 percent carbon, was developed by the International Nickel Company for rocket motor cases.

All the materials obtained for the program were produced by the consumable electrode vacuum melting process. Current Boeing design practice requires vacuum melting for critically stressed steel components that are heat treated to ultimate strengths greater than 180 ksi. Vacuum melting reduces the inclusions content, increases toughness, and reduces material anisotropy (Refs. 2, 3, and 4).

Materials for the program were received from the suppliers in the form of 3- by 9- by 24-inch annealed billets. Three billets were obtained per alloy. Two of the three 300M billets were from the same heat. The billets of the remaining alloys were all from different vacuum melt heats. At least two vacuum melt heats of each alloy were from different parent air melt heats. Since the materials were from different heats, variations of composition

existed between billets of the same alloy. Evaluation of the various heats provided an indication of the extent of the property changes resulting from compositional variations. The billet suppliers, applicable specifications, and heat data are listed in Table I.

Table II describes the forging histories of the billets. Because the amounts of reduction and the forging temperature affect the mechanical properties, the forging processes will be considered in the analysis of the test results. The annealing treatments used after forging are described in Table III.

The chemical compositions of the materials are given in Table IV. This table lists the results of the supplier's heat analysis and the results of a billet analysis performed at Boeing. Generally, there were no major discrepancies between the two analyses. However, the billet analyses indicated slightly higher levels of phosphorous and sulphur and lower (0.00-0.03 percent) carbon contents.

When the materials were received, each billet was ultrasonically inspected with 5/64-inch indications as the basis for rejection (Ref. 5). Except for one 9Ni-4Co-0.30C billet (Heat 3931145), all the billets satisfactorily passed ultrasonic inspection. The rejected billet passed inspection after cropping. This billet appeared to have been severely forged at too low a temperature.

Following ultrasonic inspection, cross sections were cut from the ends of the billets (Fig. 1) and macroetched. Pictures of the macroetched cross sections are shown in Figs. A-1 through A-6 in Appendix A. The Maraging 250 billet displayed the most pronounced flow structures (Fig. A-5). No voids or shuts were observed on any of the sections. However, edge cracks were observed along the sides of one of the 9Ni-4Co-0.30C billets (Fig. A-3c). These cracks were removed by milling the sides of the billet.

Evaluation of annealed billet microstructures at the positions shown in Fig. 1 revealed alloying element segregration in the form of longitudinal grain direction banding. These areas of segregation probably developed during freezing of the ingot. When the ingots were forged, the segregated areas were elongated and compressed into narrow bands. With the exception of 300M, banding was observed in the microstructure of at least one heat of each alloy. The Maraging 250 displayed the most severe banding. Figures A-7 through A-12 of the Appendix show the microstructures of the as-received billets.

Table I Material Sources and Heat Data

Alloy	Specification	Supplier	Heat Number	Size Air Melt (Tons)	Size Vacuum Melt (Tons)	Vacuum Melt Ingot Diameter (inches)
4330 V-Modified	BMS 7-122	Republic	3960633	70	4	24
		Latrobe	C10157	32	-	20
		Latrobe	C57046	13	-	30
H-11 Modified	BMS 7-80	Vanadium	09110	--	3	20
		Vanadium	09099	--	3	20
		Vanadium	08990	--	3	20
9Ni-4Co-0.30C (Cr,Mo)	BMS 7-182	Republic	3930852	3.65	3.5	24
		Republic	3931144	20	3	24
		Republic	3931145	20	3	24
300 M	BMS 7-26 (Class I)	Vanadium	09715	--	3	30
		Republic	+3951531(P)	70	10	32
		Republic	+3951531(R)	70	10	32
Maraging (18%)Ni) 250	AMD 64BP	Allegheny	24676	12	-	17
		Vanadium	09148	--	3	20
		Republic	3930879	70	4.5	24
9Ni-4Co-0.45C	AMS 6542	Republic	3882720	70	4.5	24
		Republic	3931141	70	3	24
		Republic	3931120	70	3	24

*Boeing Material Specification.

+Two billets from same heat, billets P and R.

Table II ***Material Forging History***

Alloy	Heat Number	*Forging Ratio	Forging History
4330 V-Modified	3960633	16.8	24 inch ingot; heated to 2200°F and press-forged to 6 by 9 inches; reheated to 2000°F and press-forged to 3 by 9 inches
	C10157	11.6	20 inch ingot; heated to 2050°F and press-forged to 11 inch square, reheated to 1975°F and hammer-forged to 3 by 9 inches
	C57046	26.2	30 inch ingot; press-forged to 6-3/4 inch square, reheated and hammer-forged to 3 by 9 inches
H-11 Modified	09110	11.6	20 inch ingot; heated to 2200°F and press-forged to 3 by 9 in.
	09099	11.6	20 inch ingot; heated to 2200°F and press-forged to 3 by 9 in.
	08990	11.6	20 inch ingot; heated to 2200°F and press-forged to 3 by 9 in.
9Ni-4Co-0.30C	3930852	12.9	24 inch ingot; heated to 2100°F and press-forged to 3-1/2 by 10 inches
	3931144	16.8	24 inch ingot; heated to 2200°F and press-forged to 10 inch square, reheated to 2000°F and press-forged to 3 by 9 inches
	3931145	16.8	24 inch ingot; heated to 2200°F and press-forged to 10 inch square, reheated to 2000°F and press-forged to 3 by 9 inches
300 M	09715	11.6	20 inch ingot; heated to 2125°F and press-forged to 3 by 9 in.
	3951531	29.8	32 inch ingot; heated to 2300°F and hot-rolled to 23 by 10 inches, reheated to 2100°F and press-forged 3 by 9 inches
Maraging (18% Ni) 250	24676	8.4	17 inch ingot; heated to 2150°F and forged to 3 x 9 inches
	09148	11.6	20 inch ingot; heated to 2100°F and press-forged to 3 by 9 in.
	3930879	16.8	24 inch ingot; heated to 2300°F and press-forged to 16 inches square, reheated to 2100°F and press-forged to 3 by 9 inches
9Ni-4Co-0.45C	3882720	16.8	24 inch ingot; heated to 2100°F and press-forged to 8 by 16 inches, reheated to 2100°F and press-forged to 3 by 9 inches
	3931141	12.9	24 inch ingot; heated to 2100°F and press-forged to 3-1/2 by 10 inches
	3931120	12.9	24 inch ingot; heated to 2100°F and press-forged to 3-1/2 by 10 inches

* Ratio of ingot cross-sectional area to final billet cross-sectional area

Table III Annealing Treatments

Alloy	Heat Number	Annealing Treatment
4330 V-Modified	3960633 C10157 C57046	1250°F/12 hr/FC 1650°F/14 hr/FC 25°F per hr to 1100°F 1650°F/14 hr/FC 25°F per hr to 1100°F
H-11 Modified	08990 09099 09110	1975°F/2 hr FC + 1650°F/2 hr/AC + 1600°F/2 hr/FC 1975°F/2 hr FC + 1650°F/2 hr/AC + 1600°F/2 hr/FC 1975°F/2 hr FC + 1650°F/2 hr/AC + 1600°F/2 hr/FC
9Ni-4Co-0.30C	3930852 3931141 3931145	1150°F/36 hr/AC 1150°F/36 hr/AC 1150°F/36 hr/AC
300M	09715 *3951531P *3951531R	1400°F/2 hr/FC 1250°F/12 hr/FC
Maraging-250	24676 09148 3930879	1500°F/1 hr/WQ 1700°F/3 hr/AC 1615°F solution heat treatment
9Ni-4Co-0.45C	3882720 3931141 3931120	1150°F/36 hr/AC 1150°F/36 hr/AC 1150°F/36 hr/AC

FC - Furnace Cool
AC - Air Cool
WQ - Water Quench

* Two billets from same heat, billets P and R.

Table IV Chemical Composition

Alloy	Heat Number	Analysis Source	C	Mn	Si	P	S	Ni	Cr	Mo	V	Co	Al	Ti
4330 V-Mod.	3960633	B	.31	.83	.27	.008	.007	1.84	.89	.44	.09	--	--	--
		S	.32	.79	.29	.005	.005	1.79	.89	.43	.08	--	--	--
	C57046	B	.32	.76	.29	.008	.008	1.74	.81	.41	.09	--	--	--
		S	.33	.80	.31	.004	.005	1.75	.81	.40	.06	--	--	--
	C10157	B	.28	.80	.38	.009	.007	1.84	.90	.44	.08	--	--	--
		S	.31	.80	.35	.006	.006	1.83	.84	.44	.08	--	--	--
H-11 Modified	08990	B	.37	.30	.91	.019	.009	.15	5.22	1.28	.36	--	--	--
		S	.38	.22	.93	.010	.004	--	4.85	1.38	.51	--	--	--
	09099	B	.36	.30	.92	.013	.008	.15	5.10	1.30	.36	--	--	--
		S	.41	.21	.86	.010	.004	--	4.83	1.38	.54	--	--	--
	09110	B	.37	.28	.93	.009	.008	.15	5.15	1.20	.43	--	--	--
		S	.41	.20	.88	.010	.008	--	5.12	1.30	.52	--	--	--
9Ni-4Co-0.30C	3930852	B	.32	.13	.03	.007	.008	7.59	1.13	.70	.10	4.52	--	--
		S	.32	.16	.01	.005	.007	7.62	1.03	.94	.08	4.25	--	--
	3931144	B	.32	.28	.02	.01	.007	7.53	1.00	.95	.06	4.25	--	--
		S	.32	.24	.01	.008	.006	7.37	.99	.98	.06	4.38	--	--
	3931145	B	.30	.21	.02	.01	.008	7.42	.99	.99	.06	4.32	--	--
		S	.31	.21	.01	.007	.006	7.40	.99	.99	.06	4.40	--	--
300M	09715	B	.43	.85	1.62	.014	.006	1.74	.94	.41	.08	--	--	--
		S	.43	.67	1.59	.010	.004	1.78	.89	.40	.10	--	--	--
	3951531P	B	.39	.82	1.55	.012	.009	1.73	.86	.43	.09	--	--	--
	3951531R	B	.38	.84	1.54	.010	.006	1.84	.75	.44	.09	--	--	--
		S	.40	.86	1.61	.008	--	1.78	.88	.42	.09	--	--	--

Table IV Chemical Composition (Concluded)

Alloy	Heat Number	Analysis Source	C	Mn	Si	P	S	Ni	Cr	Mo	V	Co	Al	Ti
Maraging 250	24676	B	.016	.04	.10	.007	.007	18.69	--	4.95	--	7.95	.10	.54
		S	.014	.03	.039	.001	.003	18.81	--	4.79	--	7.73	.10	.57
	09148	B	.015	.03	.10	.007	.005	18.62	--	4.92	--	7.96	.15	.40
		*S	.020	.04	.09	.006	.006	18.21	--	4.87	--	7.64	.11	.43
	3930879	B	.030	.10	.10	.005	.008	18.05	--	5.08	--	7.66	.15	.40
		**S	.022	.10	.09	.005	.006	17.83	--	4.88	--	7.23	.09	.40
9Ni-4Co-0.45C	3882720	B	.42	0.09	.03	.003	.011	7.90	.33	.22	.10	4.26	--	--
		S	.44	.15	.02	.004	.009	7.82	.29	.30	.09	3.95	--	--
	3931141	B	.44	.19	.02	.01	.009	7.79	.32	.29	.08	4.03	--	--
		S	.46	.19	.01	.003	.008	7.65	.32	.29	.08	4.00	--	--
	3931120	B	.45	.20	.02	.01	.012	7.82	.33	.30	.08	3.98	--	--
		S	.46	.20	.01	.004	.009	7.66	.33	.30	.08	4.03	--	--

B - Boeing Billet Analysis

S - Suppliers Analysis

* B-0.006, Z-0.018, Ca-0.05

** B-0.003, Z-0.002, Ca-0.06

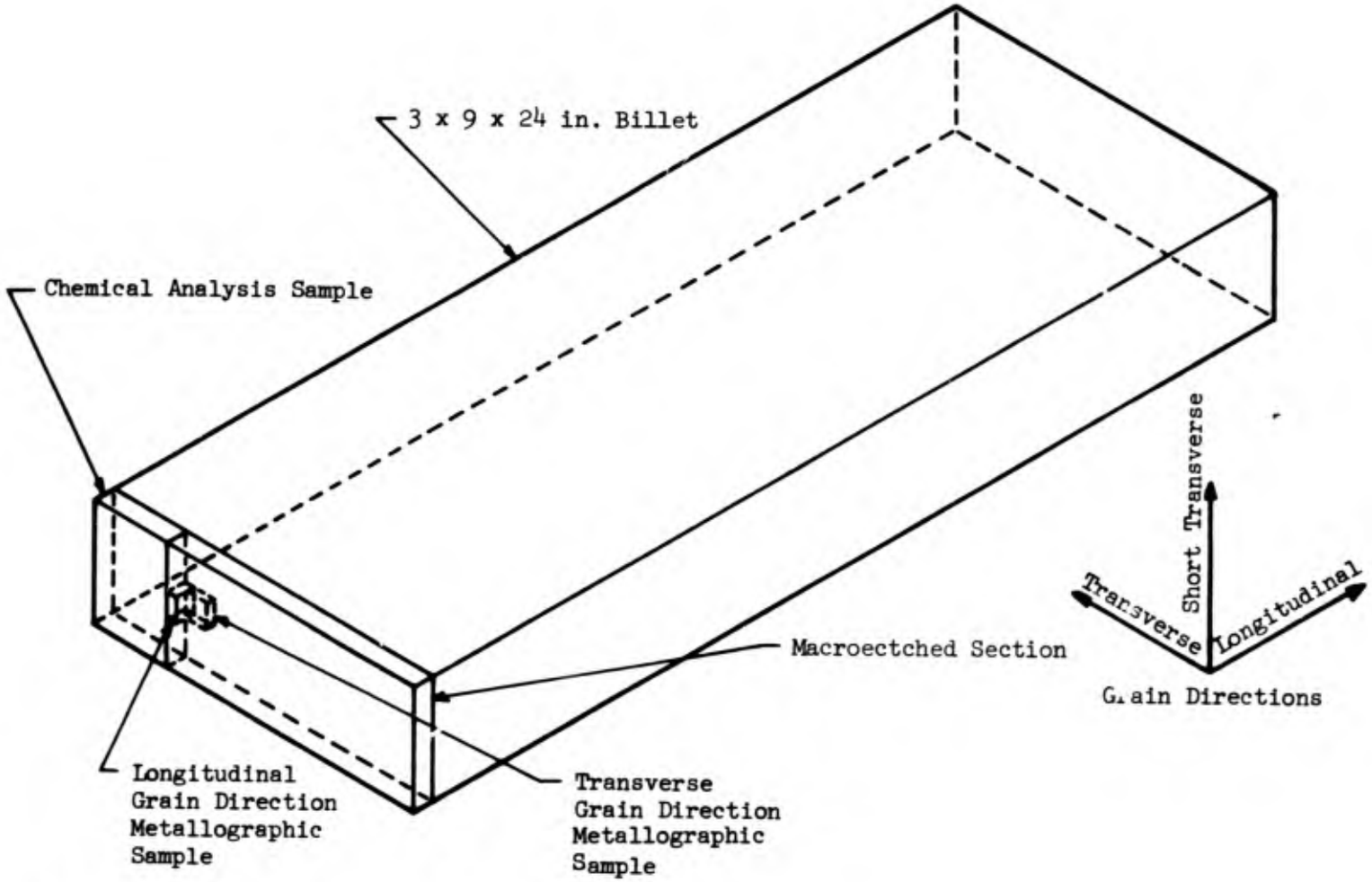

Figure 1. Positions of Samples

3.0 TESTING METHODS AND SPECIMEN CONFIGURATIONS

The materials evaluation conducted in this program was based on seven types of testing:

- Tensile
- Precracked Charpy Impact
- Plane Strain Fracture Toughness
- Sustained-Loading of Fatigue Cracked Notched Bend Specimens in Salt Water
- Sustained-Load Alternate Immersion of Unnotched Bend Specimens in Salt Water
- Notched Tension-Tension Fatigue
- Stress Rupture of Hydrogen Charged Notched Tensile Specimens

All the testing was performed at either -65°F or at room temperature. Room temperature testing was selected to provide data for comparison with available data in the literature and -65°F testing was considered to reveal the lowest fracture toughness encountered in these alloys over the SST service temperature range.

In this section, the specimen preparation procedures and testing methods are discussed. These subjects are related to all phases of the program. Deviations from the specimen preparation procedures or test methods are discussed in the applicable sections.

3.1 SPECIMEN PREPARATION PROCEDURES

Initially, coupons were cut from the billets and machined into heat treatment blanks. The shapes of the blanks were similar to the final specimen shapes except that 0.025-inch minimum of excess material was left on all surfaces. This excess allowed for removal of decarburization and warpage after heat treatment. Austenitizing and normalizing was performed in controlled atmosphere furnaces to further insure against decarburization. The heat treatments used are described in subsequent sections. Finish machining was performed by grinding after heat treatment and was carefully controlled (Ref. 6) to prevent the formation of untempered martensite due to excessive heating.

3.2 SPECIMEN IDENTIFICATION

Each specimen of the program was stamped with a code letter and number. The code letter identified the alloy and type of heat treatment as indicated below.

Code	Alloy	Type of Heat Treatment
A	4330 V-Modified	Quench-Temper
B	H-11 Modified	Quench-Temper
C	9Ni-4Co-0.30C	Quench-Temper
D	300M	Quench-Temper
E	Maraging 250	Solution Treat and Age
F	9Ni-4Co-0.45C	Quench-Temper
G	9Ni-4Co-0.45C	Bainitic

The billet locations of any given specimens can be identified in terms of the specimen's letter code and number by referring to the billet cutting diagrams, Figs. A-13 through A-30 in Appendix A. Specimens with their longitudinal axis parallel to the billet length dimension were denoted longitudinal specimens, whereas specimens with their axis parallel to the width or thickness dimension were denoted transverse and short-transverse specimens, respectively.

3.3 TENSILE TESTING

Tensile testing was performed in room temperature air using the round tensile specimen configurations shown in Fig. 2. Testing was conducted at a rate of 0.005 in./in./min to yield and then at 0.1 in./in./ min to failure. The results of the tensile test included ultimate strength, 0.2 percent offset yield strength, percent elongation in a 1-inch gage length, reduction of area, and modulus of elasticity. Load-deflection curves to failure were obtained for the specimens tested during the "Heat Treatment Study" phase of the program. All the tensile testing was conducted in accordance with ASTM E21-587 procedures.

3.4 PRECRACKED CHARPY IMPACT TESTING

Charpy specimens of standard dimensions (Fig. 3) were tested at -65°F. Prior to testing, the specimens were fatigue cracked at the root of the notch to a depth of approximately 0.02 inches. This precracked charpy test was

considered to be a more sensitive toughness test. After precracking, the specimens were tested as standard charpy specimens. The toughness values were calculated as energy to fracture divided by the fracture face area which was determined by multiplying the average fracture face depth by the specimen width. The specimens were cooled to -65°F in a bath of dry ice and alcohol.

3.5 NOTCHED BEND SPECIMEN FRACTURE TOUGHNESS TESTING

The susceptibilities of the steels to unstable crack growth at stresses below the yield strength was evaluated by plane strain fracture toughness testing (Refs. 7, 8). Both the longitudinal and transverse grain directions of all the billets were fracture toughness tested. The four-point-load notched bend specimen used for this testing is shown in Fig. 4. Because the billets were 3 inches thick and the notched bend specimen was 7-1/2 inches long, it was not possible to test the short-transverse grain direction of the billets.

Notched bend specimens were precracked in a Sonntag SF-10-U fatigue machine with a cantilever bending fixture (Fig. 5). The specimens were cycled at 1800 cycles per minute until the combined depth of the fatigue crack and notch was approximately 0.30 inches. The final maximum fatigue cyclic stress-intensity (K) imposed on the specimen was not allowed to exceed 40 ksi$\sqrt{\text{in.}}$ This limitation minimized the size of the yield zone at the tip of the fatigue crack.

Testing of the fatigue cracked notched bend specimens was accomplished in a Tinius-Olsen tensile machine as shown by Fig. 6. The specimens were loaded to failure at a rate of 14,400 pounds per minute. With this loading rate, the maximum outer fiber bending stress rate was 10^3 psi per second. As the specimens were loaded, load-deflection curves were recorded. The deflection was measured in terms of testing machine crosshead movement with a class PD-IM deflectometer. After failure, the average depth of the notch plus fatigue crack on the fracture face was measured with a machinists scale. A cold box cooled by releasing pressurized nitrogen gas was used for the -65°F testing. Thermocouples were attached to the test fixture and specimen to verify the test temperature. All specimens were soaked at -65°F for not less than 1/2 hour prior to testing.

The load levels used to calculate the critical-stress-intensity (K_{IC}) was the load at deviation from linearity on the load deflection curve. Figure 7

illustrates the four types of load-deflection curves obtained with P_{DL} denoting the load at deviation from linearity. Curve A shows linearity up to the maximum load which indicates negligible slow growth. The majority of the curves obtained during the program were of this type and the load used to compute K_{IC} was P_{max}. Curve B indicates slow growth of the crack starting at Point P_{DL}, the deviation from linearity, which was then used to compute K_{IC}. Curve C illustrates the classical case of plane strain indicated by "pop-in" of the crack. Curve D indicates some slow growth, starting at P_{DL}, prior to the "pop-in" of the crack. Load measured at point P_{DL} was therefore used to compute the plane strain stress intensity in each case, except curve A, where P_{DL} coincided with P_{max}. In this evaluation, "pop-in" below the maximum load was a rarity. When the K_{IC} values were computed, no correction was made for the plastic zone at the tip of the crack.

To obtain valid K_{IC} values, limitations of the stress-intensity factor formula (Fig. 4) require that the ratio of nominal bending stress at the tip crack (σ_n) to the 0.2 percent offset tensile yield strength (σ ys) be one or less than one ($\sigma_n / \sigma_{ys} \leq 1$). The notched bend specimen size selected for this investigation resulted in predominantly valid test results.

3.6 SURFACE FLAWED SPECIMEN FRACTURE TOUGHNESS TESTING

Most of the fracture toughness testing was performed with the four-point-load notched bend specimen. However, a limited number of surface flawed specimens were tested to verify the results of the notched bend test. The surface flawed specimen configuration and stress intensity formula are given in Fig. 8.

The surface flawed specimens were precracked by tension fatigue cycling in an 180,000 pound capacity electrohydraulic testing fixture using a stress ratio of R = 0.06 and a cyclic rate of 120 cpm. Fatigue-crack growth was observed optically with a 50X calibrated telescope similar to that shown in Fig. 9. When the crack had fully initiated around the periphery of the electrical discharge machined flaw, fatigue cycling was stopped. The specimens were then loaded to failure at a gross-area stress rate of 10^3 psi per second. The maximum load (P_{max}) was used to calculate K_{IC}. The surface flawed specimen K_{IC} values were considered valid, when the ratio of gross area stress (σ_g) to 0.20 percent yield strength (σ_{ys}) was one or less ($\sigma_g / \sigma_{ys} \leq 1$).

3.7 SUSTAINED LOADING OF FATIGUE CRACKED NOTCHED BEND SPECIMENS IN SALT WATER

The combined action of salt water and static-tensile-stress causes cracks to propagate in high strength steels. To evaluate salt water crack growth resistance, fatigue cracked notched bend specimens, identical to notched bend specimens used for the fracture toughness testing (Fig. 4), were sustained-loaded in salt water at stress-intensity levels (K_{Ii}) below the critical-stress-intensity level, K_{IC}. In the presence of salt water, the fatigue cracks propagate until they reached the critical crack length necessary for rapid fracture. The results of this testing were plotted as curves of "K_{Ii}/K_{IC} vs. Time-to-Failure".

Figure 10 shows the notched bend specimen sustained-loading apparatus. The specimens were placed in the teflon-coated environmental cylinder and loaded at 14,400 pounds per minute to the desired stress-intensity level. The cylinder was then filled with salt water such that the precracked notched bend specimen was submerged to a depth of 1 to 1-3/8 inches. The initial applied sustained-load was maintained to failure, or until a 10,000 minute test period had elapsed. Specimens removed from the salt water prior to failure were fractured in air and examined for evidence of crack-growth. In this investigation a 3.5 percent NaCl-distilled water solution was used as a standard environment.

3.8 SUSTAINED-LOAD ALTERNATE IMMERSION TEST

Alternate immersion testing was performed with smooth-bend specimens (Fig. 11) to evaluate the stress corrosion resistance of the alloys. The specimens were sustained-loaded to 80 percent of their yield strength by applying bend moments to the ends of the specimens, as shown by Fig. 12.

The stress level at the center of the specimen was measured in terms of jig leg deflection and was checked with strain gages. With the exception of a 1- by 2-inch test area at the specimen center, the specimens were protected from corrosion with a coating of "Organo Ceram".

After stressing, the specimens were placed on a 4-foot diameter ferris wheel as shown in Fig. 13. The rotation speed was such that the specimen was immersed in an aqueous 3.5 percent NaCl solution eight minutes of each hour. This salt water solution was changed once a week. The time required

for the specimens to fail provided a measure of the susceptibility to stress corrosion. A specimen was considered to have failed when complete fracture had occurred or when the fracture specimens were held together by only a small section of metal. The alternate immersion test procedures are discussed in detail by Dreyer (Ref. 9).

Because the time-to-failure depends on the specimen surface condition (Ref. 9), the machining and finishing procedures used were the same for all specimens. Following heat treatment, the specimens were ground to final dimensions with a nominal 32 RHR surface finish. The specimens were then stress relieved at 50°F below the tempering temperature to transform any untempered martensite which might have formed during machining. The oxide film produced by the stress relieving was removed by dry abrasive blasting. The Maraging 250 specimens were not stress relieved but were abrasive blasted.

3.9 STRESS RUPTURE TEST OF HYDROGEN CHARGED SPECIMENS

Round notched tensile specimens were charged with hydrogen and then sustained-loaded in creep machines at various stress levels. The test specimen configuration used is shown in Fig. 14. The 0.003-inch notch radius resulted in a stress concentration factor of approximately 5 ($K_t = 5$). Following finish machining the root of the notch was polished with a rotating wire of diameter 0.006 inches in a slurry of oil and abrasive. When the finishing operations were completed, the specimens were magnetic particle inspected (Ref. 10) for cracks. The notch root radius and specimen diameter at the root of the notch were measured with a contour projector. With the exception of Maraging 250, the specimens were given a postmachining stress relief at 50°F below the tempering temperature.

The specimens were charged with hydrogen by electroplating with 0.0005 inch of bright cadmium using a "Rofco Super XL" brightener and a current density of 30 amp/ft^2 (Ref. 11). Prior to plating the specimens were cleaned by dry-abrasive blasting. Following plating, each specimen was inspected at low magnification (2-30X) to insure complete coverage at the root of the notch. The specimens were not given a postplate bake. However, the specimens were stored at room temperature for two weeks minimum prior to testing.

Two unplated specimens were tensile tested in room temperature air at a loading rate of 2,500 pounds per minute to determine the notched strength of the steels.

3.10 NOTCHED FATIGUE TESTING

A limited number of flat fatigue specimens of the configuration shown in Fig. 15 were tested in the Sonntag SF-10-U fatigue machine. The 0.250-inch hole at the center of the specimen resulted in a stress concentration factor of approximately 2.5 ($K_t = 2.5$). All the specimens were cycled at 1800 cycles per minute using a stress ratio of 0.06 (R = 0.06).

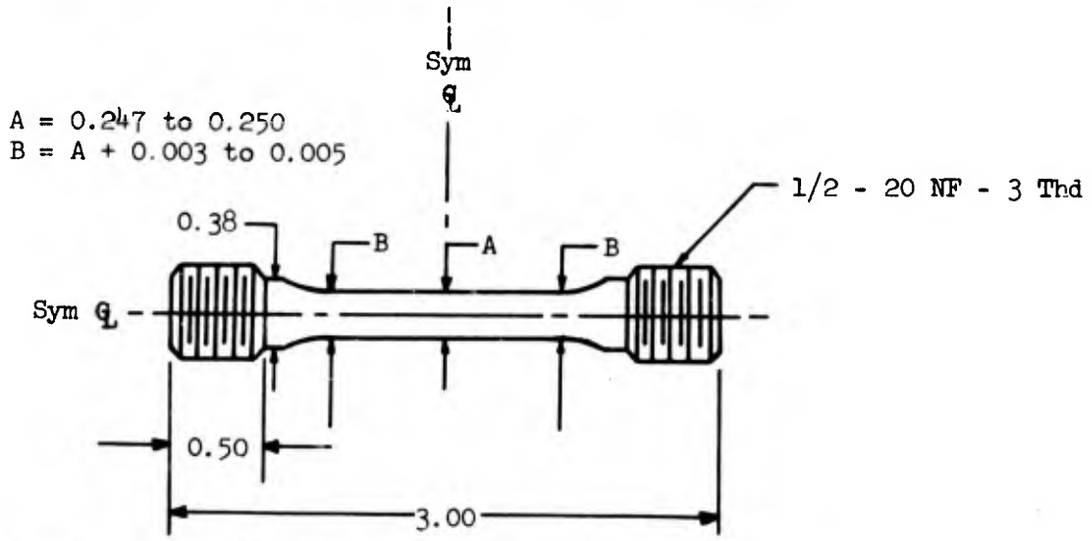

Figure 2. Tensile Specimen

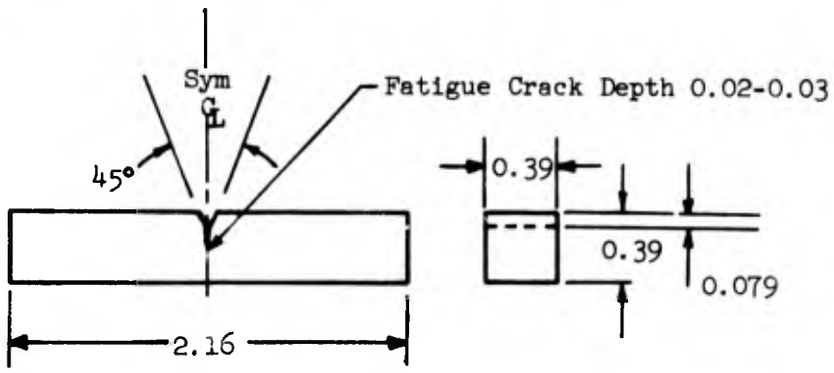

Figure 3. Precracked Charpy Specimen

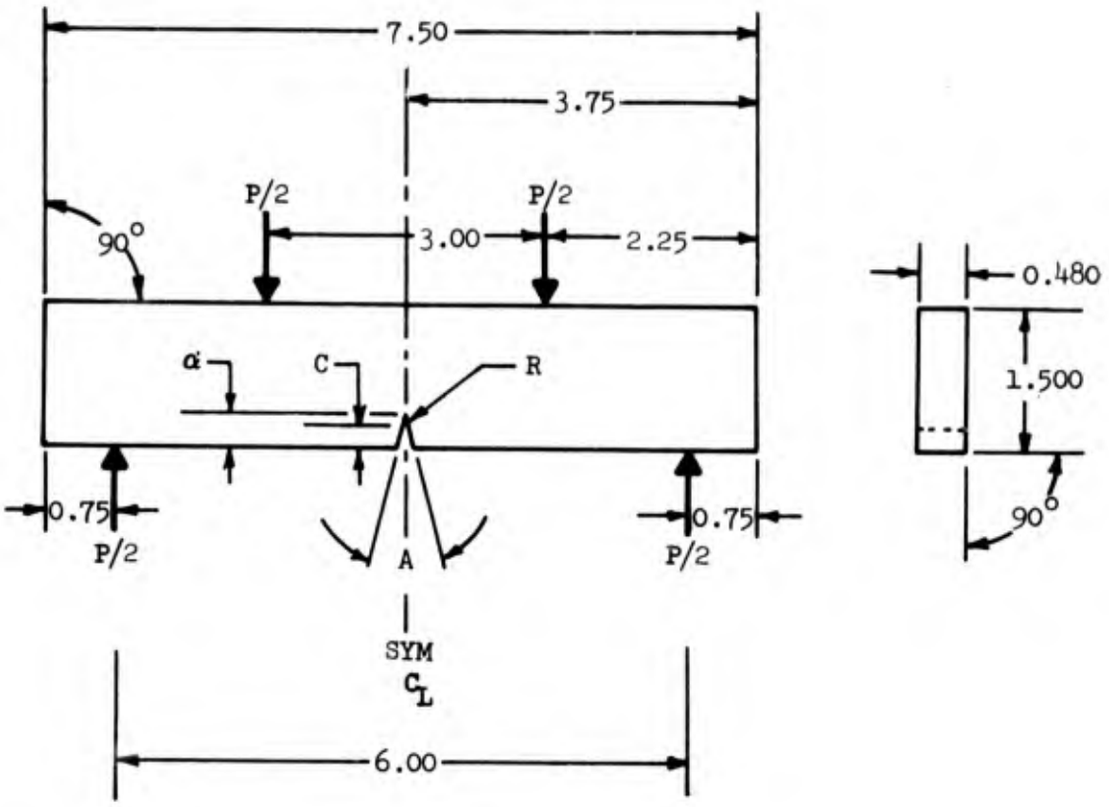

A = 45° notch angle
R = 0.011 max. notch radius
C = 0.225 ± 0.001 notch depth
α = notch depth, plus average fatigue crack depth
B = 0.480 ± 0.001 specimen width
W = 1.500 ± 0.001 specimen depth
L = 1.50 moment arm
All dimensions in inches

σ_n = nominal bending stress at crack tip

$$K = \frac{PL}{BW^{3/2}} \left\{ \left(\frac{1}{1-\mu^2} \right) \left[34.7\left(\frac{a}{w}\right) - 55.2\left(\frac{a}{w}\right)^2 + 196\left(\frac{a}{w}\right)^3 \right] \right\}^{1/2}$$

$$\sigma_n = \frac{4.5\ P}{B\ (W-a)^2}$$

Figure 4. Notched Bend Specimen and Stress Intensity Formula

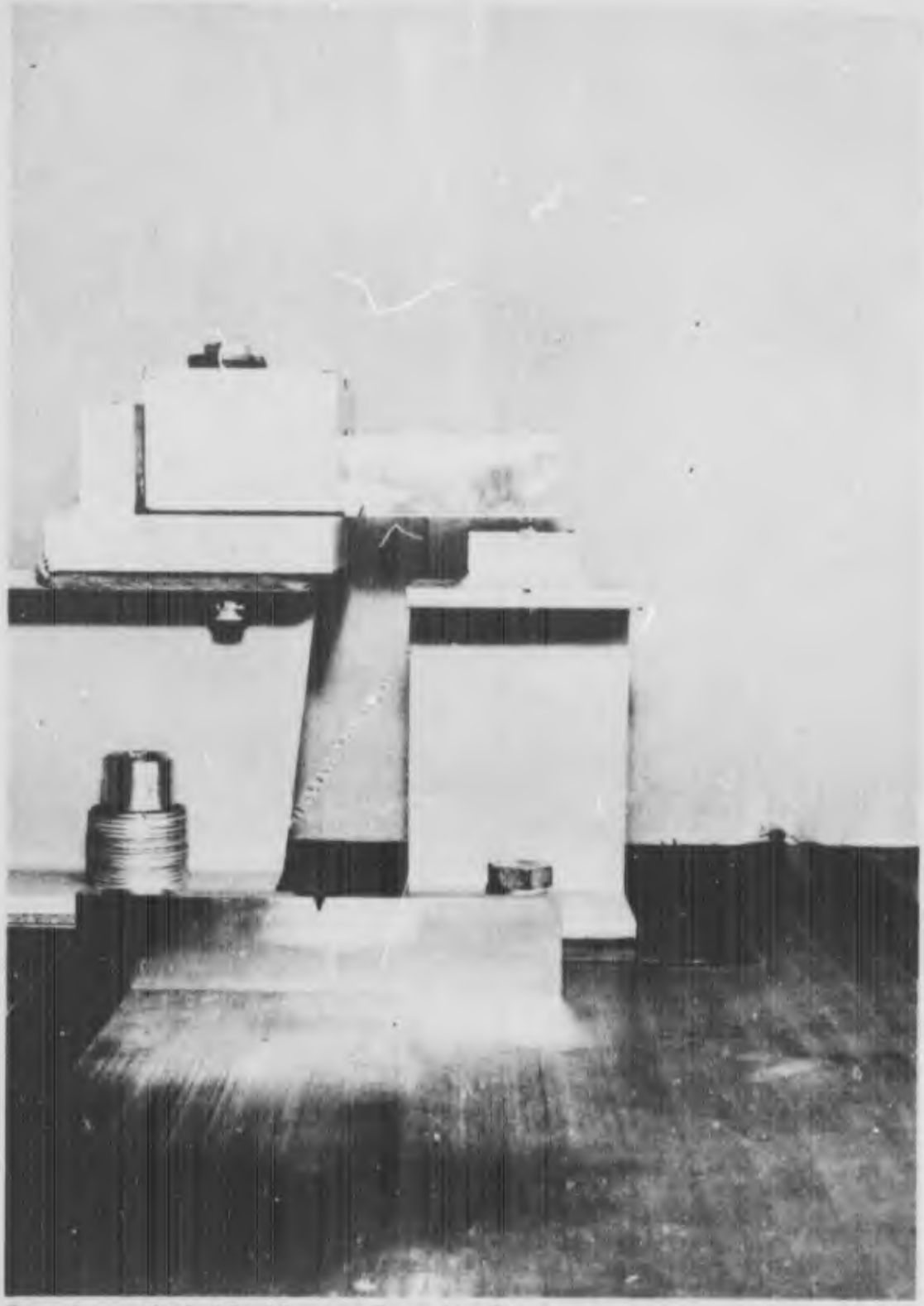

Figure 5. Notched Bend Specimen Precracking Fixture

Figure 6. Notched Bend Specimen Test Apparatus

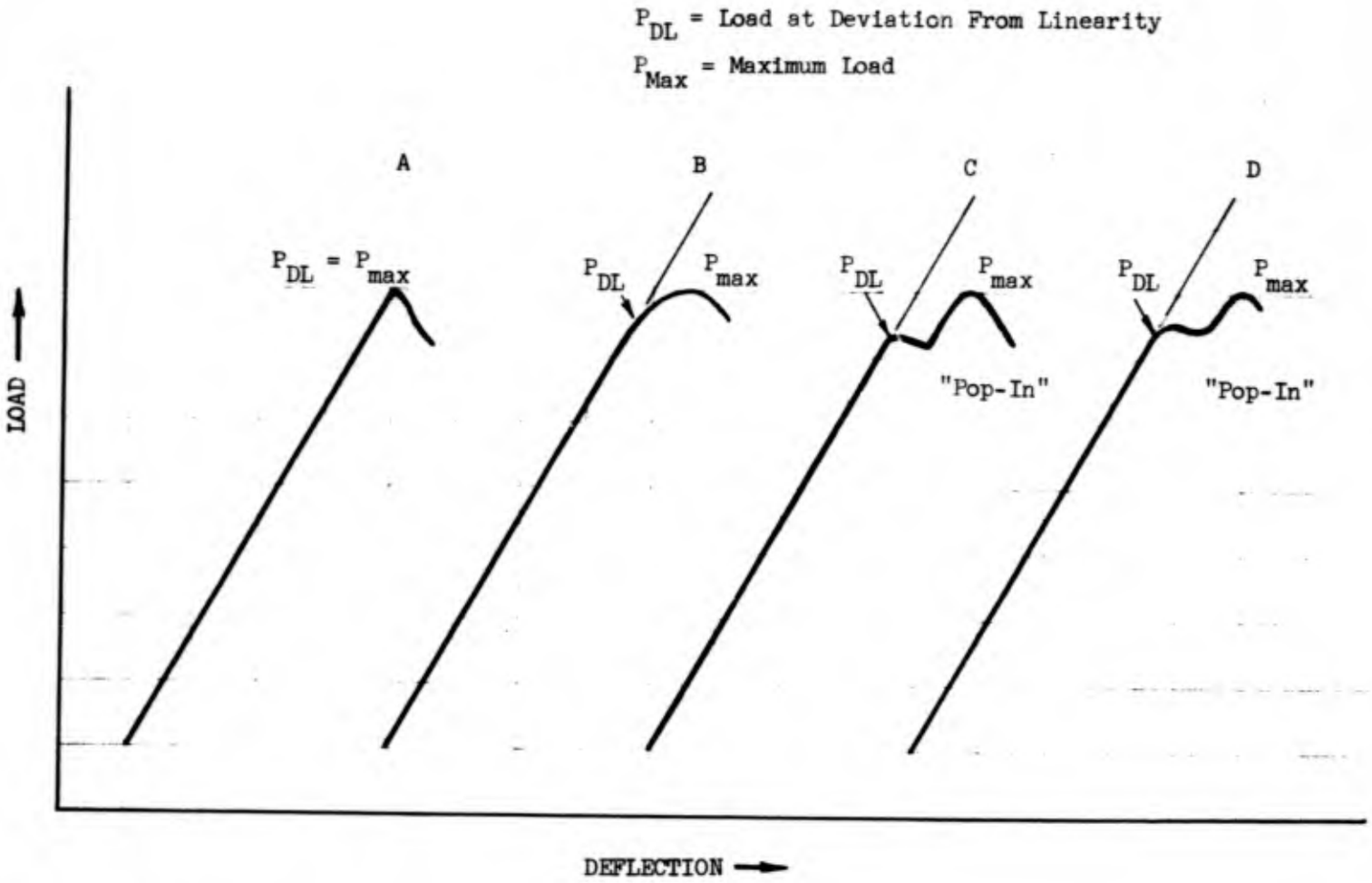

D6A 10093-2

Figure 7. Typical Notched Bend Specimen Load-Deflection Curves

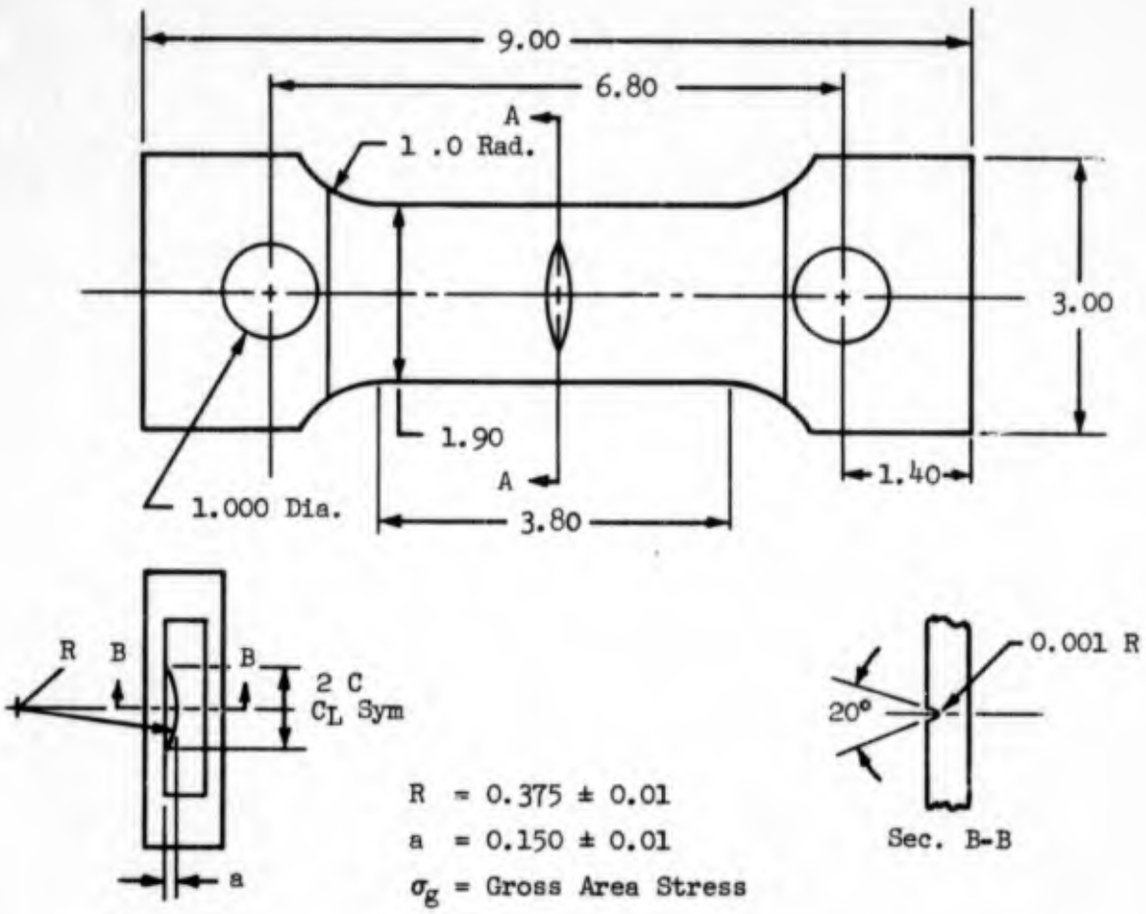

$$K_{IC} = \frac{1.95\ \sigma_g \sqrt{a}}{\Phi}$$

$$\Phi = \int_0^{\pi/2} \left(1 - \frac{c^2 - a^2}{c^2} \sin^2 \theta\right)^{1/2} d\theta$$

Figure 8. Surface-Flawed Specimen and Stress Intensity Formula

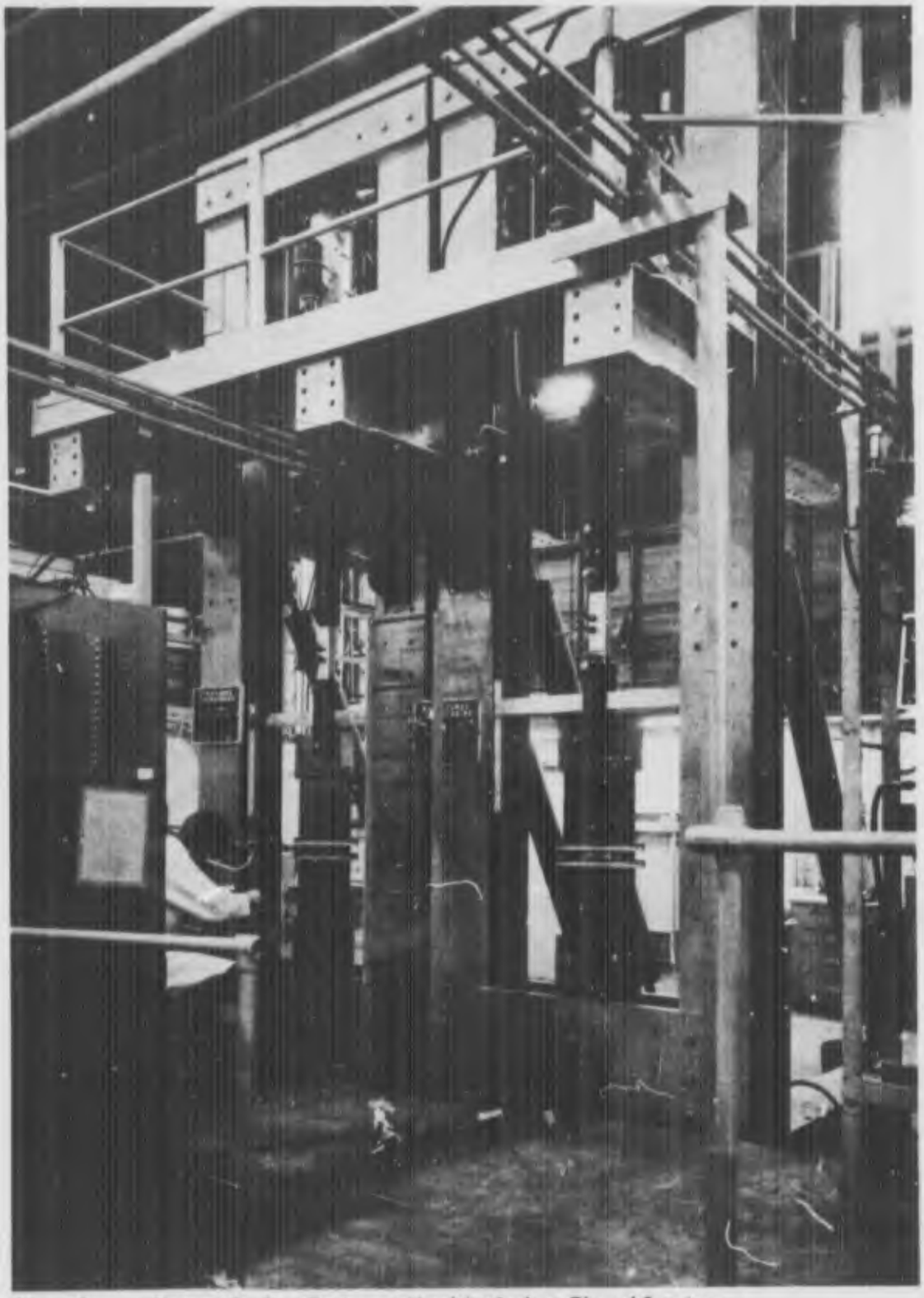

Figure 9. Fatigue Cycling Equipment Used for Surface-Flawed Specimen

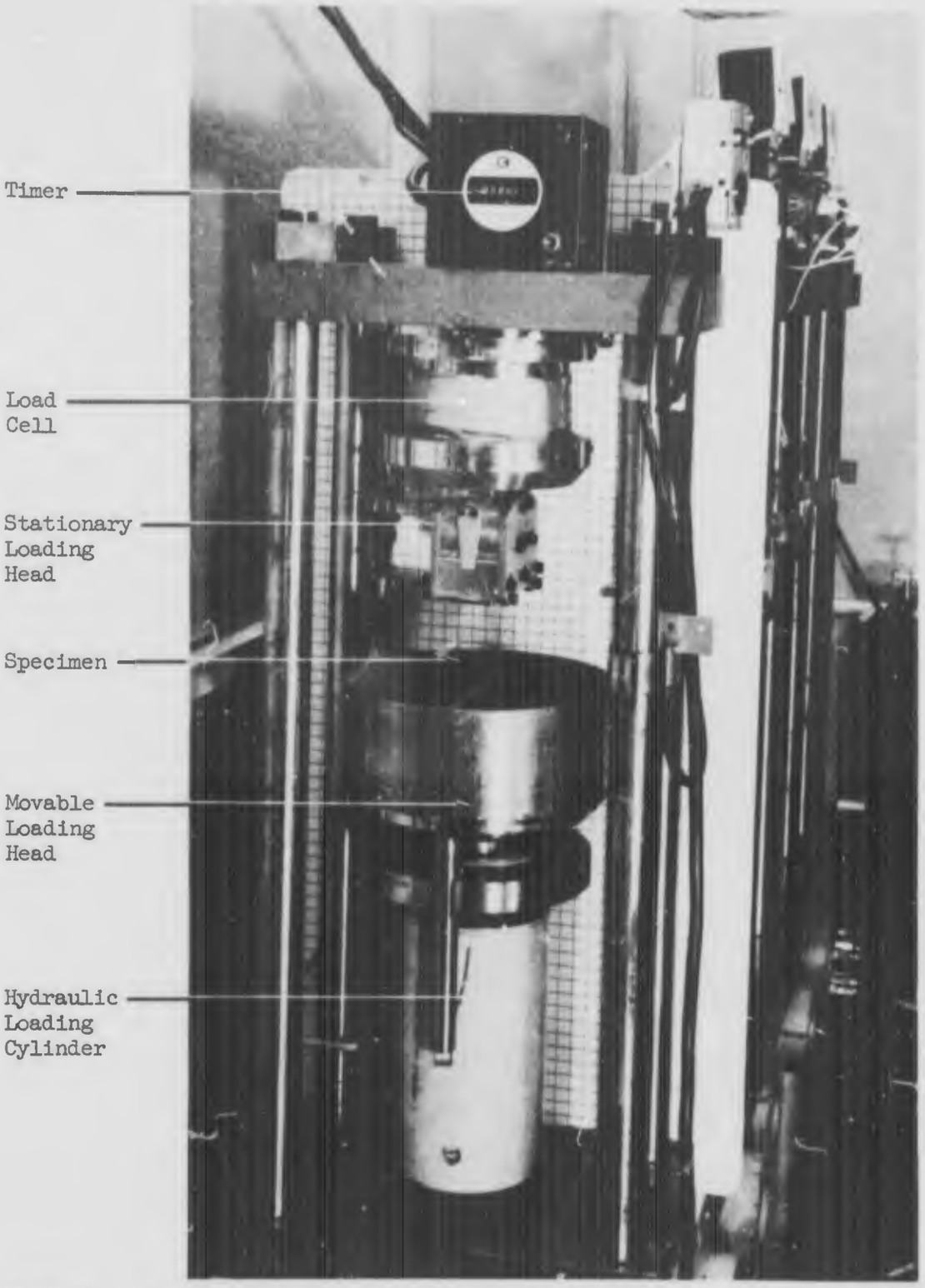

Figure 10. Notched Bend Specimen Sustained-Loading Apparatus

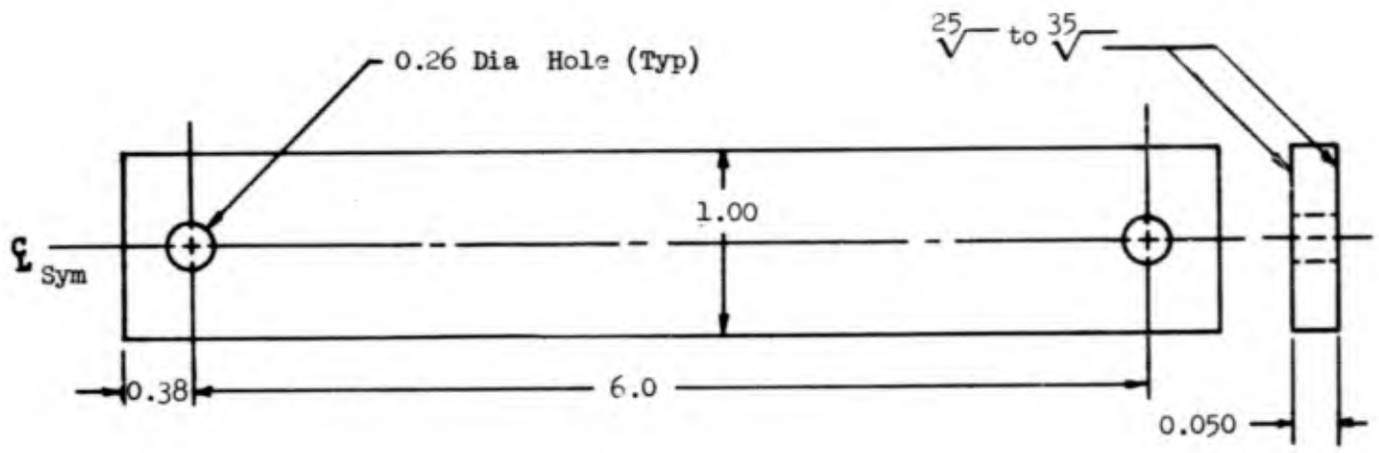

D6A 10093-2

Figure 11. Alternate Immersion Specimen

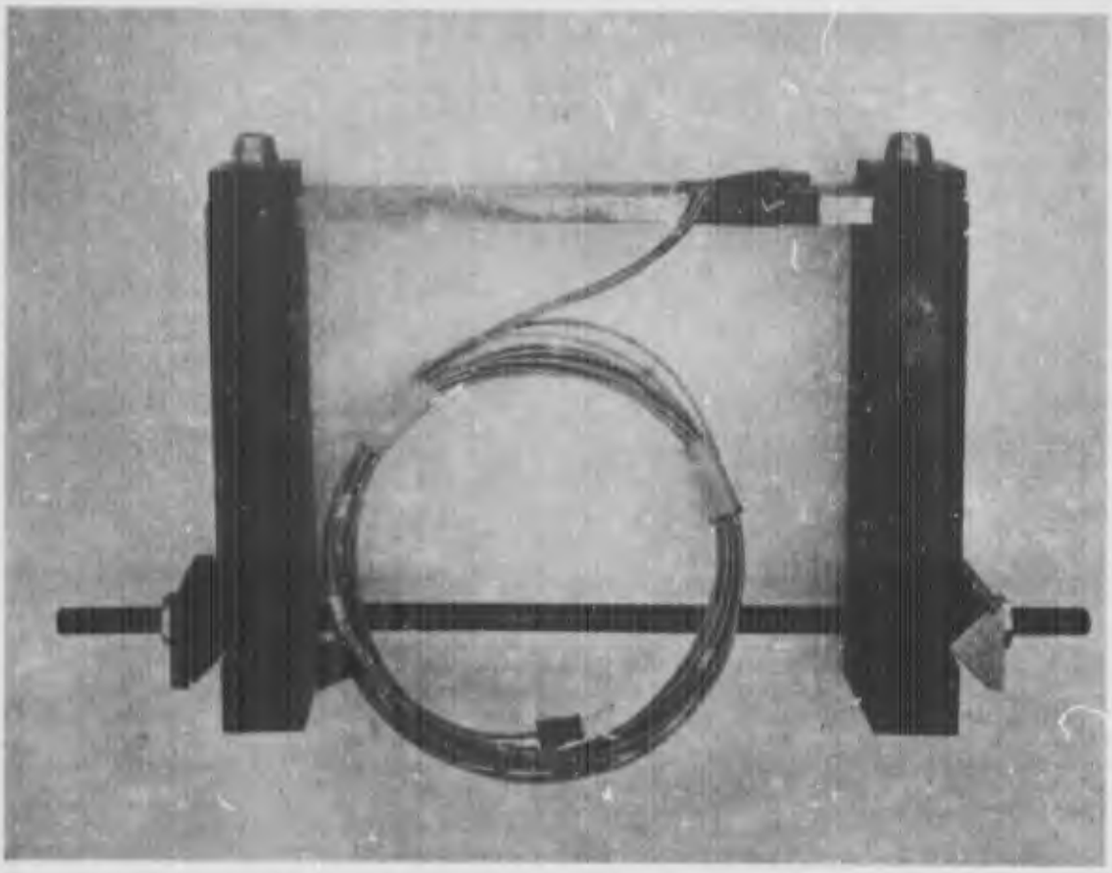

Figure 12. Sustained-Stress Alternate Immersion Specimen Fixture

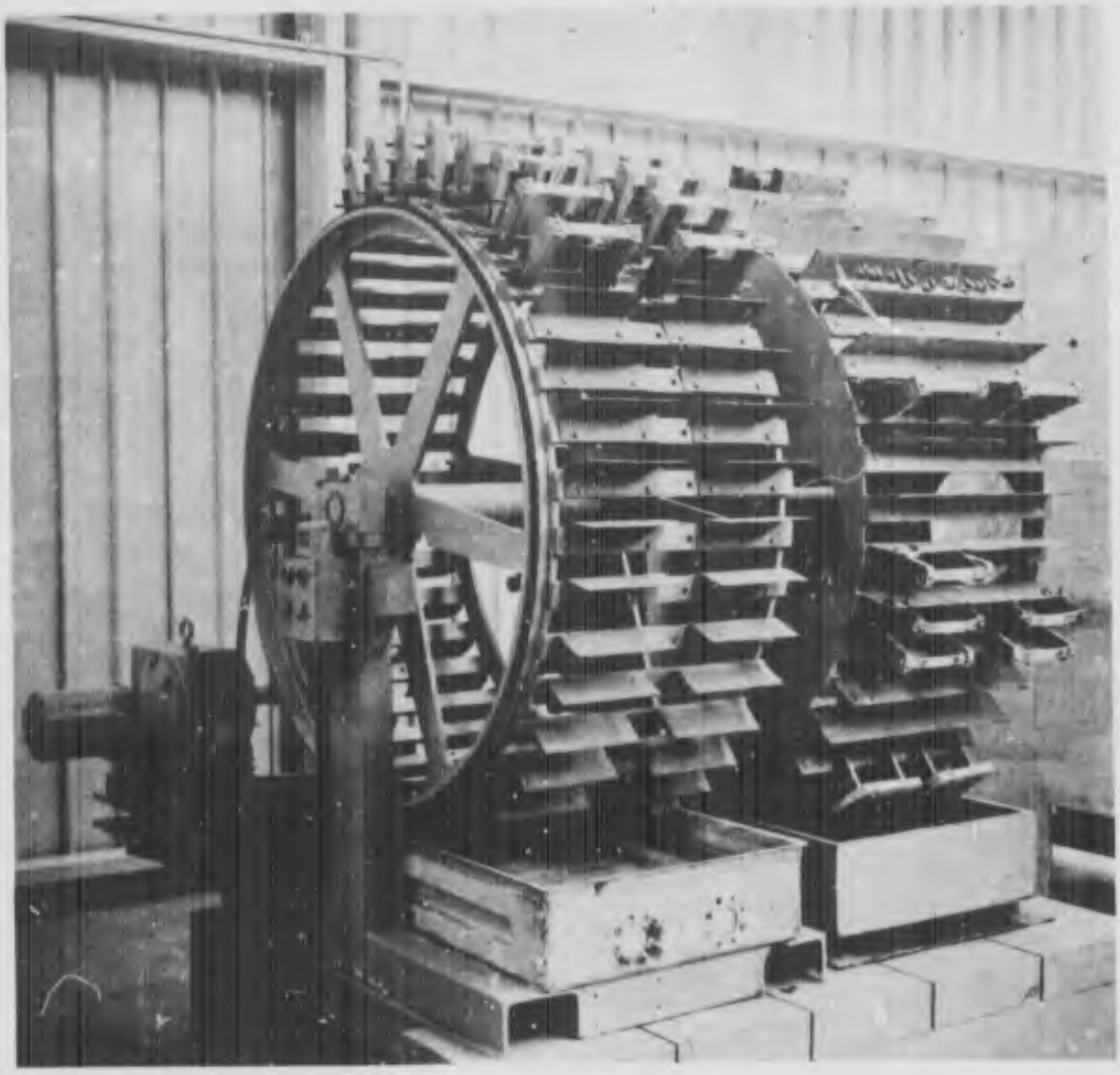

Figure 13. Alternate Immersion Test Apparatus

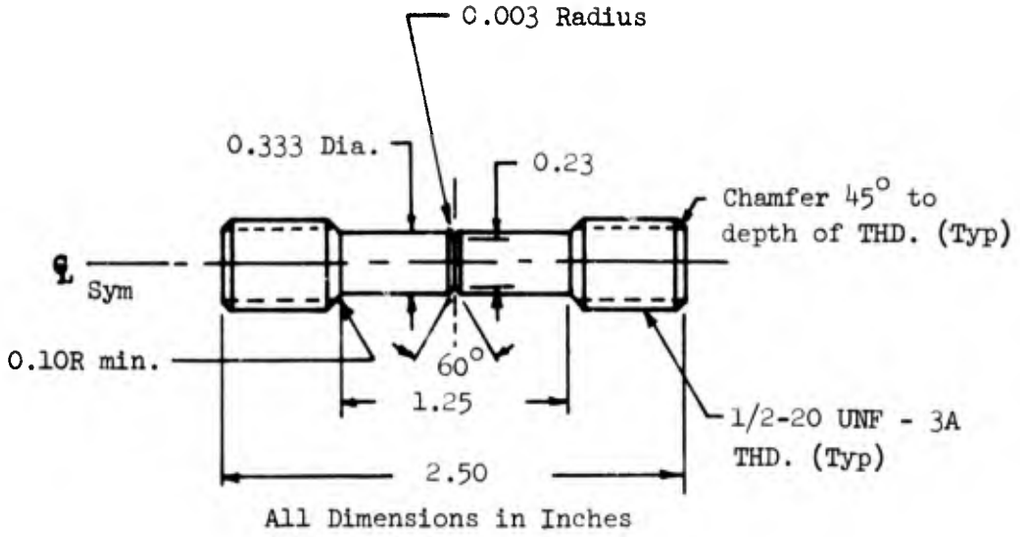

Figure 14. Round Notched Tensile Specimen

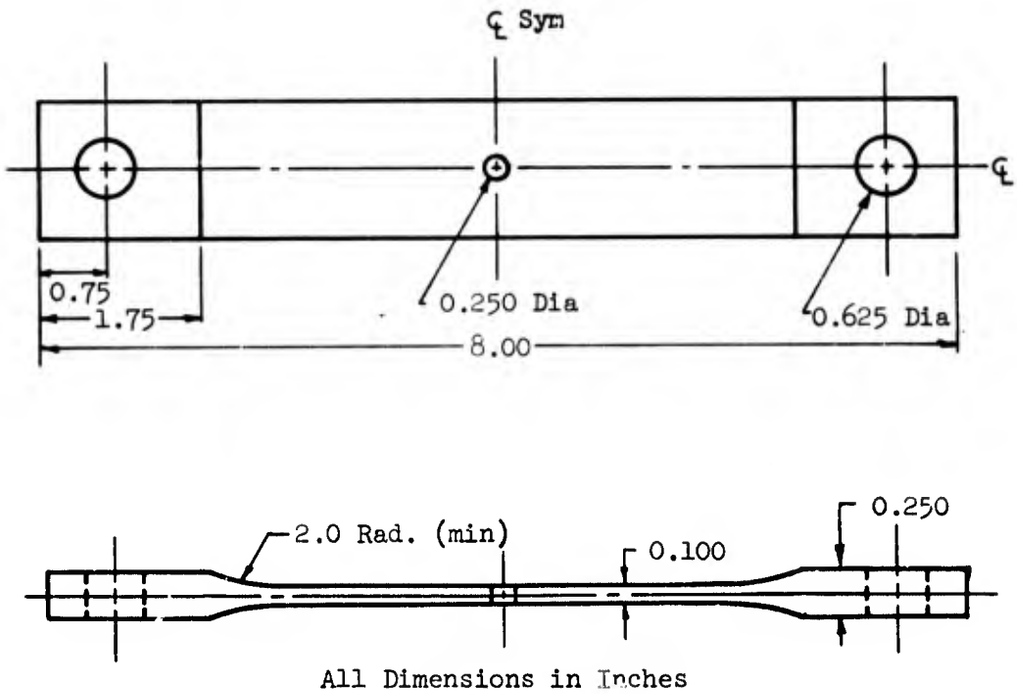

Figure 15. Fatigue Specimen

4.0 HEAT TREATMENT STUDY

An understanding of how the strength and toughness of a steel vary with heat treatment is required for selecting the thermal condition that gives the best combination of strength and toughness. The strength, toughness, and heat treatment relationships are also necessary in establishing the temperature and time controls needed to achieve a specific thermal condition.

In this section of the report, the strength and fracture toughness are reported for several different heat treatments of each alloy. The heat treatments that gave the best combination of strength and toughness were used for subsequent phases of the program such as stress corrosion (Sec. 7.0) and fatigue testing (Sec. 10.0).

4.1 PROCEDURE

Table V lists the heat treatments that were tested. Two tensile and four notched bend fracture toughness specimens were tested per heat treatment. Except for 9Ni-4Co-0.45C, each alloy was given a single type of heat treatment. For example, the Maraging 250 steel was tested only in the solution treated and aged condition, while the 300M, 4330 V-Mod, H-11 Mod and 9Ni-4Co-0.30C alloys were tested only in the quench-temper condition. The 9Ni-4Co-0.45C steel, however, was tested in both the quench-temper and bainitic conditions. The bainitic treatment included a quench from the austenitizing temperature into a salt bath, which was maintained at a constant temperature above the M_s (Martensite-Start) temperature. At this constant temperature, referred to as the bainitic treatment temperature, the austenite transformed to bainite. To insure that there was no temperature rise during quenching, a large (approximately 48 cu ft) salt bath was used.

Since the alloys evaluated were primarily intended for high strength applications, most of the specimens were heat treated to ultimate strengths greater than 220 ksi. To keep the size of the program within reasonable limits, all specimens were taken from the transverse grain direction of the billets and only specimens from one heat of each alloy were tested. The specimen configurations, specimen preparation procedures, and testing methods are described in Sec. 3.0. All the tensile specimens were tested at room temperature, whereas half of the notched bend fracture toughness specimens were tested at -65°F

and half at room temperature. Because steels often display a ductile-to-brittle transition behavior, low temperature toughness testing was considered necessary. The -65°F temperature was selected because it is representative of the minimum SST service temperature.

4.2 RESULTS

Tables VI and VII, respectively, list the tensile and fracture toughness test results for the different heat treatments. The amounts of austenite in several of the tensile specimens after testing are given in Table VIII. This table also gives some austenite data for heats which were tested during subsequent phases of the program. Figure 16 through 23 are plots of the property data as a function of a heat treatment variable such as tempering temperature or aging temperature.

4.3 4330 V-MODIFIED

The ultimate and yield strengths increased as the tempering temperature was decreased from 700°F to 400°F (Fig. 16). The toughness, however, was a minimum at tempering temperatures of 500 and 600°F. The sharp decrease of -65°F toughness at tempers of 600 and 500°F was a result of the so-called "500°F embrittlement," sometimes called "irreversible temper embrittlement."

Studies have shown (Ref. 12) that this type of embrittlement results from the transition of the carbide precipitate from epsilon carbide to cementite and the appearance of platelet cementite early in the third stage of tempering. Because the embrittlement is precipitation related, it depends on the tempering time, tempering temperature, and composition. Electron micrographs (Figs. 24 through 26) show the change in carbide precipitation from ϵ-carbide to Fe_3C.

The 500°F temper produced slightly higher -65°F toughness and higher strength than a 600°F temper, therefore a 500°F temper was selected as the optimum heat treatment. Although a 400°F temper yields higher strength and toughness, 400°F was considered too low and restricted for the application of the material at moderately elevated temperatures. Furthermore, 400°F may be too low to relieve residual thermal stress and transform or stabilize austenite retained from quenching.

4.4 H-11 MODIFIED

Figure 17 shows how the strength and toughness of H-11 Modified varied with tempering temperature. Compared with the other alloys tested, the change of strength with respect to tempering was quite rapid. For example, within the tempering range of 1025°-1175°F (150°F range) the strength varied from 270 to 250 ksi. Therefore, to achieve a specific strength level, requires closer tempering temperature control than with steels such as 4330 V-Modified or 300M.

No toughness data was obtained for the 1025°F temper because the notched bend specimens failed during precracking. However, by extrapolation (Fig. 17) the K_{IC} value was estimated to be less than 30 ksi$\sqrt{in.}$ Of all the steels tested, the H-11 Modified steel had the lowest toughness. Therefore, a relatively low strength (220 ksi ultimate) 1100°F temper was selected for further evaluation.

Microstructures for this H-11 type tool steel are included in Figs. 28 through 30. A secondary hardening reaction is reported for this steel at about 950°F (Ref. 13). The lowest tempering temperature applied to this alloy on this program was 1025°F which is well into the range for precipitation of alloy carbides referred to as secondary hardening. The presence of cementite has been reported at 1020°F (Ref. 14) based on electron diffraction analysis. It is probable that the plate-like carbides of Figs. 28 and 29 are Fe_3C. The increasing occurrence of the rounded carbides from Figs. 28 through 30 indicates the further growth of the lower energy alloy carbides at the expense of the less stable Fe_3C. The carbides are probably predominantly $M_{23}C_6$. No signs of recovery or recrystallization are observed until the steel has been tempered well past the aging peak. However, once recovery begins softening is very rapid as shown on Fig. 17.

4.5 9Ni-4Co-0.30C

The yield and ultimate strength of the 9Ni-4Co-0.30C (Cr, Mo) steel increased (Fig. 18) to a maximum when the tempering temperature was increased from 800°F to 950°F. This strength increase may have been a so-called secondary hardening effect or possibly the result of the precipitation of intermetallics. The change in microstructure corresponding to this peak in the strength properties is shown in Figs. 31 through 33. The alloy carbide or intermetallic precipitates responsible for the secondary hardening are evident

in the electron micrograph showing the overaged microstructure tempered at 1050°F (Fig. 33). Because the strength was a maximum and the -65°F deviated only slightly from the room temperature toughness, a 950°F temper was selected as optimum. However, it should be recognized that a significant increase of fracture toughness can be gained with only a slight decrease of strength by tempering at 1000°F.

Before tempering, the 9Ni-4Co-0.30C steel was subcooled at -100°F for two hours to transform austenite retained from quenching. Without this subcool, the yield strength was decreased approximately 10 ksi while the ultimate strength and fracture toughness were slightly increased (Tables VI and VII). Study of the retained austenite data (Table VIII) shows that the specimens from Heat 3930852 contained a higher percentage of retained austenite (3.5-5 percent) than the specimens from Heats 3931144 and 3931145. The reasons for the larger amounts of retained austenite in Heat 3930852 were not evident, since no significant differences of chemistries existed between the heats. However, the billet from Heat 3930852 was forged at a higher temperature (2100° vs. 2000°F, Table II) and received slightly less forging reduction.

Components fabricated from 9Ni-4Co-0.30C should be subcooled prior to tempering to provide higher yield strengths and to reduce the in-service possibility of retained austenite transforming to untempered martensite. Transformation during service of the retained austenite to untempered martensite results in severe microstructural strains which increase the susceptibility to stress corrosion, reduce fatigue life, and decrease the resistance to hydrogen embrittlement.

4.6 300M

The 750°F temper produced lower values of ultimate strength and toughness than a 600 or 400°F temper (Fig. 19). Although 400°F resulted in higher -65°F toughness and higher strength, a 600°F temper was selected as optimum because of the higher yield strength which would result in better compression properties. The 600°F tempering temperature also results in superior metallurgical stability which is required for elevated temperature applications. The loss of yield strength at the 400°F temper suggested that 400°F was too low to relieve residual stress or to transform austenite retained from quenching. Further investigation is needed before the loss of yield strength at 400°F can be

fully understood.

The composition of 300M is similar to that of 4340 steel, except that 300M contains approximately 1.5 percent additional silicon. When tempered at 600°F, 4340 has a minimum toughness due to "500°F embrittlement". The addition of silicon in the 300M retards the precipitation of cementite to higher tempering temperatures which results in the "500°F embrittlement" occurring above 600°F as seen by the sudden drop in fracture toughness of the 750°F tempered specimens. It appears from this study that 600°F is about the highest tempering temperature that should be attempted in this alloy. The microstructures revealing onset of the 500°F embrittlement are seen in Figs. 34 through 36. Cementite has been identified in a 300M structure tempered at 750°F (Ref. 14), therefore it is probable that the large carbides appearing in Fig. 38 are cementite. Silicon additions have been reported to increase the severity of this embrittlement when it finally occurs (Ref. 15). The additional silicon also gives 300M a higher strength than 4340 at an equivalent tempering temperature.

4.7 MARAGING (18 PERCENT Ni) 250

The alloying elements in Maraging steel suppress the formation of ferrite causing austenite to transform to a so-called body centered cubic martensite during slow cooling. This martensite is soft (R_C = 28-34) and machinable. Maraging steels derive their strengthening properties from a precipitation hardening mechanism. The major precipitate identified in this steel at peak hardness obtained at 900°F for 9 hours has been reported (Ref. 16) as Ni_3Mo. A second precipitate has been tentatively identified as Ni_3Ti. Micrographs of precipitates obtained during aging of this alloy are shown in Figs. 37 through 40.

Figs. 20 and 21 show that the fracture toughness decreased with increasing strength. The rate of decrease of -65°F toughness, however, appeared to be less than the rate of decrease of room temperature toughness. There is the possibility that this may not have been a real effect since there was a high degree of K_{IC} scatter.

Other Investigations have shown that 900°F is the most satisfactory aging temperature. However, aging for periods longer than about 8 to 9 hours generally results in overaging. For subsequent testing, a 900°F/3 hour age was

selected as the optimum aging treatment. In practice, the degree of aging should be limited to the extent needed to achieve the required strength. This restriction provides for the maximum toughness.

4.8 9Ni-4Co-0.45C (QUENCH AND TEMPER)

The strength of the quench and tempered 9Ni-4Co-0.45C increased and toughness decreased when the tempering temperature was lowered from 600°F to 400°F (Fig. 22). At a 500°F temper there was no evidence of irreversible temper embrittlement. It is probable that the high alloy content of this steel would retard the precipitation of cementite to above the 600°F maximum tempering temperature investigated in this program. At the low temperatures investigated, the precipitates shown in Figs. 41 through 43 are probably epsilon carbide or intermetallics. Even though the steel was subcooled prior to tempering, the austenite content after tempering was approximately 3 to 5 percent (Table VIII). Because the alloy is generally considered for applications in the 260-280 ksi ultimate strength range, a 500°F temper was selected for further evaluation. Furthermore, a 400°F tempering temperature was considered too low for stability.

4.9 9Ni-4Co-0.45C (BAINITIC)

Reducing the bainitic treatment temperature from 550°F to 475°F resulted in the ultimate strength being decreased from 234 ksi to 270 ksi and the K_{IC} values being decreased from approximately 116 ksi $\sqrt{in.}$ to about 88 ksi $\sqrt{in.}$ (Fig. 23). Because of these rapid property changes, stringent control of the salt bath temperature was required to obtain a specific strength level. The typical acicular bainitic structures are shown in Figs. 44 and 45.

Lowering the bainitic treatment temperature from 475°F to 455°F had no significant effect on the strength or toughness properties. The 455°F treatment was apparently too close to the M_s temperature resulting in formation of mixed structure. Since the highest possible strength was desired, a 475°F bainitic treatment was selected for further evaluation. If a 455°F treatment had been selected, no gain of strength would have been realized.

After bainitic treatment, 3 to 5 percent austenite was detected in the bainitic structure (Table VIII). Consideration should be given to reheating the material to the bainitic treatment temperature following the air cool when the material is removed from the salt bath. Such a treatment would temper any

untempered martensite that formed during the air cool, relieve residual thermal stresses, and probably reduce the amount of retained austenite. Representatives of the Republic Steel Company have indicated that this post salt bath temper provides slight increases in the yield strength.

At a strength level of about 270 ksi, the bainitic treatment gave higher toughness than the quench-temper treatment. The toughness of the quench-tempered material was approximately 24 percent lower at -65°F and 36 percent lower at room temperature.

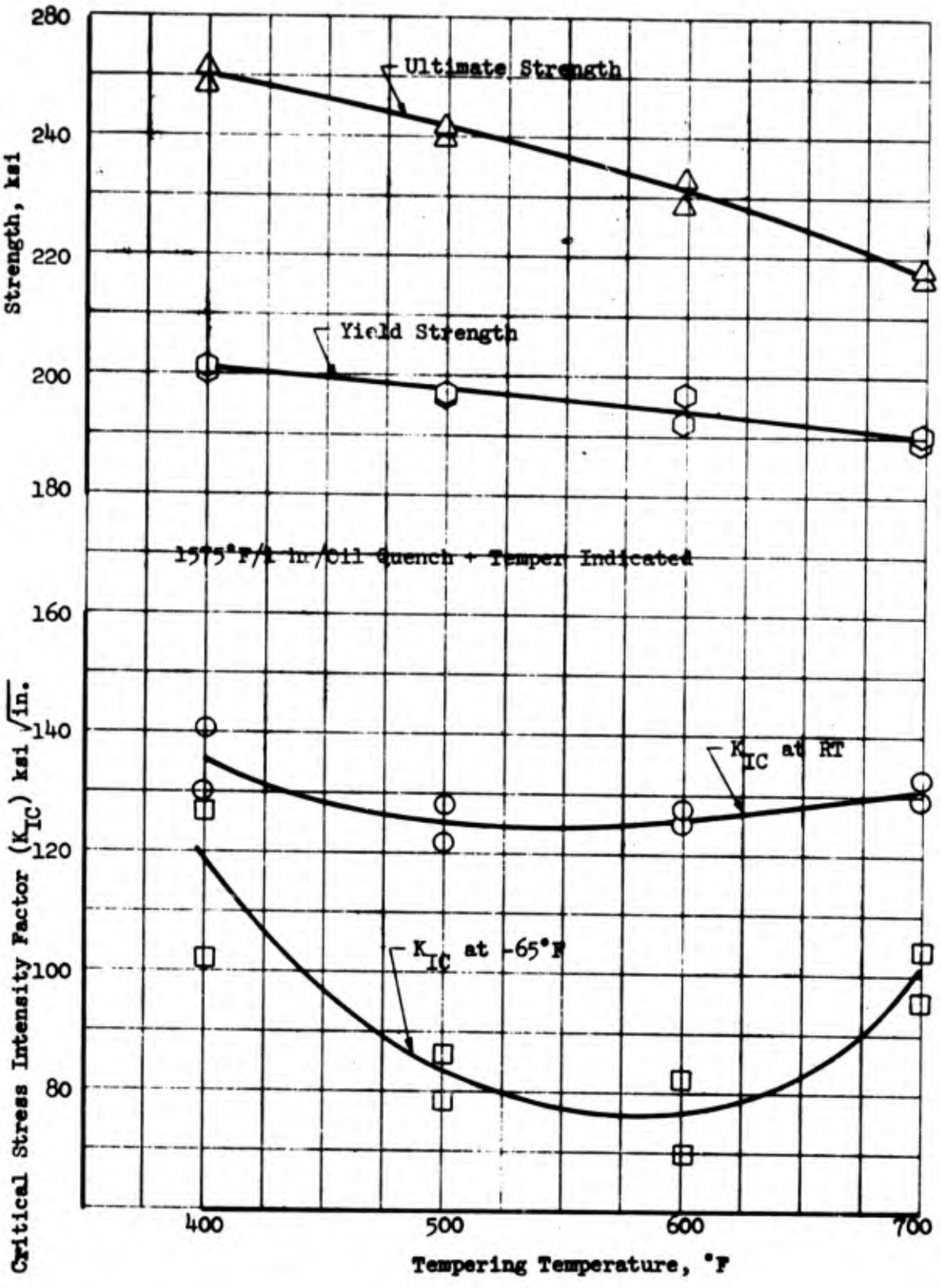

Figure 16. Effect of Tempering Temperature on Strength and Toughness of 4330 V-Modified, Heat No. C57046

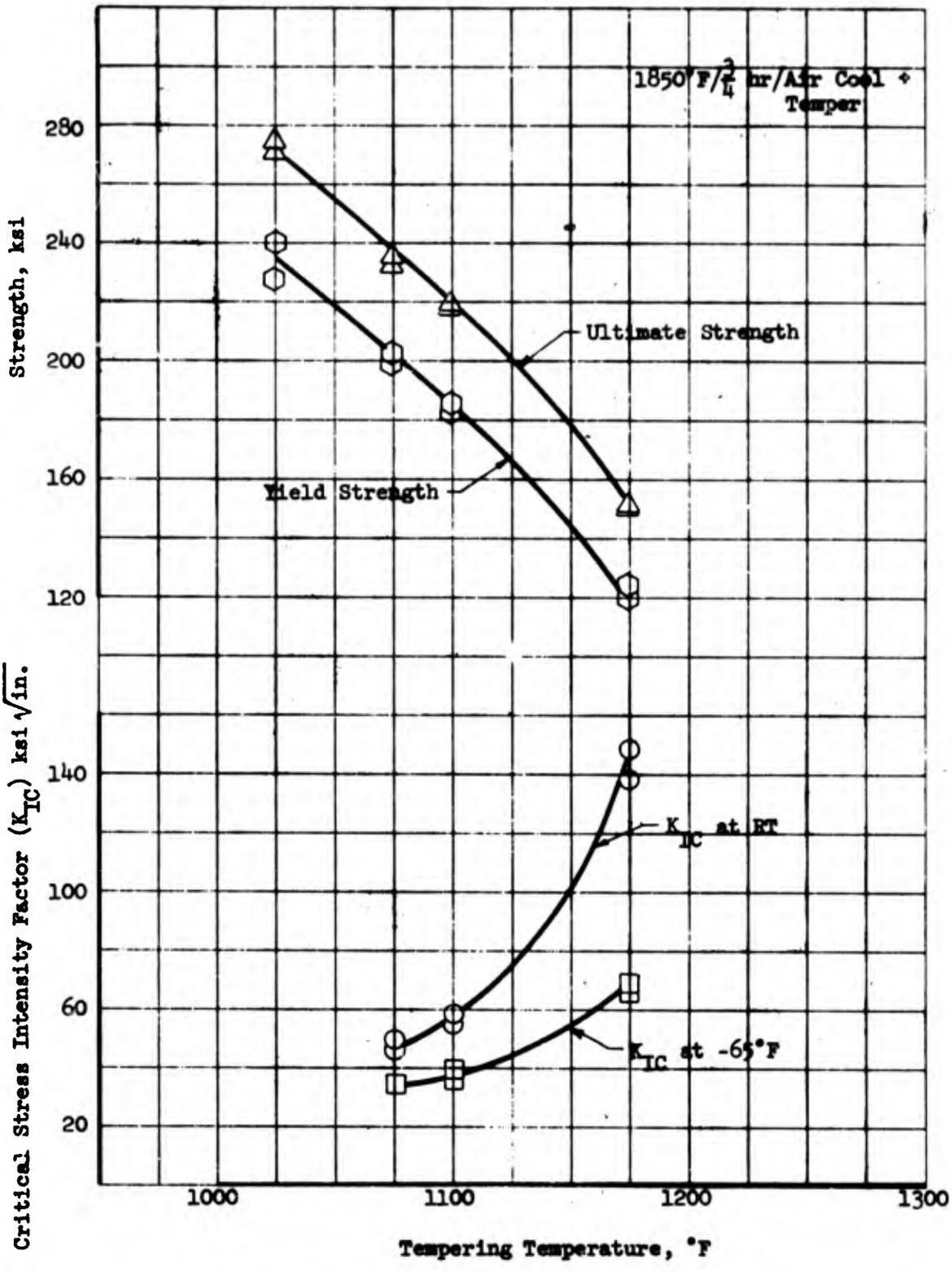

Figure 17. Effect of Tempering Temperature on Strength and Toughness of H-11 Modified, Heat No. 09110

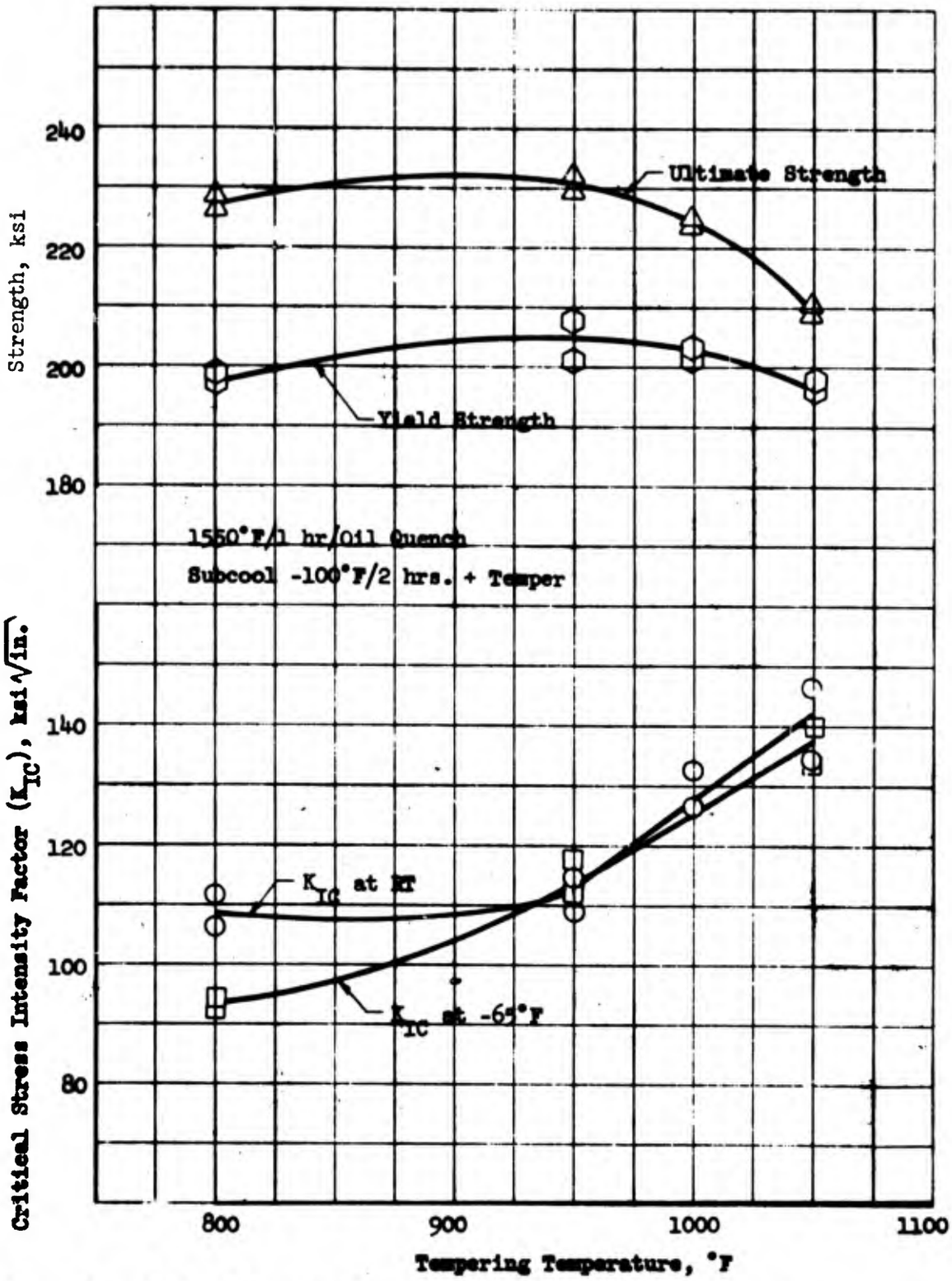

Figure 18. Effect of Tempering Temperature on Strength and Fracture Toughness of 9Ni-4Co-0.30C, Heat No. 3930852

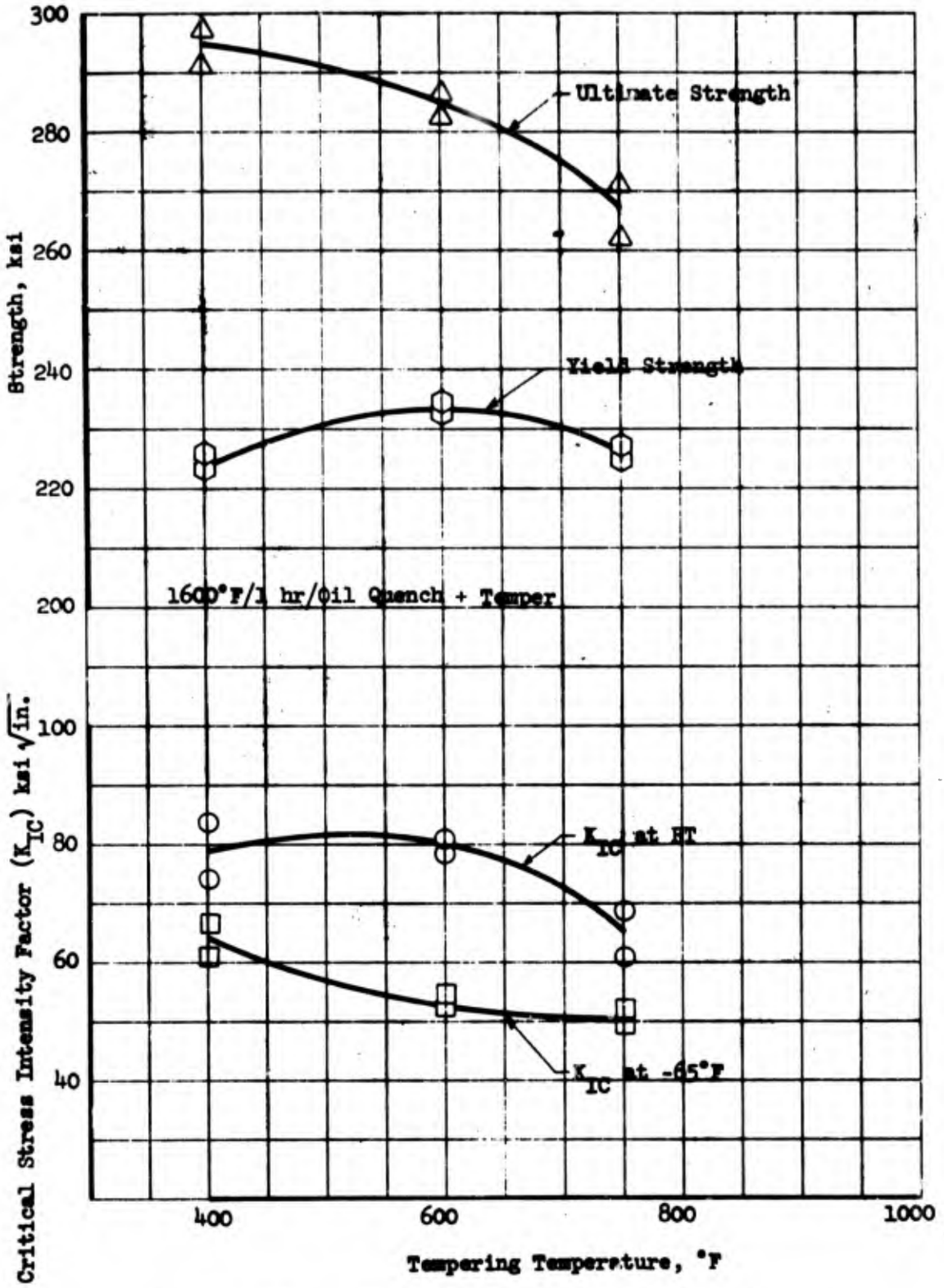

Figure 19. Effect of Tempering Temperature on Strength and Toughness of 300M, Heat No. 09715

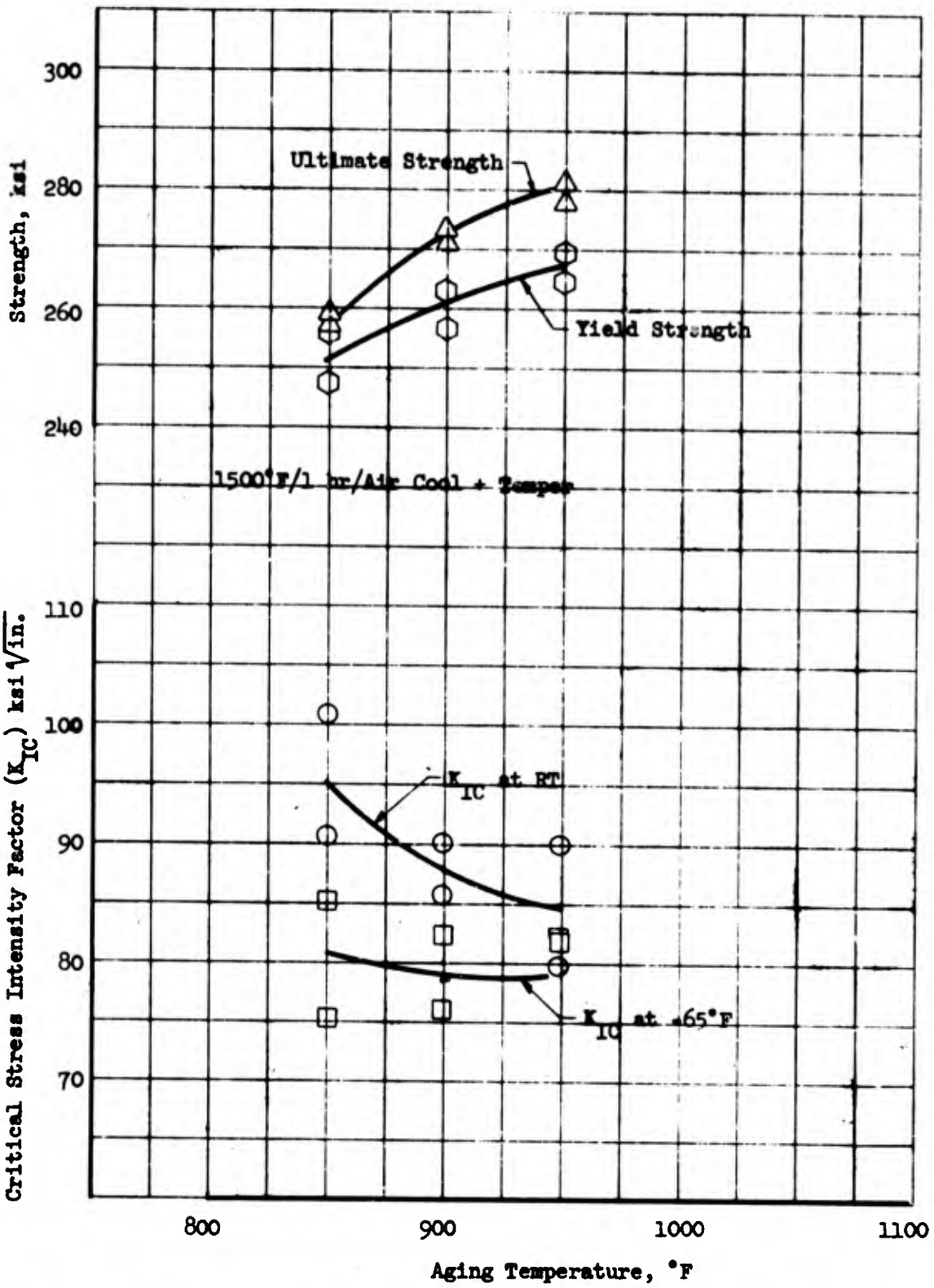

Figure 20. Effect of 3-Hour Age on Strength and Toughness of Maraging 250, Heat No. 24676

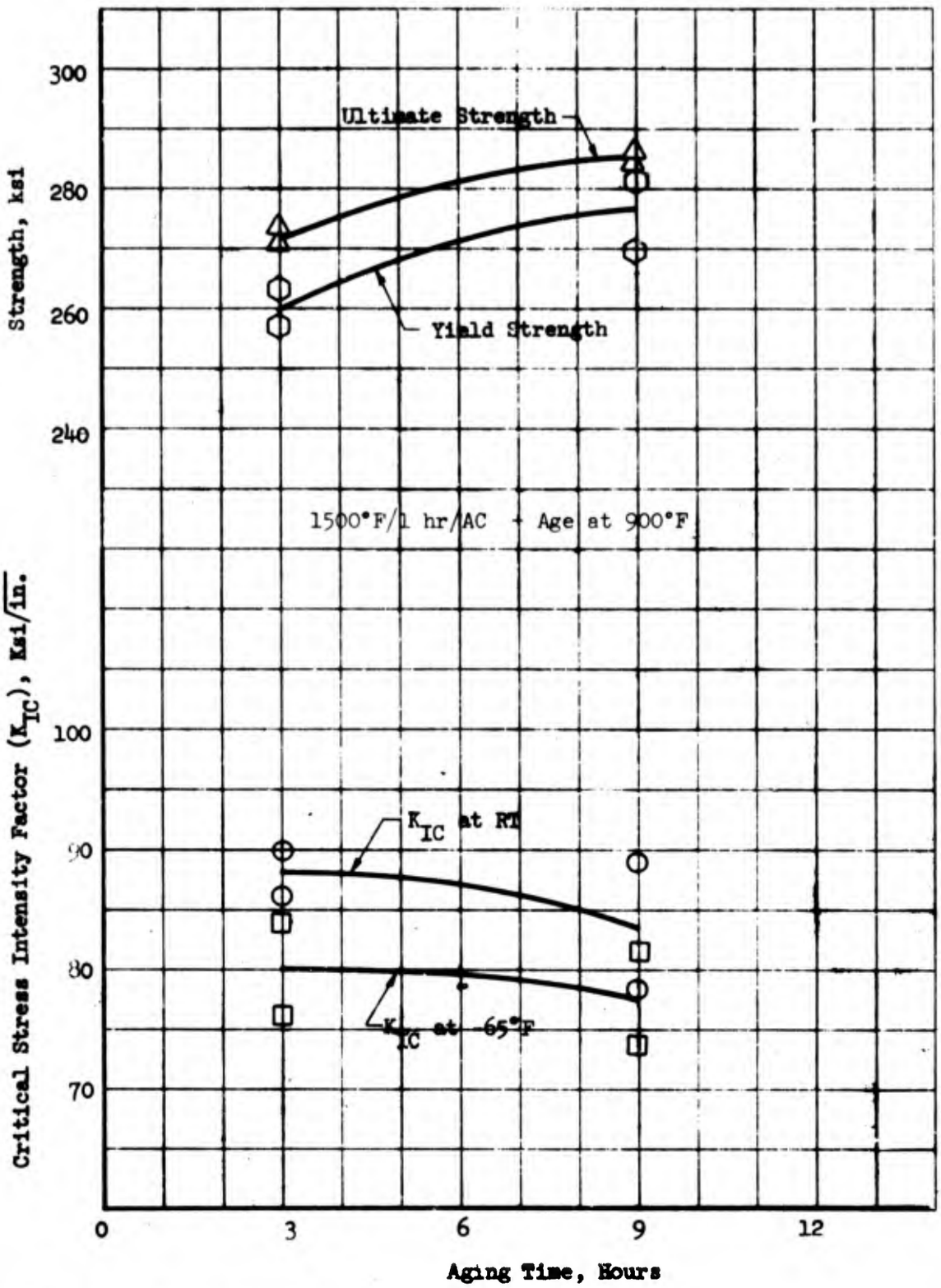

Figure 21. Effect of 900° F Aging Treatment on Strength and Toughness of Maraging 250, Heat No. 24676

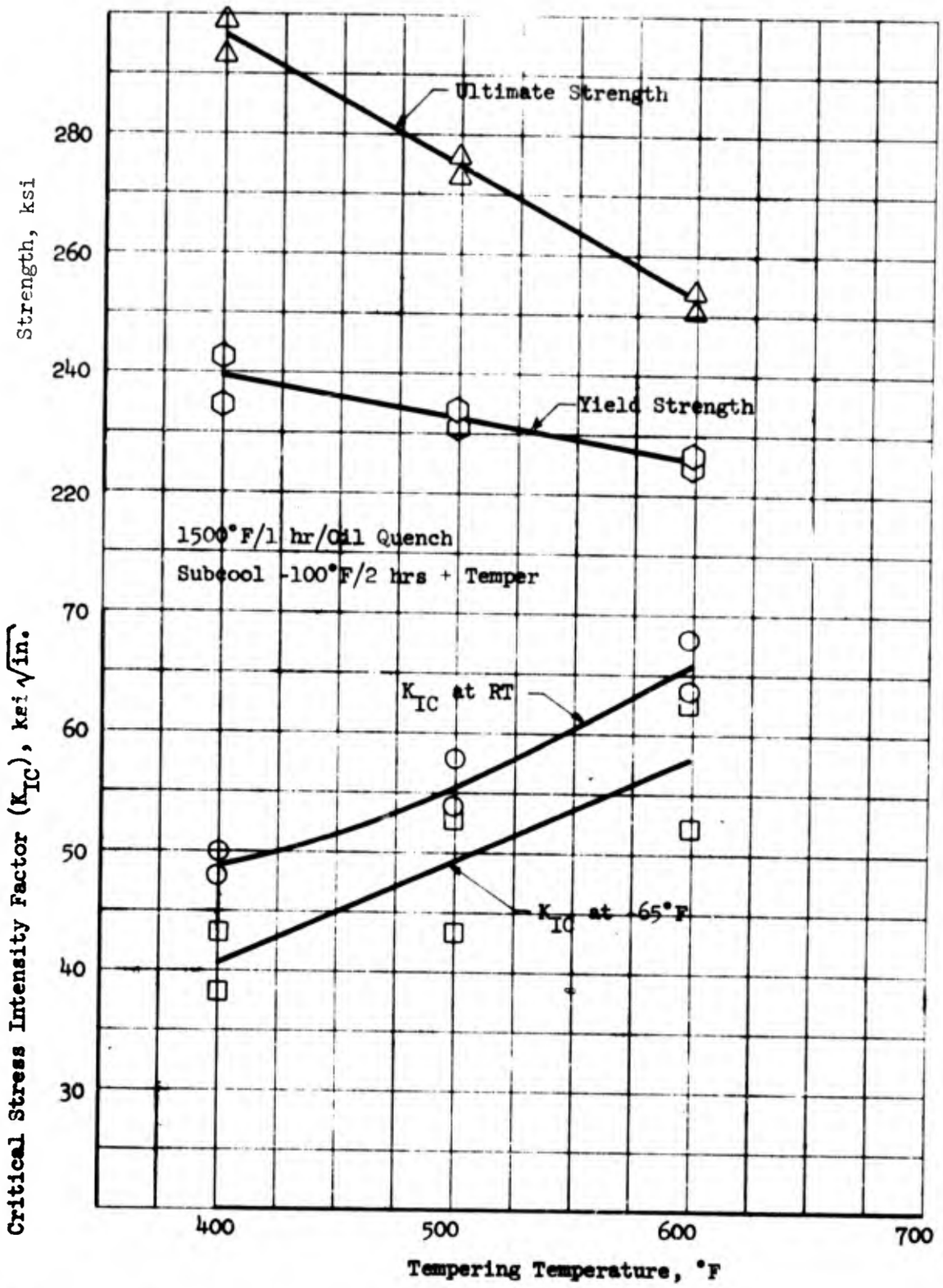

Figure 22. Effect of Tempering Temperature on Strength and Toughness of 9Ni-4Co-0.45C, Heat No. 3931141

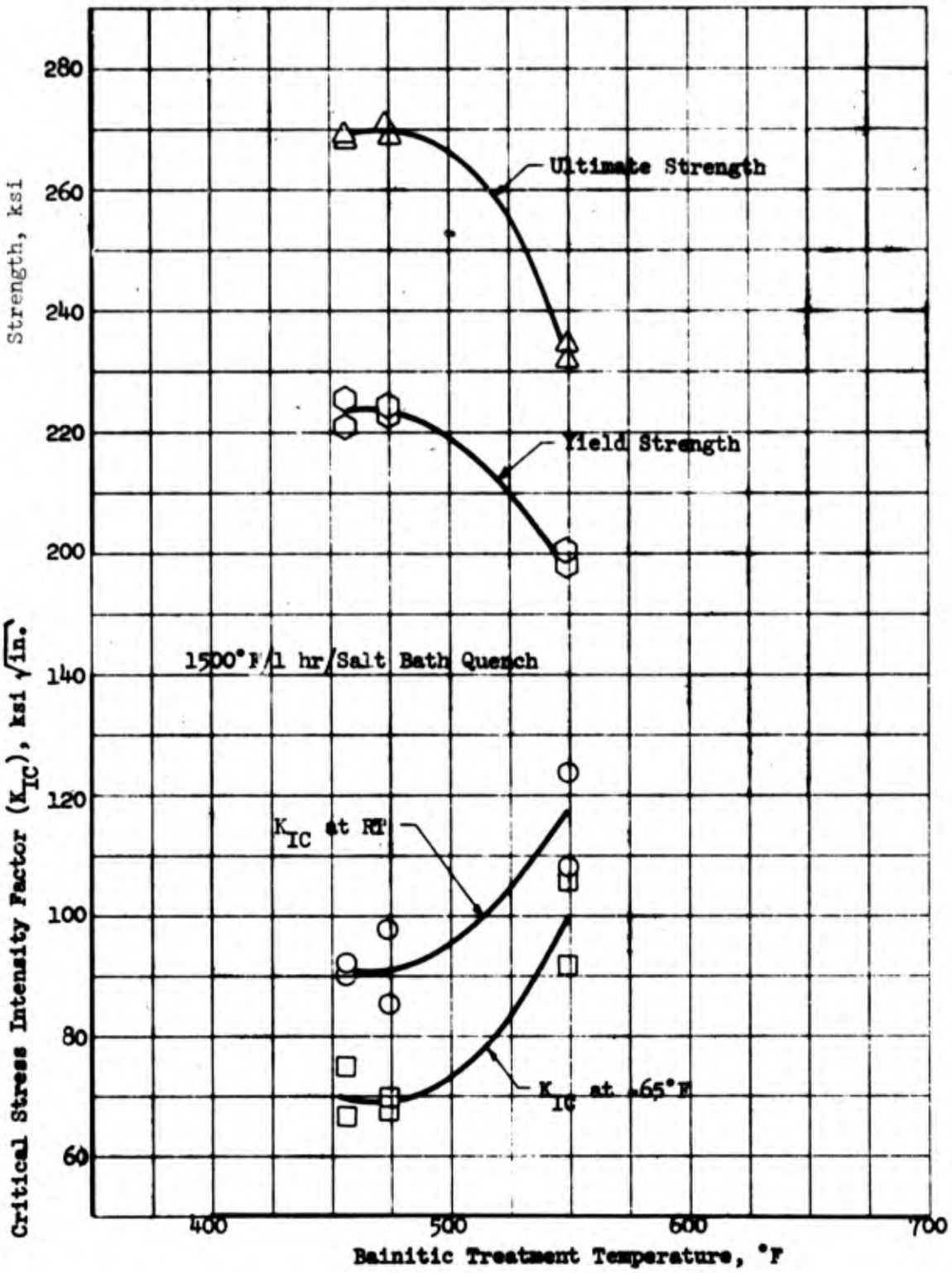

Figure 23. Effect of Bainitic Treatment Temperature on Strength and Toughness of 9Ni-4Co-0.45C, Heat No. 3931141

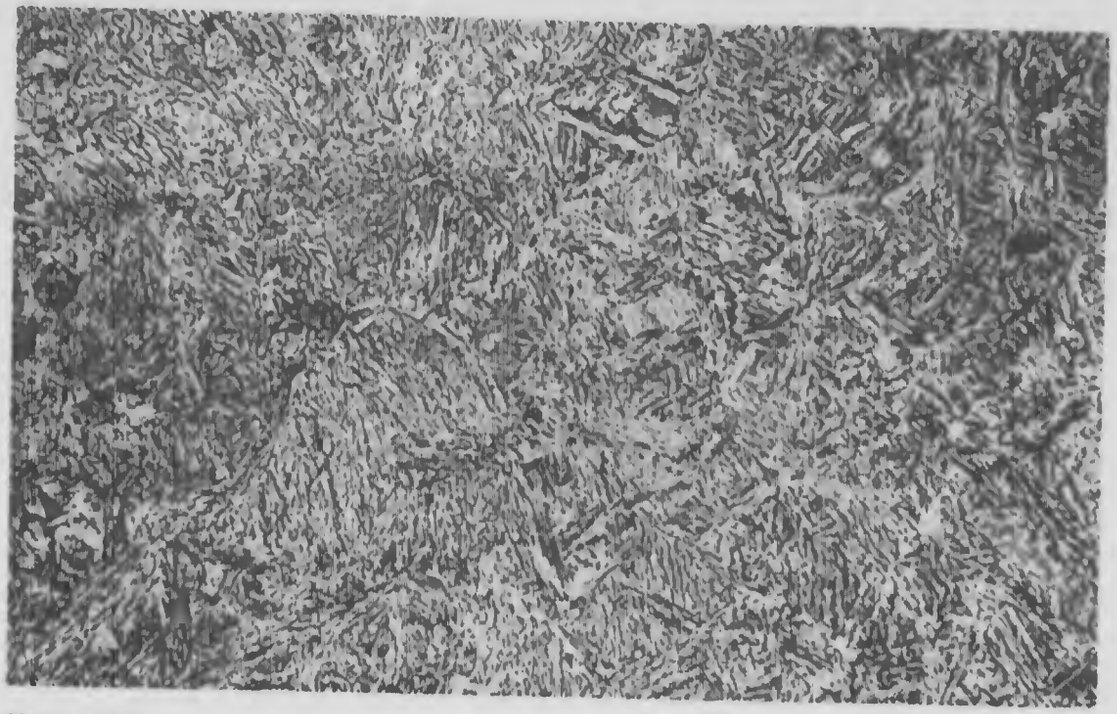

Mag: 500X

Nital Etch

Mag: 15,400X

Bioden Replica

Figure 24. Micrographs of 4330 V-Modified double-tempered at 500°F (see Table V)

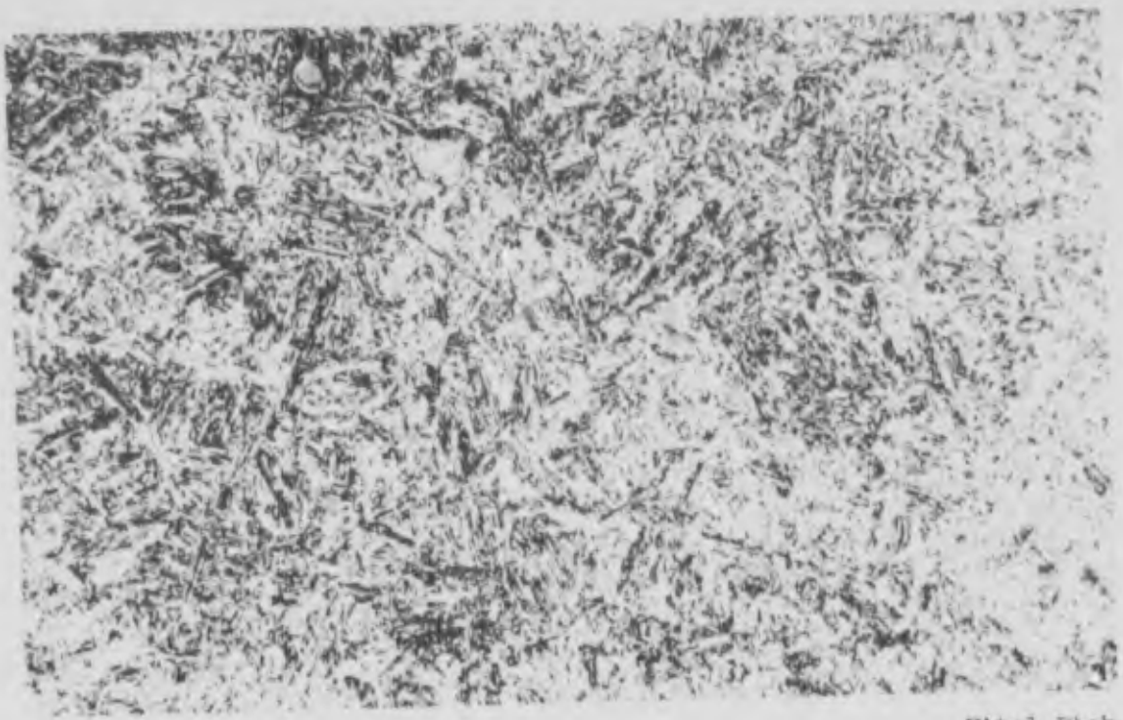

Nital Etch

Mag: 500X

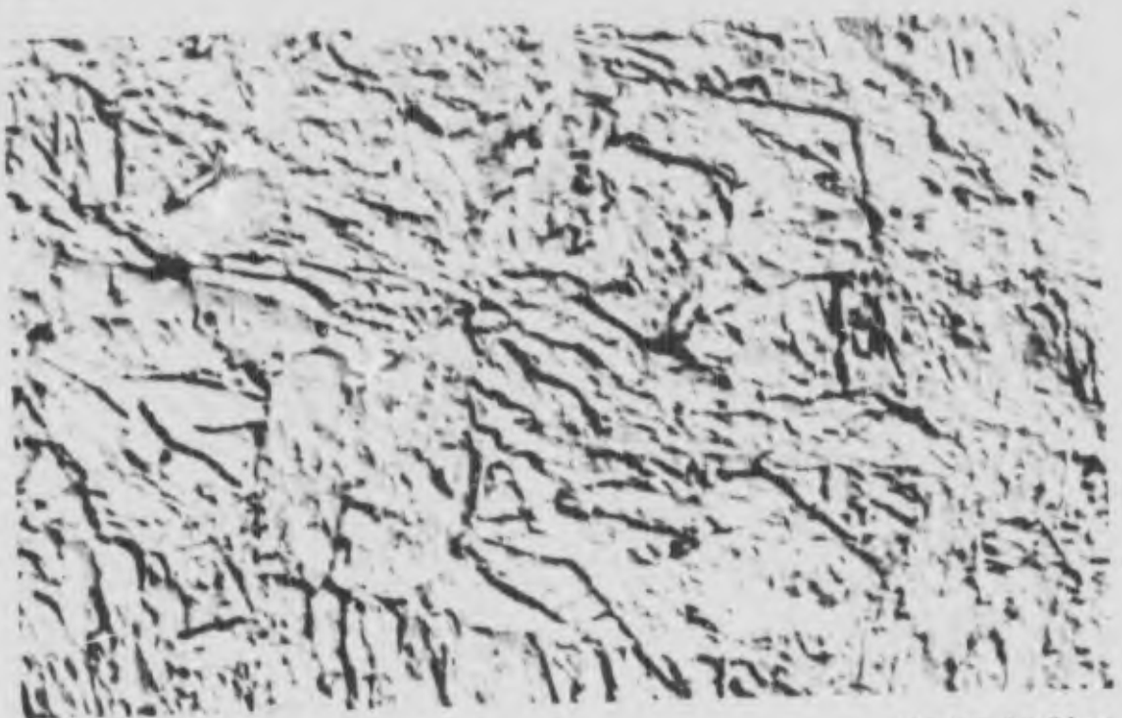

Bioden Replica

Mag: 15,400X

Figure 25. Micrographs of 4330 V-Modified double-tempered at 600°F (see Table V)

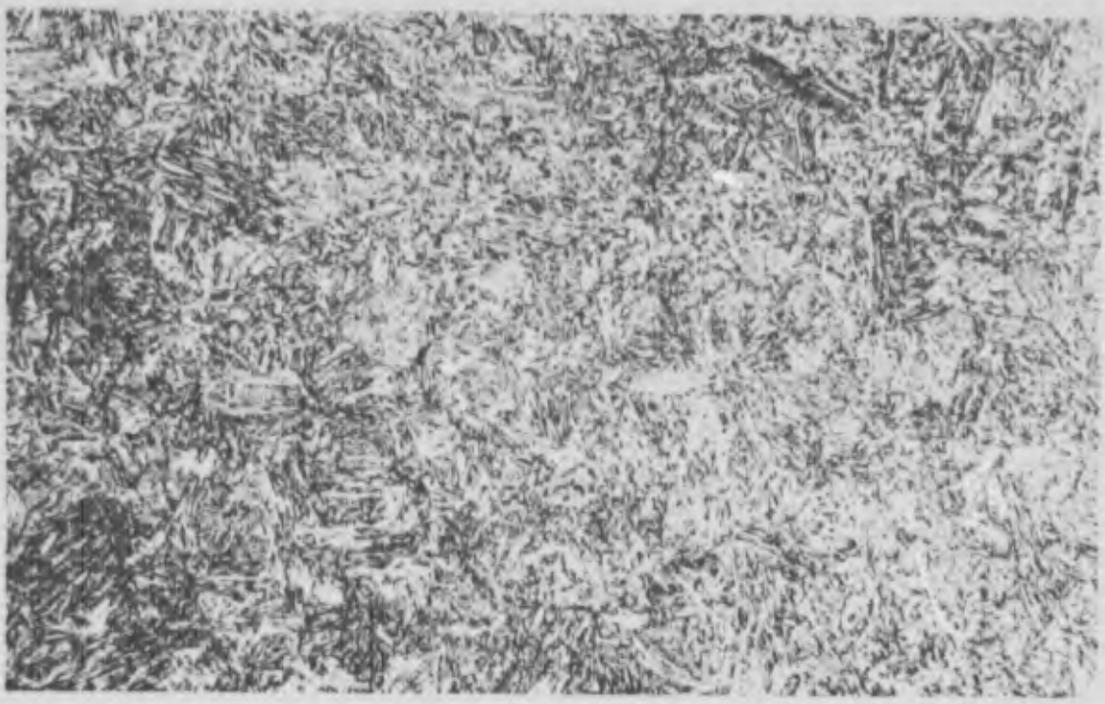

Mag: 500X Nital Etch

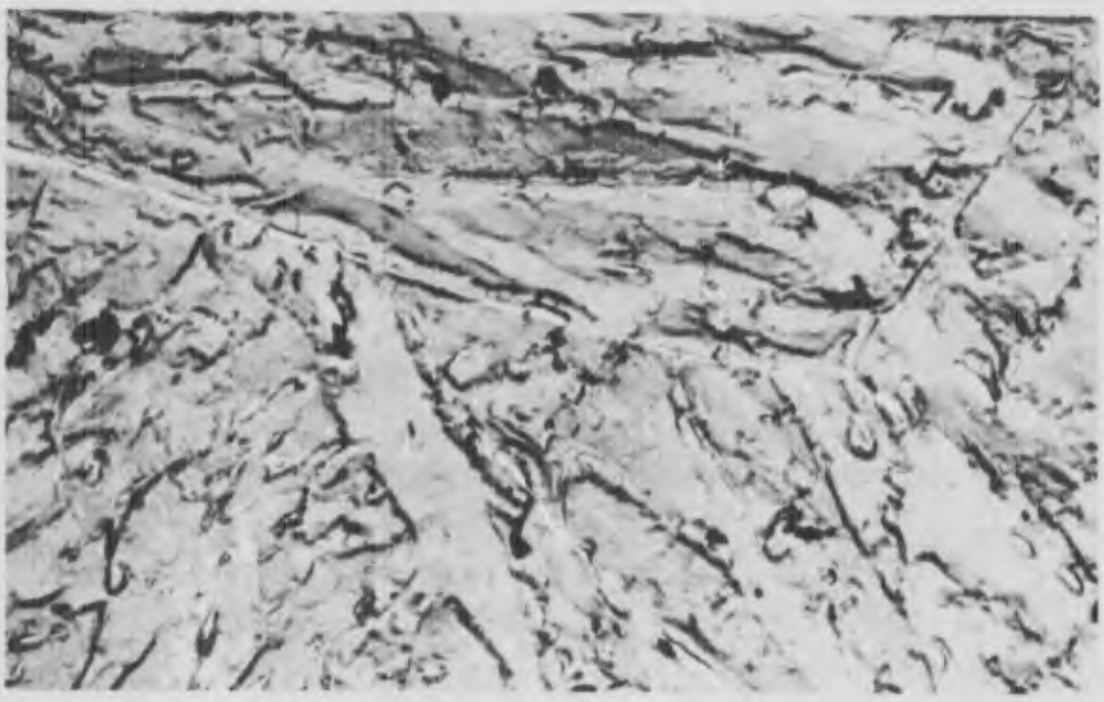

Mag: 15,400X Bioden Replica

Figure 26. Micrographs of 4330 V-Modified double-tempered at 700°F (see Table V)

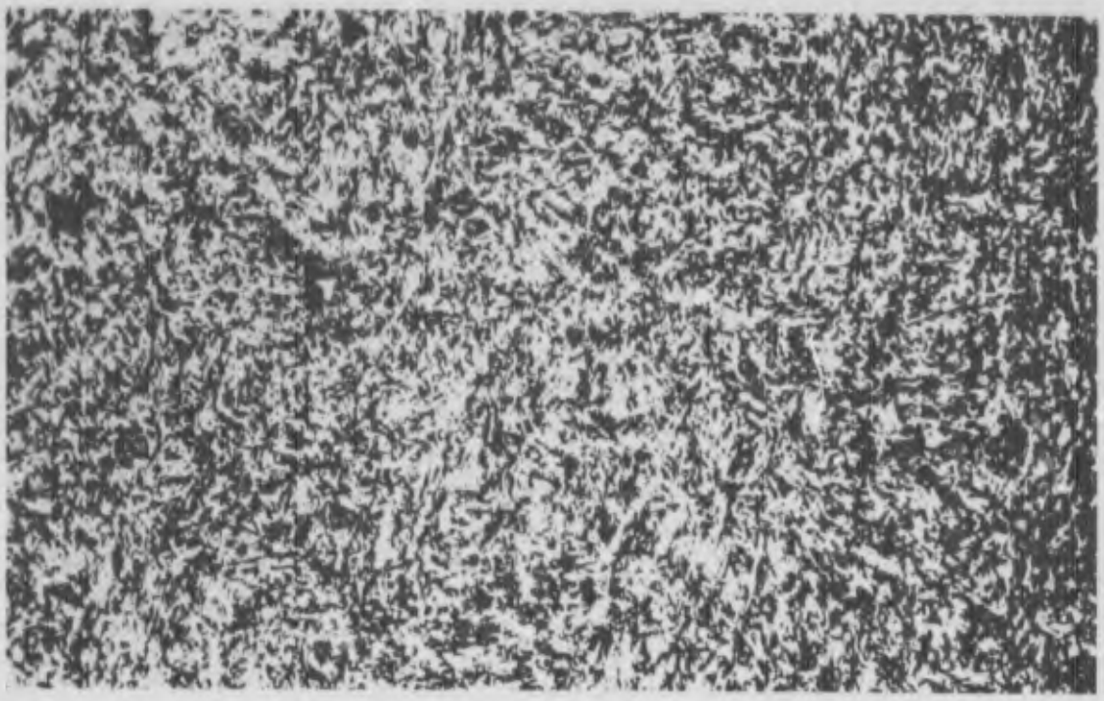

Mag: 500X Vilella's Etch

Mag: 15,400X Bioden Replica

Figure 27. Micrographs of H-11 Modified triple-tempered at 1,025° F (see Table V)

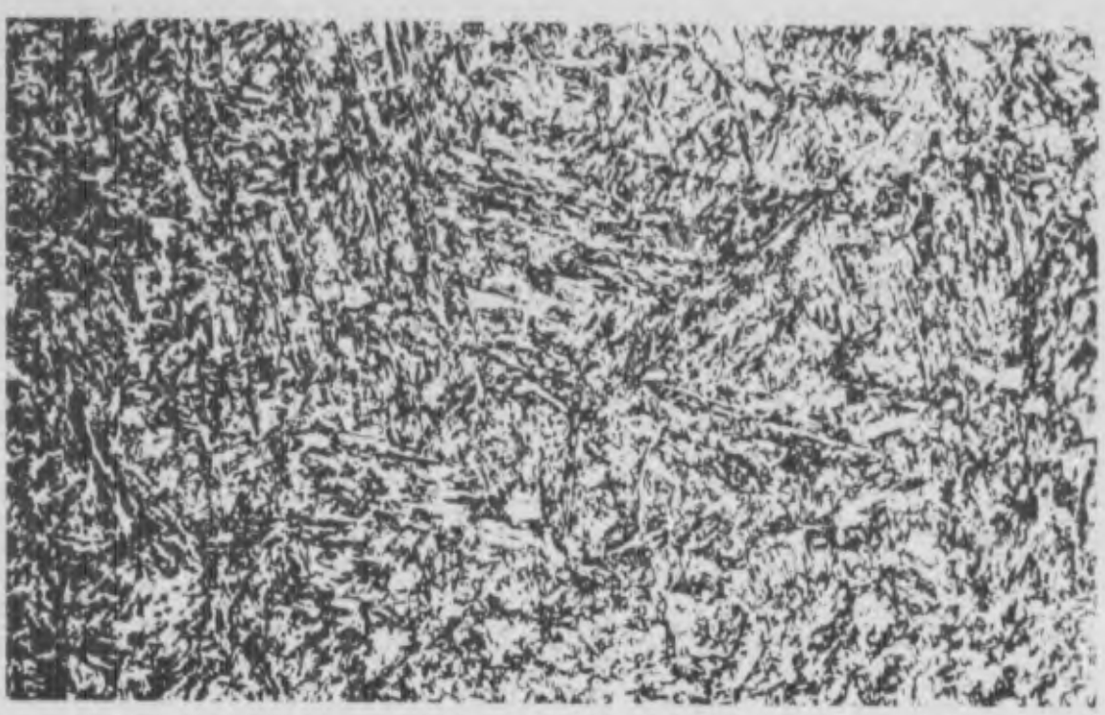

Mag: 500X Vilella's Etch

Mag: 15,400X Bioden Replica

Figure 28. Micrographs of H-11 Modified triple-tempered at 1,075°F (see Table V)

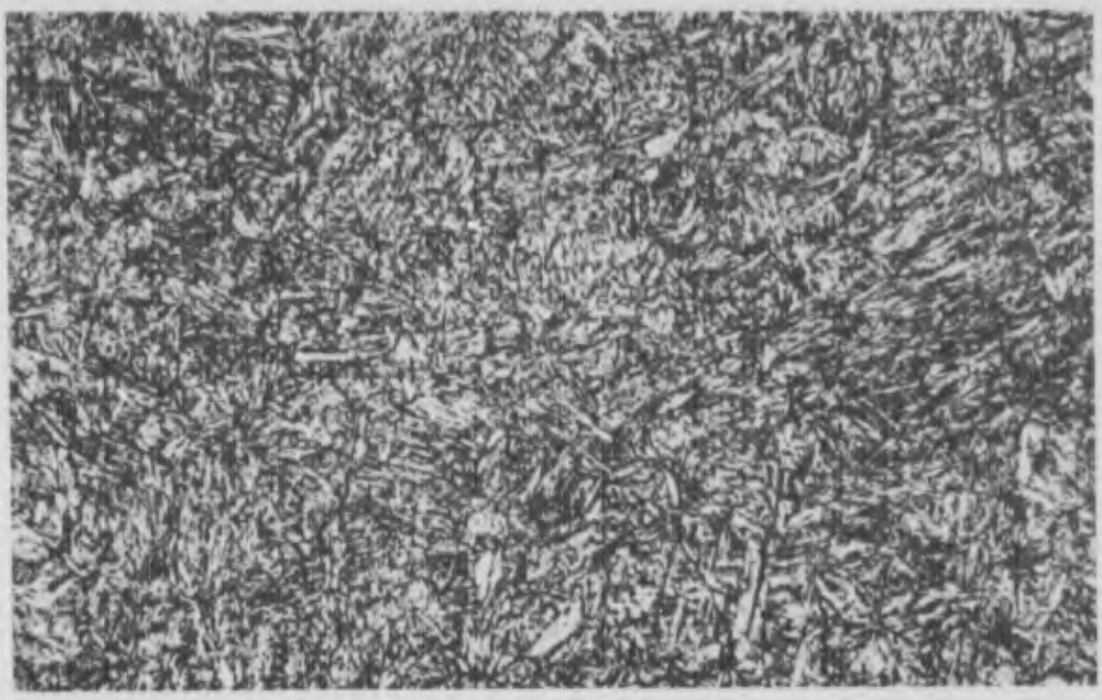

Mag: 500X Vilella's Etch

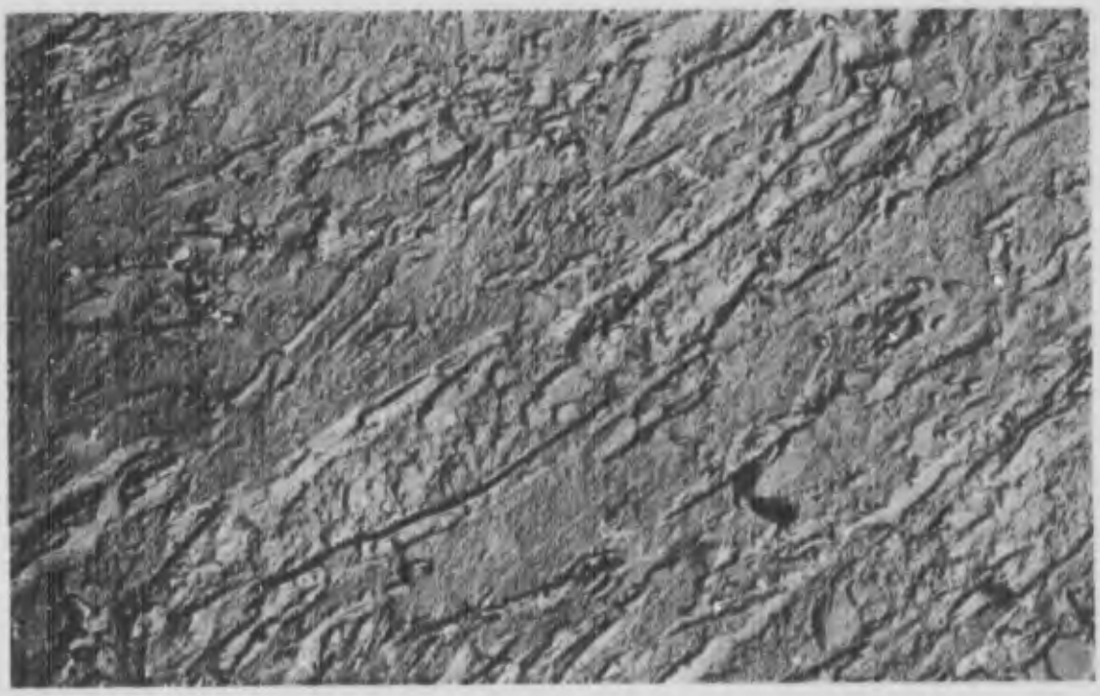

Mag: 15,400X Bioden Replica

Figure 29. Micrographs of H-11 Modified triple-tempered at 1,100°F (see Table V)

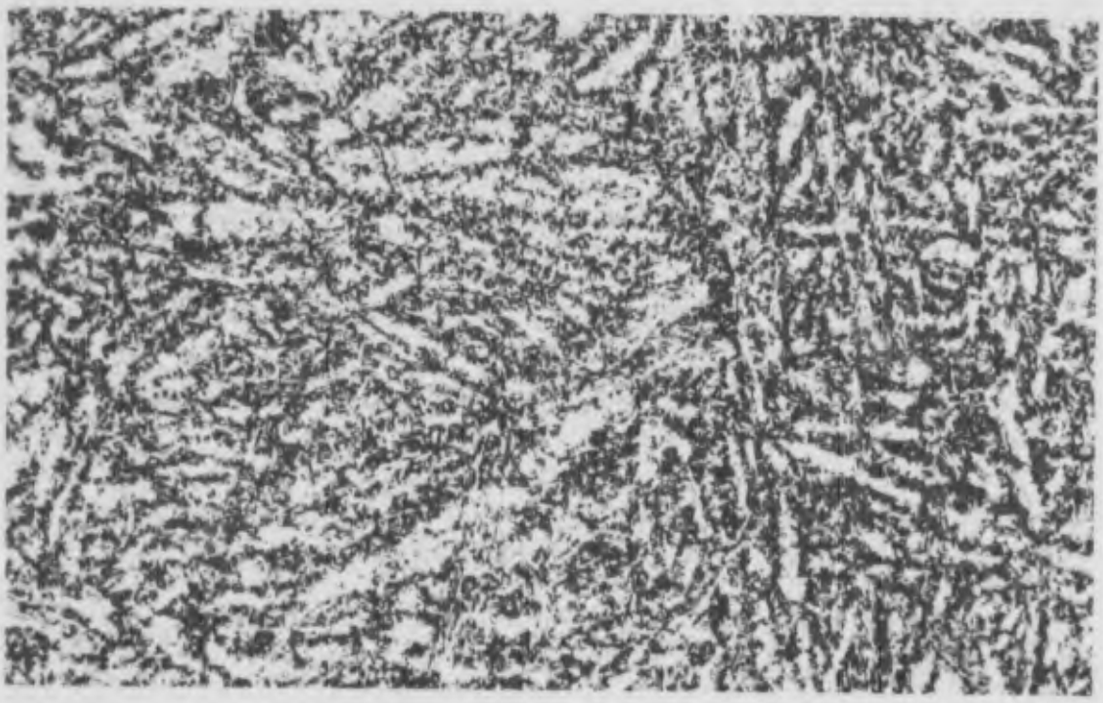

Mag: 500X Vilella's Etch

Mag: 15,400X Bioden Replica

Figure 30. Micrographs of H-11 Modified triple-tempered at 1,175°F (see Table V)

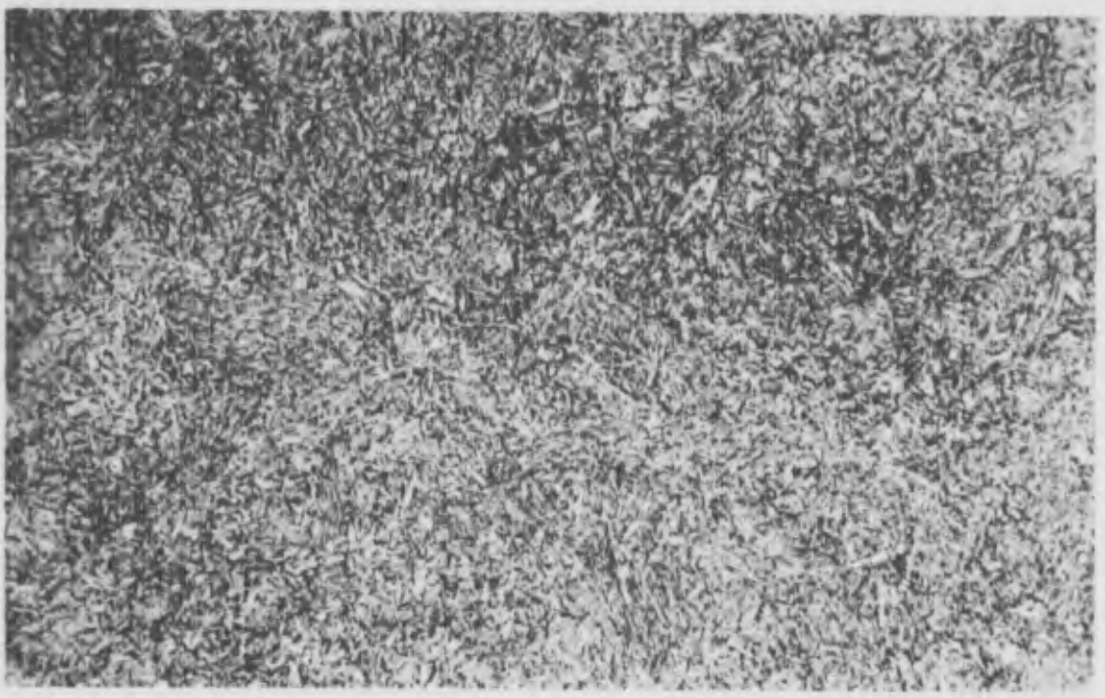

Mag: 500X Nital Etch

Mag: 15,400X Bioden Replica

Figure 31. Micrographs of 9Ni-4Co-0.30C (Cr-Mo) double-tempered at 800°F (see Table V)

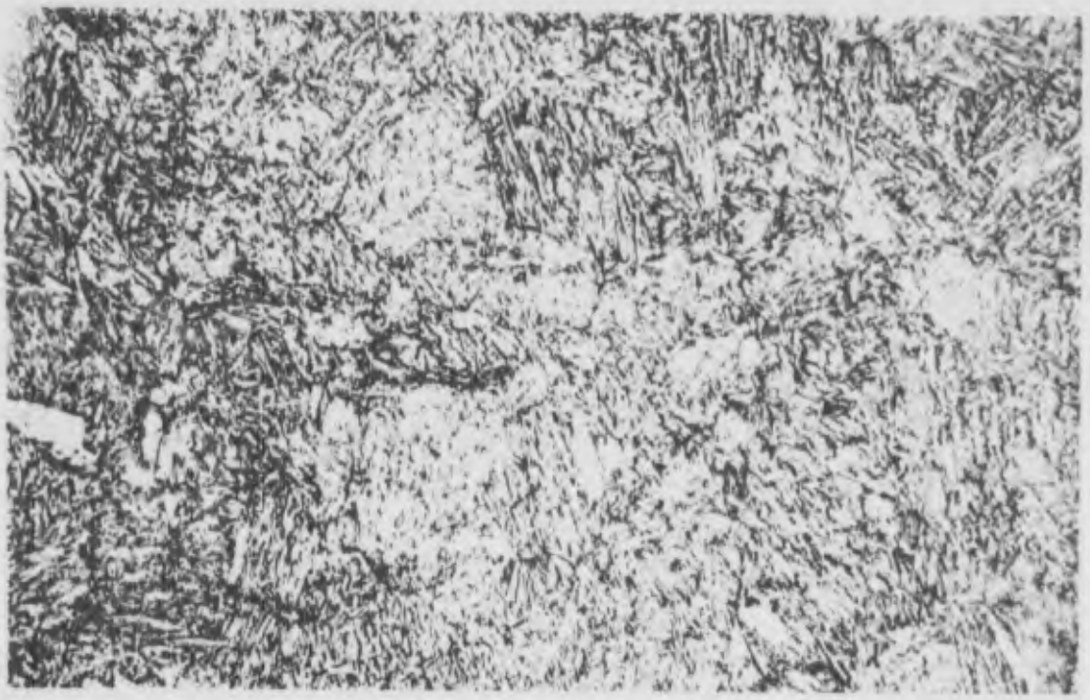

Mag: 500X Nital Etch

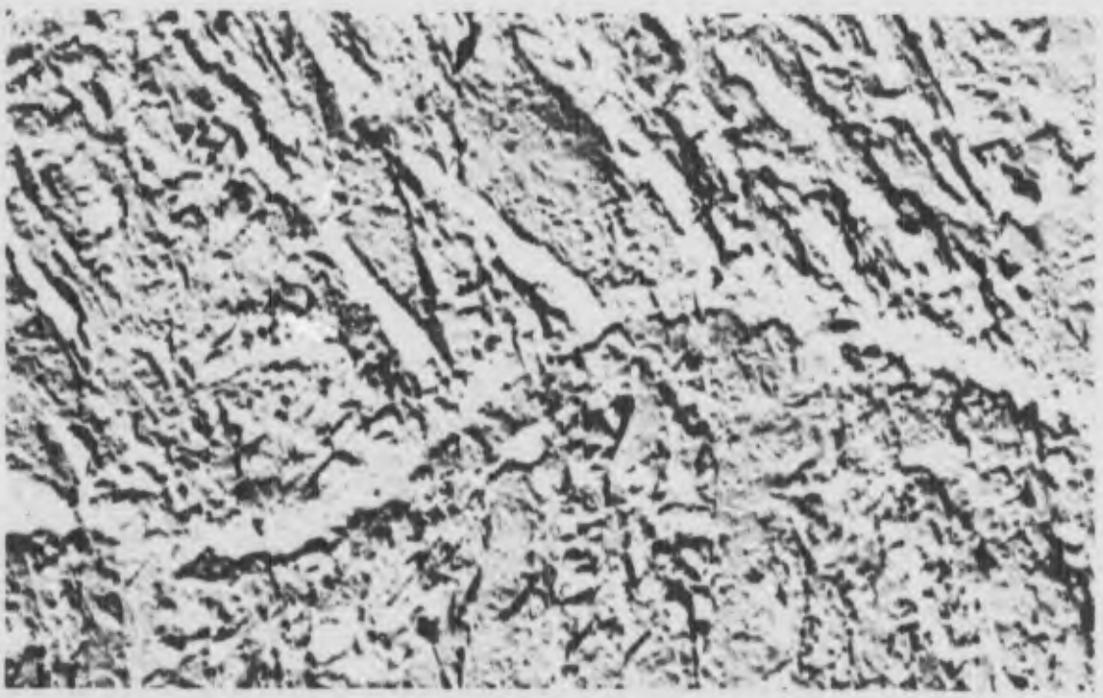

Mag: 15,400X Bioden Replica

Figure 32. Micrographs of 9Ni-4Co-0.30C double-tempered at 950°F (see Table V)

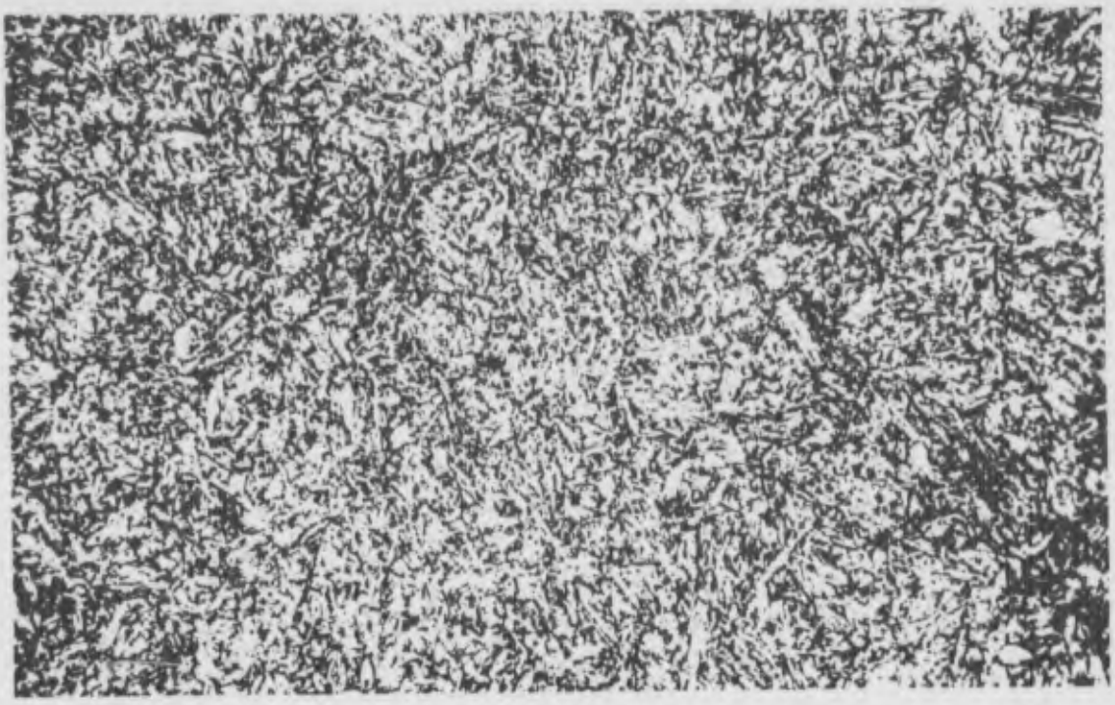

Mag: 500X

Nital Etch

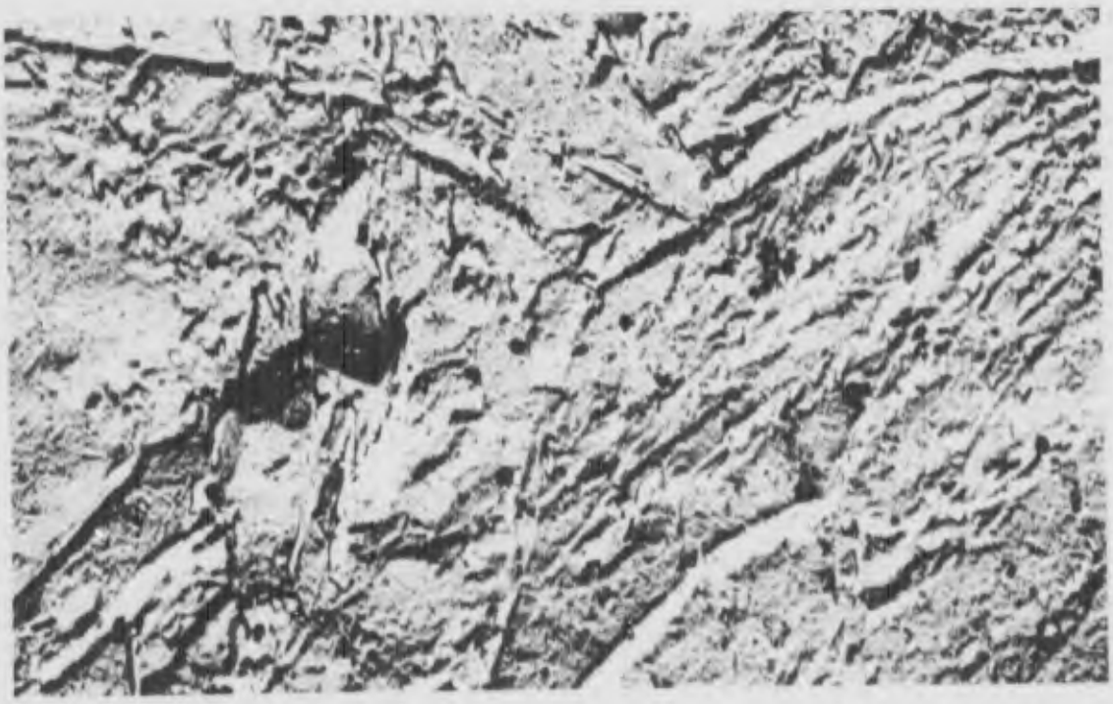

Mag: 15,400X

Bioden Replica

Figure 33. Micrographs of 9Ni-4Co-0.030C double-tempered at 1,050°F (see Table V)

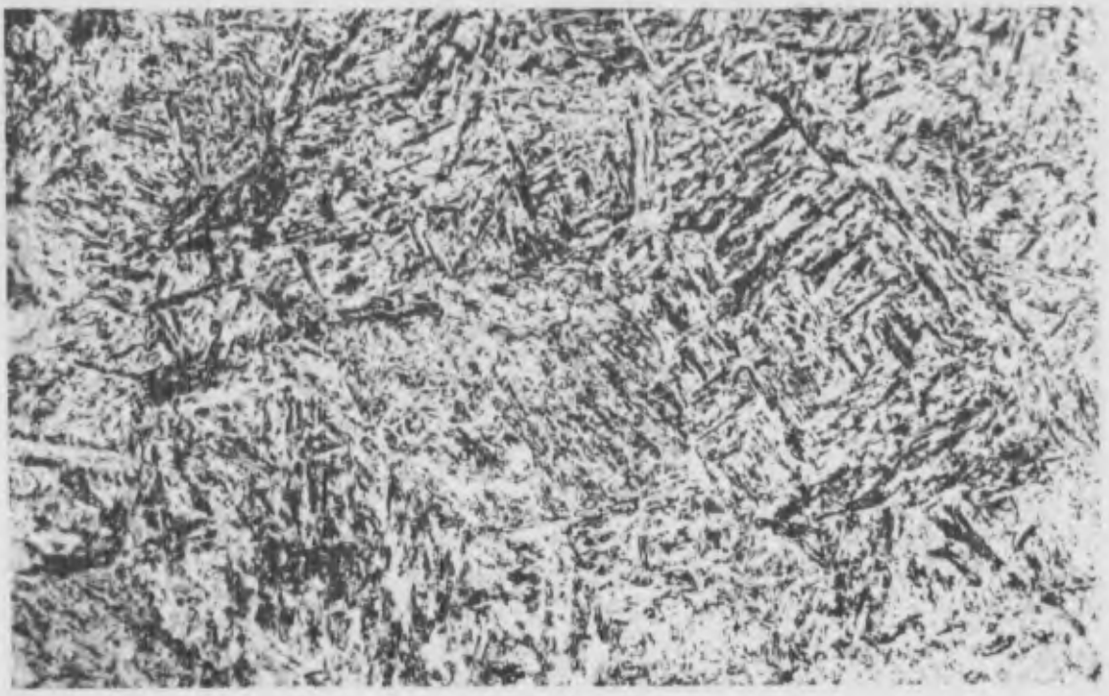

Mag: 500X Nital Etch

Mag: 15,400X Bioden Replica

Figure 34. Micrographs of 300M double-tempered at 400°F (see Table V)

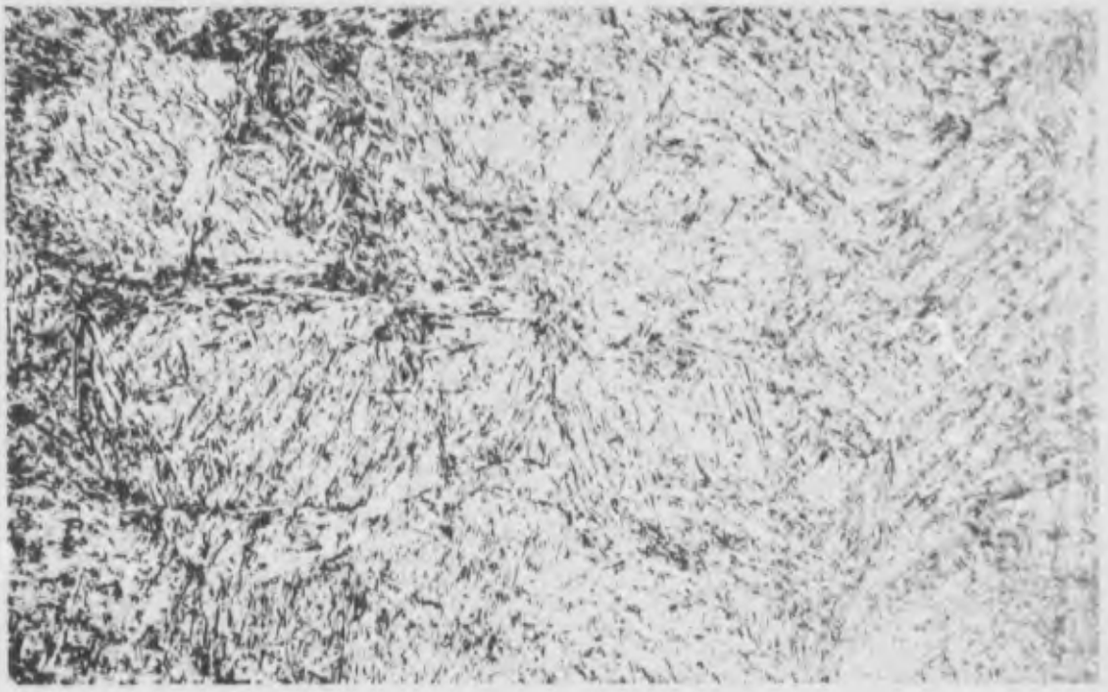

Mag: 500X Nital Etch

Mag: 15,400X Bioden Replica

Figure 35. Micrographs of 300M double-tempered at 600° F (see Table V)

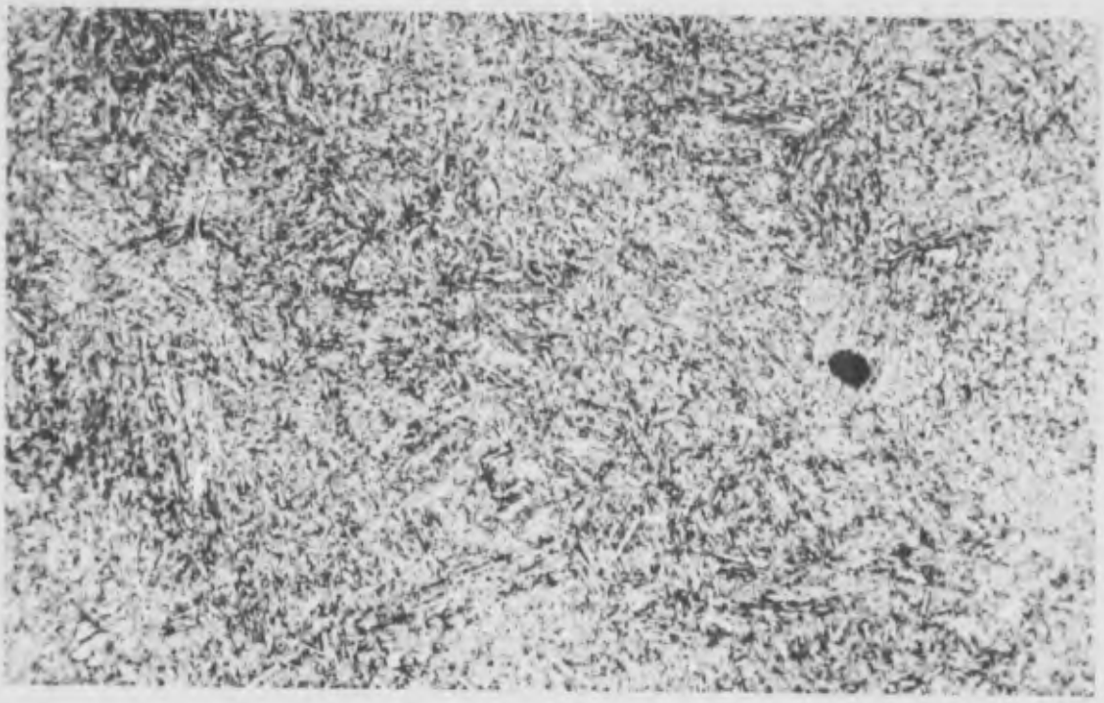

Mag: 500X

Nital Etch

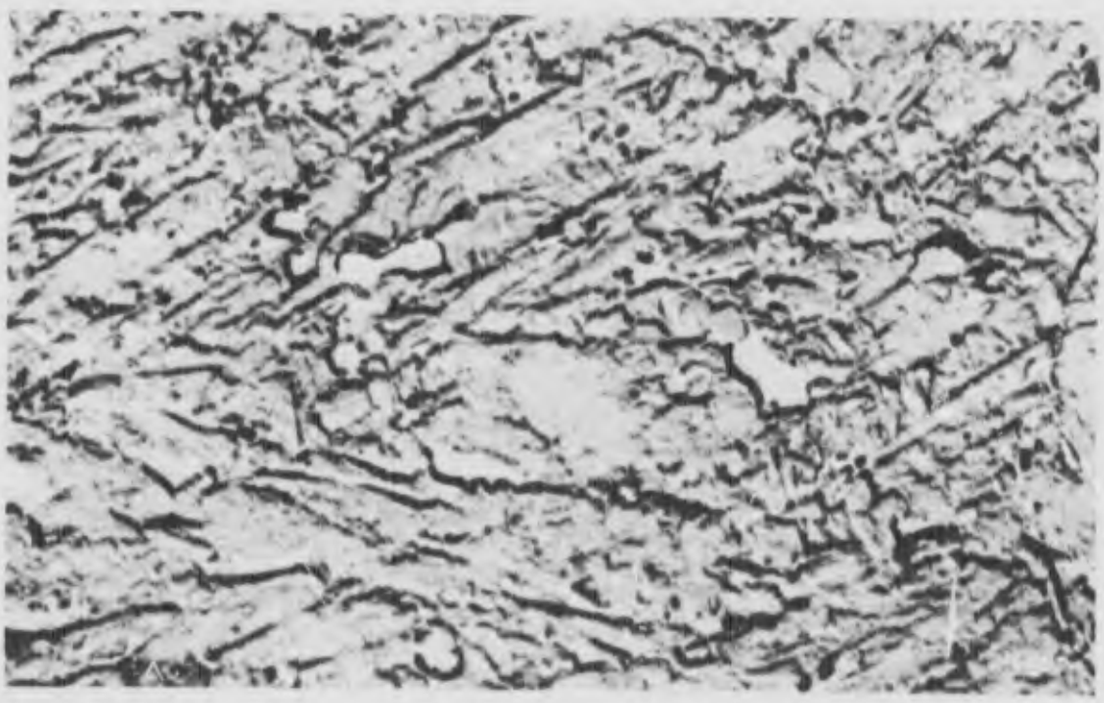

Mag: 15,400X

Bioden Replica

Figure 36. Micrographs of 300M double-tempered at 750° F (see Table V)

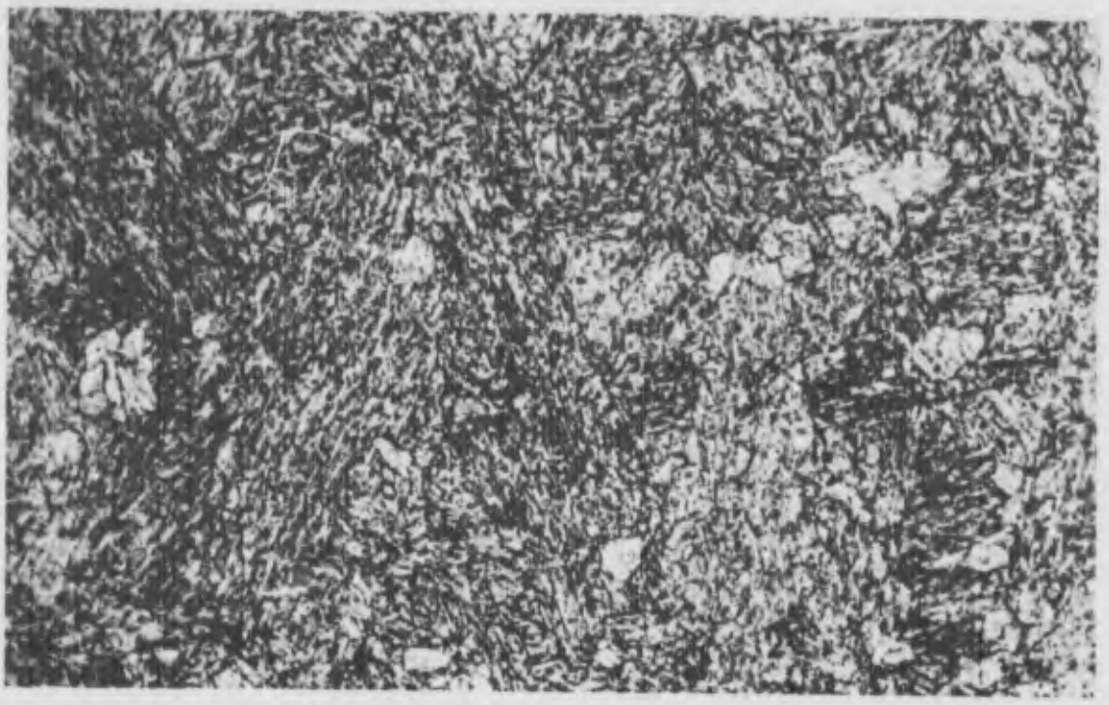

Mag: 500X

HNO_3-HF Etch

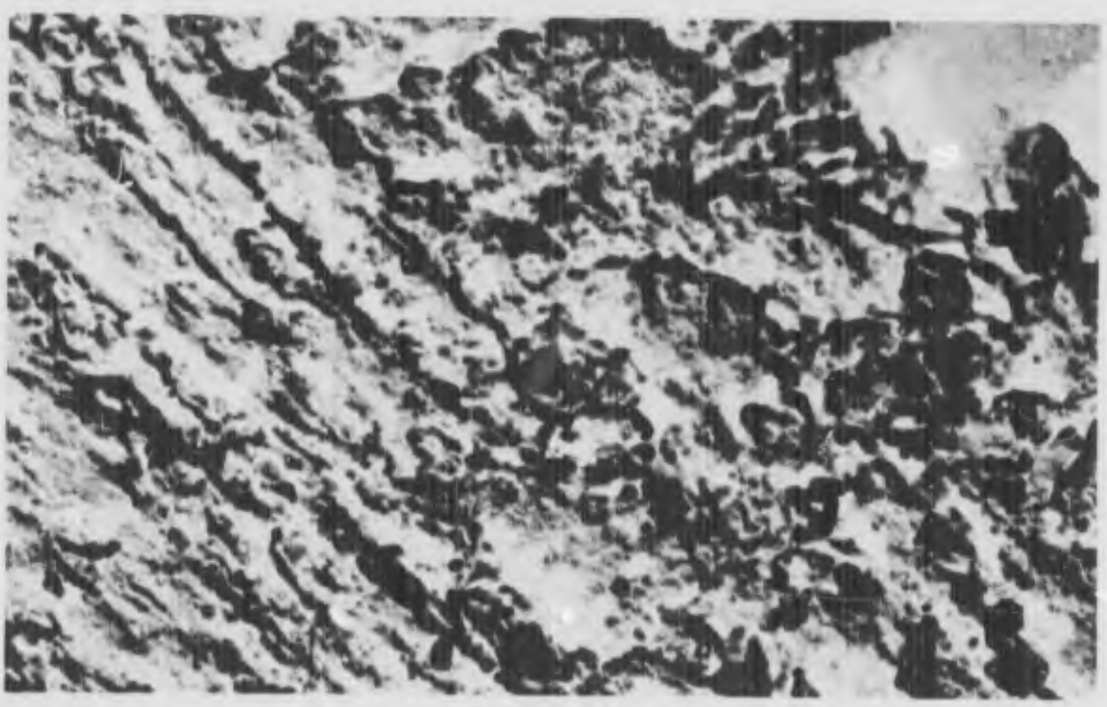

Mag: 15,400X

Bioden Replica

Figure 37. Micrographs of Maraging 250 aged 3 hours at 850° F (see Table V)

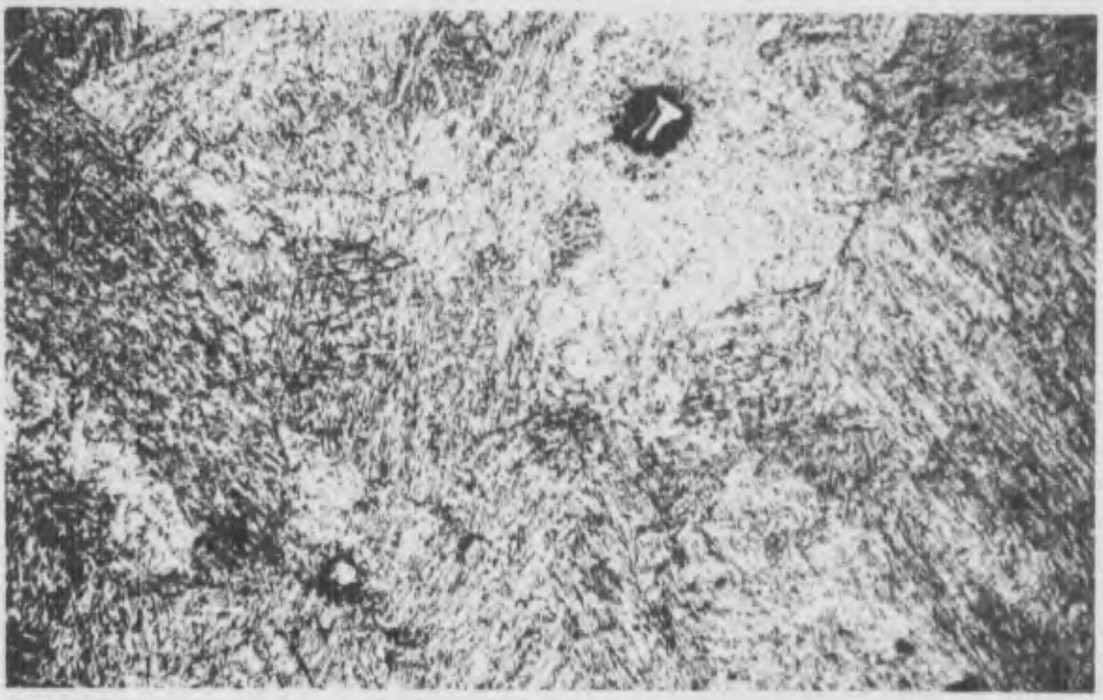

Mag: 500X HNO_3-HF Etch

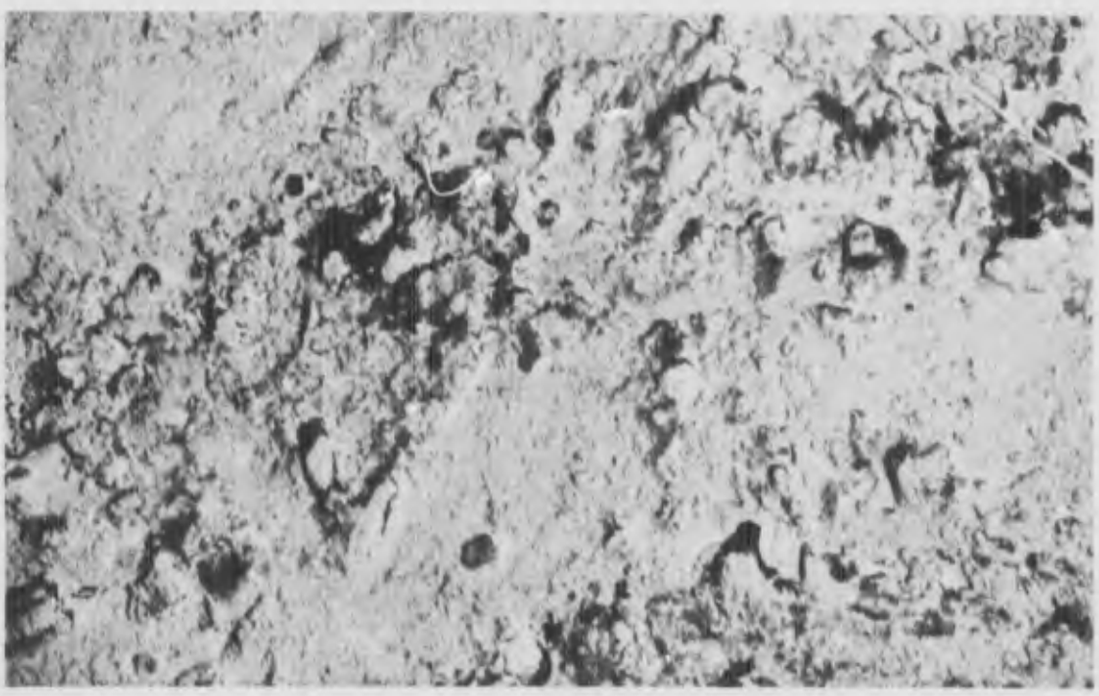

Mag: 15,400X Bioden Replica

Figure 38. Micrographs of Maraging 250 aged 3 hours at 900°F (see Table V)

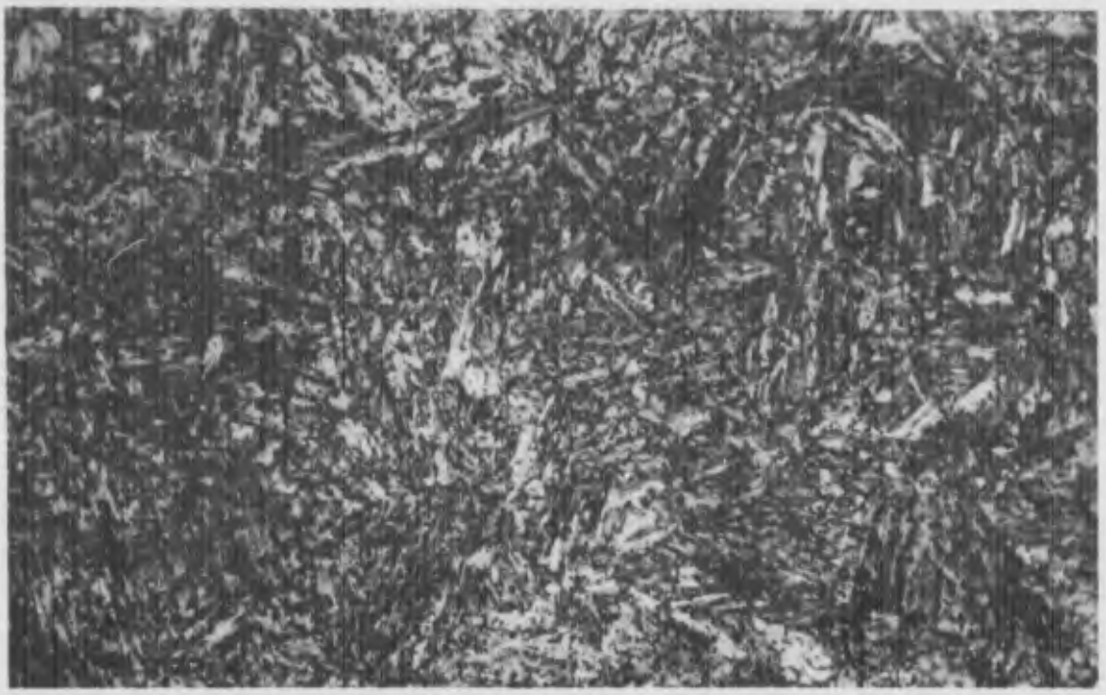

Mag: 500X HNO_3-HF Etch

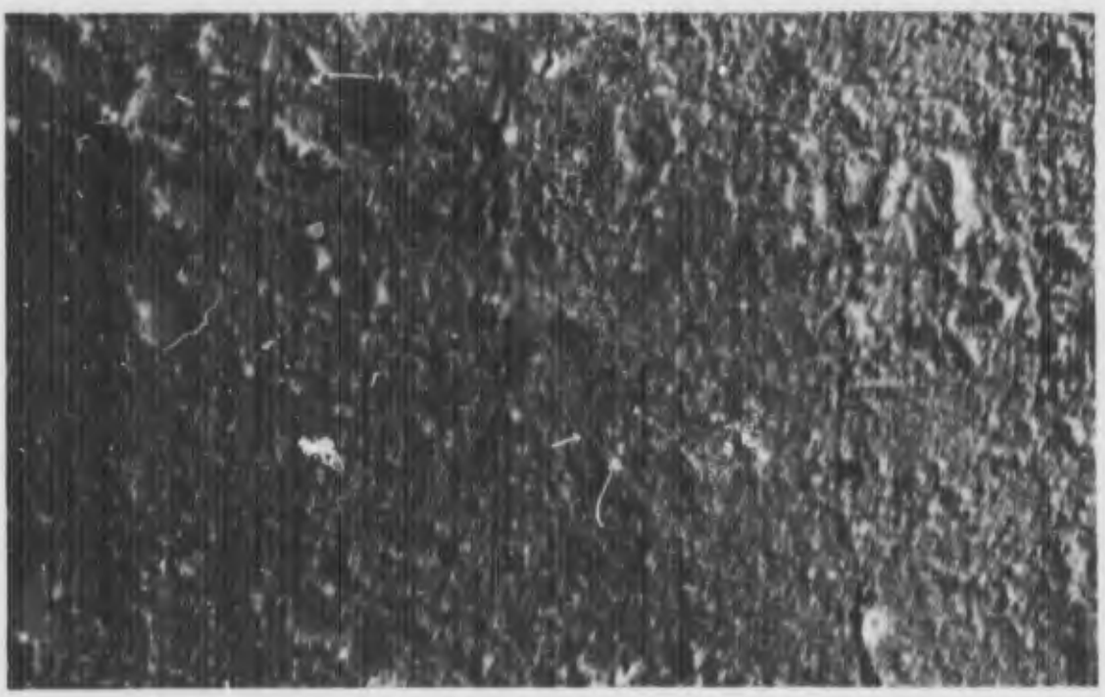

Mag: 15,400X Bioden Replica

Figure 39. Micrographs of Maraging 250 aged 3 hours at 950° F (see Table V)

Mag: 500X

HNO_3-HF Etch

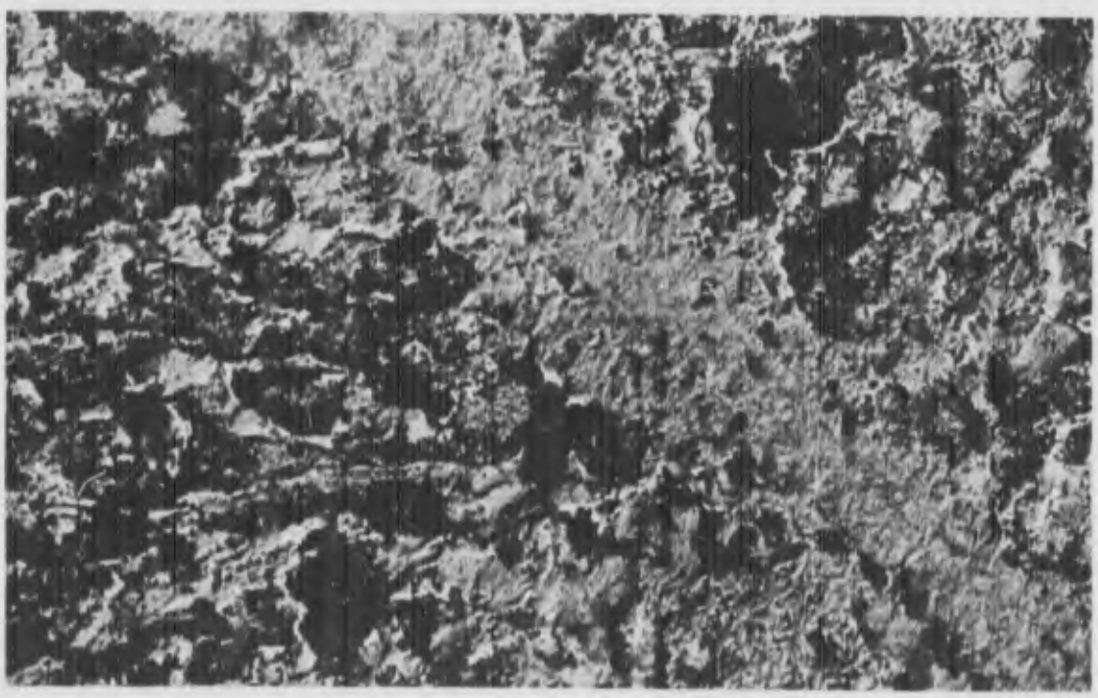

Mag: 15,400X

Bioden Replica

Figure 40. Micrographs of Maraging 250 aged 9 hours at 900°F (see Table V)

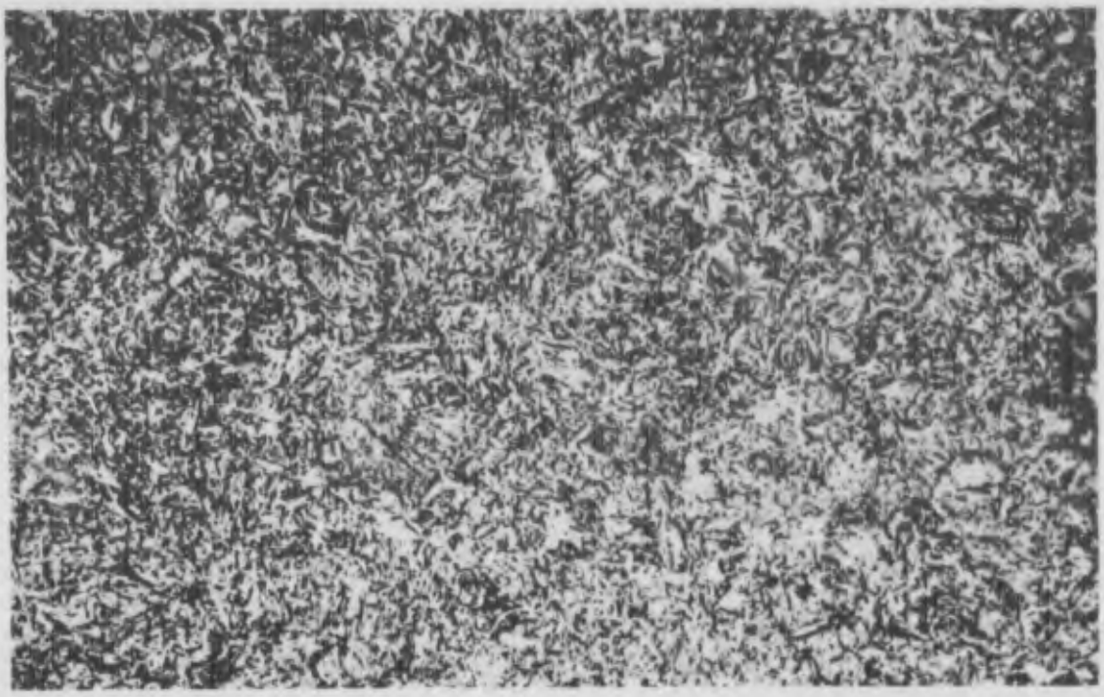

Mag: 500X Nital Etch

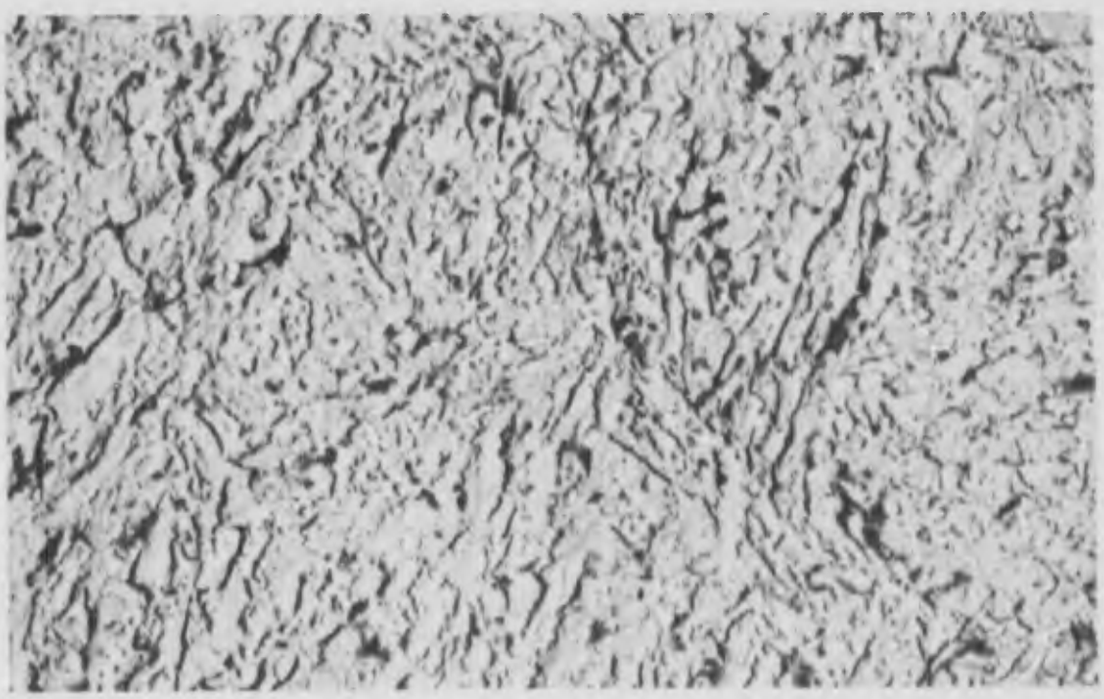

Mag: 15,400X Bioden Replica

Figure 41. Micrographs of 9Ni-4Co-0.45C double-tempered at 400° F (see Table V)

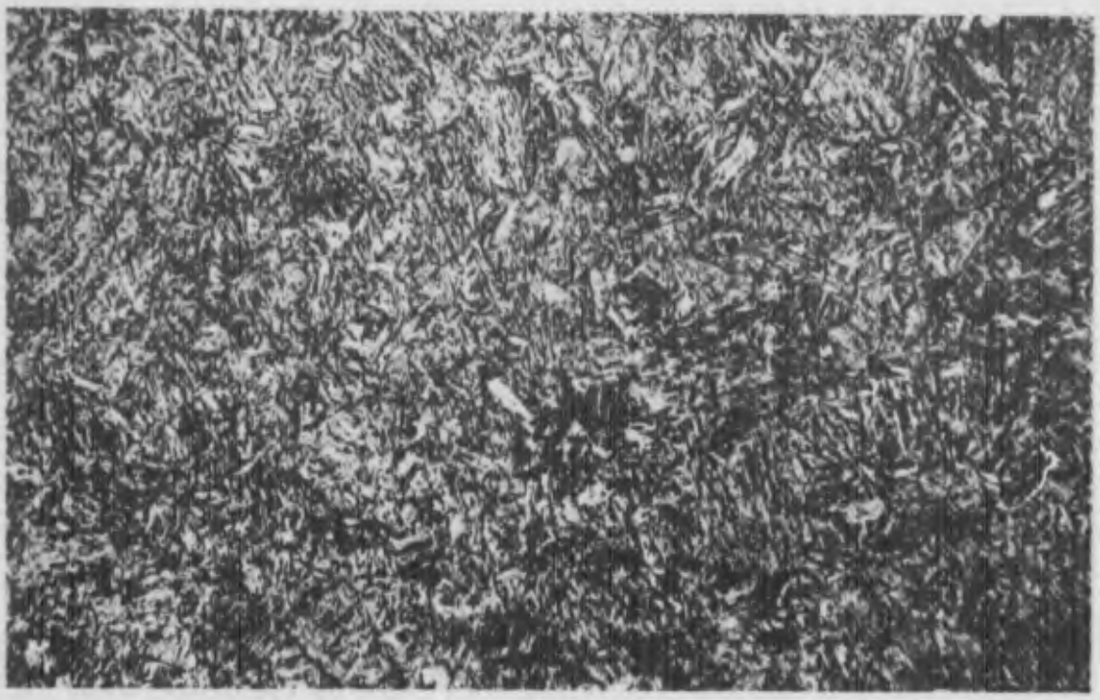

Mag: 500X Nital Etch

Mag: 15,400X Bioden Replica

Figure 42. Micrographs of 9Ni-4Co-0.45C double-tempered at 500°F (see Table V)

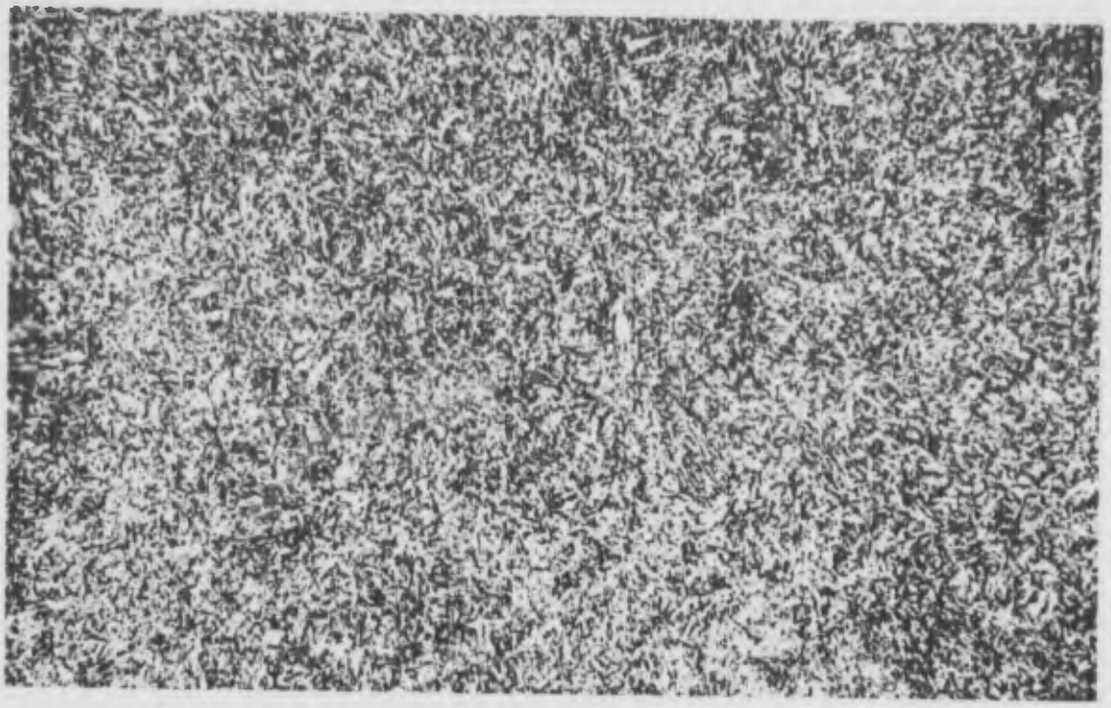

Mag: 500X

Nital Etch

Mag: 15,400X

Bioden Replica

Figure 43. Micrographs of 9Ni-4Co-0.45C double-tempered at 600°F (see Table V)

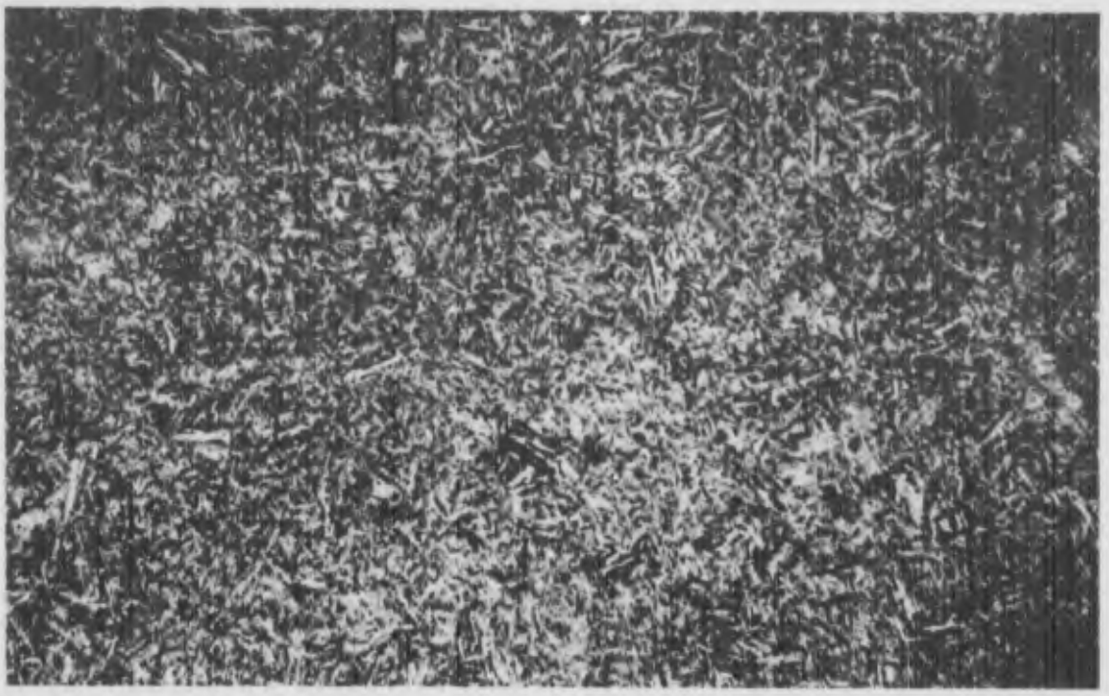

Mag: 500X Nital Etch

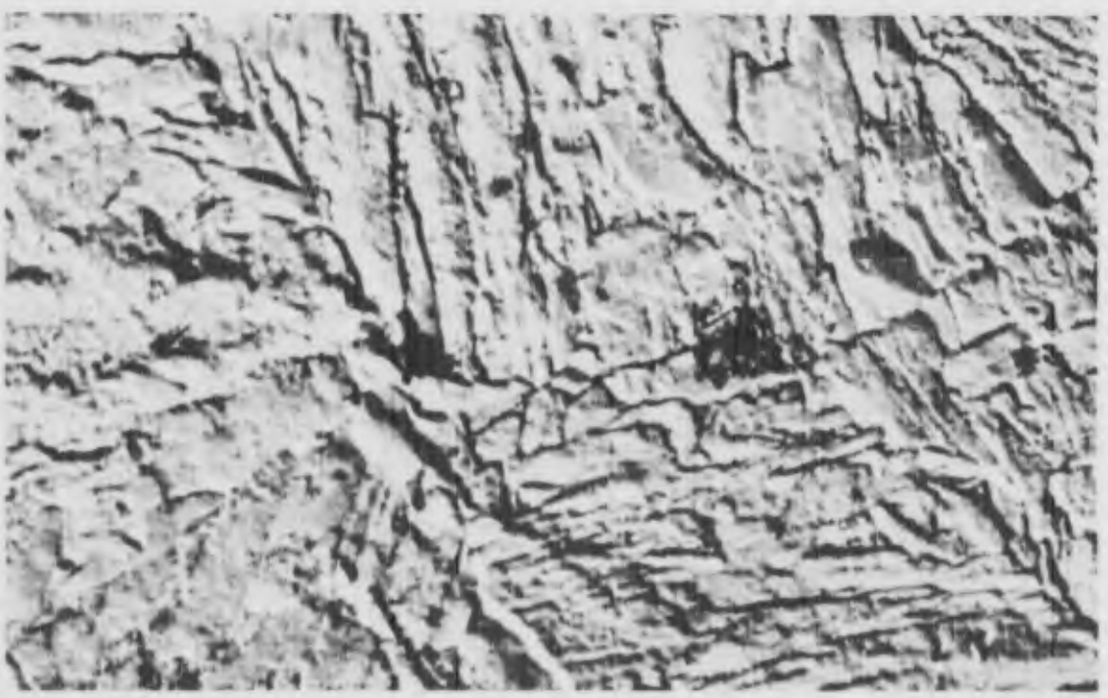

Mag: 15,400X Bioden Replica

Figure 44. Micrographs of 9Ni-4Co-0.45C bainitically quenched at 475° F (see Table V)

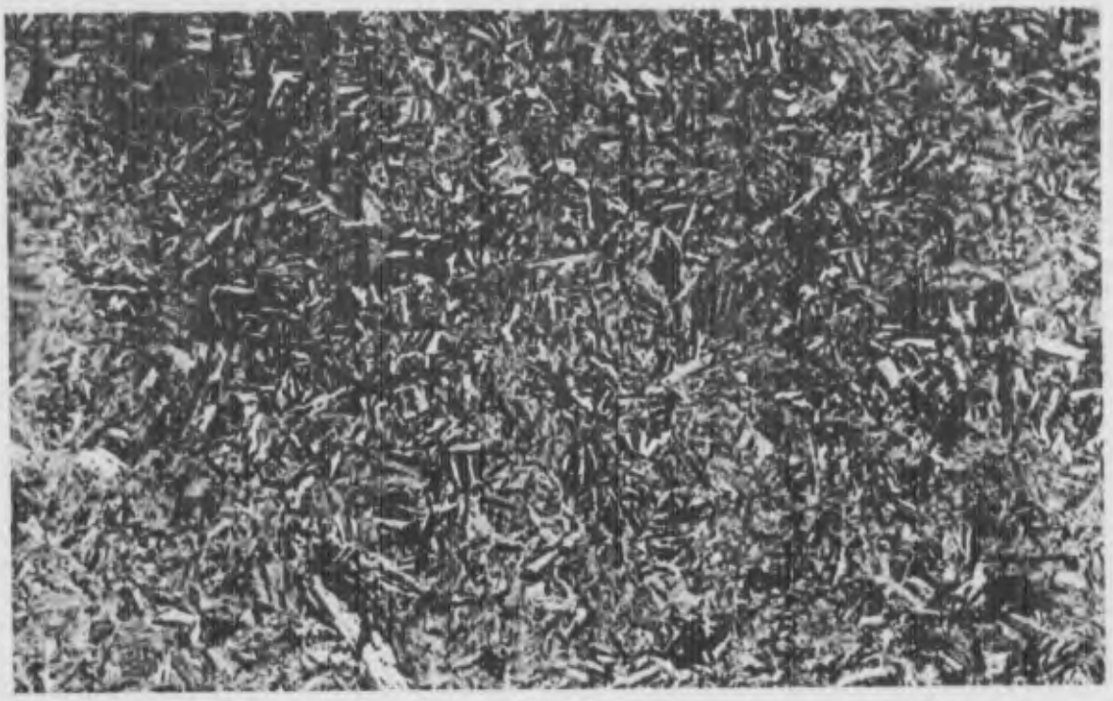

Mag: 500X Nital Etch

Mag: 15,400X Bioden Replica

Figure 45. Micrographs of 9Ni-4Co-0.45C bainitically quenched at 550° F (see Table V)

Table V ***Experimental Heat Treatments***

Alloy	Code	Heat Treatment
4330 V-Modified (Quench-Temper)	A	Normalize: 1675°F/1 hr/AC Preheat: 1250°F/1 hr Harden: 1575°F/1 hr/Oil Quench Tempering Treatments: 1) 400°F/3 hr/AC + 400°F/3 hr/AC 2) *500°F/3 hr/AC + 500°F/3 hr/AC 3) 600°F/3 hr/AC + 600°F/3 hr/AC 4) 700°F/3 hr/AC + 700°F/3 hr/AC
H-11 Modified (Quench-Temper)	B	Preheat: 1400°F/1 hr Harden 1850°F/3/4 hr/AC Tempering Treatments: 1) 1025°F/3 hr/AC + 1025°F/3 hr/AC + 1025°F/3 hr/AC 2) 1075°F/3 hr/AC + 1075°F/3 hr/AC + 1075°F/3 hr/AC 3)*1100°F/3 hr/AC + 1100°F/3 hr/AC + 1100°F/3 hr/AC 4) 1175°F/3 hr/AC + 1175°F/3 hr/AC + 1175°F/3 hr/AC
9Ni-4Co-0.30C (Quench-Temper)	C	Normalize: 1650°F/1 hr/AC Preheat: 1150°F/1 hr Harden: 1550°F/1 hr/Oil Quench Subcool: -100°F/2 hr Tempering Treatments: 1) 800°F/2 hr/AC + 800°F/2 hr/AC 2) *950°F/2 hr/AC + 950°F/2 hr/AC 3) 1000°F/2 hr/AC + 1000°F/2 hr/AC 4) 1050°F/2 hr/AC + 1050°F/2 hr/AC
300M (Quench-Temper)	D	Normalize: 1650°F/1 hr/AC Preheat: 1275°F/1 hr Harden: 1600°F/1 hr/Oil Quench Tempering Treatments: 1) 400°F/3 hr/AC + 400°F/3 hr/AC 2) *600°F/3 hr/AC + 600°F/3 hr/AC 3) 750°F/3 hr/AC + 750°F/3 hr/AC

Table V ***Experimental Heat Treatments (Continued)***

Alloy	Code	Heat Treatment
Maraging (18% Ni) 250 Solution Treat and Age	E	Solution Treatment: 1500°F/1 hr/AC Aging Treatments: 1) 850°F/3 hr/AC 2) *900°F/3 hr/AC 3) 950°F/3 hr/AC 4) 900°F/9 hr/AC
9Ni-4Co-0.45C (Quench-Temper)	F	Normalize: 1575°F/1 hr/AC Preheat: 1150°F/1 hr Harden:: 1500°F/1 hr/Oil Quench Subcool: -100°F/2 hr Tempering Treatments: 1) 400°F/2 hr/AC + 400°F/2 hr/AC 2) *500°F/2 hr/AC + 500°F/2 hr/AC 3) 600°F/2 hr/AC + 600°F/2 hr/AC
9Ni-4Co-0.45C (Bainitic)	G	Normalized: 1575°F/1 hr/AC Preheated: 1150°F/1 hr Austenitized: 1500°F/1 hr/AC Bainitic Treatments: 1) Quenched into 455°F salt bath and isothermally held 6 hr. 2) *Quenched into 475°F salt bath and isothermally held 6 hr. 3) Quenched into 550°F salt bath and isothermally held 6 hr.

*Heat treatment selected for further evaluation.

Table VI *Tensile Properties for Experimental Heat Treatments*

Alloy	Heat Number	Heat Treatment [1]	Specimen Number	Ultimate Strength (ksi)	Yield Strength 0.2% Offset (ksi)	El. % in 1 in.	RA (%)
4330 V-Modified	C57046	400°F Temper	A1A	251.1	201.6	14	55
			A2A	251.7	201.4	13	51
		500°F Temper	A1	242.5	197.9	13	55
			A2	240.7	197.5	12	53
		600°F Temper	A5	229.0	192.9	14	56
			A6	233.5	197.0	13	54
		700°F Temper	A3	217.7	190.7	13	51
			A4	218.3	190.6	12	54
H-11 Modified	09110	1025°F Temper	B1	276.2	240.0	11	40
			B2	275.0	230.9	10	35
		1075°F Temper	B1A	232.5	199.1	--	43
			B2A	235.0	201.2	12	45
		1100°F Temper	B5	219.3	185.5	14	49
			B7	219.8	184.5	13	46
		1175°F Temper	B3	151.5	120.3	18	54
			B4	150.8	122.5	16	54

[1] See Table V for complete heat treatments.

Table VI Tensile Properties for Experimental Heat Treatments (Continued)

Alloy	Heat Number	Heat Treatment [1]	Specimen Number	Ultimate Strength (ksi)	Yield Strength 0.2% Offset (ksi)	El. % in 1 in.	RA (%)
9Ni-4Co-0.30C	3930852	800°F Temper	C1	227.9	198.2	14	53
			C2	228.9	197.3	14	52
		950°F Temper	C5	230.8	208.4	14	55
			C6	232.1	201.8	14	58
		950°F Temper (No Subcool)	C1A	228.7	191.3	15	57
			C2A	228.0	191.1	15	55
		1000°F Temper	C7	225.1	203.2	16	58
			C8	225.2	202.8	15	60
		1050°F Temper	C3	220.20	199.2	15	59
			C4	219.90	198.1	16	63
300M	3951531P	400°F Temper	D1	297.1	225.6	12	37
			D2	291.2	222.0	10	38
		600°F Temper	D3	283.9	232.5	10	39
			D4	286.3	234.0	10	39
		750°F Temper	D5	270.9	227.4	11	41
			D6	262.5	225.1	12	41

[1] See Table V for complete heat treatment.

Table VI Tensile Properties for Experimental Heat Treatments (Concluded)

Alloy	Heat Number	Heat Treatment [1]	Specimen Number	Ultimate Strength (ksi)	Yield Strength 0.2% Offset (ksi)	El. % in 1 in.	RA (%)
Maraging (18% Ni)-250	24676	Aged 850°F/3 hr	E5	259.7	258.7	7	31
			E6	258.1	248.3	8	38
		Aged 900°F/3 hr	E1	273.7	264.1	7	35
			E2	272.4	258.3	6	36
		Aged 950°F/3 hr	E3	281.7	266.7	7	34
			E4	279.6	270.5	8	38
		Aged 900°F/9 hr	E7	284.8	270.4	8	36
			E8	286.2	282.3	7	34
9Ni-4Co-0.45C (Quench-Temper)	3931141	400°F Temper	F1	299.5	242.5	10	40
			F2	294.0	234.9	11	36
		500°F Temper	F3	273.7	233.8	11	44
			F4	277.8	231.9	10	44
		600°F Temper	F5	254.7	226.1	11	46
			F6	252.0	225.4	9	41
9Ni-4Co-0.45C (Bainitic)	3931141	455°F Bainitic	G7	269.4	226.6	12	45
			G8	269.6	222.4	12	47
		475°F Bainitic	G5	271.2	224.8	12	51
			G6	270.9	224.7	12	42
		550°F Bainitic	G3	233.9	199.5	17	47
			G4	235.3	200.0	14	53

[1] See Table V for complete heat treatment

Table VII *Plane Strain Fracture Toughness Data for Experimental Heat Treatments*

Alloy	Heat Number	Heat Treatment [1]	Specimen Number	Test Temp. (°F)	Crack Depth a (inch)	Load at Deviation P_{DL} (kips)	Max.Load P_{max} (kips)	K_{IC} (ksi$\sqrt{in.}$)	σ_n/σ_y
4330 V-Modified	C57046	400°F Temper	A19A	RT	.29		29.42	130.3	0.936
			A20A	RT	.29	31.95	32.35	141.5	1.02
			A21A	-65	.29		28.70	127.1	
			A22A	-65	.30	22.65	25.45	102.[illegible]	
		500°F Temper	A19	RT	.33	25.50	26.20	122.0	.89
			A20	RT	.30	28.10	28.30	127.0	.92
			A21	-65	.33		18.10	86.5	
			A22	-65	.39		14.80	78.9	
		600°F Temper	A27	RT	.33	26.70	28.20	127.8	.94
			A28	RT	.30	27.80	28.40	125.5	.93
			A29	-65	.31	15.20	15.30	70.0	
			A30	-65	.29	18.60		82.5	
		700°F Temper	A23	RT	.24	33.00	36.50	132.1	1.02
			A24	RT	.29	29.10	29.70	129.0	.98
			A25	-65	.30		21.10	95.5	
			A26	-65	.26		24.90	104.0	
5Cr-Mo-V	09110	1075°F Temper	B33	Rt	.28		10.50	45.6	.33
			B34	RT	.29		11.04	48.9	.35
			B31	-65	.32		7.30	34.2	
		1100°F Temper	B27	RT	.32		12.65	59.3	.46
			B28	RT	.30		12.55	56.7	.44
			B29	-65	.29		8.60	38.1	
			B30	-65	.30		8.80	39.8	
		1175°F Temper	B23	RT	.37	29.00	37.6	149.0	1.75
			B24	RT	.37	27.20	37.1	139.5	1.65
			B25	-65	.32		14.30	67.0	
			B26	-65	.31		14.30	65.8	

[1] See Table V for complete heat treatment

Table VII *Plane Strain Fracture Toughness Data for Experimental Heat Treatments (Continued)*

Alloy	Heat Number	Heat Treatment [1]	Specimen Number	Test Temp. (°F)	Crack Depth a (inch)	Load at Deviation P_{DL} (kips)	Max. Load P_{max} (kips)	K_{IC} (ksi$\sqrt{in.}$)	σ_n/σ_y
9Ni-4Co-0.30C	3930852	800°F Temper	C19	RT	.29	24.30	24.70	107.5	.79
			C20	RT	.27		26.35	112.1	.82
			C21	-65	.35	18.95	19.50	94.0	
			C22	-65	.32	19.90	20.80	93.4	
		950°F Temper	C27	RT	.29	24.70	29.20	109.4	.77
			C28	RT	.31	25.10	26.70	115.2	.81
			C29	-65	.28	25.95	26.45	112.2	
			C30	-65	.27		27.50	117.0	
		950°F Temper (No Subcool)	C33	-65	.31		23.80	109.5	
			C34	-65	.30	23.80	24.50	107.6	
		1000°F Temper	C31	RT	.31		29.10	133.9	.95
			C32	RT	.32	27.10	28.60	127.1	.90
		1050°F Temper	C23	RT	.29	30.20	33.00	134.9	.97
			C24	RT	.27	34.30	37.60	146.0	1.06
			C25	-65	.35		28.40	140.8	
			C26	-65	.33	28.05	30.35	134.0	
300M	395153	400°F Temper	D19	RT	.31	16.05	17.45	73.9	.48
			D20	RT	.31	18.20	18.30	83.8	.54
			D21	-65	.30	14.60	14.80	66.1	
			D22	-65	.28		13.85	60.1	
		600°F Temper	D23	RT	.29	17.55	17.75	77.8	.48
			D24	RT	.30		17.70	80.0	.49
			D25	-65	.30		11.70	53.0	
			D26	-65	.30		11.50	52.0	
		750°F Temper	D27	RT	.29	13.55	15.75	60.0	.38
			D28	RT	.30	15.10	15.40	68.3	.43
			D29	-65	.28		11.80	51.2	
			D30	-65	.30		10.95	49.5	

[1] See Table V for complete heat treatment.

Table VII Plane Strain Fracture Toughness Data for Experimental Heat Treatments (Continued)

Alloy	Heat Number	Heat Treatment [1]	Specimen Number	Test Temp. (°F)	Crack Depth a (inch)	Load at Deviation P_{DL} (kips)	Max. Load P_{max} (kips)	K_{IC} (ksi$\sqrt{in.}$)	σ_n/σ_y
Maraging (18% Ni) 250	24676	Aged 850°F/3 hr	E27	RT	.30		22.52	101.9	.58
			E28	RT	.29	20.64	21.72	91.5	.52
			E29	-65	.31		16.40	75.5	
			E30	-65	.28		19.60	85.0	
		Aged 900°F/3 hr	E20	RT	.30	19.00	19.20	86.0	.48
			E22	RT	.29	20.30	20.60	90.0	.50
			E19	-65	.32	15.35	15.85	83.8	
			E21	-65	.32	13.95	15.30	75.6	
		Aged 950°F/3 hr	E23	RT	.31	19.55	21.00	89.6	.48
			E24	RT	.30	17.55	18.75	79.5	.42
			E25	-65	.31	18.00	18.30	82.8	
			E26	-65	.30	18.60	19.20	84.0	
		Aged 900°F/9 hr	E31	RT	.30		19.68	89.0	.46
			E32	RT	.28	18.10	18.20	78.5	.41
			E33	-65	.30		16.30	73.6	
			E34	-65	.31		17.7	81.4	
9Ni-4Co-0.45C (Q + T)	3931141	400°F Temper	F19	RT	.31	13.20	13.30	60.7	.37
			F20	RT	.30		12.90	58.3	.35
			F21	-65	.30		11.80	53.4	
			F22	-65	.30		10.65	48.2	
		500°F Temper	F23	RT	.30		14.20	64.1	.40
			F24	RT	.30	15.15	15.20	68.1	.42
			F25	-65	.30		14.05	63.5	
			F26	-65	.30		11.80	53.2	
		600°F Temper	F27	RT	.54	11.52	11.64	78.9	.51
			F28	RT	.30	16.38	16.70	74.0	.47
			F29	-65	.30		16.30	73.6	
			F30	-65	.31		13.50	62.1	

[1] See Table V for complete heat treatment

Table VII *Plane Strain Fracture Toughness Data for Experimental Heat Treatments (Concluded)*

Alloy	Heat Number	Heat Treatment [1]	Specimen Number	Test Temp. (°F)	Crack Depth a (inch)	Load at Deviation P_{DL} (kips)	Max. Load P_{max} (kips)	K_{IC} (ksi $\sqrt{in.}$)	σ_n/σ_y
9Ni-4Co-0.45C (Bainitic)	3931141	455°F Bainitic	G31	RT	.35	18.20	18.35	90.3	.58
			G32	RT	.33	19.30	20.30	92.2	.59
			G33	-65	.33		14.00	66.9	
			G34	-65	.33	15.85	16.15	75.8	
		475°F Bainitic	G27	RT	.31		18.70	86.0	.55
			G28	RT	.31		21.45	98.7	.63
			G29	-65	.32	14.40	15.20	67.5	
			G30	-65	.34		14.20	69.4	
		550°F Bainitic	G23	RT	.28	25.00	28.80	108.2	.79
			G24	RT	.29	28.20	30.10	124.9	.91
			G25	-65	.30		23.40	105.8	
			G26	-65	.29		20.90	92.6	

[1] See Table V for complete heat treatment.

Table VIII ***Retained Austenite Data***

Alloy	Heat Number	Specimen Number	Heat Treatment	% Retained Austenite
300M	3931531	A2A	400°F Temper	None Detected
		A20	600°F Temper	None Detected
Maraging-250	24676	E5	850°F/3 hr Age	4
		E7	900°F/3 hr Age	4
		E4	950°F/3 hr Age	3.5
		E9	900°F/9 hr Age	2.5
9Ni-4Co-0.30C	3930852	C2	*800°F Temper	3.5
		C9	*950°F Temper	5.0
	3931144	C11	*950°F Temper	None Detected
	3931145	C17	*950°F Temper	1.5
9Ni-4Co-0.45C	3931120	FD4B	*500°F Temper	3.5
	3931141	F2	*400°F Temper	5.0
	3931141	G7	455°F Bainitic	5.0
		FE2B	475°F Bainitic	3.5
	3931120	FH2B	475°F Bainitic	5.0

* Subcooled prior to tempering.

5.0 PROPERTY VARIATIONS BETWEEN HEATS

Differences of composition, melting practice, and forging history affect the tensile and toughness properties, and directionality of billet material. Therefore, to obtain representative tensile and toughness data requires the testing of billets with varying process histories. This section of the report compares the tensile and toughness properties of billets from different heats with different forging histories.

5.1 PROCEDURE

Tensile, notch bend fracture toughness, and precracked charpy impact specimens from three billets of each alloy were tested according to the schedule of Table IX. Each of the billets were from a different heat, except that two billets of 300M were from the same vacuum melt heat. Since the billets were from different heats, slight differences of composition existed between the billets. The melting and forging history differences between the billets of the 9Ni-4Co and H-11 Modified alloys were limited because the billets of these alloys were supplied by a single vendor.

Table IX Schedule of Heat-to-Heat Testing

Tests	Test Temperature	Grain Direction	Number of Specimens Tested Per Billet
Tensile	RT	L T ST	2 2 2
Fracture Toughness	RT	T	2
	-65°F	L T	2 2
Precracked Charpy Impact	-65°F	L T ST	3 3 3

The billets of Maraging 250, 4330 V-Modified and 300M were received from more than one source. The complete histories of the materials, including chemistries, heat data, forging history, and annealing treatments, are described in Sec. 2.0.

Specimens were sawed from the billets, machined into heat treatment blanks, and identified as described in Sec. 3.0. The specimens were then given the optimum heat treatments selected for further evaluation during the "Heat Treatment Study" phase of the program (Sec. 4). Table V gives a detailed description of the heat treatments. All the specimens of an alloy were not heat treated in a single batch. This may have produced some slight difference of properties between specimens. However, the thermal processing was conducted in a heat treatment laboratory which allowed for much closer control than would normally be obtained with production processing.

The specimen configurations after final machining and the testing methods used to test the tensile, notched bend fracture toughness, and precracked charpy specimens are described in Sec. 3, "Testing Methods and Specimen Configurations."

5.2 RESULTS

Table X lists the detailed results of the tensile testing and Tables XI through XVII list the detailed results of the plane strain fracture toughness testing. The precracked charpy impact data is tabulated in Table XVIII.

In a few instances, data was not obtained as was scheduled per Table IX. For example, incorrect short-transverse tensile data was obtained for Maraging Heat 24676 because the specimens were inadvertently tested in the solution treated condition rather than in the aged condition. Further, no charpy impact data was obtained from 9Ni-4Co-0.45C heat 3931141 because the available material was needed for other types of testing.

5.3 STRENGTH PROPERTIES

The ultimate and yield strengths of the billets of each alloy were generally within a range of 10 ksi (Fig. 46). Exceptions were the 9Ni-4Co-0.30C and Maraging 250 steels. One of the three Maraging 250 heats contained approximately 0.14 percent more titanium (Table IV) than the other two heats. Since titanium is one of the major strengthening elements of Maraging steels (Ref. 17),

this heat had higher strength properties. If the heat with excessive titanium is neglected, the ranges of yield strength and ultimate strength were 241-247 ksi and 251-256 ksi, respectively.

The wide variation of 9Ni-4Co-0.30C yield strength was confined to the billet from heat 3930852. The average yield strengths of this billet in the longitudinal, transverse, and short-transverse grain directions were 205, 201, and 190 ksi, respectively. The 10 ksi decrease in the short-transverse direction was the primary cause of the wide range of yield strength. If this low short-transverse data is neglected, the range of yield strengths was 198-208 ksi.

In Sec. 4, "Heat Treatment Study," it was noted that the 9Ni-4Co-0.30C alloy is subcooled prior to tempering to transform austenite and to increase the yield strength. Austenite measurements (Table VIII) indicated that specimens from heat 3930852 contained 3-5 percent austenite, while specimens from the other two heats contained 0-1.5 percent austenite. This suggested that the higher austenite content contributed to the scatter of yield strength.

5.4 REDUCTION OF AREA PROPERTIES

The reduction of area (RA) is the most structure-sensitive parameter that is measured in the tension test. Therefore, its most important aspect is that it is used as an indication of material quality and directionality. Experience at Boeing has shown that a decrease of RA from a level of 10-15 percent in billet stock provides a warning that the material quality is substandard for good service performance.

The average and range of RA values in three grain directions are shown in Fig. 47. As was expected, the RA was lowest in the short-transverse grain directions. With the exception of Maraging 250, the average RA values in the short-transverse direction were greater than 30 percent. The low short-transverse RA of the Maraging 250 material was predictable, since micrographs of this steel displayed a higher degree of alloying element segregation than any of the other alloys (Figs. A-7 through A-12, Appendix A).

The average values of Maraging 250 short-transverse RA were about 15 percent. Improvement of the Maraging 250 RA properties can be gained by forging at lower temperatures. The billets tested in this investigation were heated to 2150 to 2100°F for the final forging step (Table II). RA values of 20-30 percent have been reported for Maraging die forgings forged at

temperatures less than 1950°F (Ref. 18). However, improved RA properties can probably be realized in most steel billet stock by die forging at lower temperatures.

Study of RA data (Fig. 47) reveals an interesting trend. The steel with lesser amounts of alloying elements such as 300M, 4330 V-Modified, and H-11 Modified displayed a lower degree of RA anisotropy, while the steels with larger amounts of alloying element displayed a higher degree of RA anisotropy. The degree of RA anisotropy tended to increase as the percentage of alloying elements increased. This was reasonable, since the higher alloy content increased the chances for segregation during ingot solidification. This greater tendency for segregation illustrates that a higher degree of process control is required when melting and forging steels with high alloying element contents. Tighter control is necessary to reduce the directionality and to obtain good short-transverse RA properties.

5.5 FRACTURE TOUGHNESS PROPERTIES

The ranges of fracture toughness data for a given alloy (Fig. 48) were produced by both toughness variations within the billets and by toughness variations between heats. Following is a discussion of these toughness variations. To simplify the discussion, each alloy is discussed separately.

5.5.1 4330 V-Modified

The ranges of 4330 V-Modified fracture toughness were primarily caused by toughness variations between heats. For example, the average room temperature fracture toughness of the three heats were 85, 100, and 124 ksi $\sqrt{\text{in.}}$, respectively, while the range of scatter between duplicate tests from a given billet were less than 10 ksi $\sqrt{\text{in.}}$ Study of the forging history (Table II) shows that the higher toughness heat received nearly twice as much forging reduction as the lower toughness heats. This greater forging reduction apparently improved the grain refinement, thereby increasing the toughness. To verify this improvement of refinement, attempts were made to determine the austenitic grain sizes of specimens from the three heats. These attempts, however, were unsuccessful. None of the etches tried resolved the prior austenitic grain size.

The intermediate toughness heat received less forging reduction

(20-inch diameter ingot) than the lower toughness heat (24-inch diameter ingot). However, the intermediate toughness heat contained slightly less carbon (Table IV) and had an approximately 10 ksi lower ultimate strength.

Extraction replica fractographs from the fracture faces of broken notched bend specimens are shown in Fig. 51. The fracture faces of the high toughness heat were almost completely free of extracted particles, while numerous symmetrically shaped particles were visible on the surface of the low toughness heat. These particles became larger as the toughness decreased. The presence of these particles, which have not yet been identified, was apparently related to the differences of fracture toughness between the heats.

The RA data (Fig. 47) gave no indication that there were significant differences of toughness between the heats of 4330 V-Modified. This points out the desirability of including a toughness requirement in a material specification.

5.5.2 H-11 Modified

The ranges of fracture toughness of H-11 Modified (Fig. 48) were primarily caused by specimen location variations within the billets. The range of -65^{o}F transverse fracture toughness for all three heats was less than 10 ksi in. If one of the six tests is neglected, the room temperature transverse grain direction fracture toughness of the three heats was within a range of 8 ksi The most significant difference of fracture toughness between the heats was in the longitudinal grain direction. The fracture toughness properties of the H-11 Modified were expected to be similar since there were few process differences between the billets. All the billets were supplied by the same vendor and received the same amount of forging reduction.

5.5.3 9Ni-4Co-0.30C

The difference between duplicate fracture toughness tests from the billets of 9Ni-4Co-0.30C were less than 6 ksi $\sqrt{\text{in.}}$, except for a duplicate test in the longitudinal direction of heat 3930852 where the K_{IC} values were 99.0 and 113.1 ksi $\sqrt{\text{in.}}$ This good repeatability indicated that the ranges of K_{IC} values (Fig. 48) were primarily caused by toughness variations between the heats.

The average values of duplicate fracture toughness tests are listed below:

Heat	Transverse Grain Direction		Longitudinal Grain Direction
	K_{IC} @ RT (ksi$\sqrt{in.}$)	K_{IC} @ -65 (ksi$\sqrt{in.}$)	K_{IC} @ -65 (ksi$\sqrt{in.}$)
3930852	112	115	106
3931144	116	101	107
3931145	121	104	119

Heat 3930852, which received slightly less forging reduction at a higher temperature, generally had lower toughness.

5.5.4 300M

Only two heats of 300M were tested. The average room temperature K_{IC} values of the heats were about 68 and 79 ksi$\sqrt{in.}$ Differences between duplicate tests were less than 6 ksi$\sqrt{in.}$ The heat with the higher toughness received nearly twice as much forging reduction (Table II). The high toughness heat was forged from a 32-inch diameter ingot and the low toughness heat was forged from a 20-inch diameter ingot. The additional forging reduction improved the grain refinement (Fig. 50). For both 300M and 4330 V-Modified, increased amounts of forging reduction produced significant increases of fracture toughness. This observation illustrates that forging history has an important effect on toughness.

5.5.5 Maraging 250

Considering that the ultimate strength of the Maraging steel varied from 251-272 ksi, the scatter of fracture toughness (Fig. 48) was relatively low. The range of duplicate fracture toughness test of a given billet was generally less than 10 ksi $\sqrt{in.}$

The average K_{IC} values for the heats were as follows:

Heat Number	Ultimate Strength	Transverse		Longitudinal
		K_{IC} @ RT (ksi$\sqrt{in.}$)	K_{IC} @ -65 (ksi$\sqrt{in.}$)	K_{IC} @ -65 (ksi$\sqrt{in.}$)
24676	271	88	80	83
09148	251	91	87	105
3930879	251	99	90	121

As was expected, the toughness of the high strength heat was lower than the toughness of the other two heats.

The differences of -65°F toughness between the transverse and longitudinal grain direction related to the amount of forging reduction. The heat that exhibited the least directionality received a lesser amount of forging reduction. The most pronounced directionality occurred in the heat with highest forging reduction.

5.5.6 9Ni-4Co-0.45C

The differences between duplicate fracture toughness tests of quench-temper 9Ni-4Co-0.45C were less than 10 ksi$\sqrt{in.}$ Therefore, the ranges of fracture toughness (Fig. 48) were primarily due to toughness variations between heats. The average room temperature K_{IC} values of the three heats were 58, 66, and 76 ksi$\sqrt{in.}$ These differences of fracture toughness between the heats were less distinguishable at -65°F.

The scatter between duplicate fracture toughness test of bainitically treated 9Ni-4Co-0.45C was considerably greater than that obtained with quench-temper specimens. While the scatter of duplicate tests of the quench-temper material was less than 10 ksi$\sqrt{in.}$, the scatter of duplicate room temperature test of bainitically treated 9Ni-4Co-0.45C ranged from 10 to 23 ksi$\sqrt{in.}$ This indicated that the fracture toughness properties of the bainitic structure were more sensitive to chemistry and structural variations within the billets. Further evidence of this was given by the observation that the differences of toughness between the transverse and longitudinal grain was greater with the bainitic structure than with the quench-temper structure. Review of the room temperature data (Table XVII) revealed that the toughness of bainitically treated material was higher at positions closer to the center of the billets.

The average transverse grain direction fracture toughness properties for both the bainitic and quench-temper structures are compared below:

Heat	K_{IC} @ RT (ksi$\sqrt{in.}$)		K_{IC} @ -65°F (ksi$\sqrt{in.}$)	
	Quench-Temper	Bainitic	Quench-Temper	Bainitic
3931141	76	90	58	68
3931120	66	94	52	80
3882720	58	83.3	52	83

Study of these data show that there was no significant correlation between the bainitic and quench-temper toughness properties. Factors, such as chemistry and forging history, that influence the toughness of the quench-temper structure did not necessarily have the same effect on the toughness of the bainitic structure.

5.6 FRACTURE TOUGHNESS AND STRENGTH RELATIONSHIPS

Figures 51 and 52 show the ranges of room temperature and -65°F fracture toughness as a function of ultimate strength in the transverse grain direction. Essentially, these figures combine the ranges of transverse grain direction fracture toughness data (Fig. 48) with the average ultimate strength data (Fig. 46). The dotted lines on the figure represent the strength and toughness relationships that were developed for one heat of each alloy in Sec. 4, "Heat Treatment Study." In some cases, 300M and 4330 V-Modified for example, the dotted lines indicated that improved toughness can be obtained at higher strength levels. However, this would require a decrease of the tempering temperature. Decreasing the tempering temperature would impair the elevated temperature stability. Lower tempering temperatures would also reduce the effectiveness of the temper as a stress relief (see Sec. 4, Heat Treatment Study).

Both Figs. 51 and 52 show that the H-11 Modified steel had inferior fracture toughness at all strength levels. Within the 220-240 ksi ultimate strength range, the fracture toughness of 9Ni-4Co-0.30C steel was superior to the fracture toughness of 4330 V-Modified. At -65°F, the toughness of the 9Ni-4Co-0.30C alloy was approximately 35 ksi$\sqrt{in.}$ higher than the fracture toughness of the 4330 V-Modified.

The room temperature fracture toughness properties of the 9Ni-4Co-0.45C (Bainitic) and Maraging 250 (Fig. 53) appear to be about equal within a strength range of about 250 to 270 ksi. However, at -65°F, the toughness of the Maraging 250 appears to be slightly higher than toughness of 9Ni-4Co-0.45C (Bainitic). Both the Maraging and 9Ni-4Co-0.45C alloys have a capability of providing higher strengths. For example, strengths of 270-300 ksi can be obtained with the Maraging 300 steel. Heats of 9Ni-4Co-0.45C with M_s temperatures of about 440°F can be bainitically treated to strengths of approximately 280 ksi (see Sec. 4). Extrapolation of the Maraging 250 and 9Ni-4Co-0.45C (Bainitic) -65°F fracture toughness to strength levels of 270-300 ksi (Fig. 52) shows that these types of steels have a potential for providing higher -65°F fracture toughness than the 300M alloy.

5.7 PRECRACKED CHARPY IMPACT PROPERTIES

Study of Fig. 53 shows that the scatter of impact properties increased at higher toughness levels. This behavior was a consequence of the increasing importance of the ductile mode of fracture at higher toughness levels. With the higher impact strength alloys such as 9Ni-4Co-0.30C and Maraging 250, the difference of grain direction became increasingly important. Comparison between the RA data (Fig. 47) and Charpy data (Fig. 53) shows that the room temperature RA was a more sensitive indicator of grain direction. For instance, with Maraging 250, the short-transverse RA was about 24 percent lower than the transverse RA. However, the charpy impact strengths were only slightly lower in the short-transverse grain direction.

The relationships between the K_{IC} values and the impact strengths at -65°F in the transverse and longitudinal grain directions are shown in Figs. 54 and 55. Examination of the plots showed that the impact strength increased rapidly with small increases of K_{IC}. This was understandable, since two different types of quantities were being compared. The impact strength is an energy term, whereas the K_{IC} term represents the state of stress at the tip of the crack for the plane strain condition. Conversion of the K_{IC} value to an energy value would have provided a comparison of similar qualities.

During the fracture toughness testing, it was found that some of the heats of a given alloy had higher toughness. Generally these differences of toughness between heats were also detected with the charpy data (Table XIX). For example, the average -65°F K_{IC} values of two heats of 300M were 54 and 45

ksi$\sqrt{\text{in.}}$, respectively, and the average impact strengths were 123 and 107 lb-in/in^2, respectively.

Although the 4330 V-Modified steel generally had higher K_{IC} values than the quench-temper 9Ni-4Co-0.45C steel, the impact properties of the two steels were about the same (Fig. 54). Also, at equivalent K_{IC} values, the quench-temper 9Ni-4Co-0.45 had higher charpy strengths than the 300M alloy. These characteristics may be a consequence of the higher strain rate associated with the Charpy tests. Generally, increasing strain rates lower the ductile-brittle transition temperature of steels (Ref. 19).

Comparison of the fracture toughness and Charpy impact properties (Figs. 48 and 53) illustrates how the two tests can lead to different conclusions about the toughness of a material. Figure 48 shows that the 4330 V-Modified had higher -65°F fracture toughness than the 9Ni-4Co-0.45C (Quench-Temper) steel. However, the -65°F Charpy data (Fig. 53) indicated that there were no significant toughness differences.

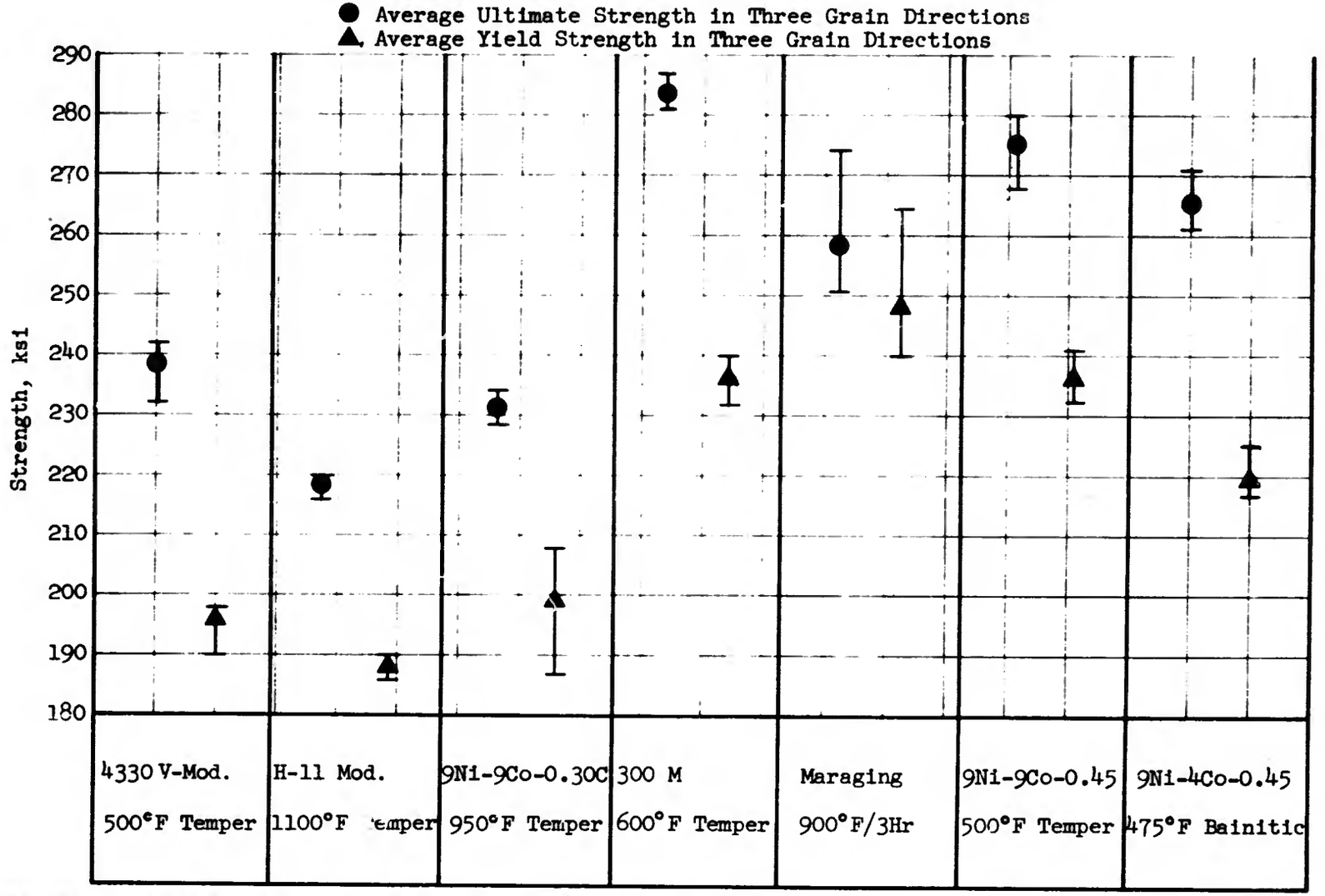

Figure 46. Room Temperature Strength Properties, Three Billets Each Alloy

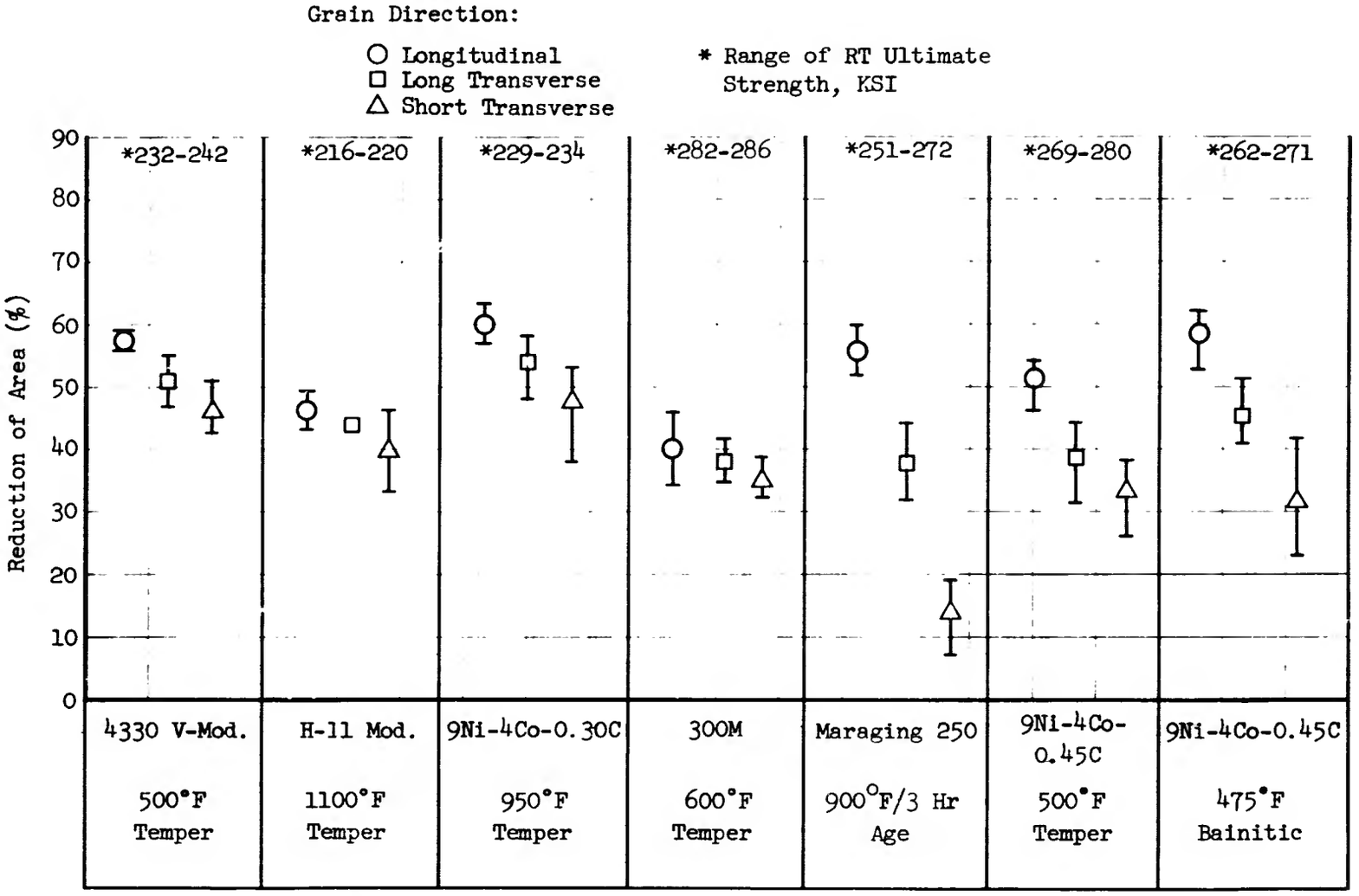

Figure 47. ***Room Temperature Reduction of Area Data, Three Billets of Each Alloy***

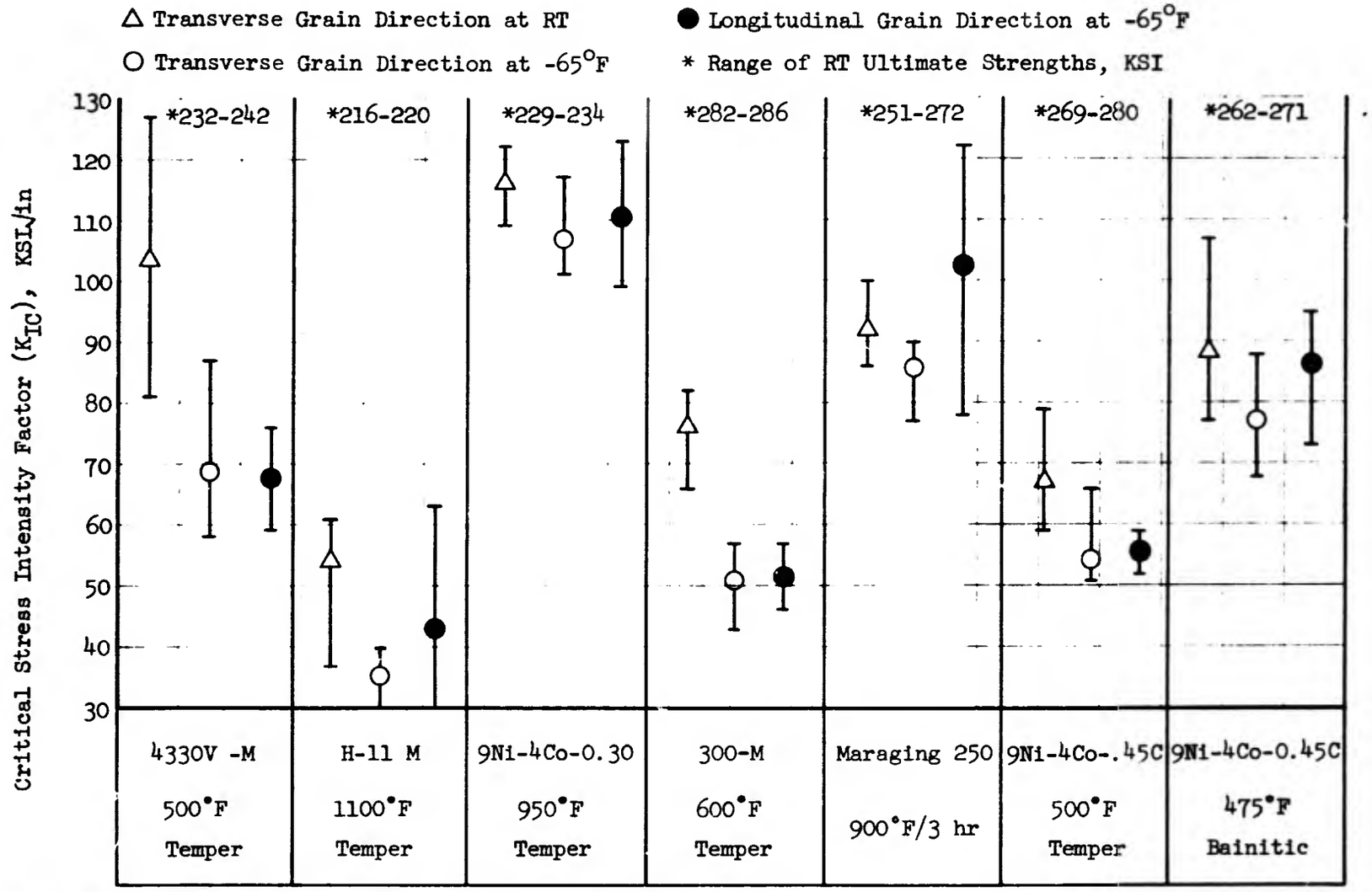

Figure 48. ***Plane Strain Fracture Toughness Data, Three Billets of Each Alloy***

DA 10093-2

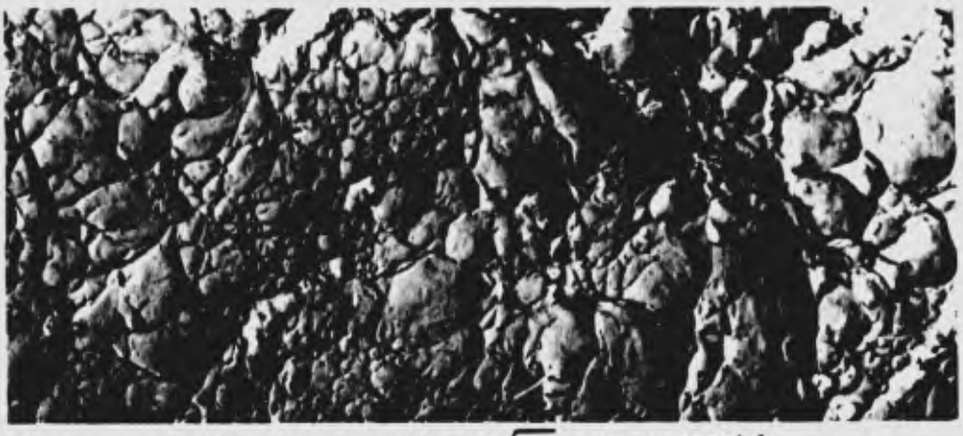

a) Specimen A19, K_{IC} = 122 ksi $\sqrt{in.}$, Heat C57046.

b) Specimen A80, K_{IC} = 104 ksi $\sqrt{in.}$, Heat 10157.

c) Specimen A87, K_{IC} = 88.2 ksi $\sqrt{in.}$, Heat 3960633.

Figure 49. Extraction Replica Fractographs from the Fracture Faces of 4330 V-Modified Notched Bend Specimen

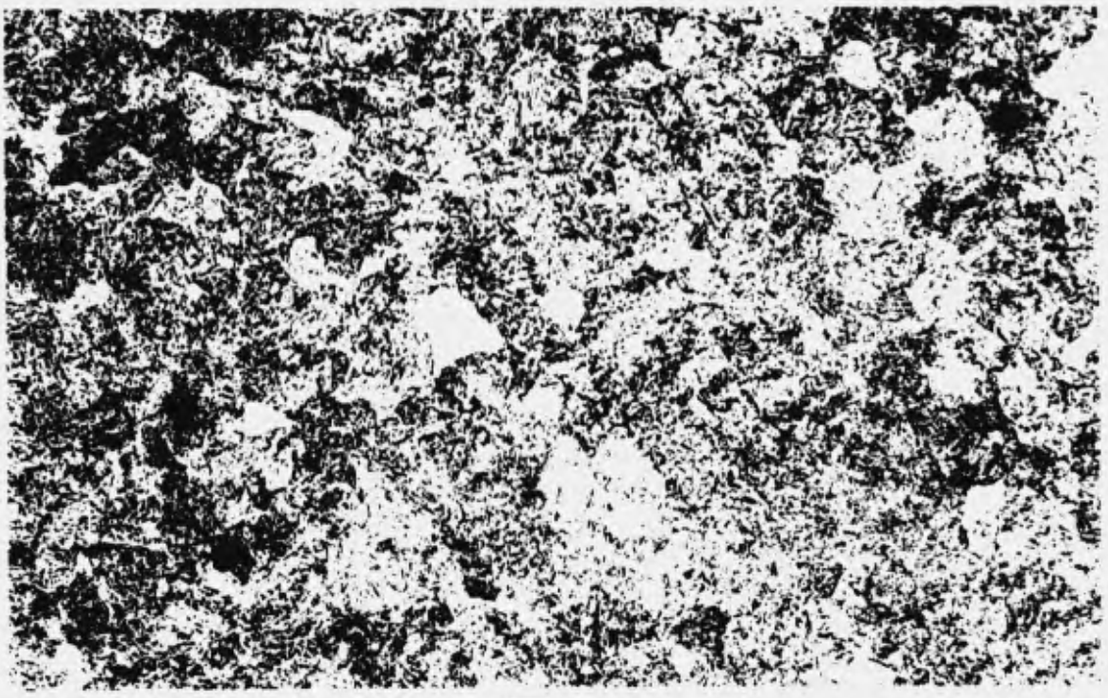

a) Heat 3931531, K_{IC}=78 ksi $\sqrt{in.}$ Mag: 100X Etchant: ADS

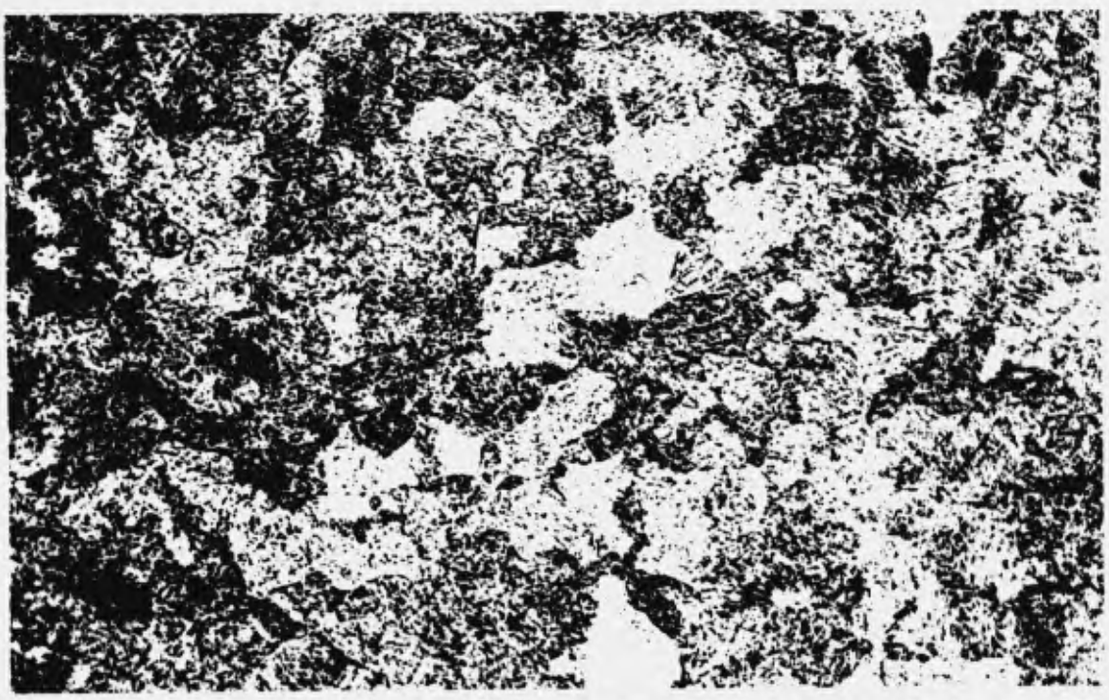

b) Heat 09715, K_{IC} = 68 ksi $\sqrt{in.}$ Mag: 100X Etchant: ADS

Figure 50. Micrographs of 300M Showing Differences in Grain Refinement, 600° F Temper

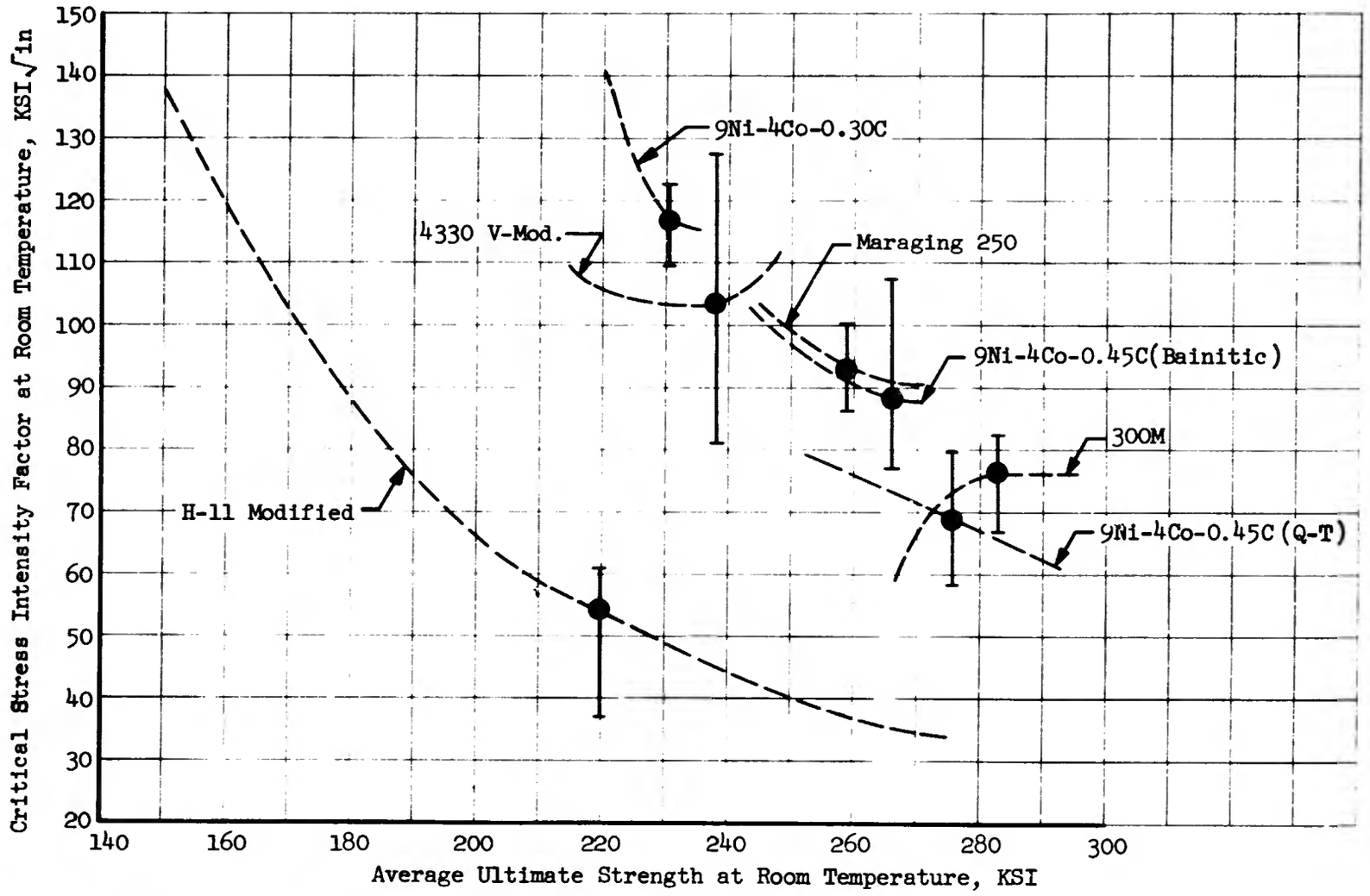

Figure 51. Strength and Room Temperature Fracture Toughness Relationships

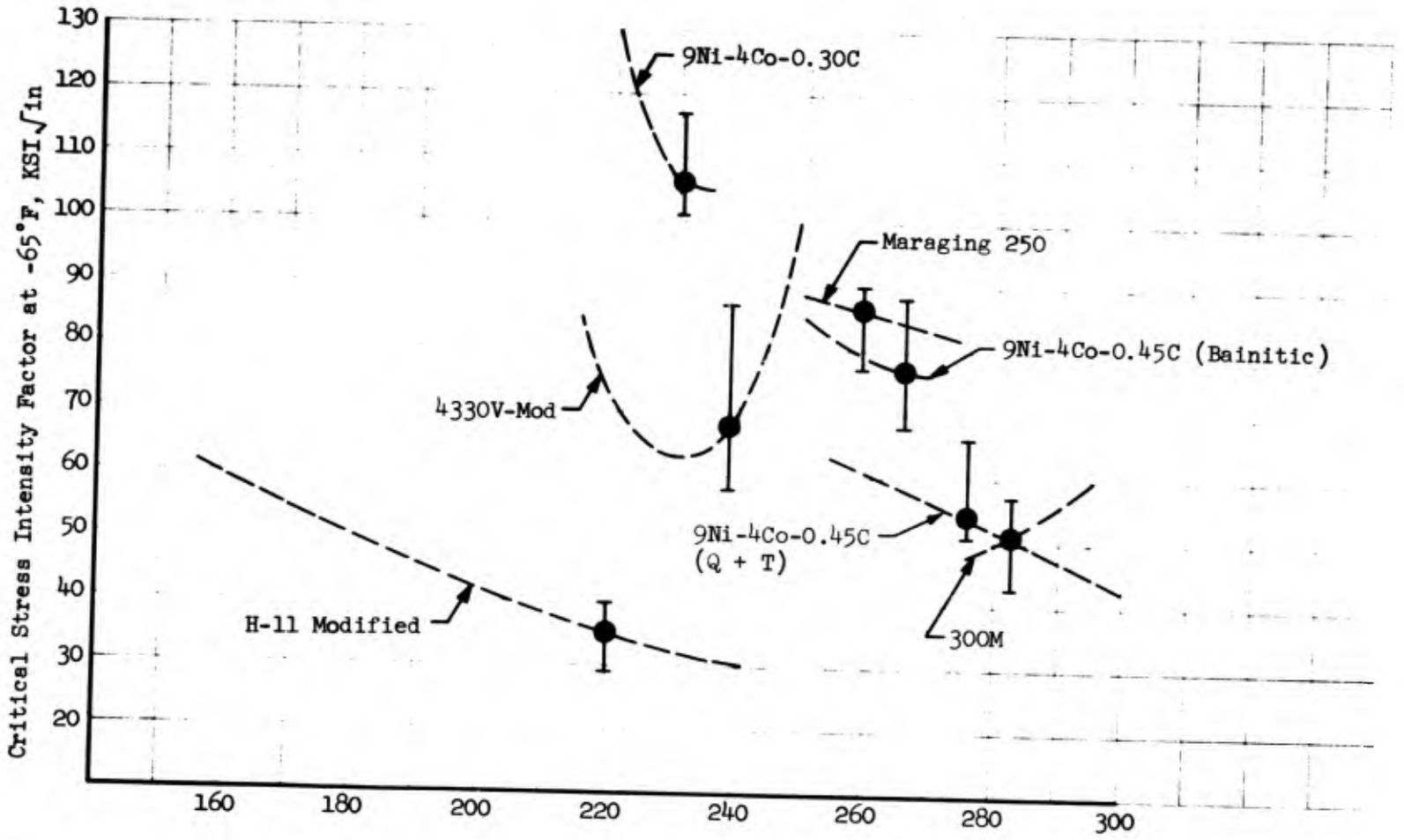

Figure 52. Strength and -65°F Fracture Toughness Relationships

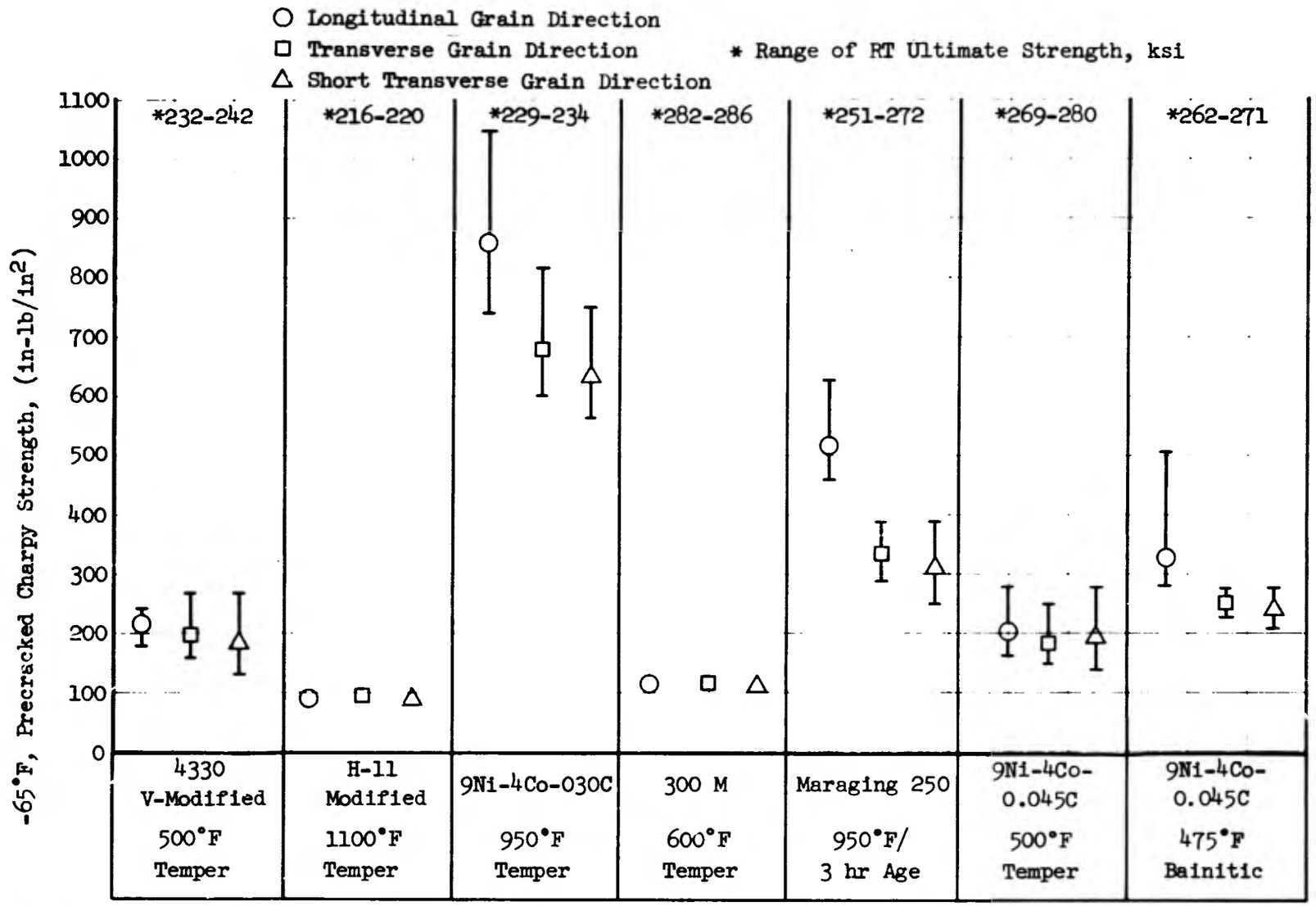

Figure 53. -65°F Precracked Charpy Data

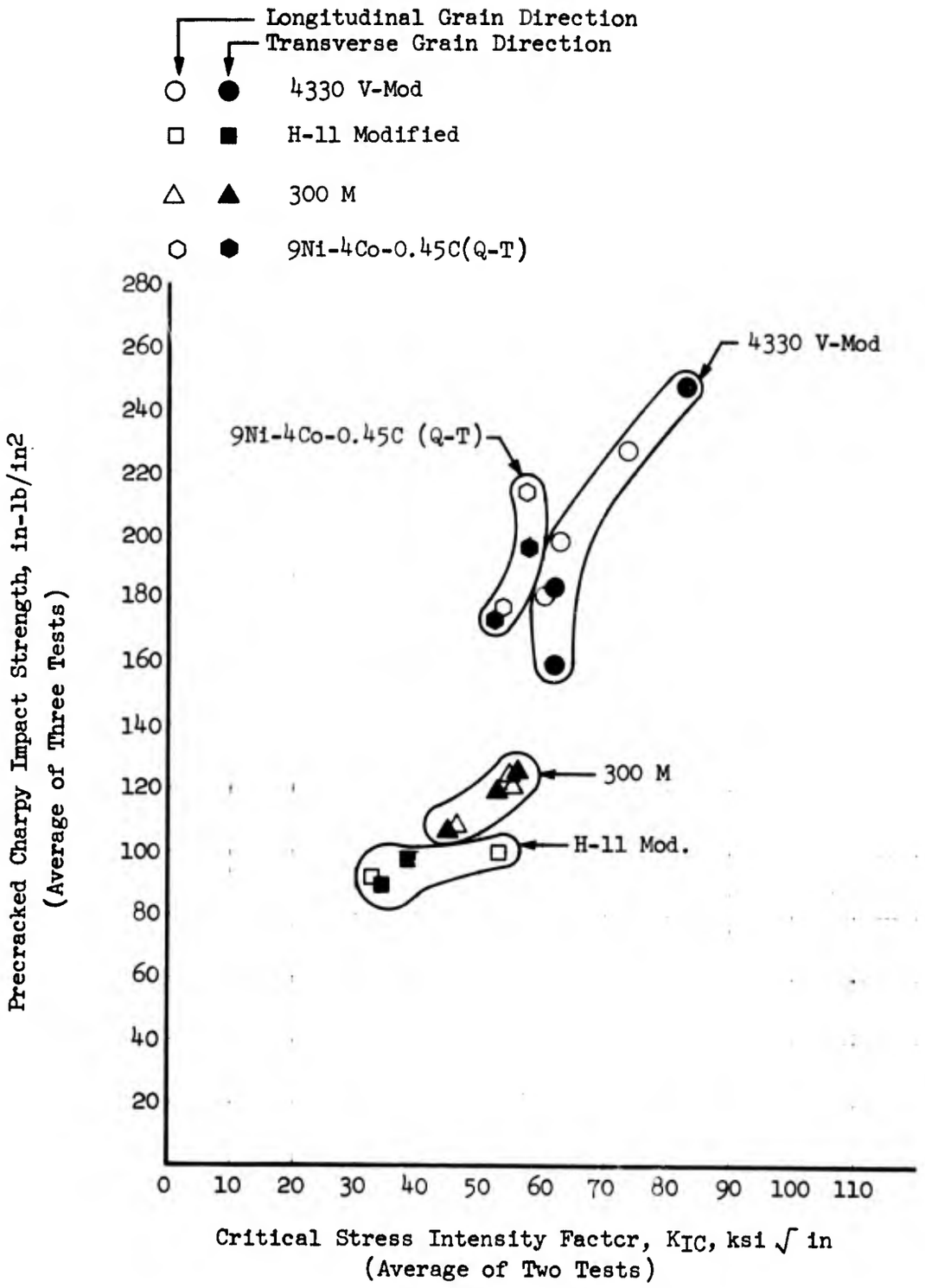

Figure 54. Comparison of Fracture Toughness and Charpy Impact Data at -65°F

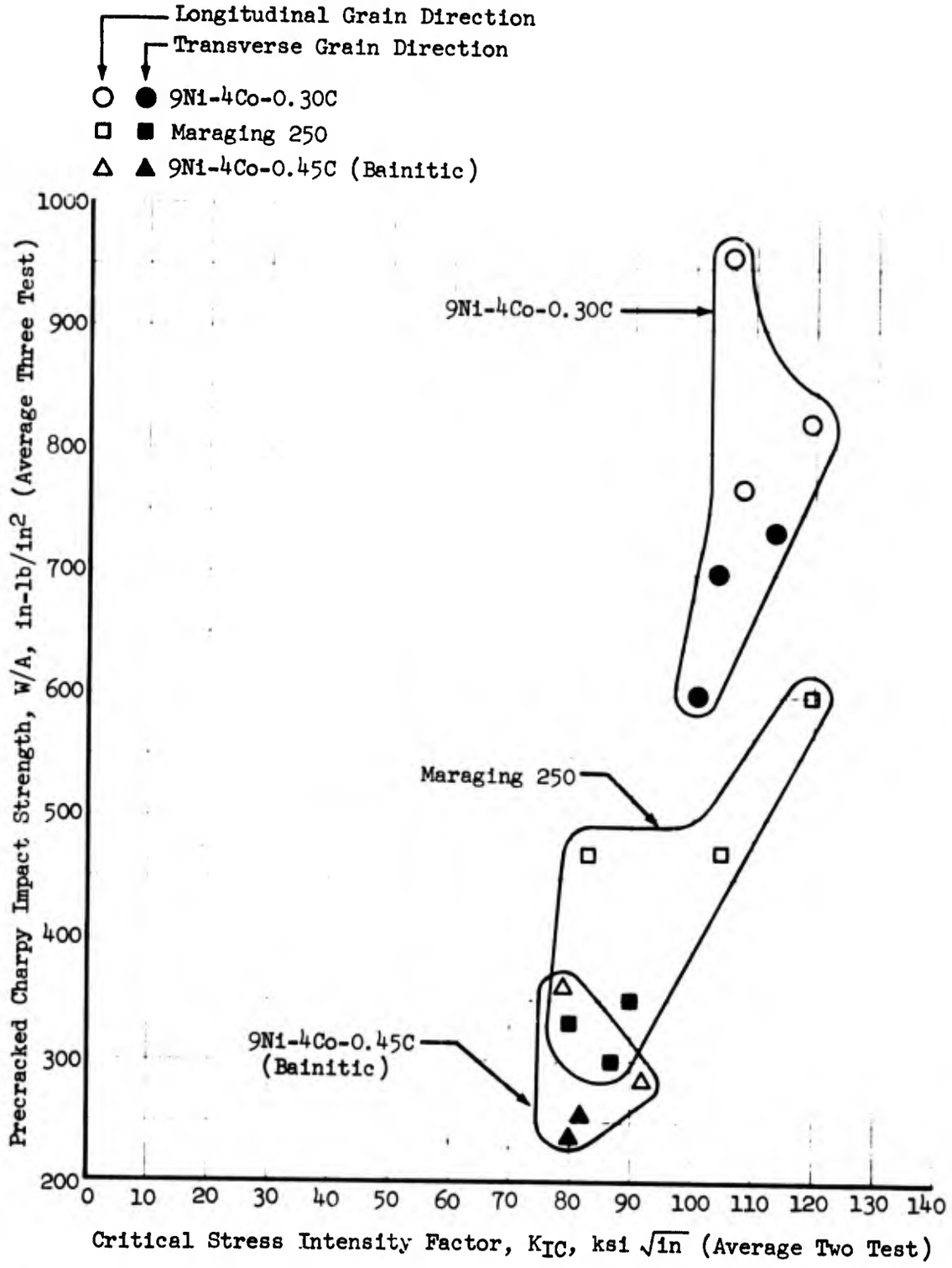

Figure 55. Comparison of Fracture Toughness and Charpy Impact Data at -65°F

Table X Room Temperature Tensile Data

Alloy	Heat Number	Specimen Number	Grain Direction	Ultimate Strength (ksi)	Yield Strength 0.2% Offset (ksi)	Elong. (% in 1 in.)	RA (%)	E (10^6 psi)
4330 V-Modified 500°F Temper	C57046	A1	T	242.5	197.9	13	55	--
		A2	T	240.7	197.5	12	54	--
		A9	L	238.6	196.7	14	59	29.5
		A10	L	240.7	197.7	14	59	29.9
		A144	ST	236.0	195.4	11	48	--
		A145	ST	237.5	197.3	12	51	--
	C10157	A11	T	234.9	192.1	12	48	29.6
		A12	T	234.2	190.2	13	52	29.8
		A13	L	234.9	191.6	13	58	29.8
		A14	L	234.5	190.7	15	58	30.6
		A146	ST	233.4	190.8	11	42	--
		A147	ST	232.5	190.8	12	43	--
	3960633	A15	T	241.1	197.7	11	47	29.0
		A16	T	241.7	198.3	10	46	29.8
		A17	L	239.5	197.5	13	58	29.4
		A18	L	241.6	200.0	13	57	29.9
		A148	ST	239.5	198.0	11	45	--
		A149	ST	240.4	200.4	11	46	--
H-11 Modified 1100°F Temper	09110	B5	T	219.3	185.5	13	45	--
		B6	T	219.5	185.0	13	42	--
		B9	L	216.6	185.4	14	49	31.5
		B10	L	217.0	186.0	13	46	30.8
		B144	ST	219.8	187.0	14	45	--
		B145	ST	220.0	187.8	14	46	--
	09099	B11	T	219.3	189.7	12	42	31.0
		B12	T	219.3	187.8	12	43	31.6
		B13	L	219.7	188.8	13	45	31.1
		B14	L	219.1	188.2	14	45	(a)
		B146	ST	229.3	197.1	12	43	--
		B147	ST	228.5	198.7	10	33	--
	08990	B15	T	220.6	189.2	13	45	30.7
		B16	T	220.1	190.1	14	44	31.6
		B17	L	217.6	188.0	14	43	31.0
		B18	L	216.2	186.2	14	49	31.7
		B148	ST	220.5	189.5	11	35	--
		B149	ST	219.7	188.6	11	35	--

Table X Room Temperature Tensile Data (Continued)

Alloy	Heat Number	Specimen Number	Grain Direction	Ultimate Strength (ksi)	Yield Strength 0.2% Offset (ksi)	Elong. (% in 1 in.)	RA (%)	E (10^6 psi)
9Ni-4Co-0.30C 950°F Temper	3930852	C5	T	230.8	208.4	14	55	--
		C6	T	232.1	201.8	14	58	--
		C9	L	229.4	199.5	15	57	27.9
		C10	L	229.4	202.0	16	58	28.9
		C144	ST	232.6	192.9	15	54	--
		C145	ST	231.9	187.2	14	54	--
	3931144	C11	T	230.9	201.2	14	48	28.7
		C12	T	232.7	201.2	14	54	28.4
		C13	L	232.7	202.0	15	59	28.1
		C14	L	232.5	201.2	16	61	27.9
		C146	ST	231.0	202.8	11	39	--
		C147	ST	232.1	201.1	12	38	--
	3931145	C15	T	231.8	200.0	15	54	28.4
		C16	T	229.7	197.9	14	55	29.0
		C17	L	230.2	199.5	16	63	28.3
		C18	L	230.9	200.6	16	62	28.3
		C148	ST	234.2	197.8	14	49	--
		C149	ST	233.1	199.0	13	53	--
300M 600°F Temper	3951531P	D3	T	283.9	232.5	10	39	--
		D4	T	283.5	234.0	10	39	--
		D9	L	284.8	238.8	12	43	29.9
		D10	L	285.7	238.5	12	39	30.3
		C144	ST	282.5	236.0	8	38	--
		C145	ST	283.0	235.1	10	35	--
	3951531R	D11	T	284.6	239.7	12	41	29.9
		D12	T	283.3	238.6	10	40	29.4
		D13	L	286.0	240.2	10	45	29.4
		D14	L	285.7	238.7	10	46	29.6
		C146	ST	281.9	232.3	10	36	--
		C147	ST	281.9	234.8	10	34	--
	09715	D15	T	281.9	235.1	10	37	29.4
		D16	T	282.2	237.2	10	35	28.7
		D17	L	284.4	237.7	9	34	29.2
		D18	L	284.4	235.5	10	35	29.7
		C148	ST	282.9	234.4	10	32	--
		C149	ST	278.6	232.0	12	35	--

Table X Room Temperature Tensile Data (Continued)

Alloy	Heat Number	Specimen Number	Grain Direction	Ultimate Strength (ksi)	Yield Strength 0.2% Offset (ksi)	Elong. (% in 1 in.)	RA (%)	E (10^6 psi)
Maraging-250 900°F/3 Hr Age	2467(	E1	T	273.7	264.1	7	35	--
		E2	T	272.4	261.2	6	36	--
		E9	L	272.5	264.0	11	55	26.6
		E10	L	272.5	261.0	11	52	30.9
	09148	E11	T	252.5	240.6	9	42	26.3
		E12	T	251.5	240.4	9	40	26.5
		E13	L	255.1	244.0	11	54	26.3
		E14	L	251.0	238.8	12	55	26.6
		E146	ST	255.1	244.9	4	7	--
		E147	ST	256.2	247.8	3	14	--
	3930879	E15	T	253.9	242.5	9	44	27.0
		E16	T	253.3	242.7	8	32	26.6
		E17	L	252.8	243.8	11	58	26.4
		E18	L	251.6	239.7	13	59	26.3
		E148	ST	253.5	246.7	5	19	--
		E149	ST	253.5	247.3	5	15	--
*9Ni-4Co-0.45C 500°F Temper	3931141	F3	T	273.7	233.8	11	44	--
		F4	T	275.7	232.8	10	44	--
		F9	L	276.8	236.8	12	54	28.4
		F10	L	274.8	236.3	12	54	28.2
		F144	ST	268.7	236.4	9	31	--
		F145	ST	273.3	237.2	12	38	--
	3931120	F11	T	276.2	237.0	7	31	27.7
		F12	T	278.3	237.1	9	40	28.2
		F13	L	279.1	234.2	11	54	27.7
		F14	L	278.0	235.6	11	51	28.0
		F146	ST	280.1	241.5	--	--	--
		F147	ST	278.5	239.4	8	26	--
	3882720	F15	T	275.6	238.4	9	38	28.3
		F16	T	273.4	234.9	10	37	27.8
		F17	L	274.2	236.1	12	46	27.7
		F18	L	274.4	236.8	12	50	28.0
		F148	ST	274.2	238.0	8	36	--
		F149	ST	275.2	239.7	10	38	--

Table X Room Temperature Tensile Data (Concluded)

Alloy	Heat Number	Specimen Number	Grain Direction	Ultimate Strength (ksi)	Yield Strength 0.2% Offset (ksi)	Elong. (% in 1 in.)	RA (%)	E (10^6 psi)
**9Ni-4Co-0.45C 475°F Bainitic	3931141	G5	T	271.2	224.8	12	51	27.5
		G6	T	270.9	224.7	12	42	28.0
		G9	L	263.2	218.5	14	60	28.4
		G10	L	266.3	220.4	14	62	28.2
		G144	ST	268.7	217.2	8	25	--
		G145	ST	268.8	219.8	8	27	--
	3931120	G11	T	265.8	220.0	11	41	27.7
		G12	T	264.4	221.4	10	49	28.2
		G13	L	264.5	218.0	13	61	27.7
		G14	L	268.0	218.3	13	59	28.0
		G146	ST	267.8	218.4	--	--	--
		G147	ST	268.0	219.8	10	42	--
	3882720	G15	T	262.9	218.6	11	47	28.3
		G16	T	262.2	216.7	11	41	27.8
		G17	L	265.1	219.2	12	54	27.7
		G18	L	265.0	218.8	12	53	28.0
		G148	ST	266.2	221.6	12	42	--
		G149	ST	265.7	223.3	11	23	--

Table XI *4330 V-Modified Plane Strain Fracture Toughness Data*

Heat Number	Specimen Number	Grain Direction	Test Temp.	Crack Depth a (inches)	Load at Deviation P_{DL} (Kips)	Max. Load P_{max} (Kips)	K_{Ic} (ksi $\sqrt{in}$)	σ_n/σ_{yd}
C57046	A19	T	RT	0.33	25.50	26.20	122.0	0.89
	A20	T	RT	0.30	28.10	28.30	127.0	0.92
	A21	T	-65°F	0.33	18.10	18.10	86.5	
	A22	T	-65°F	0.39	14.80	14.80	78.9	
	A35	L	-65°F	0.33	14.75	14.75	70.5	
	A36	L	-65°F	0.29	17.20	17.20	76.3	
C10157	A80	T	RT	0.32	22.20	23.60	104.1	0.78
	A81	T	RT	0.32	20.40	22.60	95.6	0.72
	A37	T	-65°F	0.32	13.25	13.25	62.2	
	A38	T	-65°F	0.35	12.25	12.25	60.8	
	A39	L	-65°F	0.31	14.50	14.55	66.6	
	A40	L	-65°F	0.31	12.80	12.80	58.9	
3960633	A86	T	RT	0.31	17.70	18.00	81.4	0.59
	A87	T	RT	0.32	18.80	18.80	88.2	0.63
	A41	T	-65°F	0.31	12.60	12.60	58.0	
	A42	T	-65°F	0.30	14.50	14.50	65.5	
	A43	L	-65°F	0.31	12.80	12.80	58.9	
	A44	L	-65°F	0.32	15.60	15.60	73.2	

Heat Treatment: 1575°F/1 hr/OQ + 500°F/3 hr/AC + 500°F/3 hr/AC

Table XII H-11 Modified Plane Strain Fracture Toughness Data

Heat Number	Specimen Number	Grain Direction	Test Temp.	Crack Depth a (inches)	Load at Deviation P_{DL} (Kips)	Max. Load P_{max} (Kips)	K_{Ic} (ksi $\sqrt{in}$)	σ_n/σ_{yd}
09110	B27	T	RT	0.32	12.65	12.65	59.3	0.46
	B28	T	RT	0.30	12.55	12.55	56.7	0.44
	B29	T	-65°F	0.29	8.60	8.60	38.1	
	B30	T	-65°F	0.30	8.80	8.80	39.8	
	B35	L	-65°F	0.29	14.10	14.10	62.5	
	B36	L	-65°F	0.33	9.50	9.50	45.4	
09099	B80	T	RT	0.32	12.58	12.58	59.0	0.45
	B81	T	RT	0.30	13.52	13.52	61.1	0.47
	B38	T	-65°F	0.27	7.00	7.00	29.8	
	B39	L	-65°F	0.28	8.30	8.30	36.1	
	B40	L	-65°F	0.28	6.80	6.80	29.6	
08990	B86	T	RT	0.31	8.02	8.02	36.9	0.28
	B87	T	RT	0.29	12.22	12.22	54.1	0.41
	B41	T	-65°F	0.27	8.12	8.12	34.6	
	B42	T	-65°F	0.28	8.20	8.20	35.7	

Heat Treatment: 1850°F/3/4 hr/AC + 1100°F/3 hr/AC + 1100°F/3 hr/AC + 1100°F/3 hr/AC

Table XIII 9Ni-4Co-0.30C Plane Strain Fracture Toughness Data

Heat Number	Specimen Number	Grain Direction	Test Temp.	Crack Depth a (inches)	Load at Deviation P_{DL} (Kips)	Max. Load P_{max} (Kips)	K_{Ic} (ksi $\sqrt{in}$)	σ_n/σ_{yd}
3930852	C27	T	RT	0.29	24.70	29.20	109.4	0.77
	C28	T	RT	0.31	25.10	26.70	115.2	0.81
	C29	T	-65°F	0.28	25.95	26.45	112.2	
	C30	T	-65°F	0.27	27.50	27.50	117.0	
	C35	L	-65°F	0.30	21.90	25.40	99.0	
	C36	L	-65°F	0.31	24.60	25.30	113.1	
3931144	C80	T	RT	0.31	24.90	25.80	114.2	0.82
	C81	T	RT	0.30	26.10	26.20	117.9	0.84
	C37	T	-65°F	0.30	22.30	23.00	101.0	
	C38	T	-65°F	0.30	22.40	22.40	101.2	
	C39	L	-65°F	0.29	24.10	24.10	106.8	
	C40	L	-65°F	0.31	23.60	23.60	108.6	
3931145	C86	T	RT	0.30	26.90	27.10	121.5	0.88
	C87	T	RT	0.29	27.60	28.00	122.3	0.89
	C41	T	-65°F	0.30	23.50	23.50	106.2	
	C42	T	-65°F	0.30	22.60	22.60	102.1	
	C43	L	-65°F	0.31	26.70	27.40	122.7	
	C44	L	-65°F	0.32	24.80	25.50	116.0	

Heat Treatment: 1550°F/1 hr/OQ + 950°F/2 hr/AC + 950°F/2 hr/AC

Table XIV 300M Plane Strain Fracture Toughness Data

Heat Number	Specimen Number	Grain Direction	Test Temp.	Crack Depth a (inches)	Load at Deviation P_{DL} (Kips)	Max. Load P_{max} (Kips)	K_{Ic} (ksi $\sqrt{in}$)	σ_n/σ_{yd}
3151531P	D23	T	RT	0.29	17.55	17.55	77.8	0.48
	D24	T	RT	0.30	17.70	17.70	80.0	0.49
	D25	T	-65°F	0.30	11.70	11.70	53.0	
	D26	T	-65°F	0.30	11.50	11.50	52.0	
	D35	L	-65°F	0.36	10.80	10.92	54.6	
	D36	L	-65°F	0.31	12.22	12.22	56.2	
3151531R	D80	T	RT	0.29	18.55	19.00	82.2	0.50
	D81	T	RT	0.29	18.26	18.80	81.0	0.49
	D37	T	-65°F	0.33	11.86	12.10	56.7	
	D38	T	-65°F	0.32	11.66	12.34	54.6	
	D39	L	-65°F	0.30	11.82	11.82	53.5	
	D40	L	-65°F	0.30	12.52	12.88	56.6	
09715	D86	T	RT	0.33	14.38	14.58	68.8	0.42
	D87	T	RT	0.28	15.30	15.60	66.4	0.41
	D41	T	-65°F	0.28	10.60	10.60	46.1	
	D42	T	-65°F	0.31	9.42	9.42	43.3	
	D43	L	-65°F	0.31	9.92	9.92	45.6	
	D44	L	-65°F	0.32	9.86	9.86	46.2	

Heat Treatment: 1600°F/1 hr/OQ + 600°F/3 hr/AC + 600°F/3 hr/AC

Table XV *Maraging 250 Plane Strain Fracture Toughness Data*

Heat Number	Specimen Number	Grain Direction	Test Temp.	Crack Depth a (inches)	Load at Deviation P_{DL} (Kips)	Max. Load P_{max} (Kips)	K_{Ic} (ksi $\sqrt{in}$)	σ_n/σ_{yd}
24676	E20	T	RT	0.30	19.00	19.20	86.0	0.47
	E22	T	RT	0.29	20.30	20.60	90.0	0.50
	E19*	T	-65°F	0.32	15.35	15.85	83.8	
	E21**	T	-65°F	0.32	13.95	15.3	77.0	
	E35	L	-65°F	0.31	19.25	20.8	88.6	
	E36	L	-65°F	0.34	15.95	19.15	77.9	
09148	E80	T	RT	0.31	19.70	21.30	90.6	0.54
	E81	T	RT	0.31	19.70	19.70	90.6	0.54
	E37	T	-65°F	0.33	18.00	18.00	86.1	
	E38	T	-65°F	0.31	19.25	19.25	88.6	
	E39	L	-65°F	0.32	21.80	26.4	102.5	
	E40	L	-65°F	0.32	22.90	23.95	107.3	
3930879	E86	T	RT	0.31	21.65	22.50	99.3	0.59
	E87	T	RT	0.33	20.50	20.70	98.0	0.58
	E41	T	-65°F	0.32	19.25	19.60	90.4	
	E42	T	-65°F	0.32	19.10	19.10	89.6	
	E43	L	-65°F	0.32	25.45	29.80	119.3	
	E44	L	-65°F	0.32	25.80	26.00	122.0	

Heat Treatment: 1500°F/1 hr/AC + 900°F/1 hr/AC
* Specimen 0.412 inches thick
** Specimen 0.415 inches thick

Table XV! *Quench-Temper 9Ni-4Co-0.45C Plane Strain Fracture Toughness Data*

Heat Number	Specimen Number	Grain Direction	Test Temp.	Crack Depth a (inches)	Load at Deviation P_{DL} (Kips)	Max. Load P_{max} (Kips)	K_{Ic} (ksi $\sqrt{in}$)	σ_n/σ_{yd}
3931141	F27	T	RT	0.64	11.52	11.64	78.9	0.50
	F28	T	RT	0.30	16.38	16.70	74.0	0.48
	F25	T	-65°F	0.30	14.05	14.05	63.5	
	F26	T	-65°F	0.30	11.80	11.80	53.2	
	F35	L	-65°F	0.31	12.80	12.80	57.8	
	F36	L	-65°F	0.34	12.95	12.95	58.5	
3931120	F80	T	RT	0.31	14.20	14.20	66.6	0.40
	F81	T	RT	0.30	14.55	14.70	65.8	0.40
	F37	T	-65°F	0.32	10.80	10.80	50.6	
	F38	T	-65°F	0.32	11.55	11.55	54.2	
	F39	L	-65°F	0.31	11.85	11.85	54.5	
	F40	L	-65°F	0.31	11.75	11.75	54.0	
3882720	F86	T	RT	0.30	13.00	13.00	58.8	0.36
	F87	T	RT	0.30	13.00	13.00	58.8	0.36
	F41	T	-65°F	0.31	11.60	11.60	53.4	
	F42	T	-65°F	0.32	11.05	11.15	51.8	
	F43	L	-65°F	0.30	12.05	12.05	54.5	
	F44	L	-65°F	0.31	11.30	11.30	52.0	

Heat Treatment: 1500°F/1 hr/OQ + Subcool -100°F/2 hr + 500°F/2 hr/AC + 500°F/2 hr/AC

Table XVII **Bainitically Treated 9Ni-4Co-0.45C Plane Strain Fracture Toughness**

Heat Number	Specimen Number	Grain Direction	Test Temp.	Crack Depth a (inches)	Load at Deviation P_{DL} (Kips)	Max. Load P_{max} (Kips)	K_{Ic} (ksi $\sqrt{in}$)	σ_n/σ_{yd}
3931141	G27	T	RT	0.31	18.70	18.70	80.6	0.55
	G28	T	RT	0.31	21.45	21.45	98.7	0.63
	G29	T	-65°F	0.32	14.40	15.20	67.5	
	G30	T	-65°F	0.34	14.20	14.20	69.4	
	G35	L	-65°F	0.32	20.20	20.20	94.8	
	G36	L	-65°F	0.31	18.20	18.20	83.7	
3931120	G80	T	RT	0.32	17.55	19.80	82.4	0.52
	G81	T	RT	0.31	23.00	23.80	105.8	0.67
	G37	T	-65°F	0.32	15.20	15.80	71.3	
	G38	T	-65°F	0.31	19.10	19.10	87.8	
	G39	L	-65°F	0.32	15.60	15.60	73.3	
	G40	L	-65°F	0.33	18.60	18.60	89.0	
3882720	G86	T	RT	0.31	16.70	17.20	76.9	0.51
	G87	T	RT	0.31	19.40	20.30	89.4	0.59
	G41	T	-65°F	0.32	17.90	18.30	84.0	
	G42	T	-65°F	0.32	17.40	18.30	81.7	
	G43	L	-65°F	0.31	19.70	19.80	90.6	
	G44	L	-65°F	0.31	19.70	19.70	90.6	

Heat Treatment: 1500°F/1 hr/Quenched into 475°F salt bath + 475°F/6 hr

Table XVIII $-65^{\circ}F$ **Precracked Charpy Data**

Alloy	Heat Number	Specimen Number	Grain Direction	Depth to Crack (inch)	Impact Strength W/A (in-lb/in^2)	Average Impact Strength, W/A (in-lb/in^2)
4330 V-Modified	C57046	A51	L	.270	222.6	
		A52	L	.270	237.7	227.0
		A53	L	.280	220.7	
		A45	T	.280	240.0	
		A46	T	.275	265.7	248.9
		A47	T	.280	240.9	
		A48	ST	.275	263.0	
		A49	ST	.285	216.1	246.0
		A50	ST	.285	258.9	
	C10157	A60	L	.285	178.6	
		A61	L	.280	227.3	198.2
		A62	L	.290	178.6	
		A54	T	.265	182.7	
		A55	T	.270	207.5	184.8
		A56	T	.285	164.3	
		A57	ST	.285	151.8	
		A58	ST	.280	160.9	154.8
		A59	ST	.290	151.8	
	3960633	A139	L	.280	183.6	
		A140	L	.275	182.4	181.6
		A141	L	.265	178.8	
		A133	T	.285	156.2	
		A134	T	.275	155.6	158.9
		A135	T	.270	165.1	
		A136	ST	.270	129.7	
		A137	ST	.280	150.9	142.5
		A138	ST	.280	147.3	

Table XVIII -65°F Precracked Charpy Data (Continued)

Alloy	Heat Number	Specimen Number	Grain Direction	Depth to Crack (inch)	Impact Strength W/A (in-lb/in^2)	Average Impact Strength, W/A (in-lb/in^2)
H-11 Mod	09110	B51	L	.285	103.6	
		B52	L	.295	95.7	98.6
		B53	L	.290	96.5	
		B45	T	.285	97.3	
		B46	T	.290	86.8	96.8
		B47	T	.285	106.2	
		B48	ST	.300	96.6	
		B49	ST	.290	99.1	96.6
		B50	ST	.295	94.0	
	09099	B60	L	.285	98.2	
		B61	L	.285	94.6	92.2
		B62	L	.285	83.9	
		B54	T	.285	94.6	
		B55	T	.300	98.3	96.1
		B56	T	.285	95.5	
		B57	ST	.285	96.4	
		B58	ST	.280	96.4	97.0
		B59	ST	.280	98.2	
	08990	B139	L	.290	92.1	
		B140	L	.280	95.4	90.2
		B141	L	.285	83.0	
		B133	T	.290	85.1	
		B134	T	.290	93.9	89.0
		B135	T	.295	87.9	
		B136	ST	.290	90.3	
		B137	ST	.280	87.3	89.3
		B138	ST	.290	90.3	

Table XVIII -65°F Precracked Charpy Data (Continued)

Alloy	Heat Number	Specimen Number	Grain Direction	Depth to Crack (inch)	Impact Strength W/A (in-lb/in^2)	Average Impact Strength, W/A (in-lb/in^2)
9Ni-4Co-0.30C (Cr,Mo)	3930852	C51	L	.275	911.1	960.0
		C52	L	.275	926.0	
		C53	L	.290	1043.0	
		C45	T	.275	733.3	737.0
		C46	T	.280	700.0	
		C47	T	.275	777.8	
		C48	ST	.285	747.3	714.5
		C49	ST	.280	711.8	
		C50	ST	.280	684.5	
	3931144	C60	L	.290	793.8	770.3
		C61	L	.270	780.2	
		C62	L	.280	737.0	
		C54	T	.270	596.2	601.1
		C55	T	.280	604.5	
		C56	T	.280	602.7	
		C57	ST	.275	635.2	564.9
		C58	ST	.280	486.4	
		C59	ST	.285	573.2	
	3931145	C139	L	.275	850.9	826.9
		C140	L	.275	842.6	
		C141	L	.280	787.3	
		C133	T	.270	816.0	703.5
		C134	T	.275	613.9	
		C135	T	.275	680.4	
		C136	ST	.275	668.5	630.0
		C137	ST	.270	660.4	
		C138	ST	.275	561.1	

Table XVIII -65°F Precracked Charpy Data (Continued)

Alloy	Heat Number	Specimen Number	Grain Direction	Depth to Crack (inch)	Impact Strength W/A (in-lb/in^2)	Average Impact Strength, W/A (in-lb/in^2)
300M	3951531P	D60	L	.280	116.2	119.0
		D61	L	.280	126.2	
		D62	L	.280	114.5	
		D54	T	.275	117.6	119.5
		D55	T	.280	123.4	
		D56	T	.275	117.4	
		D57	ST	.275	116.5	123.7
		D58	ST	.270	124.3	
		D59	ST	.275	130.3	
	3951531R	D51	L	.280	130.6	126.6
		D52	L	.245	118.6	
		D53	L	.280	128.8	
		D45	T	.280	135.1	126.1
		D46	T	.285	121.4	
		D47	T	.280	121.8	
		D48	ST	.290	122.8	125.4
		D49	ST	.290	125.4	
		D50	ST	.280	127.9	
	09715	D139	L	.275	107.4	108.0
		D140	L	.270	110.3	
		D141	L	.280	106.4	
		D133	T	.270	109.4	107.1
		D134	T	.270	102.8	
		D135	T	.275	109.2	
		D136	ST	.265	98.1	101.8
		D137	ST	.255	101.0	
		D138	ST	.280	106.3	

Table XVIII -65°F Precracked Charpy Data (Continued)

Alloy	Heat Number	Specimen Number	Grain Direction	Depth to Crack (inch)	Impact Strength W/A (in-lb/in^2)	Average Impact Strength, W/A (in-lb/in^2)
Maraging 250	24676	E51	L	.275	478.7	
		E52	L	.280	472.7	476.1
		E53	L	.275	476.8	
		E45	T	.270	385.8	
		E46	T	.280	329.1	331.7
		E47	T	.265	331.7	
		E48	ST	.275	314.8	
		E49	ST	.275	287.0	285.7
		E50	ST	.280	255.4	
	09148	E60	L	.280	474.8	
		E61	L	.280	482.7	472.4
		E62	L	.285	459.8	
		E54	T	.280	302.7	
		E55	T	.275	312.0	302.1
		E56	T	.275	291.7	
		E57	ST	.280	249.1	
		E58	ST	.275	267.0	288.8
		E59	ST	.280	350.4	
	3930879	E139	L	.285	627.7	
		E140	L	.280	593.6	601.6
		E141	L	.280	583.6	
		E133	T	.270	358.5	
		E134	T	.285	367.0	351.1
		E135	T	.275	327.8	
		E136	ST	.270	390.6	
		E137	ST	.280	341.8	362.0
		E138	ST	.285	353.6	

Table XVIII **–65°F Precracked Charpy Data (Continued)**

Alloy	Heat Number	Specimen Number	Grain Direction	Depth to Crack (inch)	Impact Strength W/A (in-lb/in^2)	Average Impact Strength, W/A (in-lb/in^2)
9Ni-4Co-0.45 (Q+T)	3931120	F60	L	.280	277.3	
		F61	L	.280	207.7	214.5
		F62	L	.280	163.6	
		F54	T	.285	150.9	
		F55	T	.260	149.1	196.6
		F56	T	.280	246.9	
		F57	ST	.270	139.2	
		F58	ST	.280	187.3	164.7
		F59	ST	.280	167.6	
	3882720	F139	L	.275	163.9	
		F140	L	.275	163.0	168.5
		F141	L	.275	178.7	
		F133	T	.280	159.1	
		F134	T	.280	177.3	164.9
		F135	T	.280	158.2	
		F136	ST	.285	237.5	
		F137	ST	.285	272.3	227.2
		F138	ST	.230	171.8	

Table XVIII *–65°F Precracked Charpy Data (Concluded)*

Alloy	Heat Number	Specimen Number	Grain Direction	Depth to Crack (inch)	Impact Strength W/A (in-lb/in^2)	Average Impact Strength, W/A (in-lb/in^2)
9Ni-4Co-0.45C (Bainitic)	3931120	G60	L	.285	504.5	
		G61	L	.280	293.6	362.9
		G62	L	.275	290.7	
		G54	T	.290	251.7	
		G55	T	.280	241.8	242.6
		G56	T	.290	234.7	
		G57	ST	.280	238.2	
		G58	ST	.280	226.4	226.6
		G59	ST	.285	215.2	
	3882720	G139	L	.280	283.6	
		G140	L	.280	283.6	280.9
		G141	L	.280	275.4	
		G133	T	.290	249.1	
		G134	T	.285	272.3	255.0
		G135	T	.285	243.7	
		G136	ST	.280	279.1	
		G137	ST	.285	271.4	268.0
		G138	ST	.280	253.6	

Table XIX Comparison of Fracture Toughness and Precracked Charpy Data at -65°F

Alloy	Heat Number	Transverse Grain Direction		Longitudinal Grain Direction	
		K_{Ic}, Average Two Test ($ksi\sqrt{in.}$)	W/A, Average Three Test ($in\text{-}lb/in^2$)	K_{Ic}, Average Two Test ($ksi\sqrt{in.}$)	W/A, Average Three Test ($in\text{-}lb/in^2$)
4330 V-Modified 500°F Temper	C57046 C10157 3960633	82.7 61.5 61.8	248.9 184.8 158.9	73.4 62.8 60.1	227.0 198.2 181.6
H-11 Mod 1100°F Temper	09110 09099 08990	39.0 -- 35.2	96.8 96.1 89.0	54.0 32.9 --	98.6 96.8 96.6
9Ni-4Co-0.30C 950°F Temper	3930852 393144 3931145	114.6 101.1 104.2	737.0 601.1 703.5	106.0 107.7 119.4	960.0 770.3 826.9
300M 600°F Temper	3951531(P) 3951531(R) 09715	52.5 55.7 44.7	119.5 126.1 107.1	55.4 55.1 45.9	119.0 126.6 108.0
Maraging 250 900°F/3 hr Age	24676 09148 3930879	80.4 87.4 90	331.7 302.1 351.1	83.3 104.9 120.7	476.1 472.4 601.6
9Ni-4Co-0.45C 500°F Temper	3931120 3882720	58.4 52.4	196.6 164.9	58.2 54.3	214.5 168.5
9Ni-4Co-0.45C 475°F Bainitic	3931120 3882720	79.8 82.9	242.6 255.0	81.1 90.6	362.9 280.9

6.0 TOUGHNESS TESTS VERIFICATION

This section compares the plane strain fracture toughness test results obtained with surface flawed specimens and with notched bend specimens. A majority of the fracture toughness tests of this program were conducted with notched bend specimens; however, a limited number of surface flaw specimens were tested to obtain a comparison between the two test methods.

This comparison was needed because the surface flawed specimen tests more closely approximates the types of failures that occur in service with heavy section components. Most service failures originate at surface flaws. The through-the-thickness crack of the notched bend specimen is, therefore, less realistic of actual service conditions. However, the notched bend specimen is less expensive to fabricate and test.

6.1 PROCEDURE

Two transverse grain direction surface flawed and notched bend specimens from one billet of each alloy were fabricated and tested as described in Sec. 3. The specimen billet positions were as shown in Fig. 56. The specimens of each alloy were given identical heat treatments.

6.2 RESULTS AND DISCUSSION

Figure 57 compares the notched bend and surface flawed specimen test data and Table XX lists the detailed test results. Surface flawed specimen fracture faces are shown in Fig. 58.

The K_{IC} values obtained from the two tests were within a range of 18 ksi$\sqrt{\text{in.}}$ for each alloy. The largest scatter of K_{IC} values was obtained with the billet of 300M and with the billet of H-11 Modified. If the results obtained with the latter two steels are neglected, the range of K_{IC} values was less than 10 ksi $\sqrt{\text{in.}}$ With the exception of Maraging 250, the K_{IC} values obtained with the surface flawed specimens tended to be lower than the K_{IC} values obtained with notched bend specimens.

The lower K_{IC} values can be partially explained by the fact that the surface flaw specimen more closely approximates the plane strain condition. The surface flaw periphery is longer than the notched bend specimen crack front and less constrained by the specimen surfaces. Moreover, the cross-

sectional area of the surface flawed specimen was approximately 40 percent greater than the cross-section area of the notched bend specimen.

Some of the scatter between the two tests was a consequence of billet anisotropy. The amount of forging reduction and grain refinement increases outwardly from the center of the billet. Therefore, the toughness is usually lower at the billet center. Since the surface flaw was located at the billet center (Fig. 56) and the notch of the notched bend specimen was displaced from the billet center, lower toughness values were obtained with the surface flawed specimen.

The billets of 300M and H-11 Modified, which displayed the largest amount of K_{IC} scatter (Fig. 57), received less forging work. These billets were forged from 20-inch diameter ingots, while the remaining billets were forged from 24-inch diameter ingots. This lesser amount of forging reduction caused a greater variation of toughness between the billet center and sides thus increasing the degree of test scatter.

The features on the fracture faces revealed the direction of rapid crack propagation (Fig. 58). The crack propagation of the notched specimens was primarily in the longitudinal grain direction. Crack propagation of the surface flaw was radial and varied from the longitudinal to the short-transverse grain direction. These differences of propagation direction undoubtedly have some effect on the degree of test scatter.

All the surface flawed fracture faces were similar except Maraging 250. The directional features on the fracture faces tend to indicate that the longitudinal grain direction was a preferred direction of crack growth.

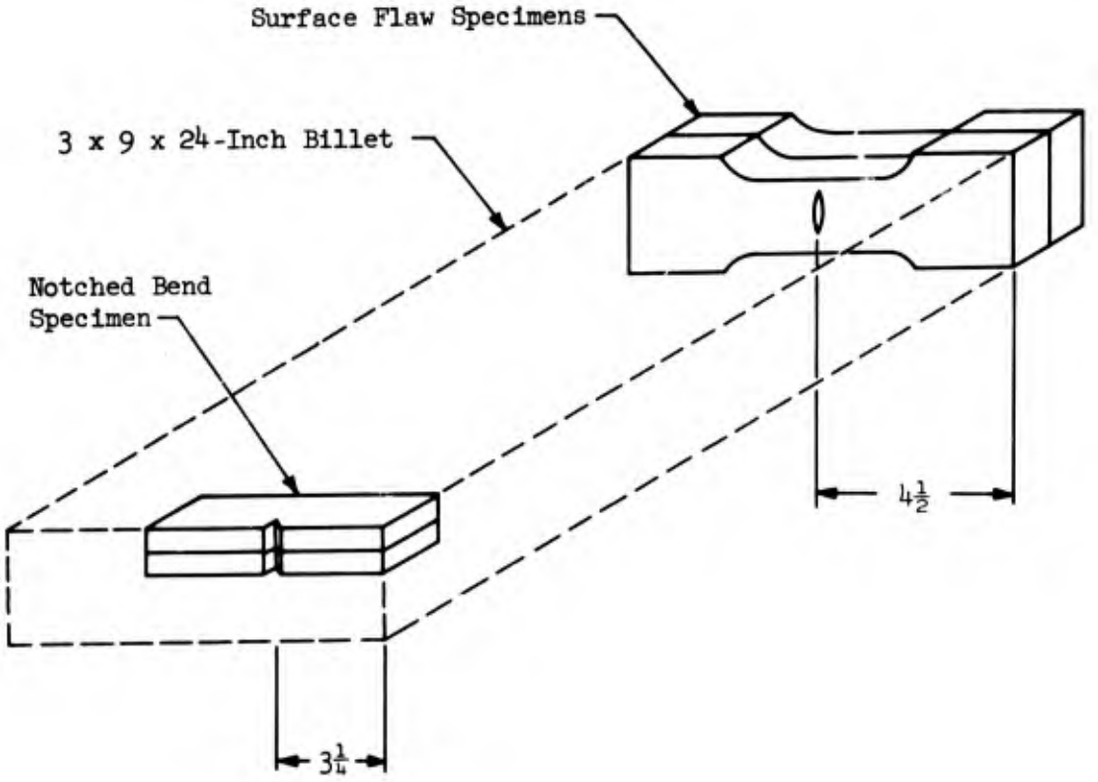

Figure 56. Notched Bend and Surface Flawed Specimen Billet Positions

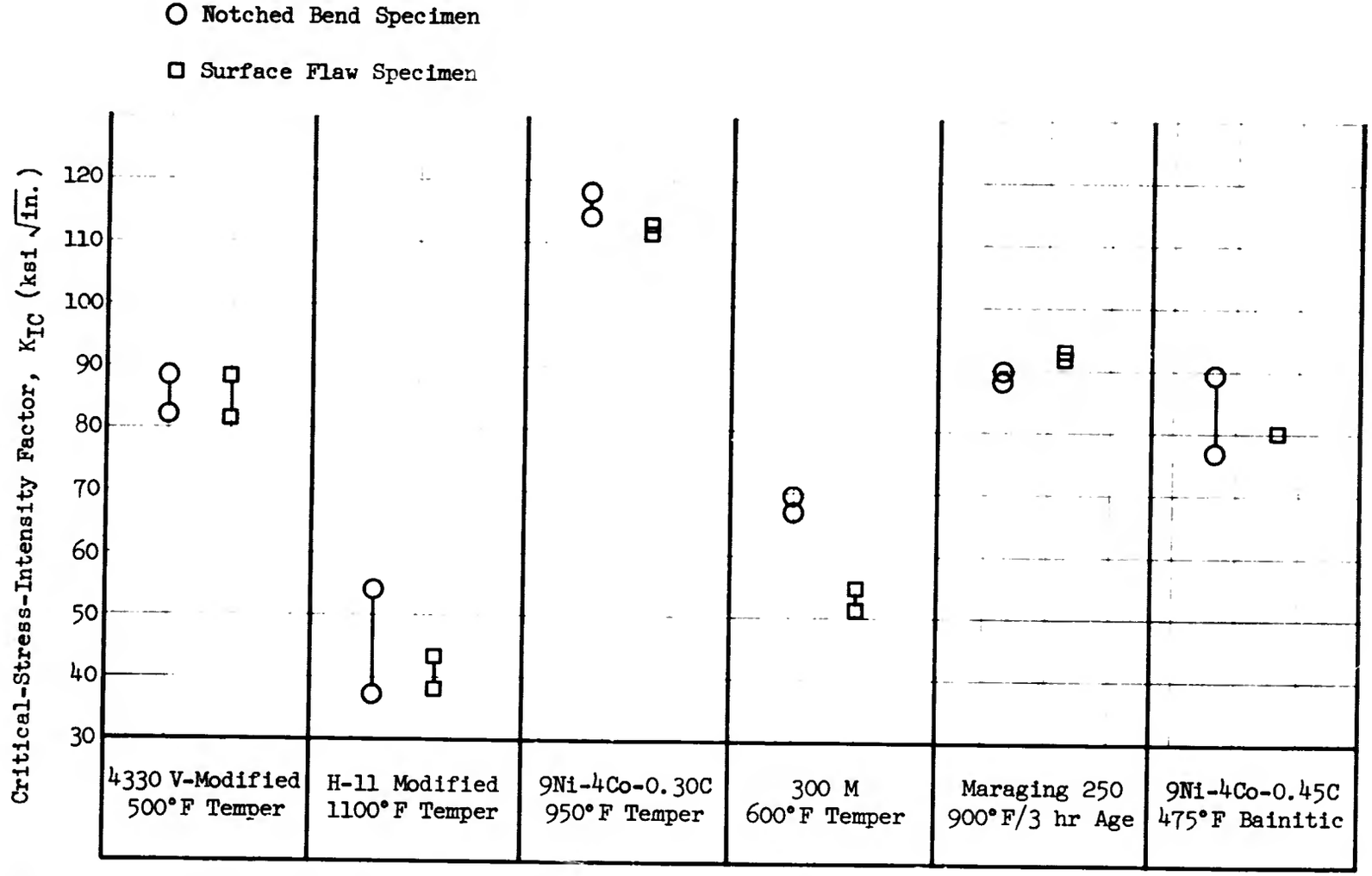

Figure 57. Comparison of Surface Flawed and Notched Bend Specimen Fracture Toughness Data

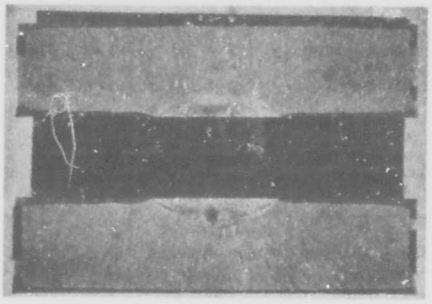

a) 300M, Specimen 63
K_{IC} = 51.1 ksi$\sqrt{in.}$

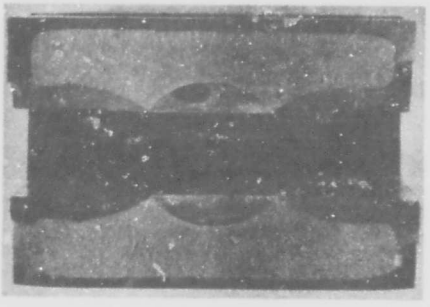

b) 4330 V-Modified,
Specimen A63
K_{IC} = 80.8 ksi$\sqrt{in.}$

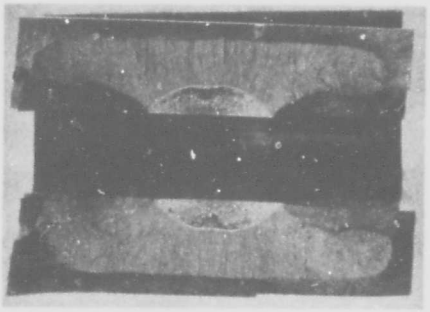

c) 9Ni-4Co-.45C
(Bainitic),
Specimen G63
K_{IC} = 79.9 ksi$\sqrt{in.}$

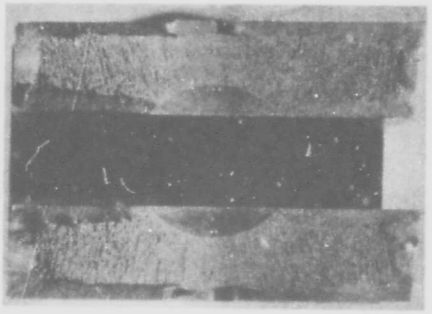

d) Maraging 250,
Specimen E63
K_{IC} = 102.3 ksi$\sqrt{in.}$

Figure 58. Surface Flawed Specimen Fracture Faces

Table XX Notched Bend and Surface Flawed Specimen Fracture Toughness Data

Alloy	Heat Number	Type Specimen	Specimen Number	a (inch)	P_{DL} (kips)	P_{max} (kips)	K_{IC} (ksi$\sqrt{in.}$)	Average K_{IC} (ksi$\sqrt{in.}$)
4330 V-Modified	3960633	Notched Bend	A86	.31	17.70	18.00	81.4	84.8
		Notched Bend	A87	.32	18.80	18.80	88.2	
		Surface Flaw	A63	.155	110.30	110.30	80.8	84.4
		Surface Flaw	A64	.155	119.10	119.10	88.0	
H-11 Modified	08990	Notched Bend	B86	.31	8.02	8.02	36.9	45.5
		Notched Bend	B87	.29	12.22	12.22	54.1	
		Surface Flaw	B63	.15	59.20	59.20	43.7	40.9
		Surface Flaw	B64	.15	52.40	52.40	38.2	
9Ni-4Co-0.30C	3931144	Notched Bend	C80	.31	24.90	25.80	114.2	116.0
		Notched Bend	C81	.30	26.10	26.20	117.9	
		Surface Flaw	C63	.15	152.00	152.00	110.8	111.7
		Surface Flaw	C64	.16	154.00	154.00	112.6	
300 M	09715	Notched Bend	D86	.33	14.38	14.58	68.8	67.6
		Notched Bend	D87	.28	15.30	16.30	66.4	
		Surface Flaw	D63	.15	70.00	70.00	51.1	52.7
		Surface Flaw	D64	.16	72.00	72.00	54.4	
Maraging 250	3930879	Notched Bend	E86	.31	21.65	22.50	99.8	98.9
		Notched Bend	E87	.33	20.50	20.70	98.0	
		Surface Flaw	E63	.17	135.00	135.00	102.3	103.2
		Surface Flaw	E64	.17	137.40	137.40	104.2	
9Ni-4Co-0.45C (Bainitic)	3882720	Notched Bend	G86	.31	16.70	17.20	76.9	83.1
		Notched Bend	G87	.31	19.40	20.30	89.4	
		Surface Flaw	G63	.155	104.00		79.8	

7.0 STRESS CORROSION SUSCEPTIBILITY

The combined action of salt water and tensile stresses has resulted in delayed failures of high strength steels (Ref. 9). Failures of this type are commonly called "stress corrosion" failures and are ordinarily thought to occur by a two-step process; crack initiation and crack-growth. To evaluate the susceptibility of six high strength steel alloys to the combined processes of crack-initiation and crack-growth, alternate immersion testing was performed with smooth, statically stressed specimens. The susceptibility of the steels to crack-growth was evaluated with precracked notched bend specimens which were sustained-loaded in salt water at stress-intensity levels (K_{Ii}) below the critical-stress-intensity level (K_{IC}).

This section of the report describes the results of both the alternate immersion and crack-growth susceptibility tests. To simplify the discussion, the results of the two tests are discussed separately.

7.1 ALTERNATE IMMERSION TESTS

7.1.1 Procedure

Specimens from two heats of 9Ni-4Co-0.45C and specimens from three heats of 4330 V-Modified, 300M, and 9Ni-4Co-0.30C were alternate immersion tested in a 3.5 percent NaCl solution as described in Sec. 3.0. All the specimens were taken from the transverse grain direction of the billets. Neither the Maraging-250 or the H-11 Modified alloys were tested because vacuum melted heats of these alloys had previously been tested at Boeing (Ref. 20). The heat treatments for the specimens are listed in Table V. Preparation of the specimens was carefully controlled to minimize differences of surface condition between the specimens, since the susceptibility of a material is affected by the surface condition (Ref. 9).

With the exception of the alloy 9Ni-4Co-0.45C (Bainitic), the specimens were loaded to 80 percent of the yield strength. The 9Ni-4Co-0.45C (Bainitic) specimens were loaded to 86 percent of their yield strength.

7.1.2 Results and Discussion

Table XXI lists the test results and Fig. 59 graphically illustrates the results by showing the scatter bands of time-to-failure. Because the times-to-failure were about the same (Fig. 59), it was not possible to differentiate between the susceptibilities of 9Ni-4Co-0.30C and 9Ni-4Co-0.45C (Bainitic) alloys. However, study of the data shows that these alloys were less susceptible than the 9Ni-4Co-0.45C (Quench and Temper), 300M or 4330 V-Modified alloys. Data from previous work (Ref. 20) indicates that the resistance of the Maraging 250 steel to stress corrosion is as good or better than that of 9Ni-4Co-0.30C and 9Ni-4Co-0.45C (Bainitic). Past work (Table XXI) has also shown that the H-11 Modified (190 ksi yield strength) has slightly better resistance to stress corrosion than 4330 V-Modified (195 ksi yield strength).

7.2 CRACK-GROWTH SUSCEPTIBILITY TESTS

7.2.1 Procedure

The procedure used for the sustained-load tests of fracture toughness specimens in salt water is described in Sec. 3. A minimum of three specimens were tested per heat of each alloy. All of the specimens were taken from the transverse grain direction of the billets. Most of the testing was conducted in a 3.5 percent NaCl distilled water solution. However, a few specimens of 300M and 4330 V-Modified were sustained loaded in room temperature air (25-35 percent relative humidity).

The NaCl concentration of the solution that was poured into the tank surrounding the specimen (Fig. 10) ranged from 3 to 4 percent, and the pH of the solution ranged from 5 to 7. These variations of solution condition were not detected until a majority of the testing had been completed. The differences of pH originated from the distilled water that was used to make up the salt solutions. Distilled water which was allowed to age for several weeks in atmospheric air had a pH of 5-6, whereas unaged distilled water generally had a pH of about 7. These changes of pH may have affected the susceptibility of the steels. If so, the differences of pH undoubtedly had some effect on the degree of test scatter. The condition of the solution was also influenced by residual salt and corrosion products left in the tank from previous tests. The tanks were not equipped with drain plugs, consequently it was not possible to thoroughly rinse and clean the tanks prior to each test.

During testing, evaporation caused the level of solution in the tank to drop. Consequently it was necessary to pour additional solution into the tank after about 4,000 minutes of test time. Initially 3.5 percent NaCl solution was added to the tank. However, during latter stages of the program, the tanks were replenished with distilled water. Although the NaCl concentrations of the fresh solutions were generally within a range of 3-4 percent, variation of the refill procedure and salt in the tank from previous tests caused the NaCl concentration to vary from about 2-7 percent (Table XXIX).

7.2.2 Results

The detailed results of the testing are given in Tables XXII through XXVIII. NaCl concentration and pH measurement taken are recorded in Table XXIX.

Several heats with different K_{IC} values were evaluated per alloy. At equivalent K_{Ii} levels, a specimen from a heat with a low K_{IC} value would be expected to fail in a shorter time than a specimen from a heat with a higher K_{IC} value, because the specimens from the higher toughness heat can tolerate a longer crack. To normalize for the differences of fracture toughness between the heats, the initially applied stress intensity level, K_{Ii}, was divided by the average transverse grain direction K_{IC} value of the heat being tested. However, the K_{IC} values of a heat varied because of billet anisotropy (see Sec. 5.0). If the K_{IC} value of a specimen was higher or lower than the average K_{IC} value, the value of K_{Ii}/K_{IC} was in error. The magnitude of this error was estimated to range from 0-10%.

Plots of "K_{Ii}/K_{IC} vs. time-to-failure" are presented in Figs. 60 through 66. These plots show scatter bands of data points for each alloy. Smooth curves were drawn through the approximate centers of this scatter bands. These smooth curves were then combined into a single plot (Fig. 67) so that the environmental sustained-loading characteristics of the alloy could be easily compared. To illustrate how the times-to-failure depend on the K_{Ii} level, the curves of "K_{Ii}/K_{IC} vs. time-to-failure" (Fig. 67) were converted to curves of "K_{Ii} vs. time-to-failure" (Fig. 68). This conversion was performed by multiplying K_{Ii}/K_{IC} by the average K_{IC} value of each alloy.

7.2.3 Threshold Levels

Threshold levels below which no crack growth occurred were established in 25-35 percent relative humidity air for the 300M and 4330 V-Modified steels. At K_{Ii}/K_{IC} levels less than about 0.85 (Figs. 60 and 63), there was no observable crack growth in air after 10,000 minutes of sustained loading. However, definite threshold values were not established in salt water for Maraging 250 and 9Ni-4Co-0.30C, since all specimens for these alloys displayed some crack growth. Specimens of 4330 V-Modified, H-11 Modified, 300M, and 9Ni-4Co-0.45C were loaded at low enough K_{Ii} levels to prevent crack growth. Therefore, it was possible to make an estimate of the threshold level. These approximations are summarized below:

Alloy	Ultimate Strength (ksi)	Estimated Threshold Level (ksi $\sqrt{\text{in.}}$)
4330 V-Modified	239	25
H-11 Modified	219	30
9Ni-4Co-0.30C	231	45
300M	283	13
Maraging 250	259	45
9Ni-4Co-0.45C (Q&T)	276	15
9Ni-4Co-0.45C (B)	266	20

These data show that almost all the alloys were susceptible to crack growth at relatively low K_{Ii} values. However, examination of Fig. 68 shows that at equivalent K_{Ii}/K_{IC} levels there were marked differences of the times-to-failure. For example, at a $K_{Ii}/K_{IC} = 0.6$, the 9Ni-4Co-0.45C (Quench-Temper) specimens failed in about 250 minutes, while the 9Ni-4Co-0.45C (Bainitic) specimens failed in about 3,000 minutes. These variations of time-to-failure were apparently caused by differences in the fracture characteristics.

7.2.4 Crack Growth Characteristics

The combined action of the salt water and sustained-load caused slow crack growth to originate from the tip of the notched bend specimen fatigue crack. This slow growth continued until the crack grew to the critical length necessary for fast crack-growth and failure. The areas of fatigue, slow, and

fast crack growth were visible on the fracture faces that were immediately removed from the salt water after failure and dried. Figures 68 through 80 show the different types of crack growth that were observed. Because all of the specimens were not directly removed from the salt water after failure, general corrosion sometimes obscured the slow crack growth. Also the shapes of the slow-growth crack fronts were often irregular. Therefore, the final crack depth measurements listed in Tables XXII through XXVIII can only be considered as estimates.

Study of the fractured specimens revealed that some of the cracks tended to grow by a branching process rather than at right angles to the axis of the specimens. Figures 81 and 82 show typical examples of crack branching. This crack branching behavior was apparently related to the size of the plastic zone at the tip of the crack.

The size of the plastic zone increases with increasing K_{Ii} levels and decreases with increasing yield strength (Ref. 7). The 300M and 9Ni-4Co-0.45C specimens, which had yield strengths greater than 215 ksi did not display any branching at low K_{Ii} levels. However, as the crack grew and the stress intensity at the tip of the crack increased, the tendency for the crack to grow by branching increased.

The Maraging 250 specimens, which had the highest yield strengths of any of the alloys tested, seldom displayed any evidence of crack branching. The H-11 Modified specimens also showed no evidence of crack branching. This was understandable, since the H-11 Modified specimen had low K_{IC} values and were thus subject to low values of stress intensity. The 4330 V-Modified and 9Ni-4Co-0.30C steels, which had relatively low yield strength and high K_{IC} values exhibited the most pronounced crack branching. When crack branching occurred, the cracks tended to grow more rapidly at the sides of the specimens (Fig. 69a & 73a).

Crack branching appeared to influence the times-to-failure. The initially flat portions of some of the curves (Fig. 68) illustrate this. At high K_{Ii} levels the initial degree of plastic yielding at the crack tip was higher and the curves were nearly flat. At lower K_{Ii} levels, where the initial degree of plastic yielding was lower, the curves rapidly dropped off.

The initially flat portions of the curves also suggested that there may have been an incubation period required for crack growth initiation (Ref. 21).

Further, work should include a study of the effect of plastic yielding at the crack tip. Also the time required for crack growth initiation should be studied.

When the final crack lengths and times in solution of 9Ni-4Co-0.30C and 4330 V-Modified specimens were compared at equivalent K_{Ii} levels, it appeared that the 9Ni-4Co-0.30C specimens had experienced a slower rate of crack growth. Fracture faces of the H-11 Modified showed only a slight amount of crack growth (Fig. 71). However, the low fracture toughness of H-11 Modified steel allowed for only a slight increase of crack length before failure.

Study of the time to failure data for the alloys with ultimate strength greater than 250 ksi showed that the 9Ni-4Co-0.45C (Bainitic) and Maraging 250 steels were more resistant to failure in the salt water environment than the 9Ni-4Co-0.45C (Quench and Temper) or 300M alloys.

7.2.5 Mode of Crack Growth

Fractographs of different crack growth regions are shown in Figs. 69 through 80. Corrosion products on some of the fracture surfaces obscured the topography of the fracture faces. However, it was observed that, with the exception of Maraging 250, the slow crack propagation was intergranular. The slow crack growth on the fracture faces of Maraging 250 was transgranular. The rapid crack growth that occurred during failure was observed to be transgranular.

Some of the fracture faces displayed a ductile band between the region of fatigue crack growth and slow crack growth (Fig. 74). It is not known if this ductile growth occurred before or after the salt water was added to the tank surrounding the specimen. Often areas of mixed intergranular and ductile growth were observed in the region of slow to fast growth.

* Data From Report No. ML-TDR-64-3, "Investigation of the Effect of Stress Corrosion on High Strength Steel Alloys," G. A. Dreyer

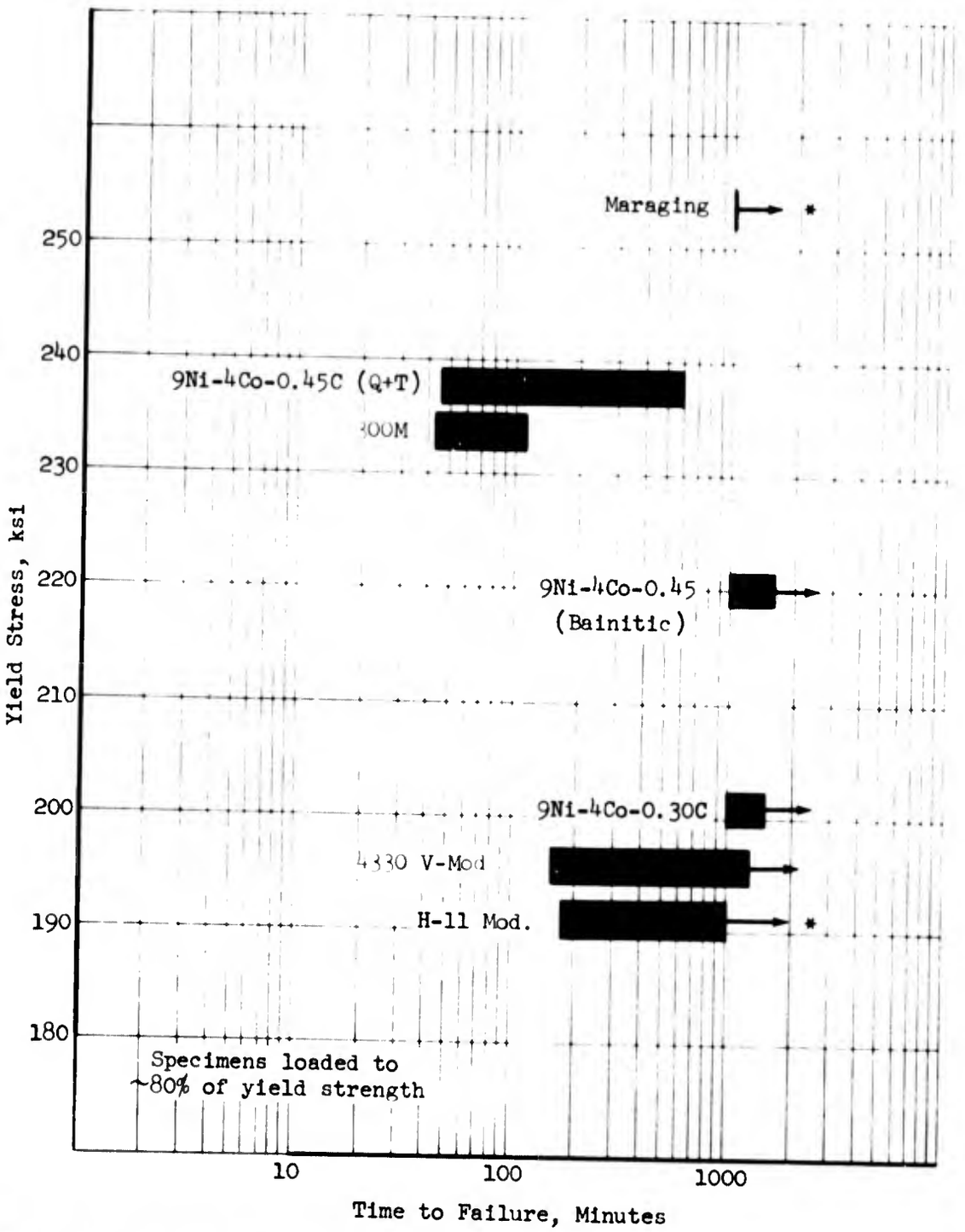

Figure 59. Alternate Immersion Data

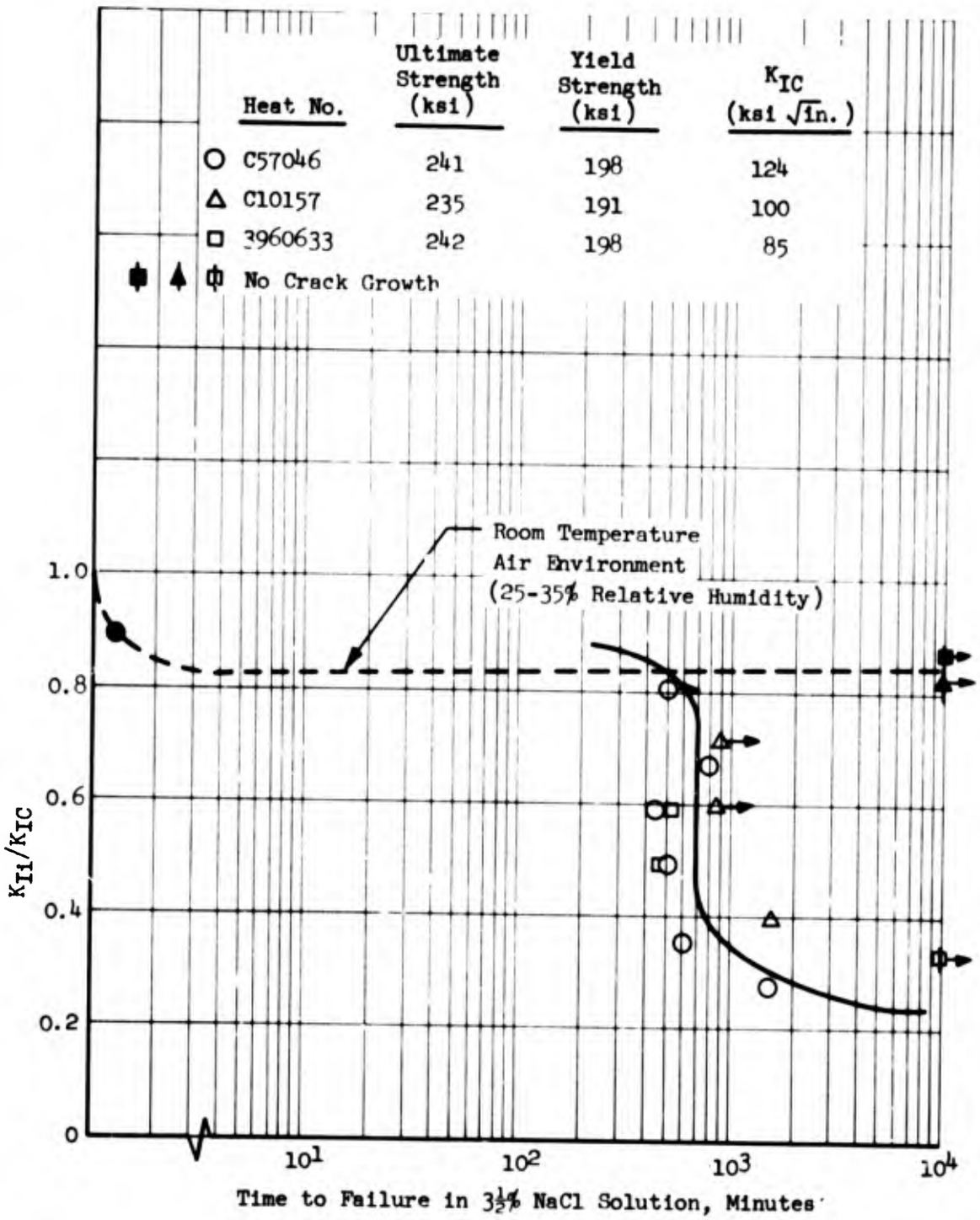

Figure 60. Sustained-Loading Characteristics of 4330 V-Modified

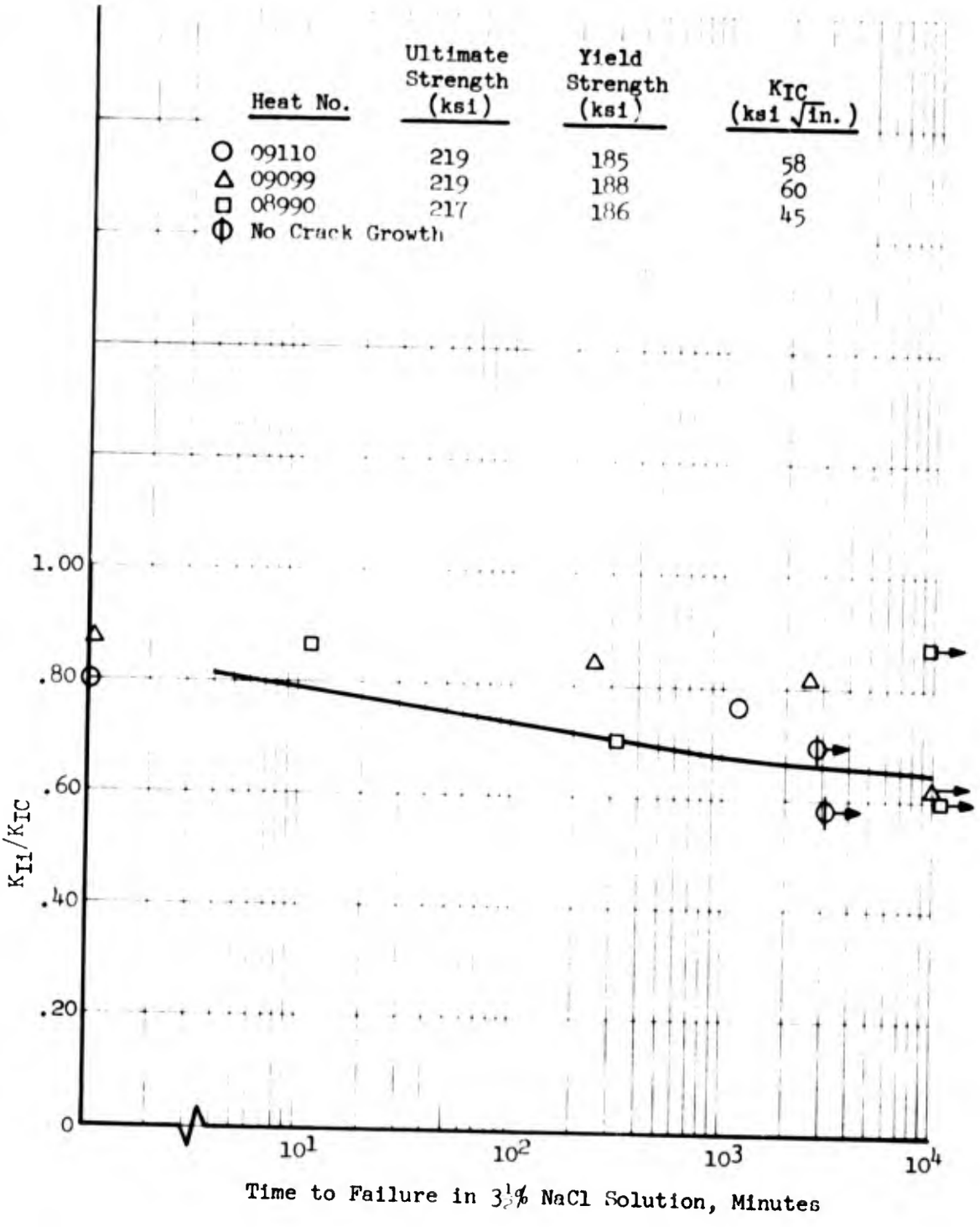

Figure 61. Sustained-Loading Characteristics of H-11 Modified

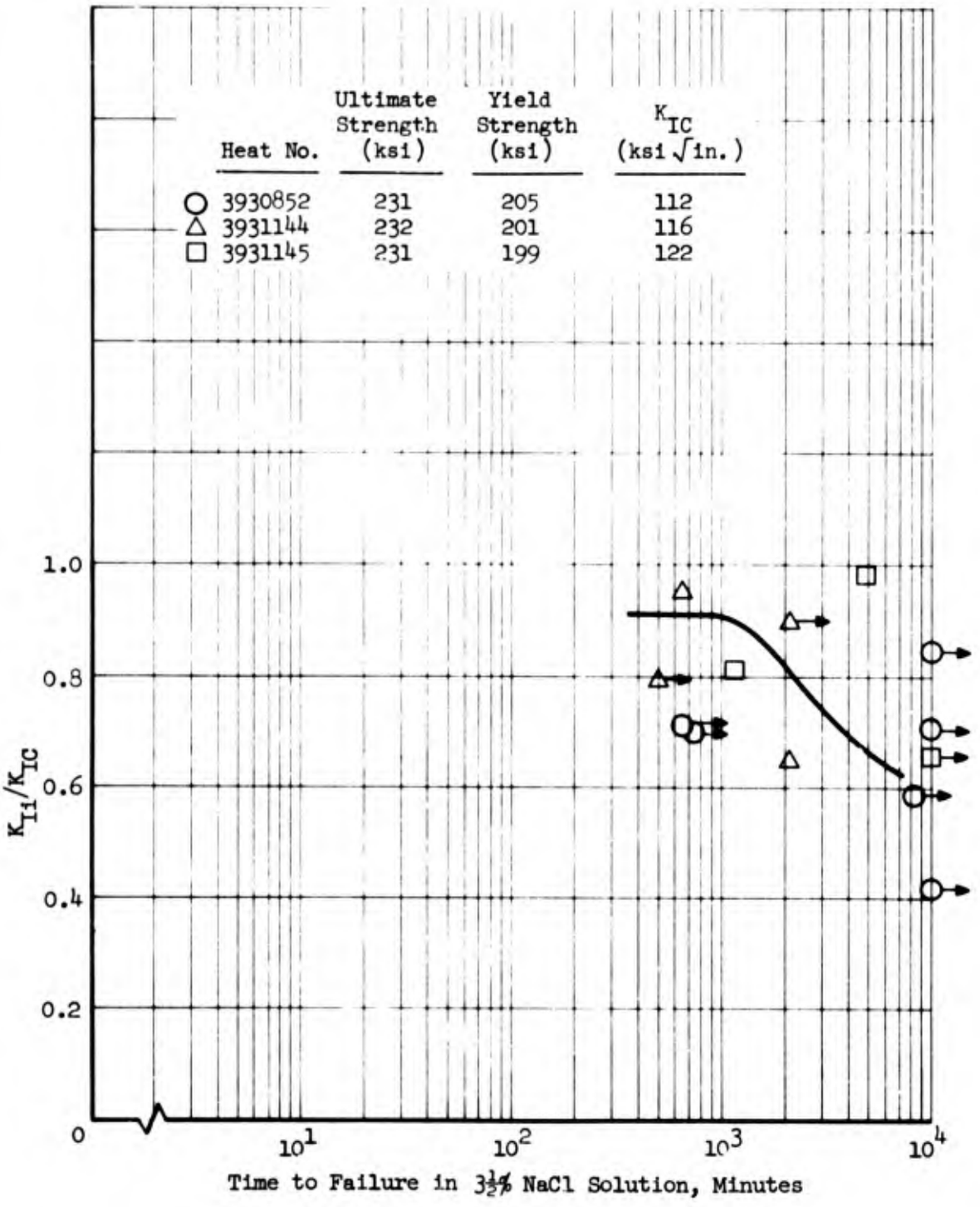

Figure 62. Sustained-Loading Characteristics of 9Ni-4Co-0.30C

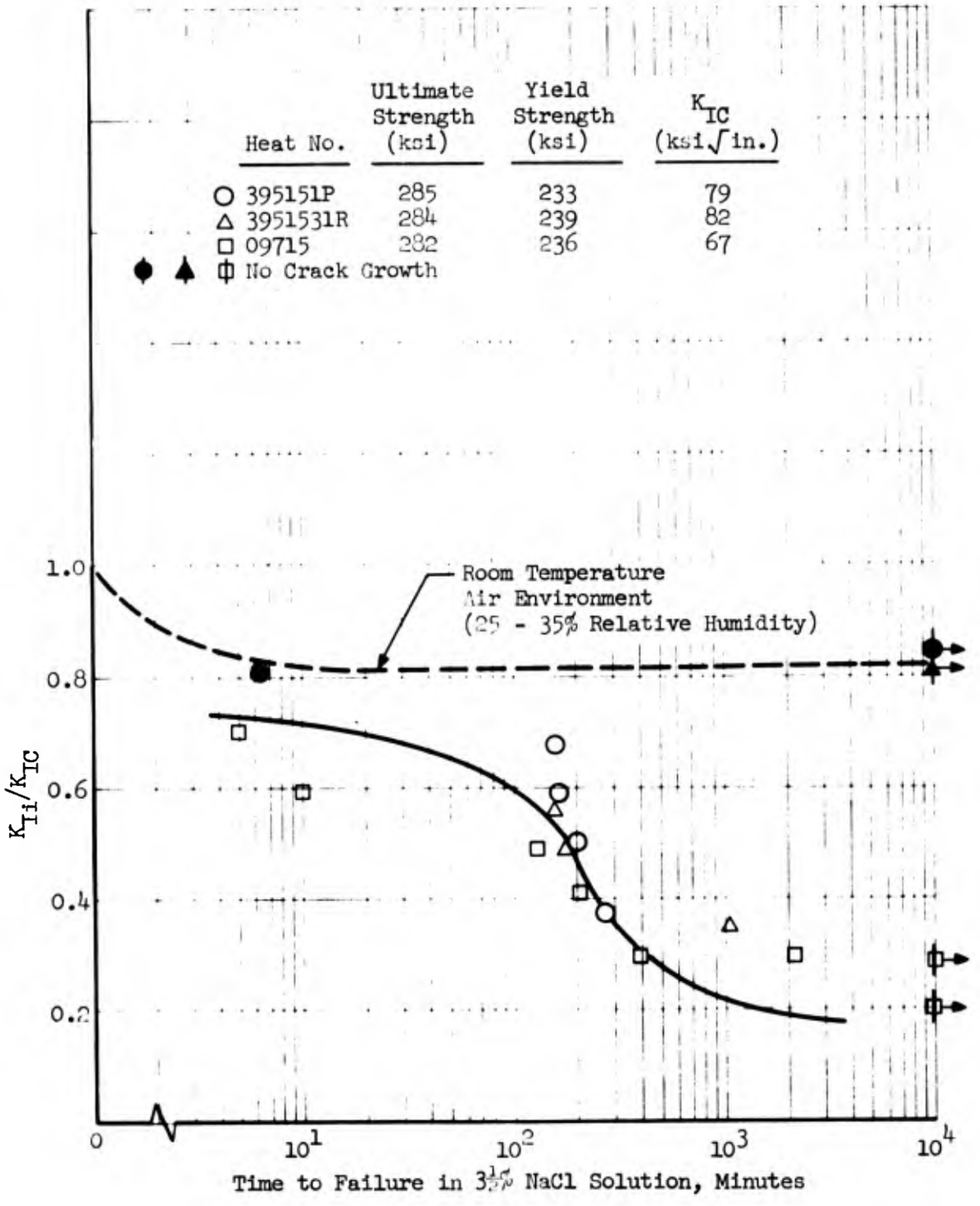

Figure 63. Sustained-Loading Characteristics of 300M

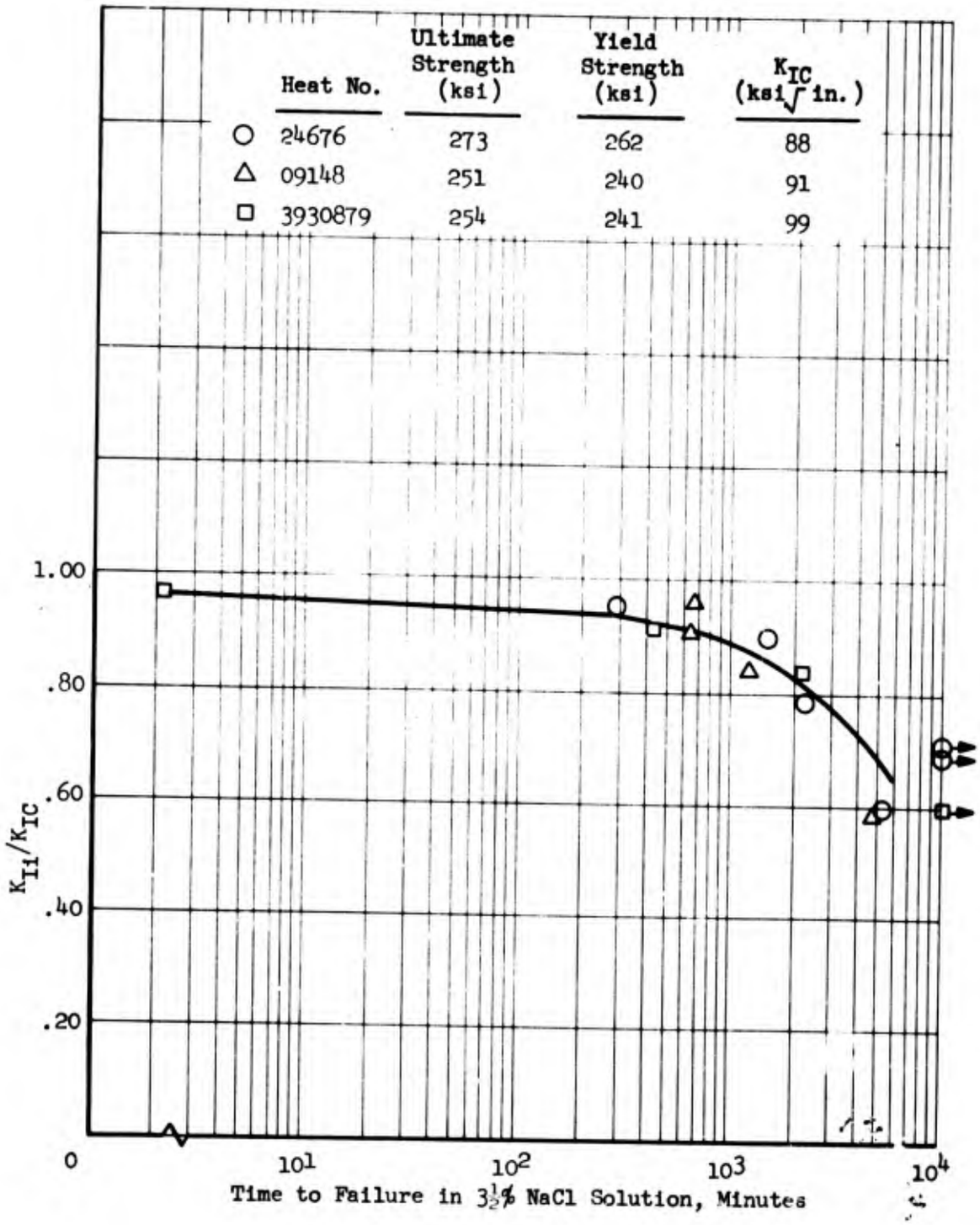

Figure 64. Sustained-Loading Characteristics of Maraging 250

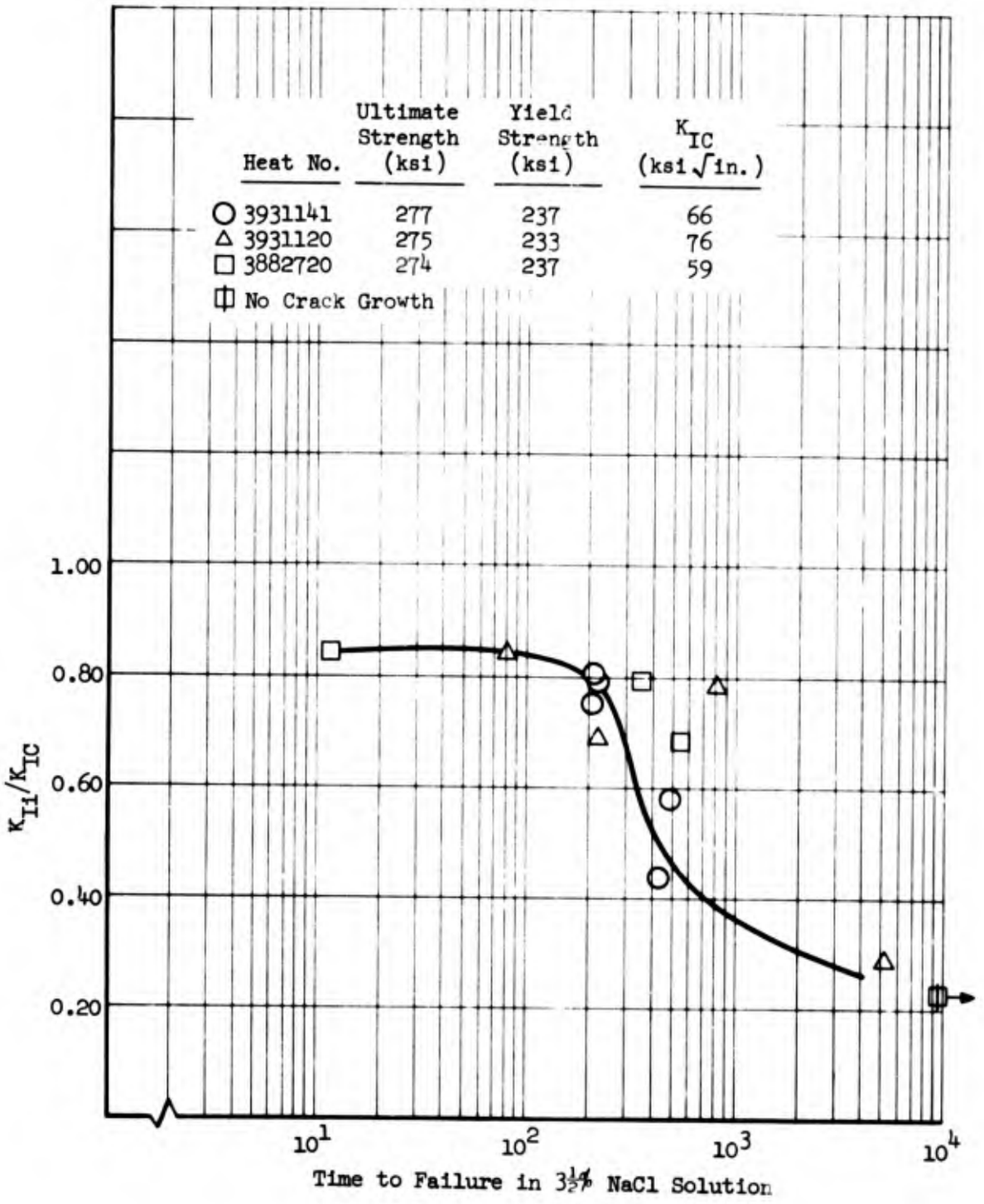

Figure 65. Sustained-Loading Characteristics of Quench-Tempered 9Ni-4Co-0.45C

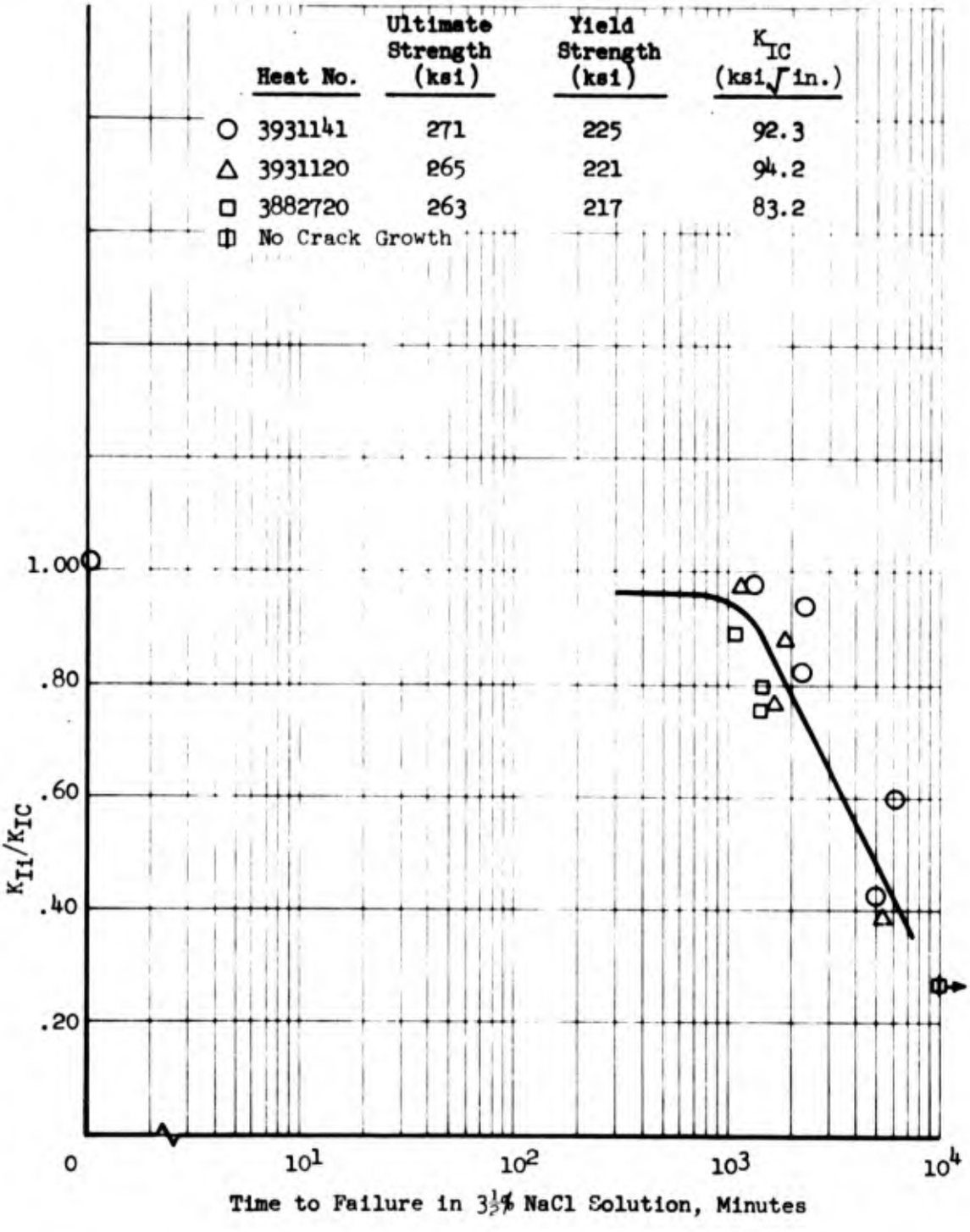

Figure 66. Sustained-Loading Characteristics of Bainitic 9Ni-4Co-0.45C

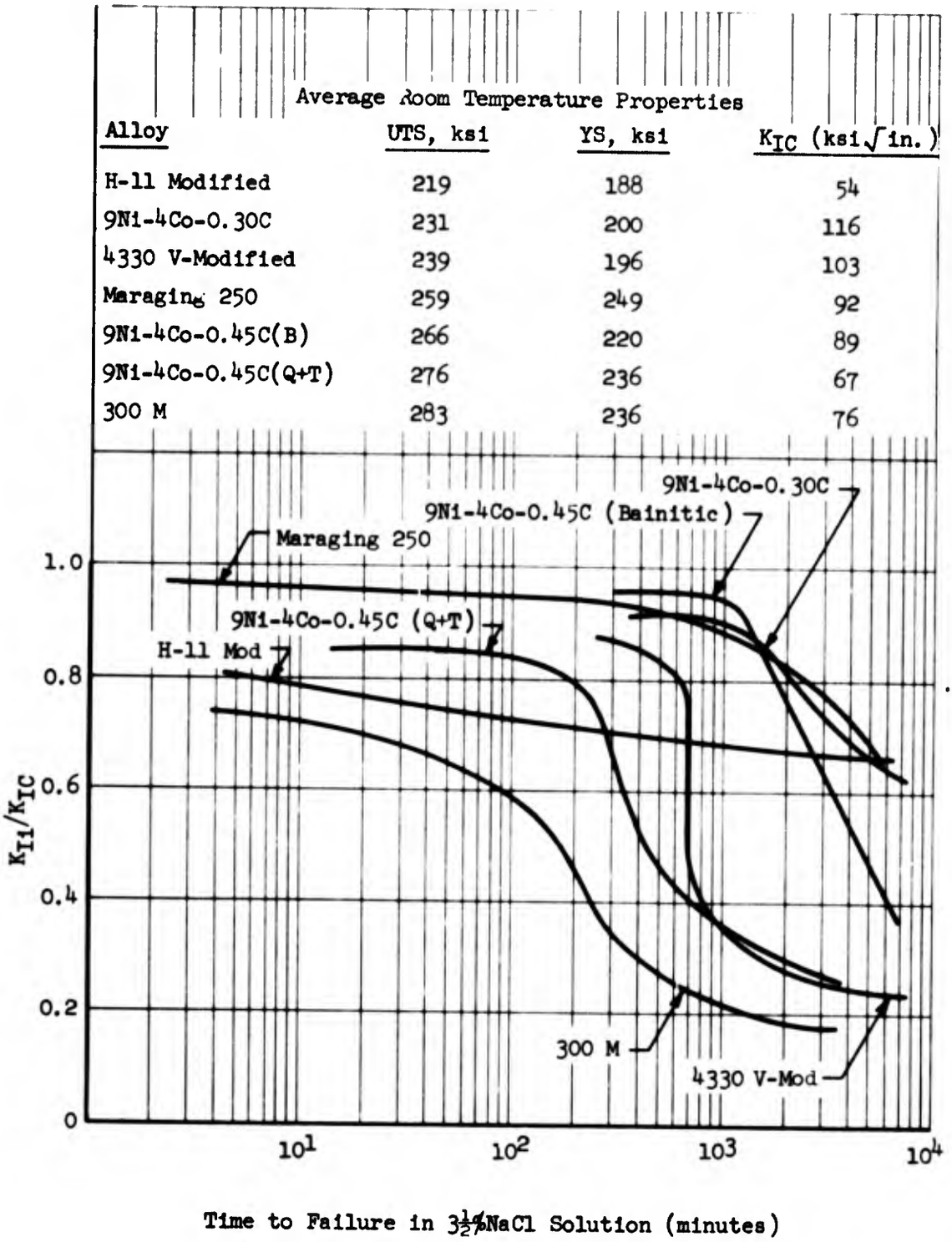

Figure 67. Summary of Sustained-Loading Characteristics

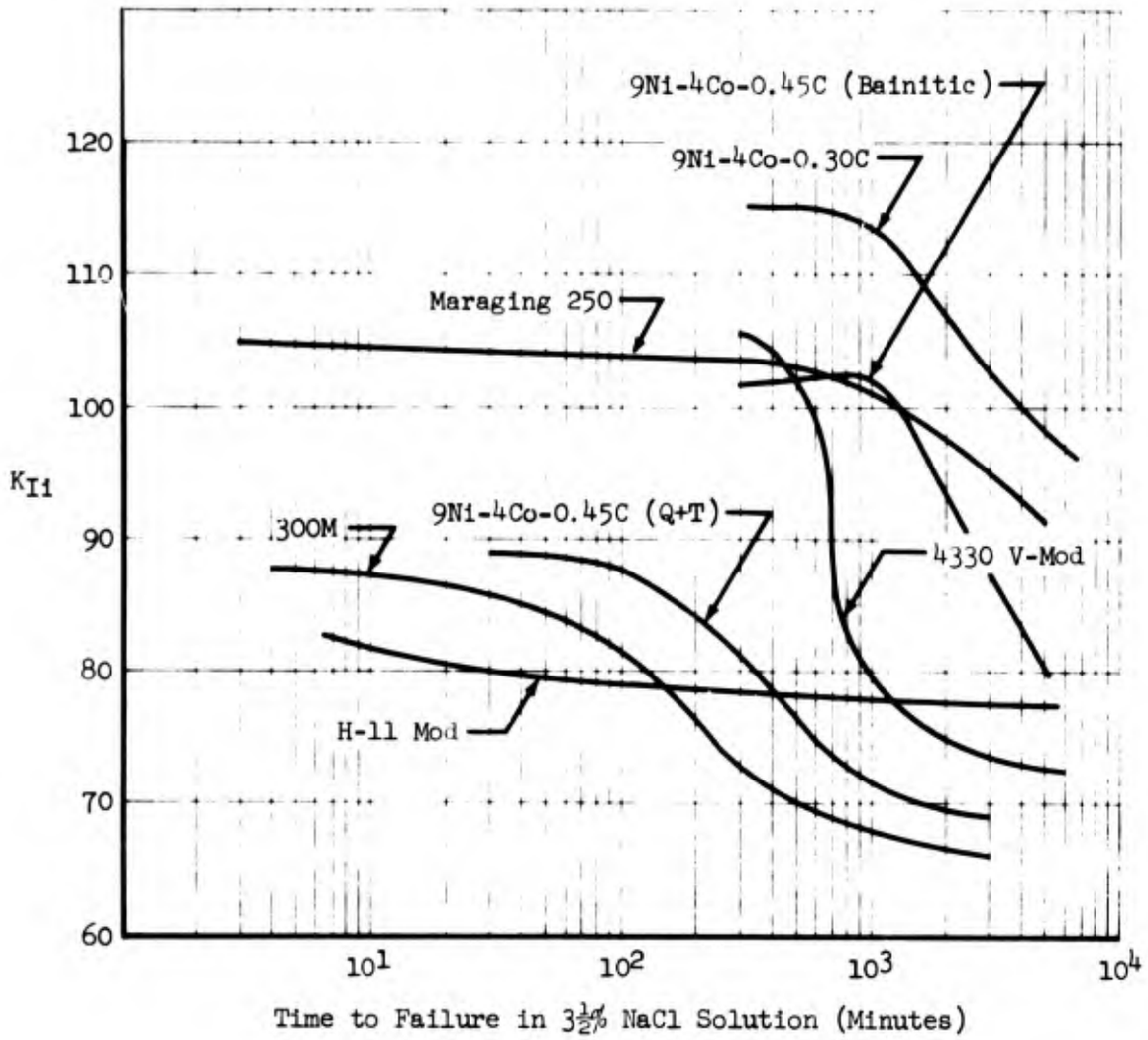

Figure 68. Sustained-Loading Characteristics as Function of K_{Ii}

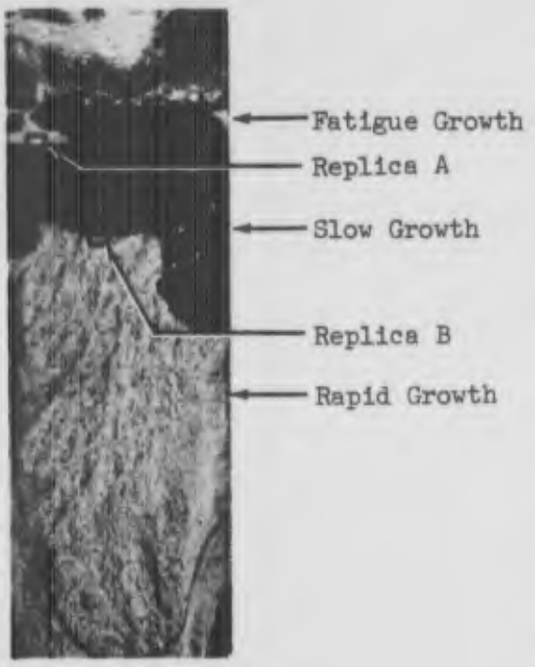

a) Fracture Face
Mag: 3X

b) Replica A, Fatigue to
Slow Growth Region
Mag: 3860X

c) Replica A, Intergranular
Slow Growth Region
Mag: 3860X

d) Replica B, Slow to Rapid
Growth Region
Mag: 3860X

Figure 69. Fracture Face and Electon Fractographs of 4330 V-Modified Specimen A83, K_{Ii} = 58.6 ksi $\sqrt{in.}$, 869 minutes in 3½% NaCl Solution

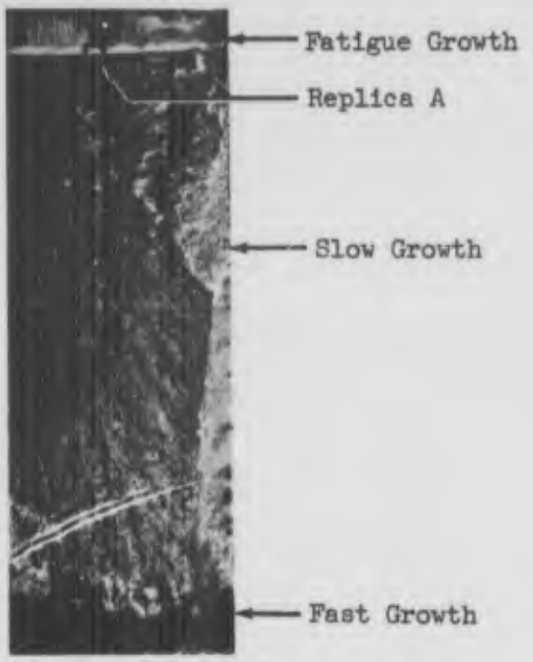

a) Fracture Face
Mag: 3X

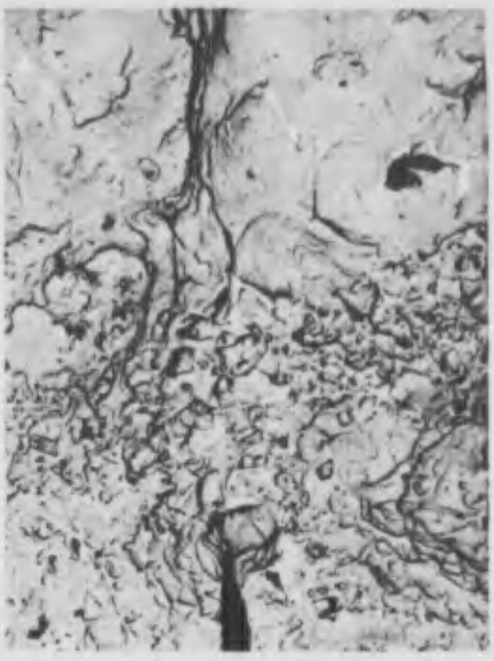

b) Replica A, Fatigue to Ductile Growth Region
Mag: 3860X

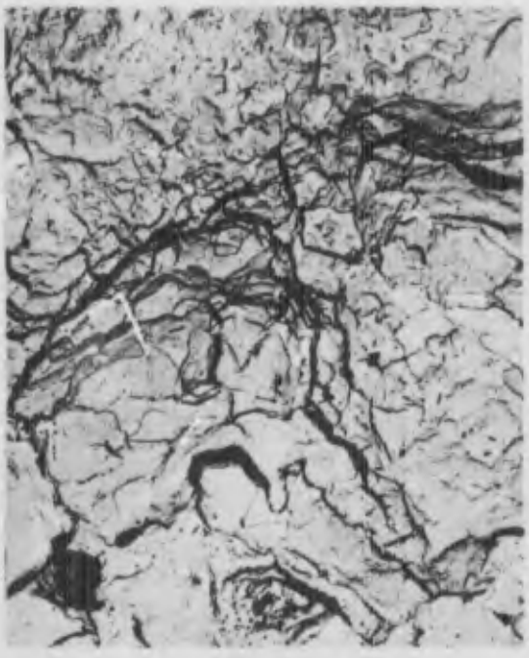

c) Replica A, Ductile Band Between Fatigue and Interangular Growth Regions
Mag: 3860X

d) Replica A, Intergranular Slow Growth Region
Mag: 3860X

Figure 70. Fracture Face and Electron Fractographs of 4330 V-Modified Specimen A74, K_{Ii} = 43.9 ksi $\sqrt{in.}$, 638 minutes in 3½% NaCl Solution

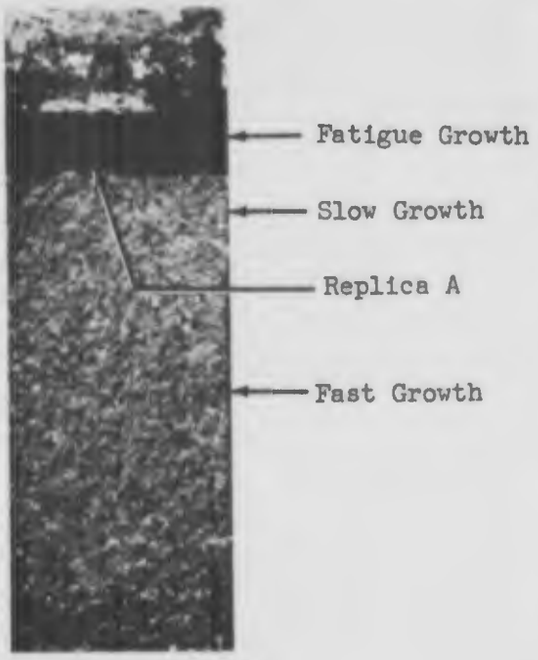

a) Fracture Face
Mag: 3X

b) Replica A, Fatigue to
Slow Growth Region
Mag: 3860X

c) Replica A, Slow
Growth Region
Mag: 3860X

d) Replica A, Slow to Fast
Growth Region
Mag: 3860X

Figure 71. Fracture Face and Electron Fractographs of H-11 Modified Specimen B90, K_{IC} = 40.2, 9868 Minutes in 3½% NaCl Solution

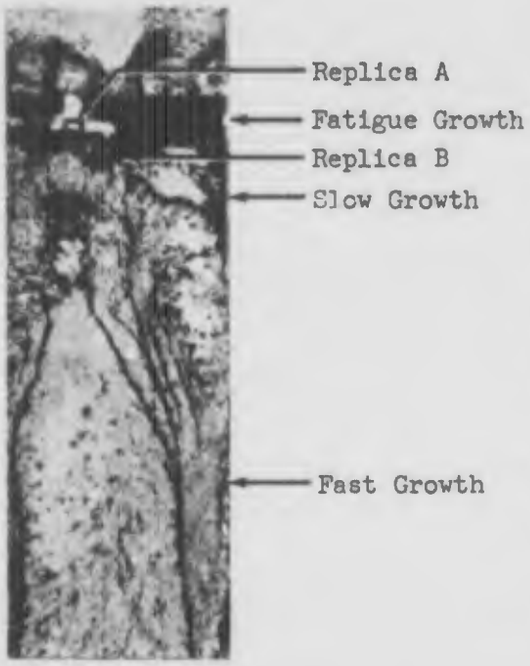

a) Fracture Face
Mag: 3X

b) Replica A, Fatigue to Slow Growth Region
Mag: 3860X

c) Replica A, Ductile Growth Region

d) Replica B, Intergranular Slow Growth Region
Mag: 3860X

Figure 72. Fracture Face and Electron Fractographs of 9Ni-4Co-0.30C Specimen C90, K_{IC} = 119.2 ksi $\sqrt{in.}$, 4821 Minutes in 3½% NaCl Solution

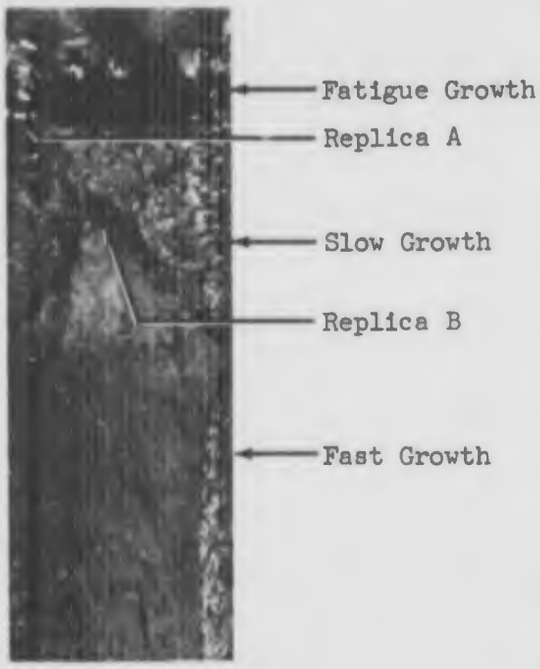

a) Fracture Face
Mag: 3X

b) Replica A, Fatigue to Intergranular Slow Growth Region
Mag: 3860X

c) Replica A, Intergranular Slow Growth Region
Mag: 3860X

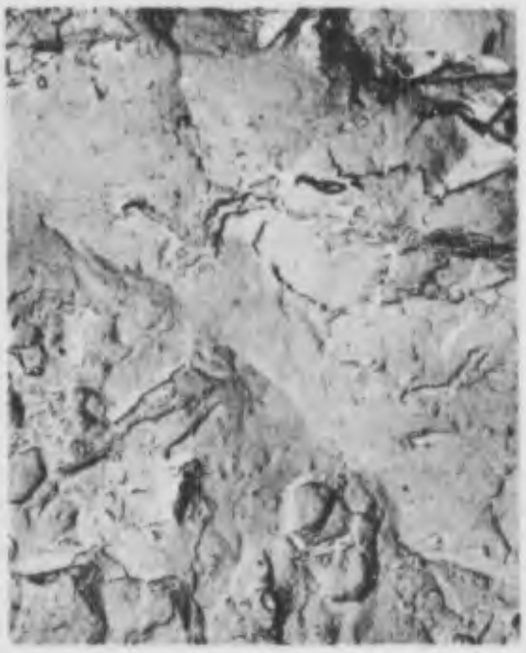

d) Replica B, Slow to Fast Growth Region
Mag: 3860X

Figure 73. Fracture Face and Electron Fractographs of 9Ni-4Co-0.30C Specimen C-75, K_{II} = 66.2 ksi $\sqrt{in.}$, 8325 Minutes in 3½% NaCl Solution

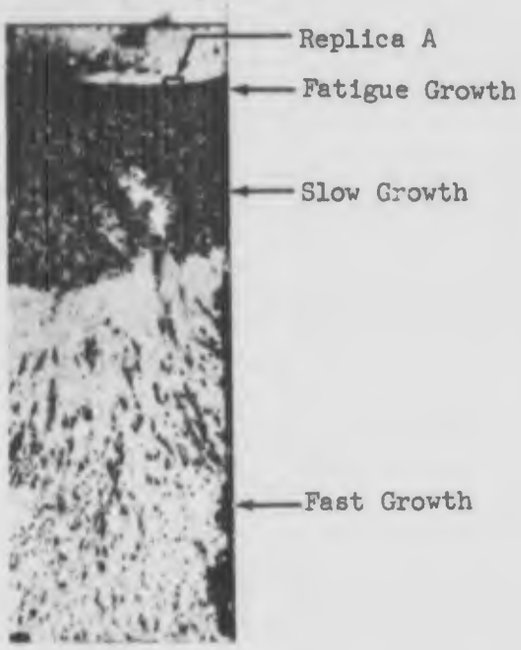

a) Fracture Face
Mag: 3X

b) Replica A, Fatigue to
Ductile Growth Region
Mag: 3860X

c) Replica A, Ductile Growth
to Intergranular Slow Growth
Mag: 3860X

d) Replica A, Intergranular
Slow Growth Region
Mag: 3860X

Figure 74. Fracture Face and Electron Fractographs of 300M Specimen D89, K_{II} = 47.3, 48 Minutes in 3½ NaCl Solution

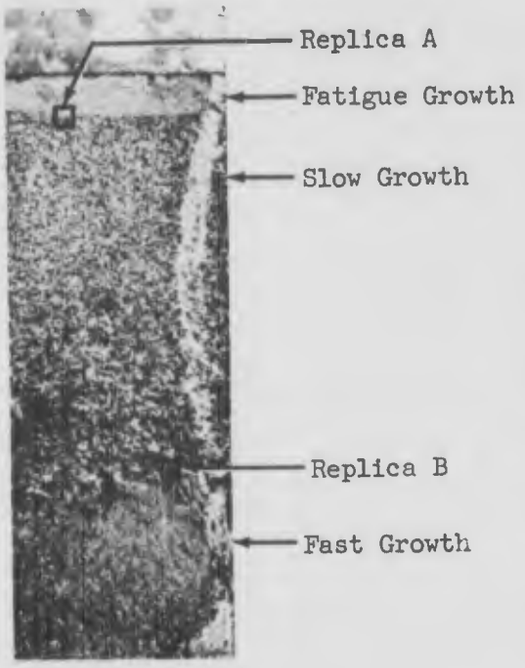

a) Fracture Face
Mag 3X

b) Replica A, Fatigue to Inter - granular Slow Growth Region
Mag: 3860X

c) Replica A, Intergranular Slow Growth Region
Mag: 3860X

d) Replica B, Slow Growth Region
Mag 3860X

Figure 75. Fracture and Electron Fractographs of 300M Specimen D87A, K_{Ii} = 20.2 ksi $\sqrt{in.}$, 201 Minutes in 3½ NaC l Solution

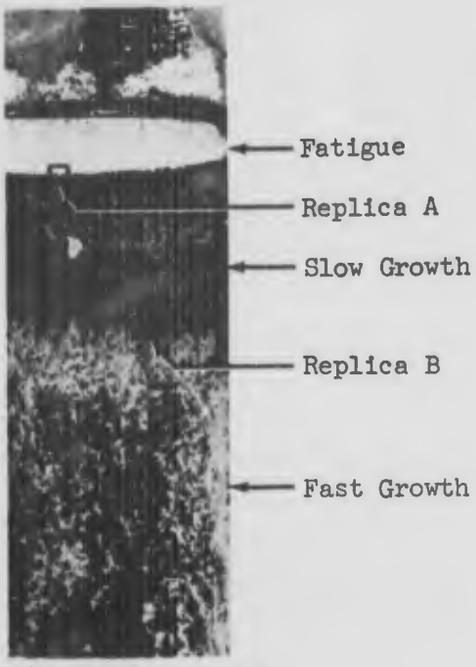

a) Fracture Face
Mag: 3X

b) Replica A, Fatigue to Slow Growth Region
Mag: 3860X

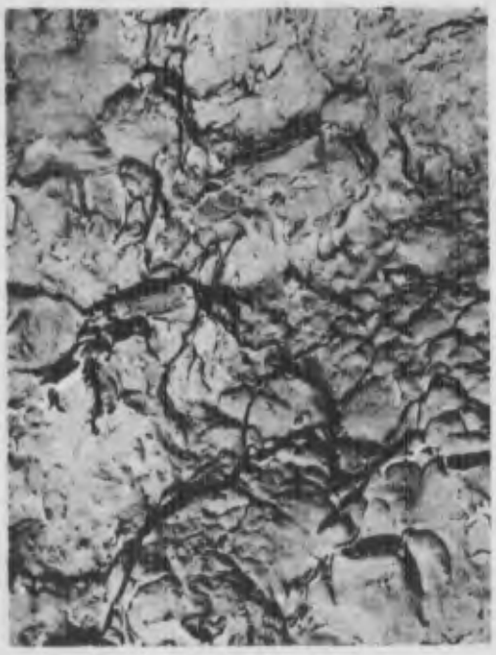

c) Replica A, Slow Growth Region
Mag: 3860X

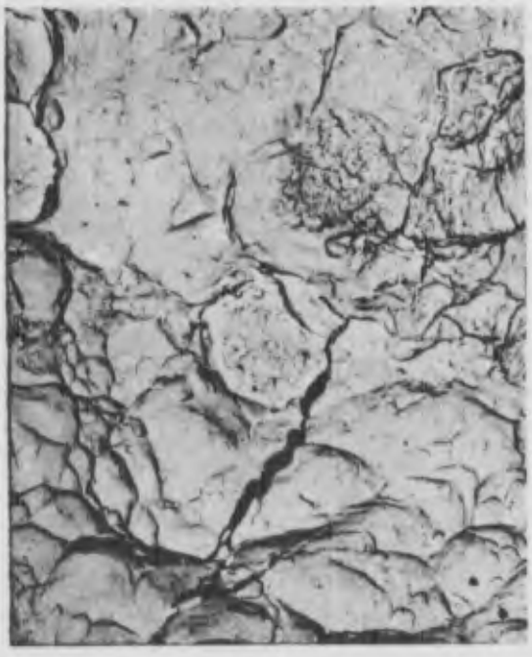

d) Replica B, Fast Growth Region
Mag: 3860X

Figure 76. Fracture Face and Electron Fractographs of Maraging 250 Specimen E74, K_{Ii} = 69.1 ksi $\sqrt{in.}$, 2336 Minutes in 3½% NaCl Solution

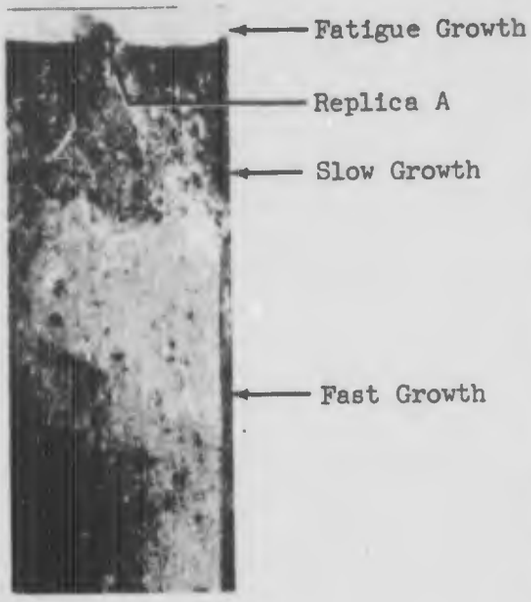

a) Fracture Face
Mag: 3X

b) Replica A, Fatigue to
Ductile Growth

c) Replica A, Ductile Growth
to Intergranular
Slow Growth Region
Mag: 3860X

d) Replica A, Intergranular
Slow Growth Region
Mag: 3860X

Figure 77. Fracture Face and Electron Fractographs of Quench-Temper 9Ni-4Co-0.45C Specimen F82, K_{Ii} = 55.7 ksi $\sqrt{in.}$, 83 Minutes in 3½% NaCl Solution

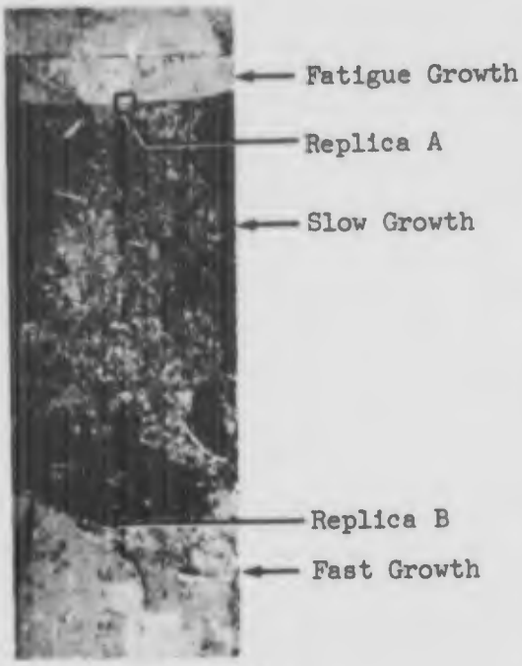

a) Fracture Face
Mag: 3X

b) Replica A, Fatigue to Slow Growth Region
Mag: 3860X

c) Replica A, Intergranular Slow Growth Region
Mag: 3860X

d) Replica B, Intergranular Slow Growth Region
Mag: 3860X

Figure 78. Fracture Face and Electron Fractographs of Quench-Temper 9Ni-4Co-0.45C Specimen F85, K_{Ii} = 19.8, 5023 Minutes in 3½% NaCl Solution

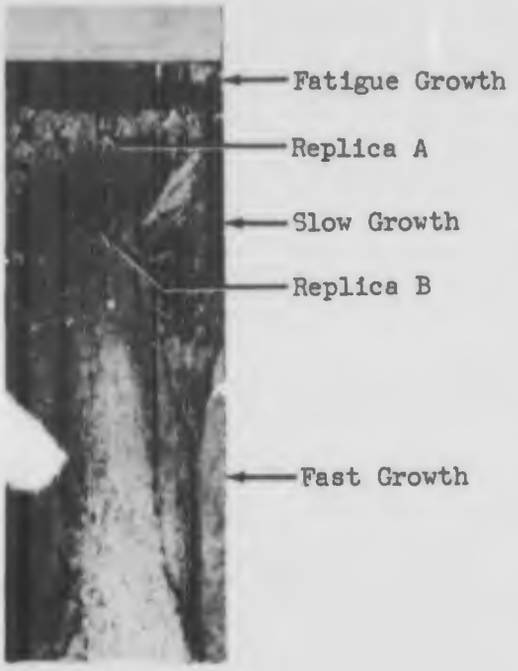

a) Fracture Face
Mag 3X

b) Replica A, Intergranular
Slow Growth Region
Mag: 3860X

c) Replica B, Near Region
of Slow to Fast Growth

d) Replica B, Fast Growth
Region

Figure 79. Fracture Face and Electron Fractographs of Bainitic 9Ni-4Co-0.45C Specimen G-74, K_{ii} = 78.4 ksi $\sqrt{in.}$, 2293 Minutes in 3½% NaCl Solution

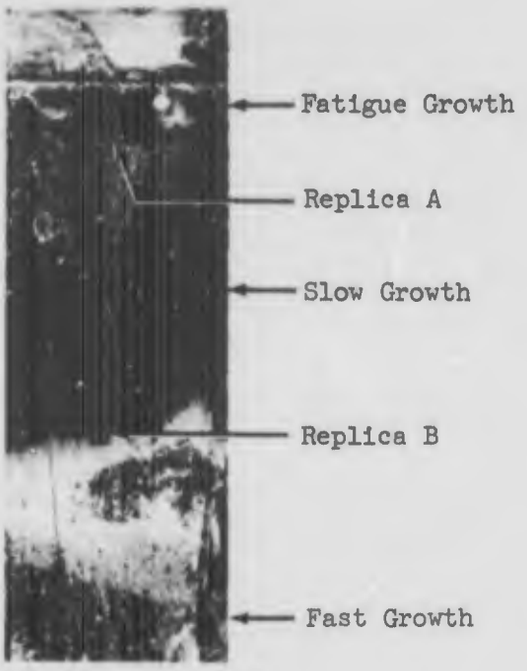

a) Fracture Face

b) Replica A, Fatigue to Slow Growth Region
Mag: 3860X

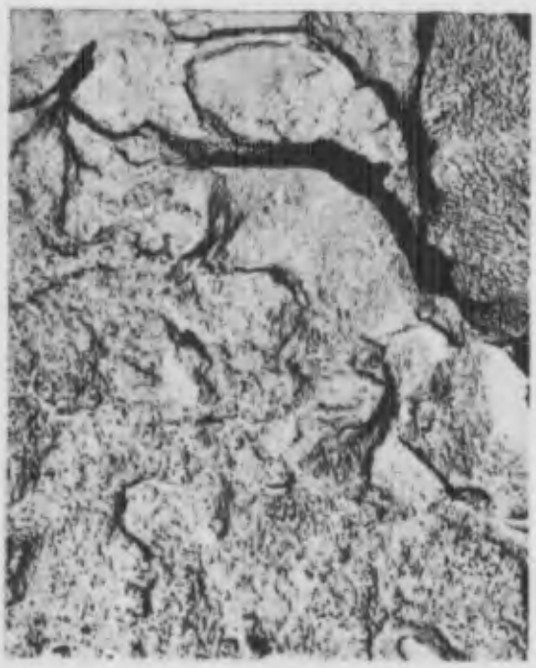

c) Replica A, Slow Growth Region

d) Replica B, Fast Growth Region

Figure 60. Fracture Face and Electron Fractographs of Bainitic 9Ni-4Co-0.45C Specimen G79, K_{II} = 41.5 ksi $\sqrt{in.}$, 5131 Minutes in 3½% NaCl Solution

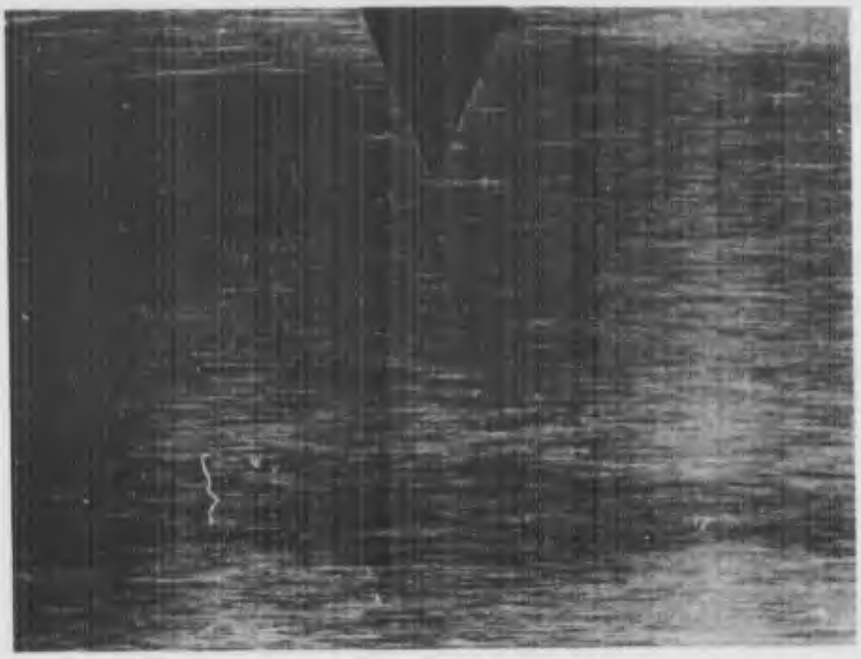

a) 4330 V-Modified, Specimen A84, Loaded for 875 minutes at K_{Ii} = 69.8,

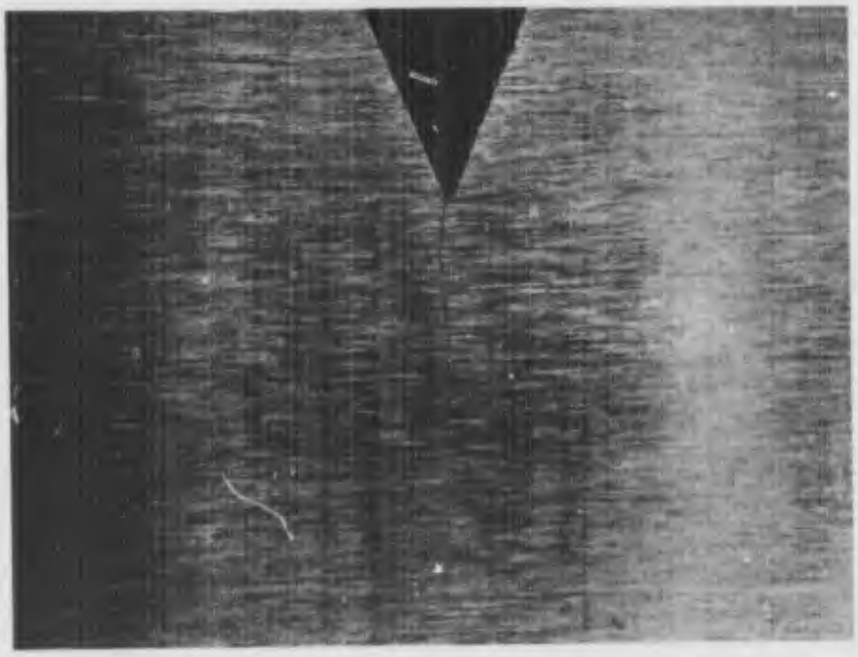

b) Maraging 250, Specimen E91, Loaded for 10,000 minutes at K_{Ii} = 59.3

Figure 81. Crack Growth of Notched Bend Specimen

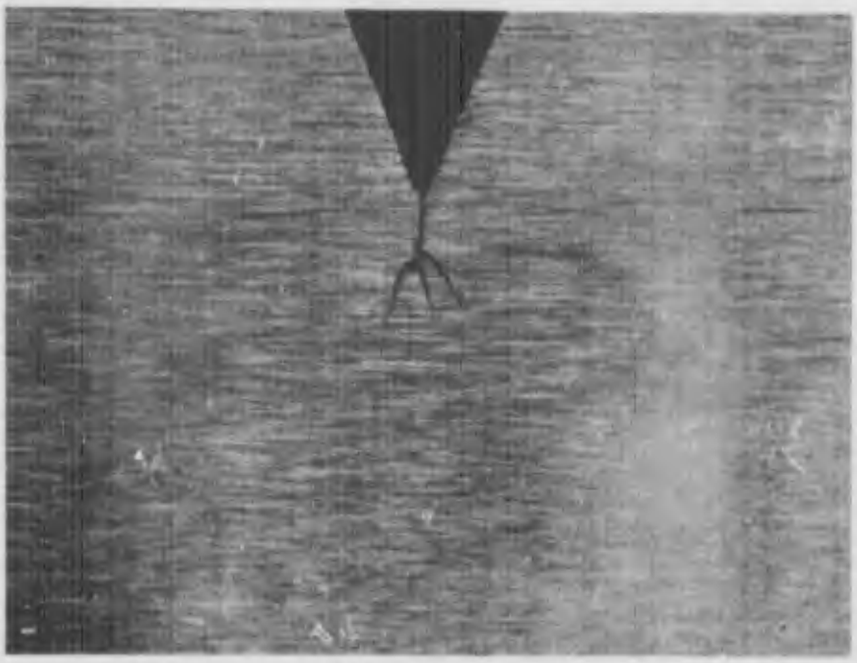

a) Specimen C83, Loaded for 656 minutes at K_{Ii} = 104.3

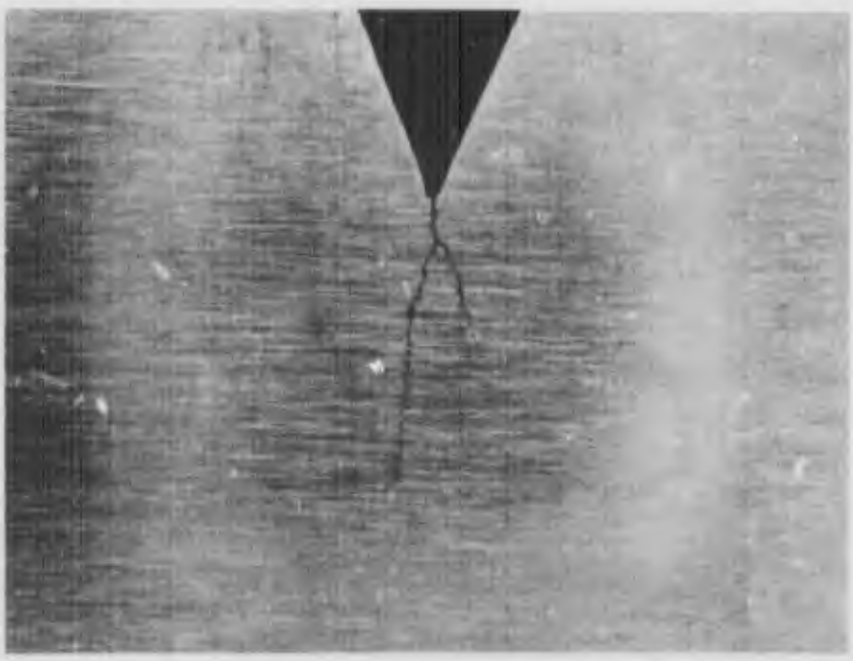

b) Specimen C91, Loaded for 10,000 minutes at K_{Ii} = 80.2

Figure 82. Crack Breaking of 9Ni-4Co-0.30C Notched Bend Specimens

Table XXI *Alternate Immersion Test Data, 3.5 Percent NaCl Solution (Continued)*

Alloy	Heat Number	Specimen Number	Yield Strength (ksi)	Sustained Stress (ksi)	Time to Failure (hours)
4330 V-Modified	C57046	A92	198	158	1416 NF
		A93			192
		A94			384
	C10157	A95	191	153	528
		A96			1176
		A97			528
	3960633	A98	198	158	264
		A99			144
		A100			144
9Ni-4Co-0.30C	3930852	C92	205	164	1536 NF
		C93			1224
		C94			1296
	3931144	C95	201	161	1488
		C96			1032
		C97			1536 NF
	3931145	C98	198	159	1368
		C99			1488
		C100			1536 NF
300 M	3951531(P)	D92	233	186	72
		D93			75-112
		D94			72
	3951531(R)	D95	239	192	75-112
		D96			41
		D97			48
	09715	D98	236	189	43
		D99			43
		D100			44

Table XXI Alternate Immersion Test Data, 3.5 Percent NaCl Solution (Concluded)

Alloy	Heat Number	Specimen Number	Yield Strength (ksi)	Sustained Stress (ksi)	Time to Failure (hours)
9Ni-4Co-0.45C (Quench & Temper)	3931120	F95	237	190	220-305
		F96			220-305
		F97			384
	3882720	F98	237	190	40
		F99			406
		F100			624
9Ni-4Co-0.45C (Bainitic)	3931120	G95	220	190	1000
		G96			1488
		G97			1536 NF
	3882720	G98	217	190	1488
		G99			1000
		G100			1536
*Maraging 250	*Billet P	Three Specimens	255	215	No failures of three specimens in 1000 hrs.
*H-11 Mod	*Billet H	B1	190	150	180
		B2			NF in 1000 hours
		B3			NF in 1000 hours

*Data from ML-TDR-64-3 "Investigation of Effect of Stress Corrosion on High Strength Steels."

Table XXII Sustained-Loading Characteristics of 4330 V-Modified in 3.5 Percent NaCl Solution

Heat Number	Specimen Number	Initial Crack Depth, a (inch)	Applied Load (Kips)	Initial Stress Intensity, K_{Ii} (ksi $\sqrt{in.}$)	(1) K_{Ii}/K_{Ic}	Time to Failure (minutes)	Estimate of Final Crack Depth (inch)
C57046	A78	.33	20.64	99.0	.80	508 NF	.62
	A77	.31	18.22	83.9	.67	801	.89
	A76	.32	15.62	73.4	.59	462	.87
	A79	.32	13.27	62.2	.50	516	.62
	A74	.32	9.37	43.9	.35	638	.94
	A31	.31	7.44	34.2	.27	1604	.91
	A75	.32	23.90	112.0	.87	*1.3	NCG
C10157	A84	.33	14.61	69.8	.70	876 NF	—
	A83	.32	12.74	59.8	.59	869 NF	0.50
	A85	.32	8.35	39.2	.39	1713	—
	A82	.32	17.45	81.8	.82	*10,000 NF	NCG
3960633	A89	.32	10.62	49.9	.59	558	.107
	A90	.31	9.04	41.6	.49	502	.103
	A91	.34	6.55	31.9	.35	10,075 NF	NCG
	A88	.32	15.72	73.8	.87	*10,000 NF	NCG

NF - No Failure
NCG - No Crack Growth
* - Room temperature and air environment (25 - 35% Relative Humidity)

(1)

Heat No.	Av. K_{Ic} ksi $\sqrt{in.}$
C57046	124.5
C10157	99.8
3960633	84.8

Table XXIII Sustained-Loading Characteristics of H-11 Modified in 3.5 Percent NaCl Solution

Heat Number	Specimen Number	Initial Crack Depth, a (inch)	Applied Load (kips)	Initial Stress Intensity, K_{Ii} (ksi$\sqrt{in.}$)	K_{Ii}/K_{IC} [1]	Time to Failure (minutes)	Estimate of Final Crack Depth (inch)
09110	B75	.27	10.88	46.4	.80	0	FAL
	B74	.31	9.45	43.5	.75	1328	---
	B77	.32	8.66	40.6	.70	2804 NF	NCG
	B76	.32	7.43	34.8	.59	3019 NF	NCG
09099	B84	.27	12.21	52.0	.86	268	---
	B82	.28	12.16	52.9	.88	0	FAL
	B83	.29	11.03	48.9	.82	2523	.31
	B85	.27	9.02	38.4	.64	10,088 NF	.32
08990	B89	.27	9.40	40.1	.882	12	---
	B90	.27	9.08	38.7	.89	9868 NF	.33
	B88	.28	7.48	32.5	.71	319	---
	B91	.27	6.41	27.3	.600	11,473 NF	.31

NF - No Failure
NCG - No Crack Growth
FAL - Failed At Load

[1]

Heat No.	Av. K_{IC} ksi $\sqrt{in.}$
09110	58.0
09099	60.0
08990	45.5

Table XXIV *Sustained-Loading Characteristics of 9Ni-4Co-0.30C in 3.5 Percent NaCl Solution*

Heat Number	Specimen Number	Initial Crack Depth, a (inch)	Applied Load (kips)	Initial Stress Intensity, K_{Ii} (ksi $\sqrt{in.}$)	[1] K_{Ii}/K_{IC}	Time to Failure (minutes)	Estimate of Final Crack Depth (inch)
3930852	C78	.32	20.36	95.5	.850	10,013 NF	.62
	C74	.30	17.42	78.8	.71	10,449 NF	.58
	C76	.30	17.30	78.8	.700	753 NF	.38
	C77	.30	17.00	79.8	.710	663 NF	.36
	C75	.32	14.40	67.5	.59	8,325 NF	.62
	C79	.32	10.80	50.6	.43	10,034 NF	.50
3931144	C84	.33	23.05	110.1	.950	656	.68
	C83	.31	22.70	104.3	.900	2,296 NF	---
	C82	.31	20.18	92.8	.800	502 NF	---
	C85	.30	16.68	75.4	.650	2,064	.80
3931145	C90	.31	25.95	119.2	.980	4,821	.71
	C88	.30	21.81	98.6	.810	1,278	.60
	C91	.30	17.41	80.2	.650	10,002	.70

NF - No Failure
NCG - No Crack Growth

[1]

Heat No.	Av. K_{IC} ksi $\sqrt{in.}$
3930852	112.3
3931144	116.0
3931145	121.9

Table XXV Sustained-Loading Characteristics of 300M in 3.5 Percent NaCl Solution

Heat Number	Specimen Number	Initial Crack Depth, a (inch)	Applied Load (kips)	Initial Stress Intensity, K_{Ii} (ksi $\sqrt{in.}$)	K_{Ii}/K_{IC} [1]	Time to Failure (minutes)	Estimate of Final Crack Depth (inch)
3951531P	D78	.33	13.47	64.4	.816	63	.61
	D76	.31	11.78	54.1	.687	176	.85
	D77	.32	10.10	47.3	.600	189	.87
	D79	.31	8.73	40.1	.510	205	.84
	D74	.32	6.23	29.2	.370	284	1.09
	D75	.29	*15.13	67.0	.850	*10,000 NF	NCG
3951531R	D82	.32	10.13	47.5	.583	163	.92
	D83	.31	8.44	38.8	.476	189	.96
	D85	.31	6.12	28.2	.346	1176	1.04
	D84	.30	*15.22	68.9	.844	*10,000 NF	NCG
09715	D89	.33	9.89	47.3	.703	48	.67
	D88	.31	8.61	39.6	.588	96	.81
	D90	.27	7.93	33.8	.500	131	.87
	D86A	.30	6.10	27.8	.413	201	.94
	D91	.30	4.47	20.2	.29	10,004 NF	NCG
	D87A	.31	4.39	20.8	.30	381	.98
	D89A	.31	4.39	20.2	.30	2,027	1.01
	D88A	.31	2.93	13.5	.20	10,000 NF	NCG

* Room Temperature and Air Environment (25-35% Relative Humidity)
NF - No Failure
NCG - No Crack Growth

[1]

Heat No.	Av. K_{IC} ksi $\sqrt{in.}$
3951531P	78.9
3951531R	81.6
09715	67.4

Table XXVI Sustained-Loading Characteristics of Maraging 250 in 3.5 Percent NaCl Solution

Heat Number	Specimen Number	Initial Crack Depth, a (inch)	Applied Load (kips)	Initial Stress Intensity, K_{Ii} (ksi $\sqrt{in.}$)	[1] K_{Ii}/K_{IC}	Time to Failure (minutes)	Estimate of Final Crack Depth (inch)
24676	E75	.29	17.88	79.2	.900	1515	.44
	E76	.32	17.82	83.5	.950	279	.52
	E74	.34	14.18	69.1	.786	2336	.59
	E77	.33	13.80	66.0	.72	9801 NF	.34
	E78	.32	13.12	61.6	.700	10,110 NF	.45
	E79	.32	11.28	52.8	.600	5296	.46
09148	E83	.32	18.34	86.0	.950	647	.42
	E82	.32	17.40	81.6	.900	616	.46
	E84	.31	16.42	75.6	.835	1239	.53
	E85	.31	11.59	53.3	589	4735	.63
3930879	E89	.32	20.22	94.9	.960	2.1	—
	E88	.32	19.18	89.9	.910	404	.42
	E90	.31	18.09	83.1	.841	2110	.42
	E91	.31	12.90	59.3	.600	10,090 NF	.66

NF - No Failure
NCG - No Crack Growth

[1]

Heat No.	Av. K_{IC} ksi $\sqrt{in.}$
24676	88.0
09148	90.6
3930879	98.9

Table XXVII Sustained-Loading Characteristics of Quench-Temper 9Ni-4Co-0.45C in 3.5 Percent NaCl Solution

Heat Number	Specimen Number	Initial Crack Depth, a (inch)	Applied Load (kips)	Initial Stress Intensity, K_{Ii} (ksi $\sqrt{in.}$)	[1] K_{Ii}/K_{IC}	Time to Failure (minutes)	Estimate of Final Crack Depth (inch)
3931141	F74	.32	14.65	68.7	.90	0	FAL
	F75	.31	13.50	62.1	.81	220	.76
	F76	.31	13.28	61.1	.80	231	.74
	F77	.31	12.44	57.3	.75	213	.89
	F78	.31	9.77	45.0	.59	*500	.93
	F79	.31	7.34	33.8	.44	445	1.06
3931120	F82	.30	12.32	55.7	.84	83	.58
	F83	.31	11.20	51.5	.78	188	.89
	F84	.31	9.79	45.0	.68	233	.87
	F85	.31	4.28	19.8	.30	5230	1.09
3882720	F88	.31	10.86	49.9	.85	12	.31
	F89	.31	10.22	47.0	.80	365	.71
	F90	.30	8.94	40.4	.69	546	.65
	F91	.30	2.87	12.9	.22	10,149 NF	NCG

* - Estimated
NF - No Failure
FAL - Failed At Load

[1]

Heat No.	Av. K_{IC} ksi $\sqrt{in.}$
3931141	76.4
3931120	66.2
3882720	58.8

Table XXVIII *Sustained-Loading Characteristics of Bainitic 9Ni-4Co-0.45C in 3.5 Percent NaCl Solution*

Heat Number	Specimen Number	Initial Crack Depth, a (inch)	Applied Load (kips)	Initial Stress Intensity, K_{Ii} (ksi $\sqrt{in.}$)	[1] K_{Ii}/K_{IC}	Time to Failure (minutes)	Estimate of Final Crack Depth (inch)
3931141	G77	.33	19.70	94.2	1.02	0.83	NCG
	G75	.31	18.75	86.3	.94	2381	.63
	G76	.33	18.70	89.4	.97	1488	.53
	G74	.31	17.03	78.4	.85	2293	.66
	G78	.32	11.80	55.4	.60	6323	.74
	G79	.31	9.02	41.5	.45	5131	.68
3931120	G83	.31	19.80	91.1	.97	1330	.45
	G82	.31	18.44	84.8	.90	1880	.59
	G84	.31	15.35	70.6	.75	1732	.59
	G85	.30	8.09	36.6	.39	4377	.82
3882720	G88	.31	16.28	74.9	.90	1021	.36
	G89	.31	14.46	66.5	.80	1536	.40
	G90	.32	13.30	62.4	.75	1537	.49
	G91	.30	5.16	23.3	.28	10,803 NF	NCG

NF - No Failure
NCG - No Crack Growth

[1]

Heat No.	Av. K_{IC} ksi $\sqrt{in.}$
3931141	92.3
3931120	94.2
3882720	83.8

Table XXIX Salt Water pH and NaCl Concentration Data

Alloy	Specimen Number	K_{Ii}/K_{Ic}	Time in Solution (minutes)	% NaCl	pH
4330 V-Modified	A91	.35	10,075	4.5	4.40
H-11 Modified	B85	.64	10,088	3.3	4.11
9Ni-4Co-0.30C	C79	.43	10,034	3.8	4.59
	C85	.65	2,064	3.3	6.61
300M	D86A	.41	1	-	5.50
			207	1.8	4.48
	A87A	.30	1	-	5.85
			381	4.7	4.82
	D88A	.20	1	-	5.60
			8,695	3.5	3.95
	D89A	.30	1	-	6.60
			2,027	6.8	4.77
	D91	.29	10,075	4.2	4.17
Maraging 250	E85	.59	4,735	3.0	7.00
	E91	.60	10,090	3.6	4.72
	E79	.60	5,296	3.2	6.95

8.0 METALLURGICAL STABILITY

Steel alloys used at elevated temperatures are required to be metallurgically stable so that deleterious property changes will not occur during the service life of the airplane. Landing gear components on the supersonic transport will be exposed to a maximum temperature of about 300°F. Since the low alloy steels are prime candidates for the landing gear, it was desirable to evaluate the alloys under consideration for metallurgical stability at 300°F.

8.1 PROCEDURE

Two tensile and five notched bend fracture toughness specimens from one heat of each alloy were exposed at a temperature 300°F or higher for 5,000 hours under a sustained stress of 40 ksi. Following exposure, the tensile specimens and two fracture toughness specimens were tested in room temperature air to determine if the exposure had an adverse effect on properties. The three remaining notched bend specimens were sustained-loaded in 3.5 percent NaCl solution to assess the effect of exposure on stress corrosion susceptibility.

Tensile and fracture toughness specimens were finish-machined prior to exposure, and the notched-bend specimens were notched and precracked after exposure. Exposure of the specimens was accomplished in standard creep machines. All the specimens were taken from the long-transverse grain direction of the billets. The exposed and unexposed materials were not heat treated together and a slight amount of scatter was therefore anticipated from heat treatment variation.

8.2 RESULTS AND DISCUSSION

The detailed results of the testing are tabulated in Tables XXX through XXXII. Figures 83 and 84, respectively, show how the exposures affect the tensile and reduction of area properties of the steels, while Fig. 85 shows the effect on fracture toughness. The susceptibilities the exposed steels to stress corrosion are compared to the susceptibilities of unexposed material in Figs. 86 through 92.

Study of Fig. 83 shows that exposures did not significantly change the ultimate or yield strength properties of the alloys. The largest change, due to exposure, was the approximate 7 ksi increase of the H-11 Mod yield strength

(Fig. 83). Because an increase of yield strength cannot be considered an adverse effect and since the ultimate strength was not affected, the small increase of the H-11 Mod yield strength was considered to be insignificant.

Examination of the reduction of area (RA) data (Fig. 84) shows that the exposure produced no significant changes of RA. One RA data point for the exposed 300M steel was about 10 percent lower than the unexposed RA values. This change was probably a result of property variations within the billets and not an effect of the exposure.

The changes of fracture toughness produced by the exposures were generally within the range of test scatter as shown by Figure 85. The toughness of the exposed material was expected to be slightly lower because of differences of billet locations between the exposed and unexposed fracture toughness specimens. The notch of the exposed notched bend specimens was approximately 1-1/4 inch closer to the billet center.

Usually the amount of forging reduction and grain refinement increases outward from the center of the billet. Therefore, the toughness is generally less at the center of the billet. The difference of properties between the center and outer portions of the billet generally decreases with increasing amounts of working.

The billets of 4330 V-Mod, H-11 Mod, and Maraging-250 received the least amount of work. The exposed Maraging-250 fracture toughness data (Fig. 85) showed that there was no decrease of fracture toughness resulting from either the exposure or the differences of billet positions. However, the fracture toughness of the 4330 V-Mod and H-11 Mod steels were decreased by the exposure. This decrease was partially attributed to lower toughness properties at the billet center. The extremely low fracture toughness data point of H-11 Mod (Fig. 85) was not considered representative and was shown by a dotted line to so indicate.

Work by L. J. Klingler, et al. (Ref. 22), has shown that the toughness of a steel, which is tempered at temperatures below the tempering temperatures of maximum "500°F Embrittlement" will decrease when exposed at 300-400°F. Data from the heat treatment study indicated that both 300M and 4330 V-Modified were tempered at temperatures less than the temperature of maximum "500°F Embrittlement". Exposure of 300M at 300°F had no significant effect on toughness (Fig. 85), thus indicating that the exposure did not result in "500°F

Embrittlement''. However, the decrease of 4330 V-Modified toughness after exposure suggests that the extent of the "500°F Embrittlement'' may have been increased. Additional stability testing of 300M and 4330 V-Modified in different temper conditions is needed to fully assess the influence of irreversible temper embrittlement on stability.

Comparison of the stress corrosion susceptibilities of the exposed and unexposed materials (Figs. 87 through 92), at higher K_{Ii}/K_{IC} levels, showed that the times-to-failure were only slightly decreased by the exposure. However, the times-to-failure of 9Ni-4Co- and Maraging-250, at lower K_{Ii}/K_{IC} levels, tended to deviate more noticeably from the unexposed material time-to-failures. Because of the high degree of scatter associated with this type of testing, difficulty was encountered in evaluating the effect of the exposure. Generally, there was no gross degradation of the stress corrosion properties due to exposure.

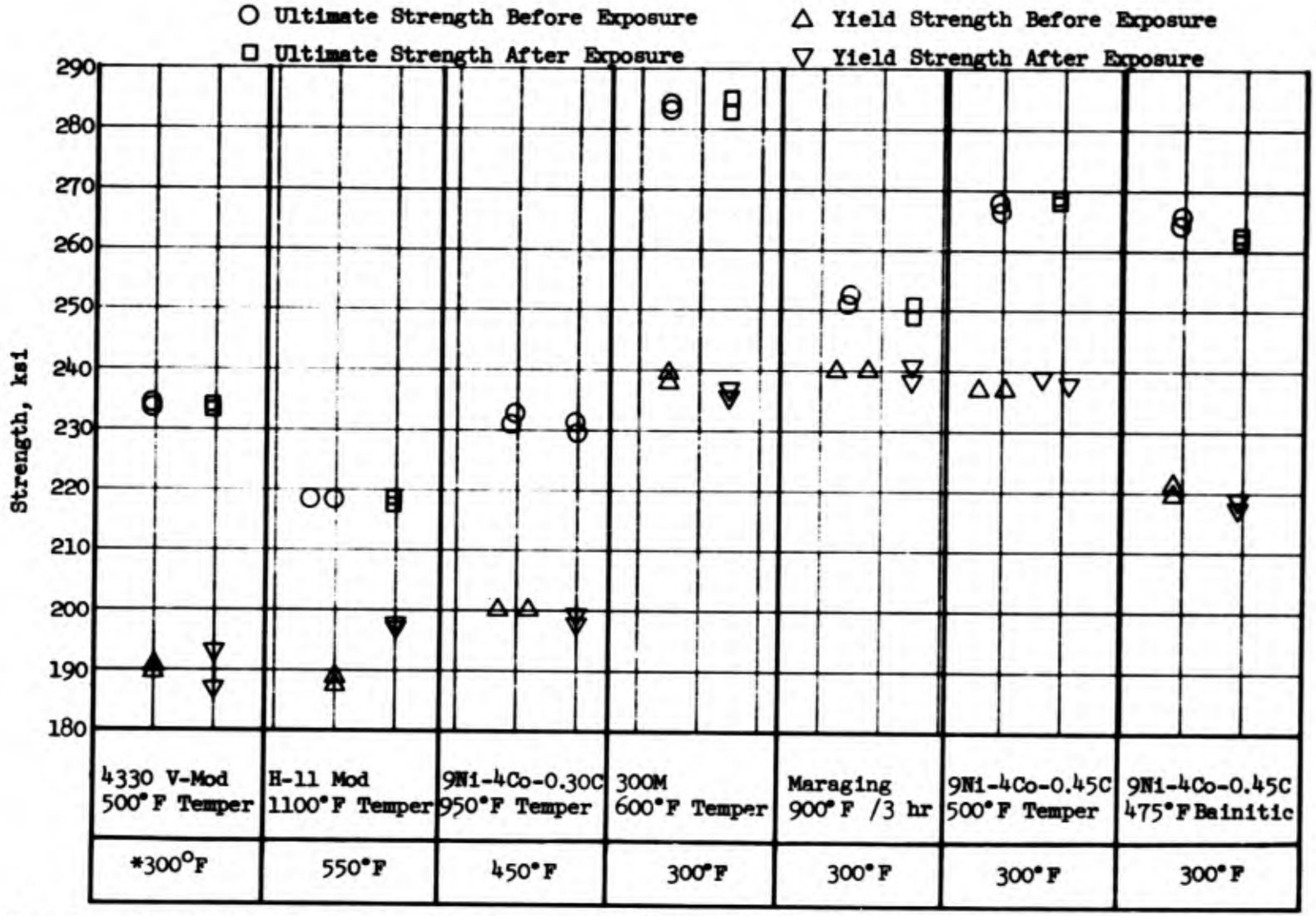

***Figure 83.** Strength Properties Before and After Exposure*

*Exposure Temperature, Specimens Exposed for 5000 hours at sustained stress level of 40 ksi.

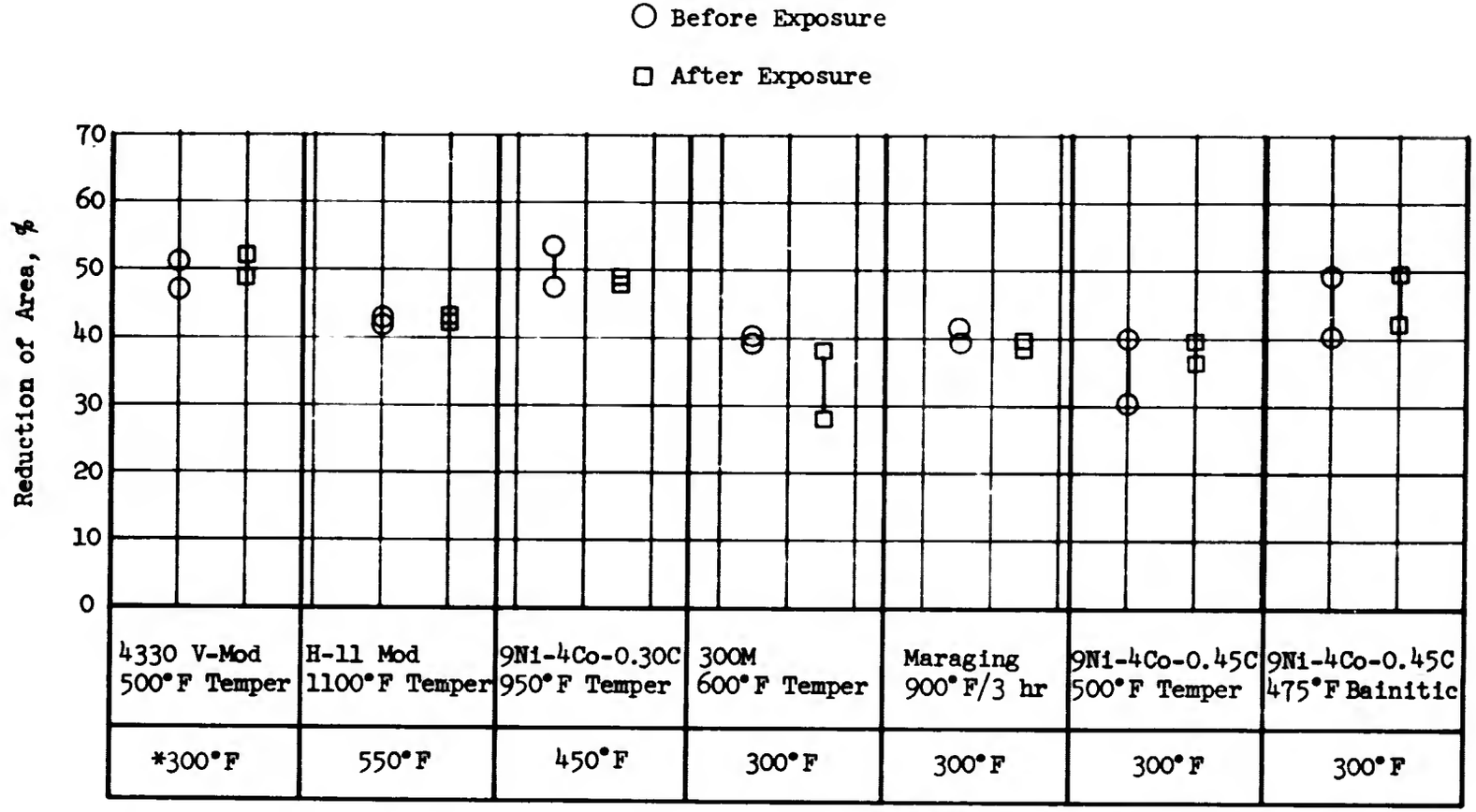

*Exposure Temperature, Specimens Exposed for 5000 hours at sustained stress level of 40 ksi.

Figure 84. Reduction of Area Properties Before and After Exposure

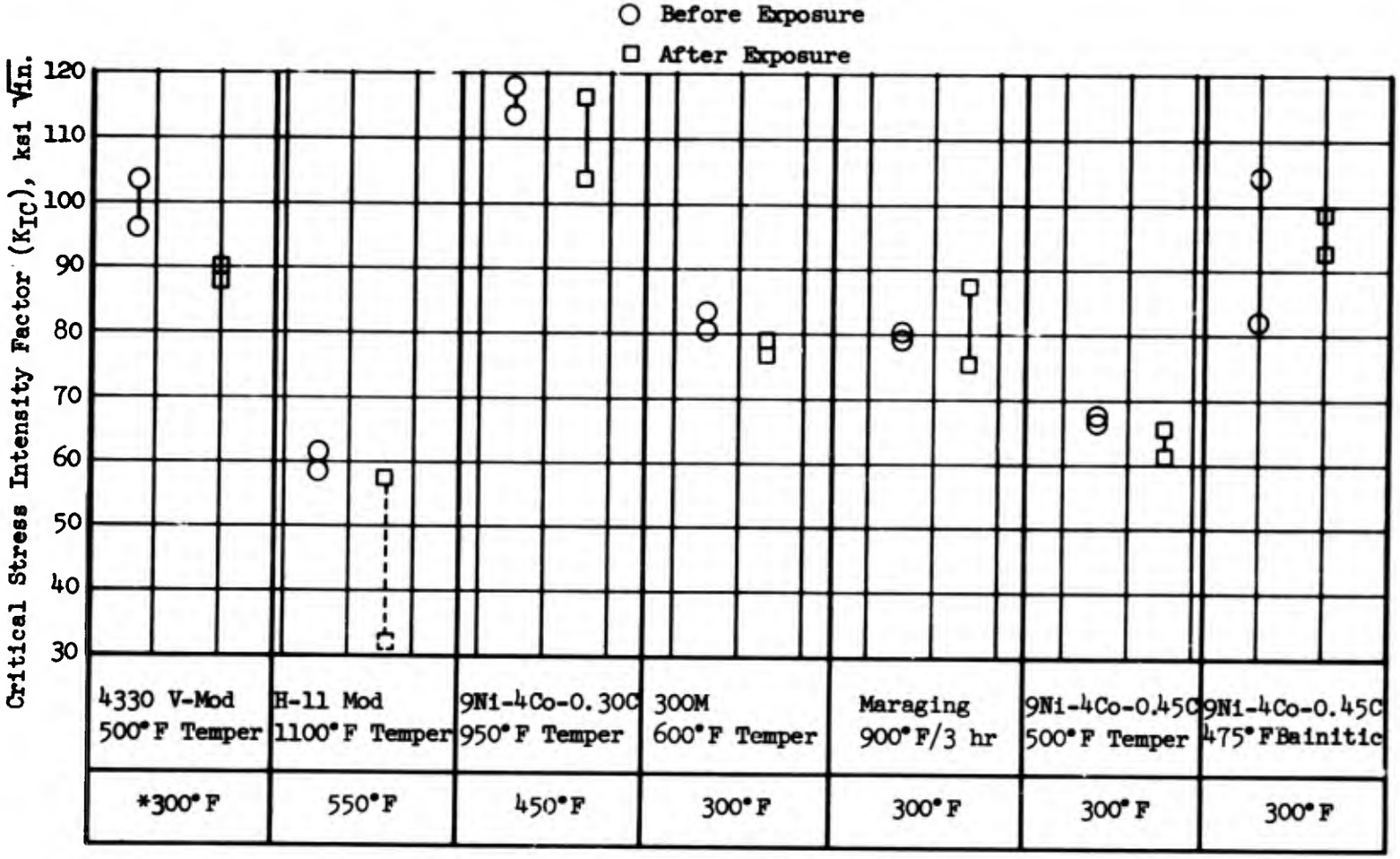

*Exposure Temperature, Specimens Exposed for 5000 hours at sustained stress level of 40 ksi.

Figure 85. ***Fracture Toughness Properties Before and After Exposure***

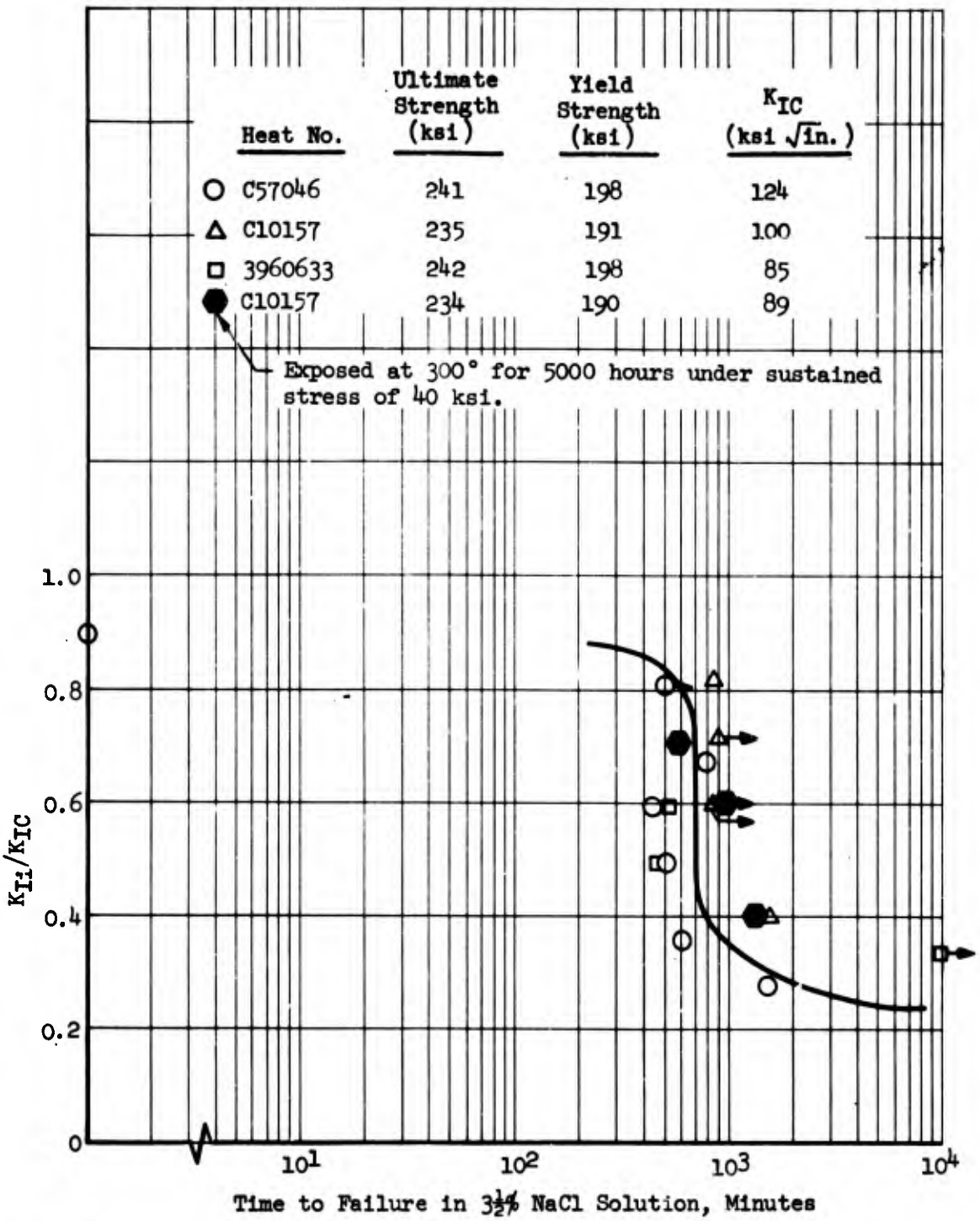

Figure 86. Sustained-Loading Characteristics of Exposed 4330 V-Modified Specimens

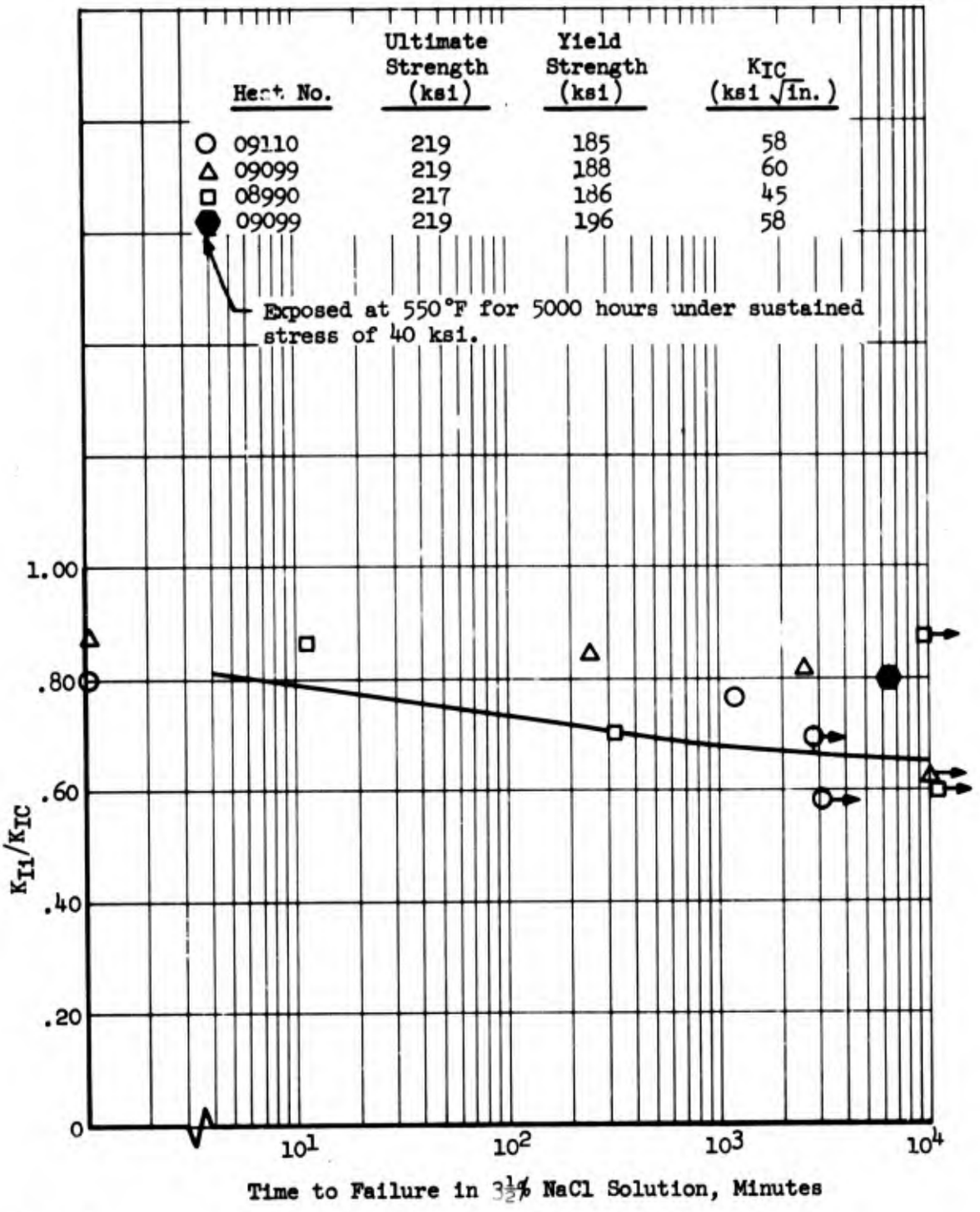

Figure 87. Sustained-Loading Characteristic of Exposed H-11 Modified Specimens

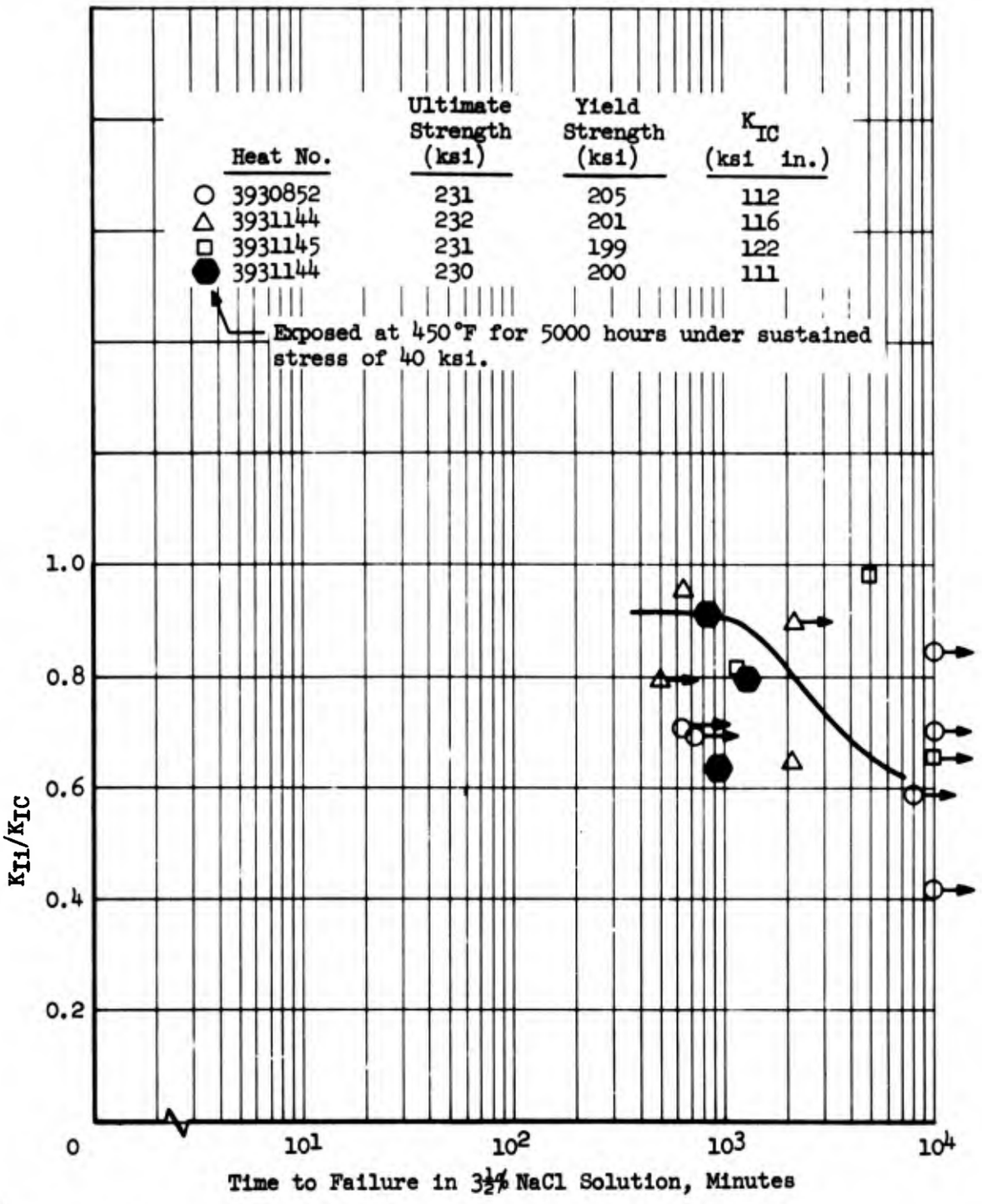

Figure 88. Sustained-Loading Characteristics of Exposed 9Ni-4Co-0.30C Specimens

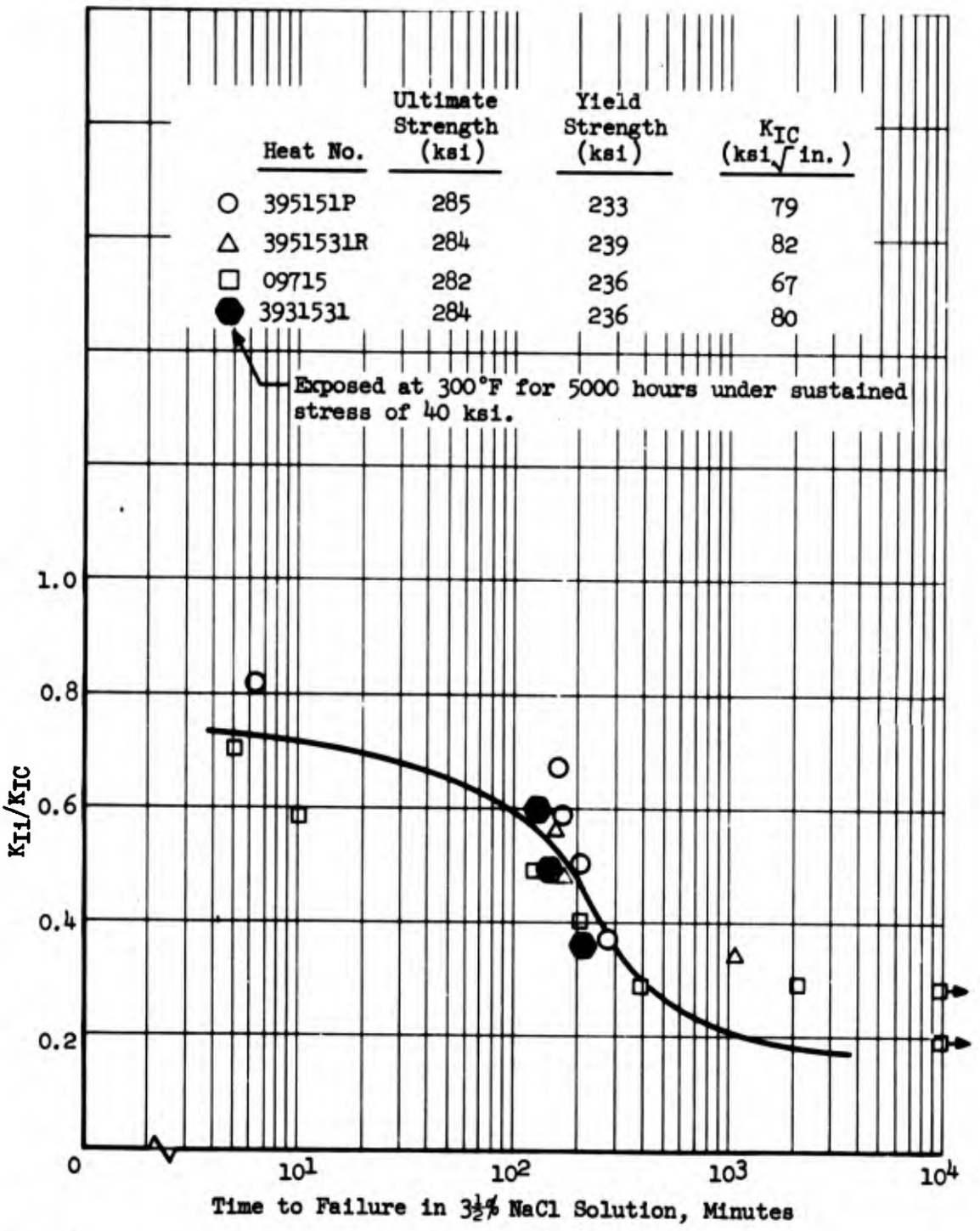

Figure 89. Sustained-Loading Characteristics of Exposed 300M Specimens

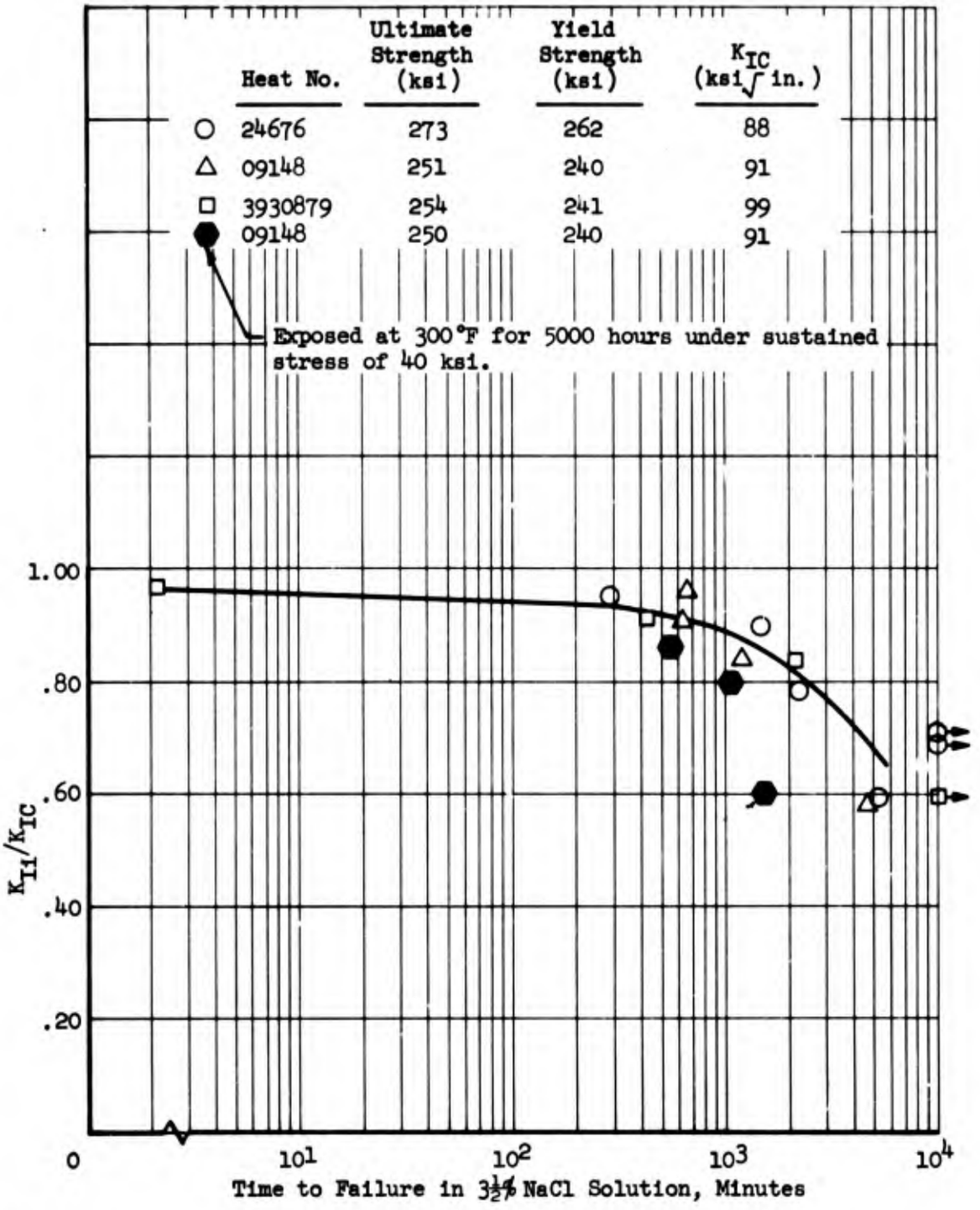

Figure 90. Sustained-Loading Characteristics of Exposed Maraging 250 Specimens

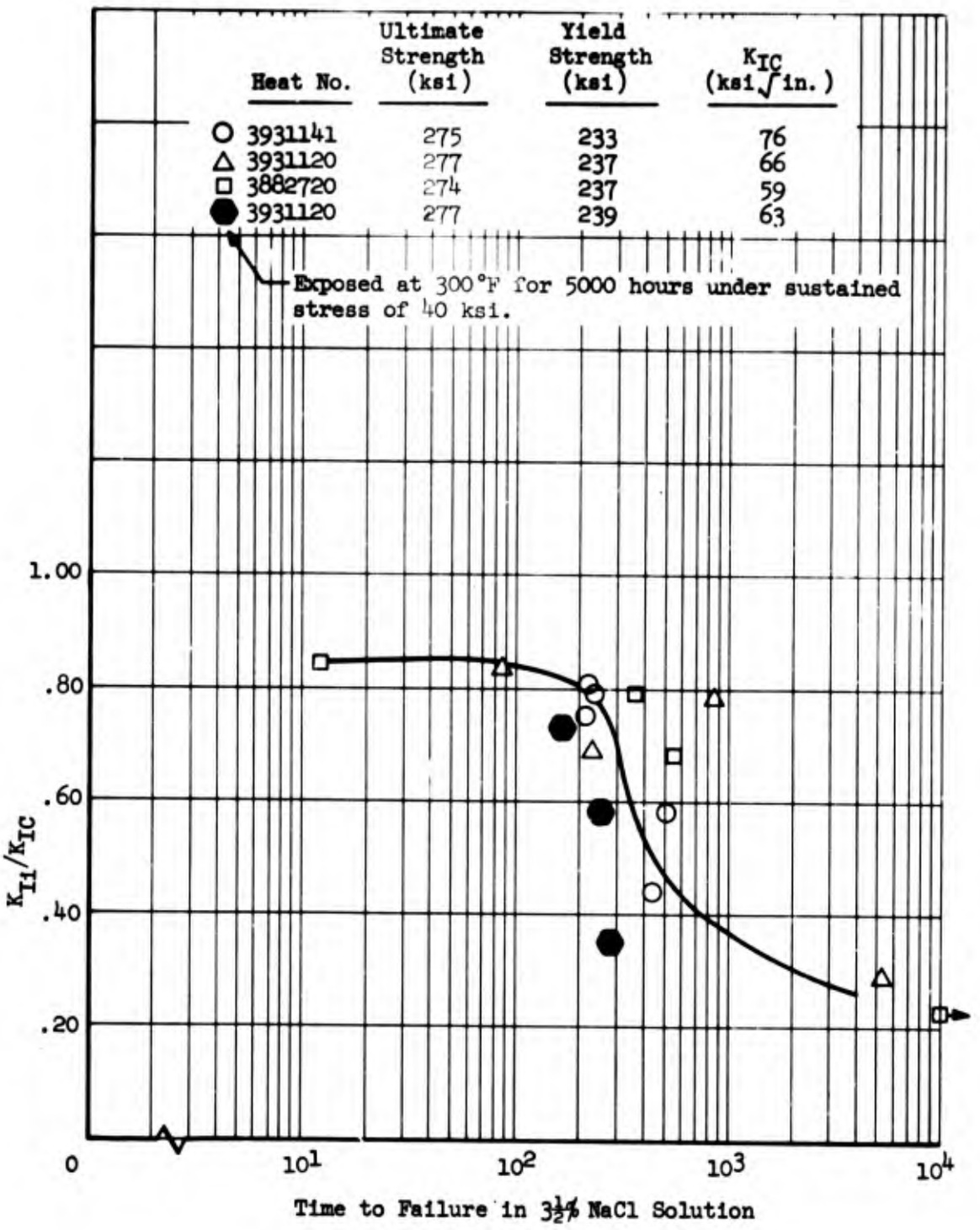

Figure 91. Sustained-Loading Characteristics of Exposed Quench and Tempered 9Ni-4Co-0.45C Specimens

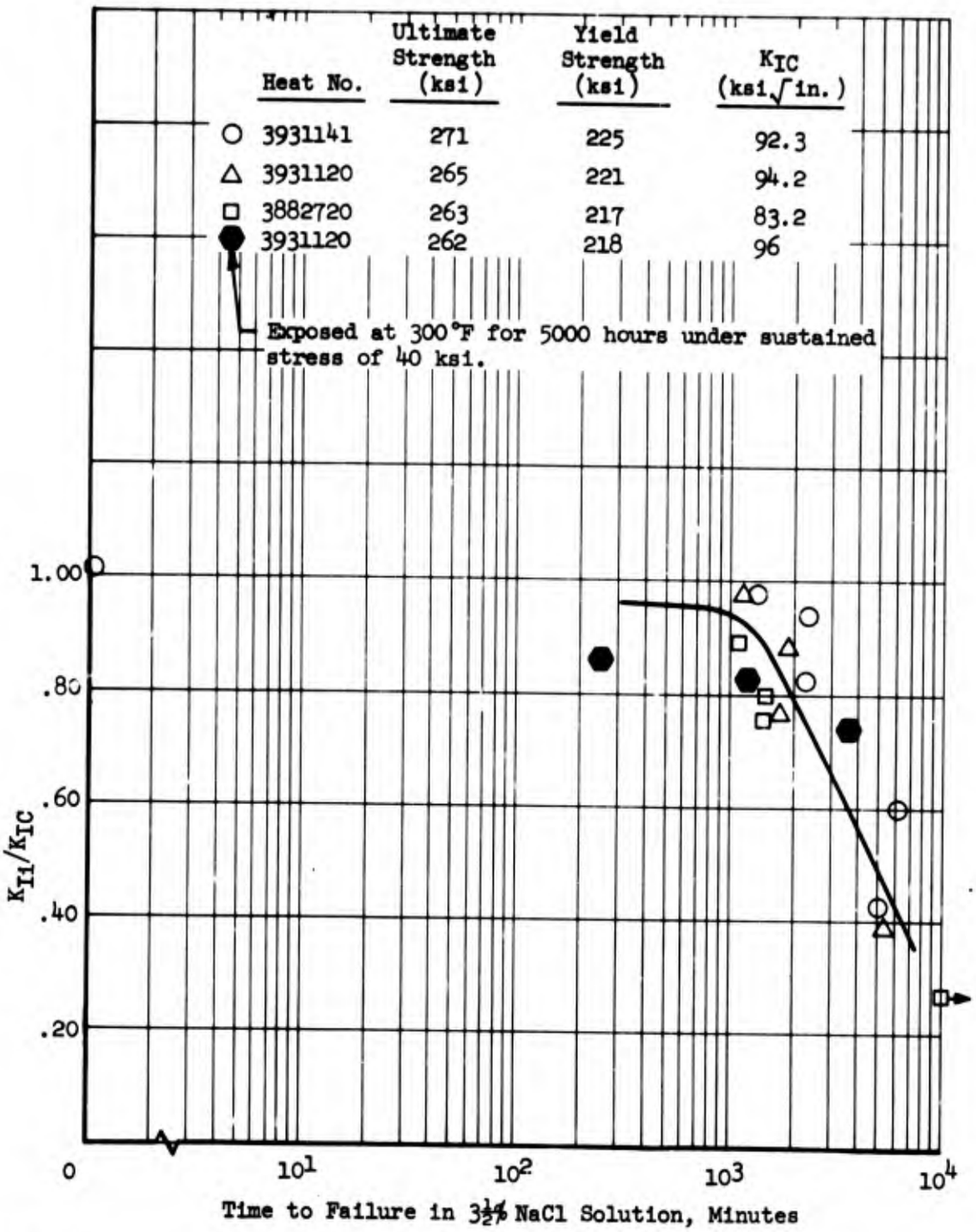

Figure 92. Sustained-Loading Characteristics of Exposed Bainitically Treated 9Ni-4Co-0.45C Specimens

Table XXX Room Temperature Tensile Data Before and After Exposure

Alloy	Heat Number	Specimen Number	Exposure Temperature [1]	Ultimate Strength (ksi)	Yield Strength (ksi)	El. (%)	RA (%)
4330 V-Modified 500°F Temper	C10157	A11	None	234.9	192.1	12	48
		A12	None	234.2	190.2	13	52
		A119	300°F	233.9	195.6	12	52
		A120	300°F	235.1	187.0	12	48
H-11 Mod. 1100°F Temper	09099	B11	None	219.3	189.7	12	42
		B12	None	219.3	187.8	12	43
		B119	550°F	219.4	196.5	13	41
		B120	550°F	220.0	197.1	13	43
9Ni-4Co-0.30C 950°F Temper	393144	C11	None	230.9	201.2	14	48
		C12	None	232.7	201.2	14	54
		C119	450°F	231.5	201.1	14	50
		C120	450°F	229.9	200.3	15	48
300 M 600°F Temper	3951531R	D11	None	284.6	239.7	12	41
		D12	None	283.3	238.6	10	40
		D119	300°F	285.7	236.7	10	38
		D120	300°F	282.7	236.4	12	28
Maraging 250 900°F/3 Hr. Age	09148	E11	None	252.5	240.6	9	42
		E12	None	251.5	240.4	9	40
		E119	300°F	251.1	241.9	9	39
		E120	300°F	249.3	239.0	9	40
9Ni-4Co-0.45C 500°F Temper	3931120	F11	None	276.2	237.0	7	31
		F12	None	278.3	237.1	9	40
		F119	300°F	278.3	239.5	10	39
		F120	300°F	277.1	239.5	10	35
9Ni-4Co-0.45C 475°F Bainitic	3931120	G11	None	265.8	220.0	11	41
		G12	None	264.4	221.4	10	49
		G119	300°F	263.3	219.4	12	49
		G120	300°F	261.8	218.0	10	42

Transverse grain direction. [1] 5000 hour and 40 ksi sustained stress exposure.

Table XXXI ***Room Temperature Fracture Toughness Data Before and After Exposure***

	Heat Number	Specimen Number	Exposure Temperature [1]	a (inch)	P (kips)	P_{max} (kips)	K_{IC} (ksi $\sqrt{in.}$)
4330 V-Modified	C10157	A80	None	.32	22.20	23.60	104.1
		A81	None	.32	20.40	22.60	95.6
500°F Temper		A121	300°F	.30	19.50	21.50	88.1
		A122	300°F	.30	19.80	22.8	89.5
H-11 Mod	09099	B80	None	.32	12.58	12.58	59.3
		B81	None	.30	13.52	13.52	61.1
1100°F Temper		B123	550°F	.31	6.60	6.60	30.4
		B124	550°F	.32	12.30	12.30	57.7
9Ni-4Co-0.30C	3931144	C80	None	.31	24.90	25.80	114.2
		C81	None	.30	26.10	26.20	117.9
950°F Temper		C121	450°F	.32	22.35	23.10	104.8
		C122	450°F	.33	24.60	25.1	117.6
300 M	3951531R	D80	None	.29	18.55	19.00	82.2
		D81	None	.29	18.26	18.80	81.3
600°F Temper		D121	300°F	.33	16.40	16.70	78.4
		D122	300°F	.32	17.20	17.30	80.7
Maraging 250	09148	E80	None	.31	19.70	21.30	90.6
		E81	None	.31	19.70	19.70	90.6
900°F/3 Hr. Age		E121	300°F	.29	19.15	21.6	84.8
		E122	300°F	.29	22.1	22.1	97.9
9Ni-4Co-0.45C	3931120	F80	None	.31	14.20	14.20	66.6
		F81	None	.30	14.55	14.70	65.8
500°F Temper		F121	300°F	.31	13.50	13.50	62.1
		F122	300°F	.31	14.20	14.20	65.3
9Ni-4Co-0.45C	3931120	G80	None	.32	17.55	19.80	82.4
		G81	None	.31	23.00	23.80	105.8
475°F Bainitic		G121	300°F	.32	19.8	19.80	92.9
		G122	300°F	.32	21.15	21.50	99.2

Transverse Grain Direction [1] 5000 hour and 40 ksi sustained stress exposure

Table XXXII Sustained-Load Data in 3.5 Percent NaCl Solution After Exposure

Alloy	Heat Number	Specimen Number	[1] Exposure	Stress Intensity Level, K_{Ii} ksi $\sqrt{in.}$	K_{IC} / K_{Ii}	Time-to-Failure Minutes
4330 V-Modified 500°F Temper	C10157	A123	300°F	62.2	.70	617
		A124	300°F	52.2	.59	995
		A125	300°F	35.0	.39	1597
H-11 Mod. 1100°F Temper	09099	B85	None	38.4	.64	10,088 NF
		B125	550°F	35.2	.80	5,743 NF
9Ni-4Co-0.30C 950°F Temper	3931144	C123	450°F	99.9	.90	878
		C124	450°F	89.0	.80	1156
		C125	450°F	72.3	.65	906
300M 600°F Temper	3951531	D123	300	47.7	.60	136
		D124		39.0	.49	150
		D125		27.9	.35	211
Maraging 250 900°F/3 Hr. Age	09148	E123	300	79.1	.86	555
		E124	300	73.1	.80	1116
		E125	300	54.8	.60	1520
9Ni-4Co-0.45C 500°F Temper	3931120	F123	300°F	47.8	.75	185
		F124	300°F	37.5	.59	228
		F125	300°F	21.9	.34	275
9Ni-4Co-0.45C 475°F Bainitic	3931120	G125	300°F	82.5	.86	225
		G124	300°F	80.0	.83	1919
		G123	300°F	72.0	.75	3681

[1] Exposed for 5000 hours at sustained stress level of 40 ksi.

9.0 HYDROGEN EMBRITTLEMENT SUSCEPTIBILITY

Severe embrittlement can be produced in steels by extremely small amounts of hydrogen. This hydrogen can be introduced in steels during melting, acid pickling, heat treatment, electroplating, or welding. Reactions of protective cadmium plating with the service environment can also introduce hydrogen into high strength steels. The processing of high strength steel aircraft components is carefully controlled to minimize hydrogen contamination. Despite this careful control failures sometimes occur in service by the mechanism of hydrogen embrittlement. This embrittlement, therefore, is a material reliability consideration that influences alloy selection.

9.1 PROCEDURE

Round notched tensile specimens taken from the transverse grain direction of one heat of each alloy were charged with hydrogen by bright cadmium plating. The specimens were then sustained-loaded at various stress levels. The loads were maintained until failure or until 300 hours had elapsed. If no failures occurred in 300 hours, the test was discontinued. The objective of the testing was to establish the "lower critical stress" below which no failure occurred within 300 hours by this severe plating process. The specimen configuration and plating procedures are described in Sec. 3.0.

Parts heat treated at Boeing to ultimate strengths greater than 220 ksi are normally protected with a porous cadmium-titanium plating. The parts are then baked at about 375^{o}F to remove hydrogen. The specimens of this investigation were given a relatively non-porous plating of bright cadmium and were not subsequently baked. Consequently, the embrittlement resulting from the plating procedures of this investigation was considerably more severe than embrittlement of normally processed parts in order to cause failure in susceptible material within reasonable testing times.

Prior to testing, the specimens were stored in room temperature air to allow for the diffusion of hydrogen. This diffusion increased the uniformity of distribution and reduced the high concentration at the specimen surfaces.

Initially, two unplated specimens of each alloy were tested to determine the notch strength. One plated specimen of each alloy was then loaded at

30 percent of the notch strength and the loads were then increased in incremental steps of 25 ksi until failure occurred. At each load increment the load was maintained for six hours minimum. Subsequent specimens were sustained-loaded at constant load level.

9.2 RESULTS AND DISCUSSION

Table XXXIII lists the detailed test results and Figs. 93 through 99 are plots of the test data. The numbers adjacent to each data point on these plots represent the stress concentration factor. The overall results are summarized by Fig. 100.

Difficulty was encountered during machining in maintaining a 0.003-inch root radius. The root radius varied from 0.002 to 0.005 inches, thereby resulting in a stress concentration factor variation of 4.4 to 6.6 (Ref. 23). Generally, the lower critical stress decreases as the stress concentration factor increases (Ref. 24). However, the rate of decrease depends on the material, heat treatment condition, and hydrogen content of the steel. Since the majority of the specimens had a stress concentration factor of 4.9, the data was analyzed to establish the lower critical stress for $K_t = 4.9$.

Accurate determination of the lower critical stress was difficult because of the variation of the stress concentration factor and because of test scatter. Consider, for example, the scatter obtained with 9Ni-4Co-0.45C (Bainitic) and 300M (Figs. 96 and 99). Two specimens ($K_t = 4.9$) from these alloys were sustain-loaded at approximately 100 ksi. One specimen of each alloy failed in less than 10 hours, while neither of the remaining two specimens failed after 300 hours. Since no specimens were tested at stress levels less than 100 ksi, accurate determination of the lower critical stress was not possible. However, it was established that the lower critical stress of 9Ni-4Co-0.45 (Bainitic) and 300M was less than 100 ksi.

Specimens of 9Ni-4Co-0.45C (Quench and Tempered) loaded in the range of 119-125 ksi, failed in times of 1 to 285 hours (Fig. 98), thus indicating that the lower critical stress was less than 119 ksi. A specimen with $K_t = 5.5$ did not fail in less than 300 hours at stress of 95 ksi. Since this was the highest loaded specimen that did not fail, a lower critical stress of 95 ksi was selected for a stress concentration factor of 4.9

Comparison of the data for the 9Ni–4Co–0.45C alloys (Figs. 98 and 99) indicates that the quench-and-tempered material was slightly more resistant to embrittlement than bainitically treated material. However, because only a limited number of specimens were tested and because of the test scatter, it was not possible to positively conclude that the 9Ni–4Co–0.45 (Bainitic) was more susceptible to embrittlement than the 9Ni–4Co–0.45C (quench-and-tempered).

The lower critical stress selected for the remaining alloys are shown in Figs. 93, 94, 95, and 97. The overall results (Fig. 100) indicated that the 9Ni–4Co–0.45C and 300M alloy were severely embrittled by the plating process relative to the other alloys tested. Generally it is thought that the susceptibility to hydrogen embrittlement increases as the ultimate strength increases. The Maraging 250, which had the fourth highest strength levels, appeared to be one of the least susceptible alloys.

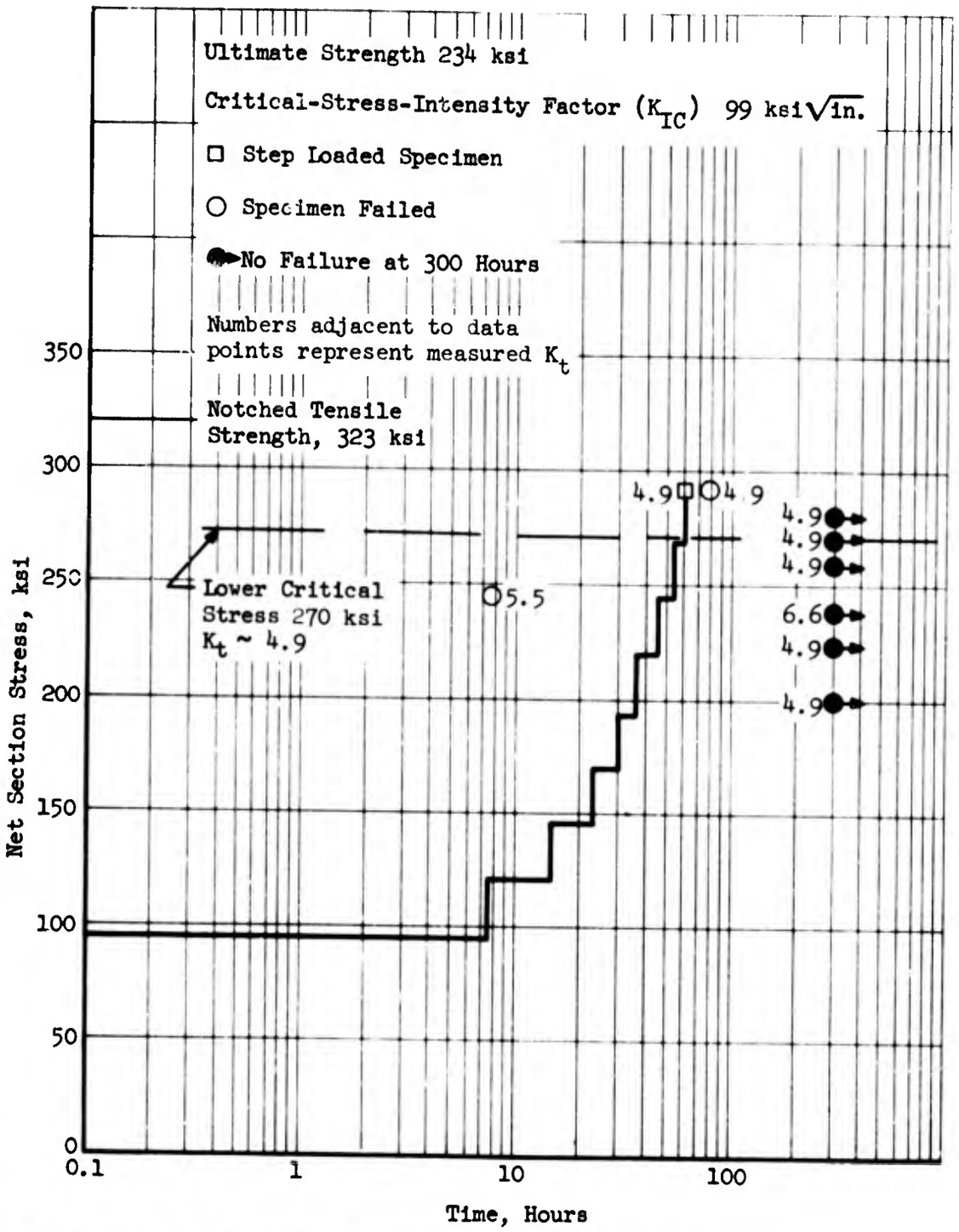

Figure 93. Delayed Failure of 4330 V-Modified Cadmium-Plated Specimens

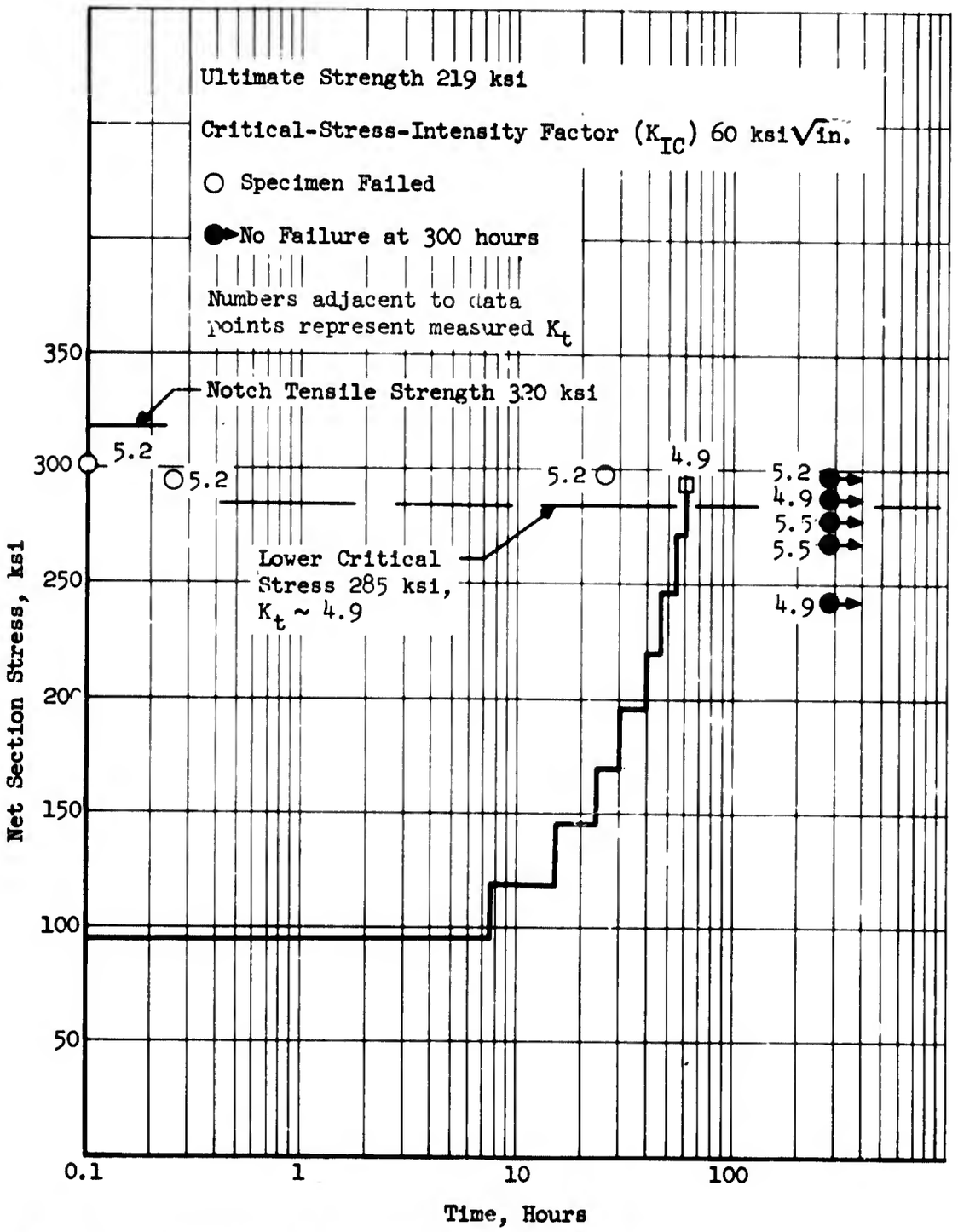

Figure 94. Delayed Failure of H-11 Modified Cadmium-Plated Specimens

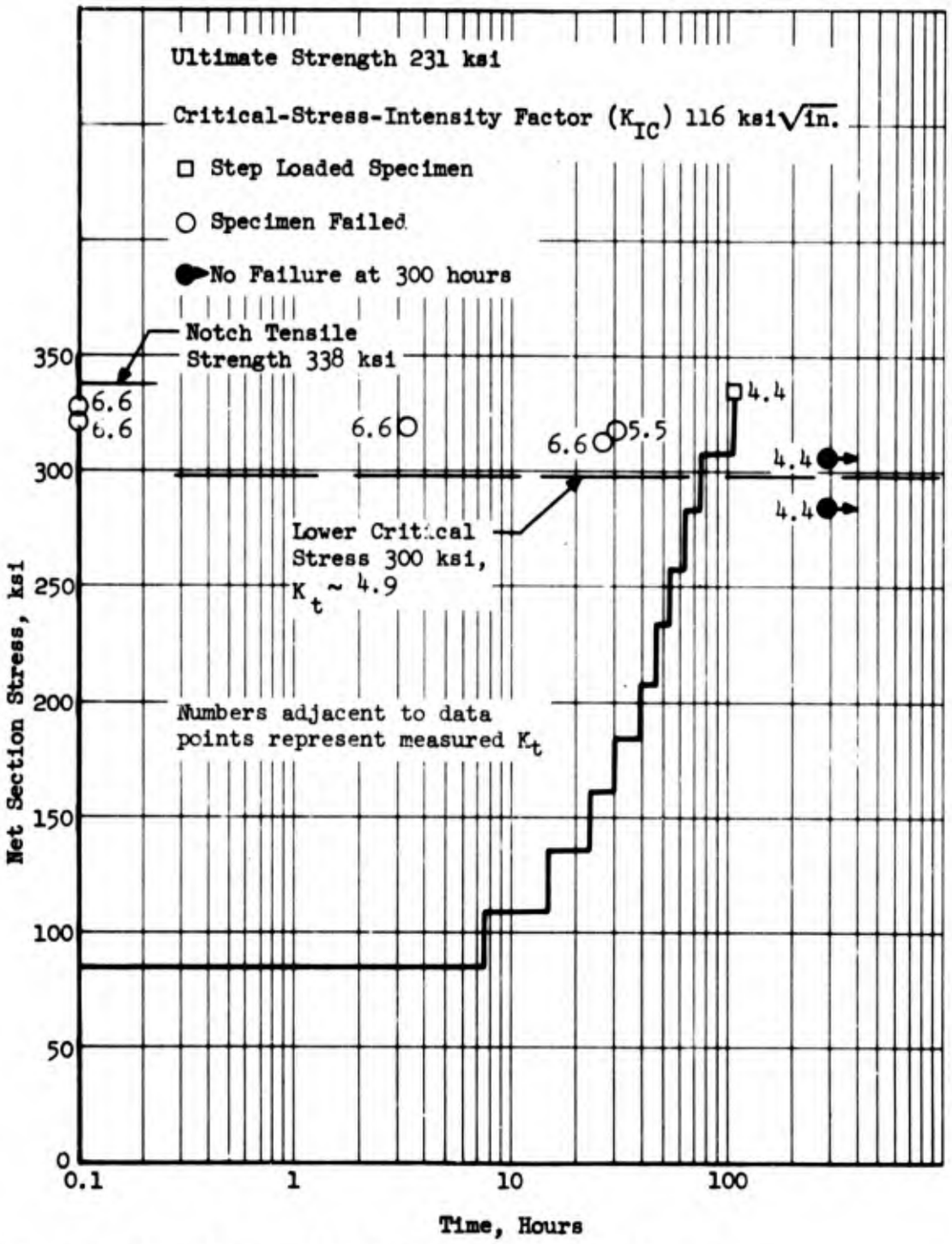

Figure 95. Delayed Failure of 9Ni-4Co-0.30C Cadmium-Plated Specimens

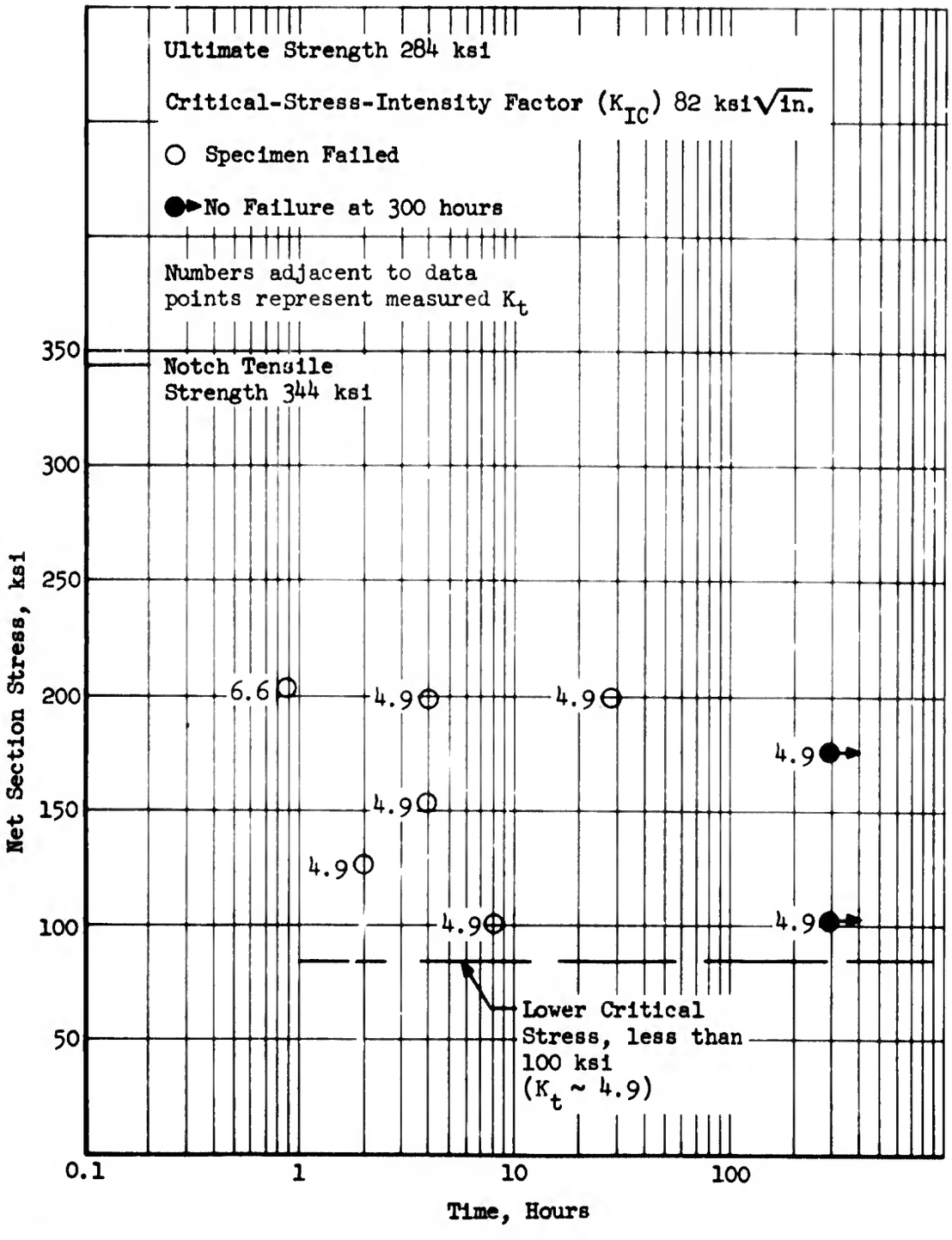

Figure 96. Delayed Failure of 300M Cadmium-Plated Specimens

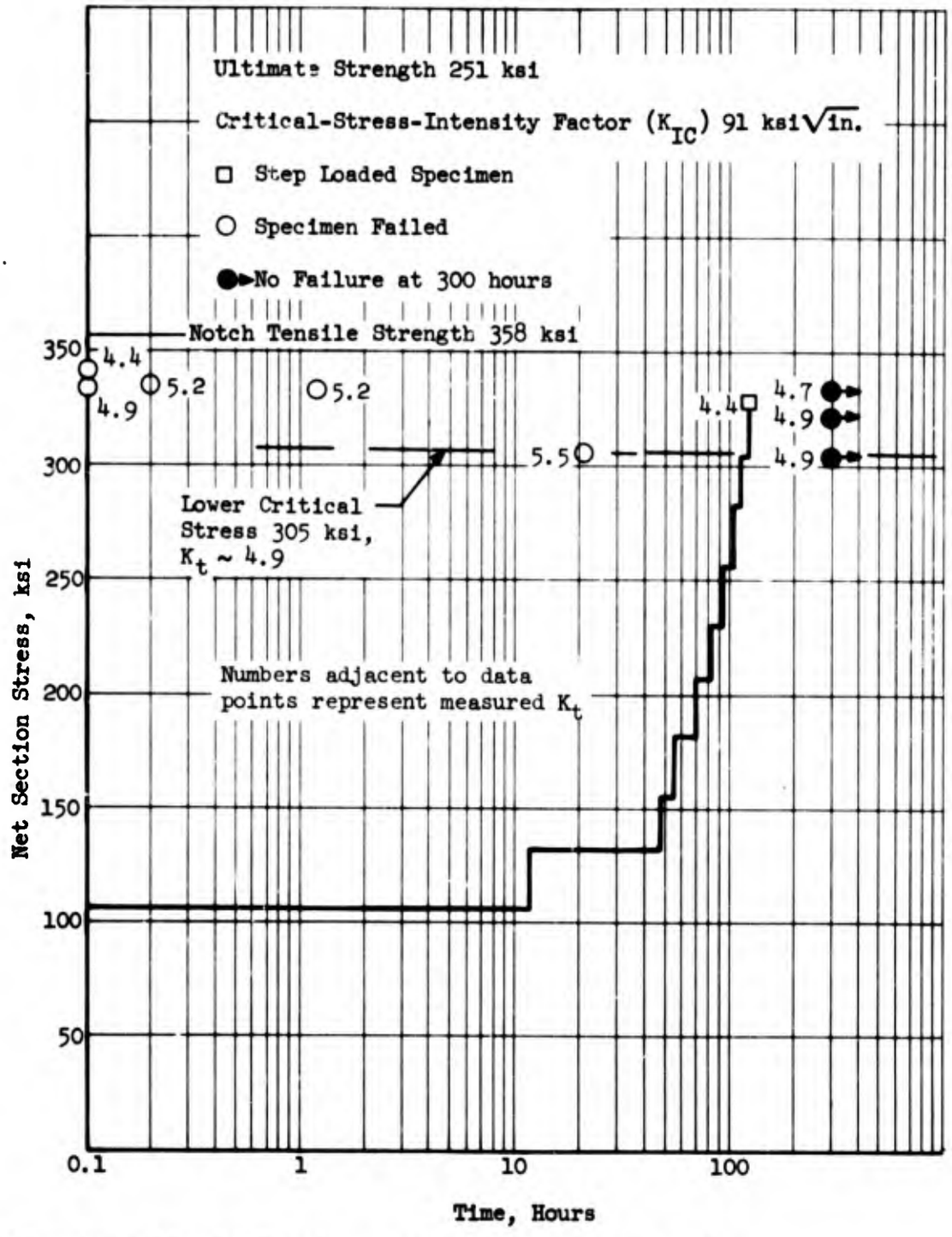

Figure 97. Delayed Failure of Maraging 250 Cadmium-Plated Specimens

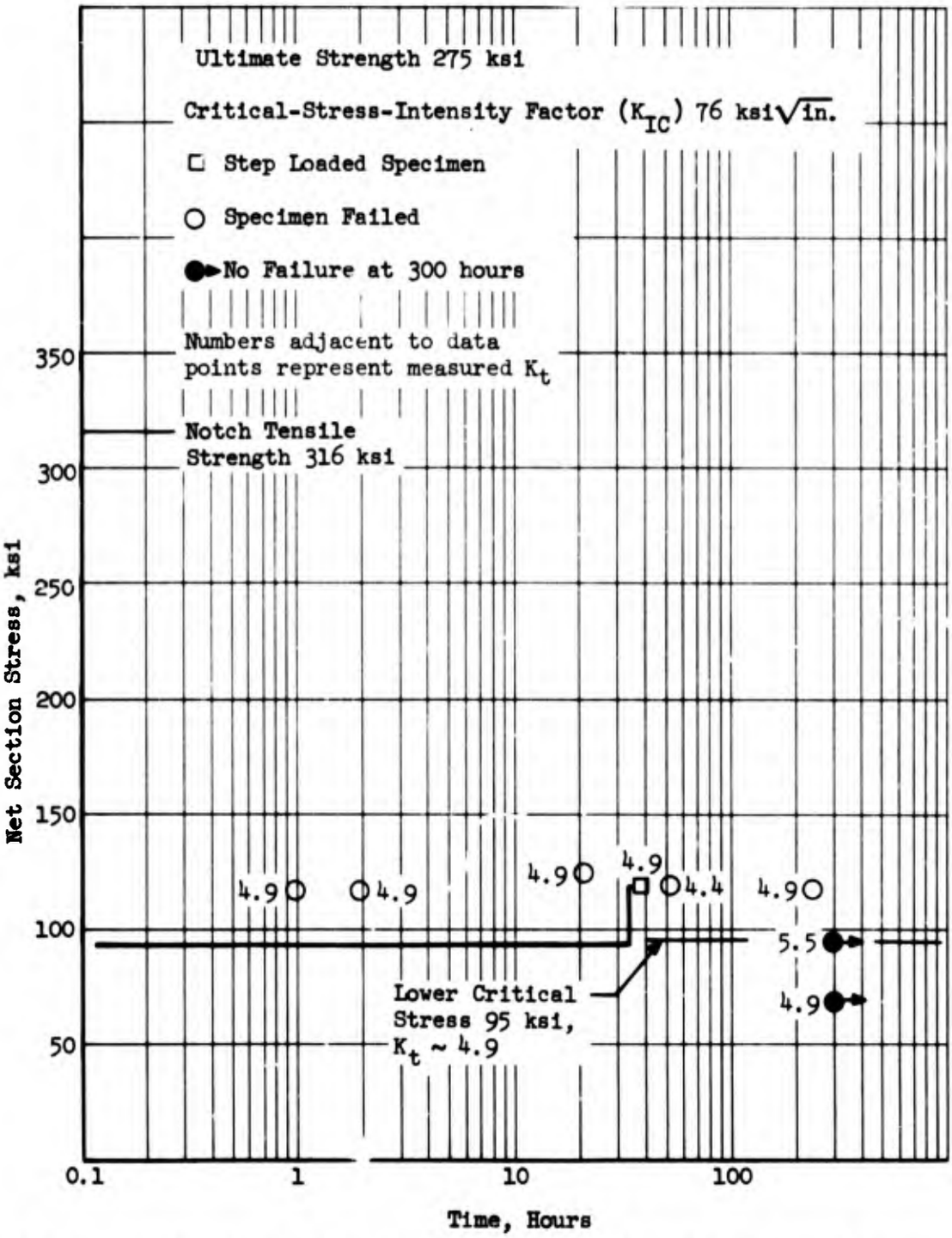

Figure 98. Delayed Failure of Quench-and-Tempered 9Ni-4Co-0.45C Cadmium-Plated Specimens

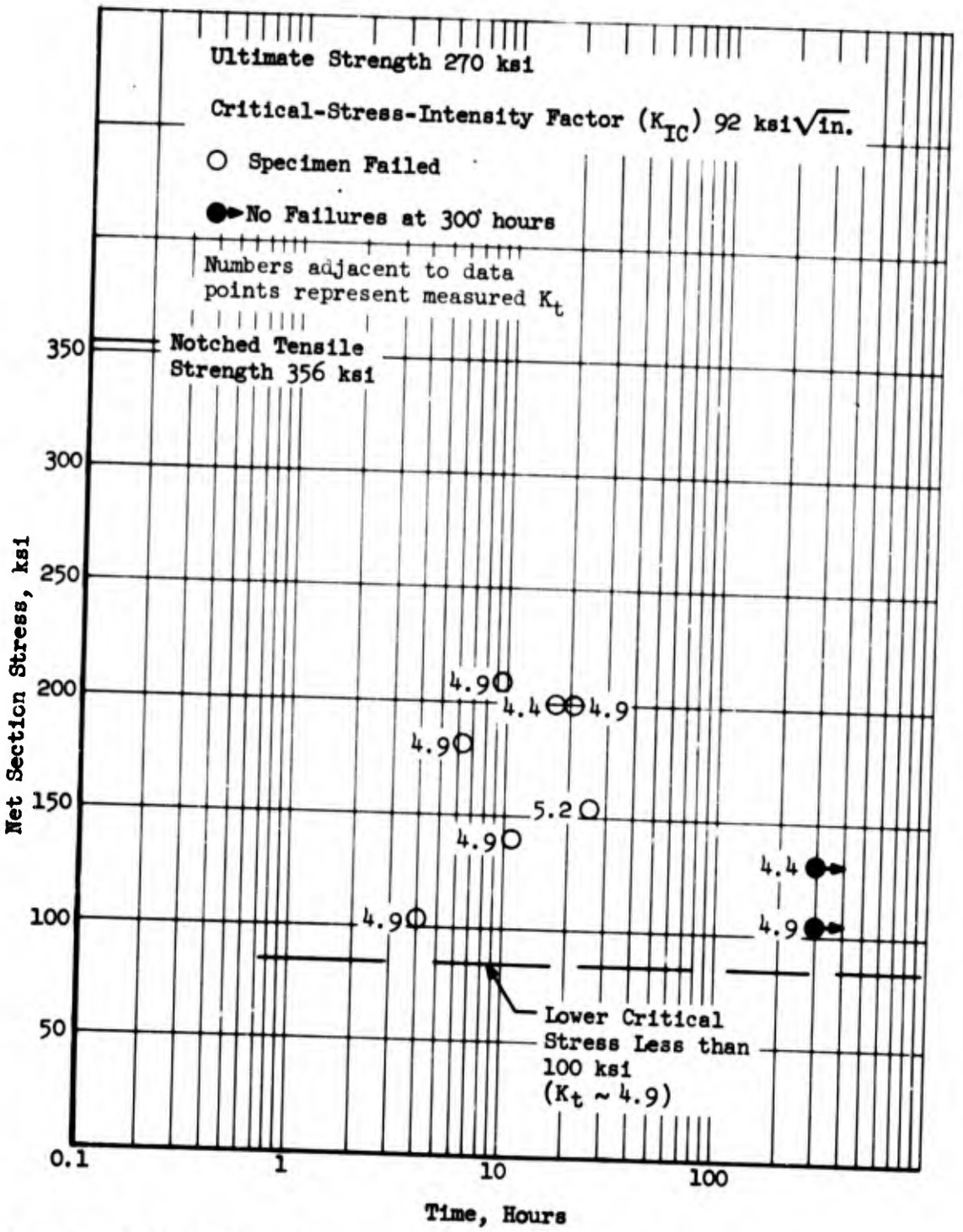

Figure 99. Delayed Failure of 9Ni-4Co-0.45C (Bainitic) Cadmium-Plated Specimens

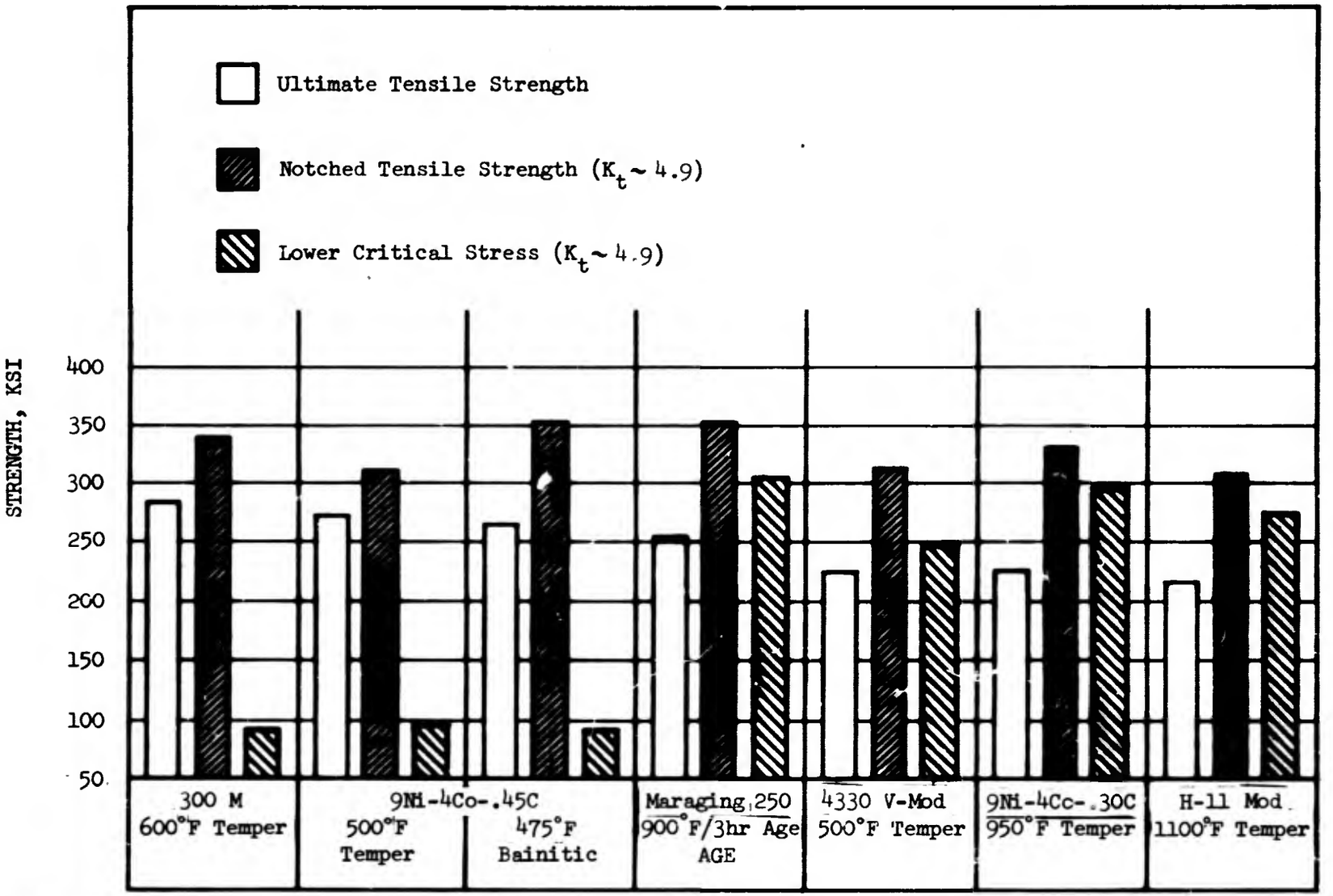

Figure 100. Hydrogen Embrittlement Susceptibilities

Table XXXIII Cadmium Plated Round Notched Tensile Specimen Data

Alloy	Heat Number	Specimen Number	Notch Diameter (inches)	Root Radius (inches)	Stress Concentration (K_t)	Notch Strength (ksi)	Sustained Stress Level (ksi)	Time at Stress (hour)
4330 V-Modified	C10157	A142	.2358	.004	4.9	+316.9	---	---
		A143	.2347	.004	4.9	+328.7	---	---
		A101	.2356	.004	4.9		* 96.8	7.9 NF
							*121.8	8.1 NF
							*146.8	8.0 NF
							*171.8	7.9 NF
							*196.8	8.0 NF
							*121.8	8.1 NF
							*246.8	8.8 NF
							*271.8	8.5 NF
							*296.8	0 FOL
		A102	.2352	.003	5.5		246.8	8 F
		A103	.2358	.004	4.9		200.0	300 NF
		A104	.2346	.004	4.9		225.0	300 NF
		A105	.2357	.002	6.6		240.0	300 NF
		A106	.2346	.004	4.9		260.0	300 NF
		A107	.2353	.004	4.9		275.0	300 NF
		A108	.2355	.004	4.9		280.0	300 NF
		A109	.2355	.004	4.9		290.0	78 F

\+ - Not Plated
* - Step Loaded
NF - No Failure
F - Failure
FOL - Failed on Loading

Table XXXIII Cadmium Plated Round Notched Tensile Specimen Data (Continued)

Alloy	Heat Number	Specimen Number	Notch Diameter (inches)	Root Radius (inches)	Stress Concentration (K_t)	Notch Strength (ksi)	Sustained Stress Level (ksi)	Time at Stress (hour)
H-11 Mod	09099	B142	.2350	.0045	4.7	+323.1	---	---
		B143	.2360	.003	5.5	+315.8	---	---
		B101	.2358	.004	4.9		* 95.8	8 NF
							*120.8	8 NF
							*145.8	8 NF
							*170.8	8 NF
							*195.8	8 NF
							*220.8	8 NF
							*245.8	8 NF
							*270.8	7.9 NF
							*295.8	0.03 F
		B102	.2364	.004	4.9		245.8	300 NF
		B103	.2353	.003	5.5		270.8	300 NF
		B104	.2354	.0035	5.2		300.0	0.01 F
		B105	.2125	.003	5.5		280.0	300 NF
		B106	.2362	.004	4.9		290.0	300 NF
		B107	.2234	.0035	5.2		300.0	27 F
		B108	.2234	.0035	5.2		300.0	300 NF
		B109	.2349	.0035	5.2		295.0	0.25 F

+ - Not Plated
* - Step Loaded
NF - No Failure
F - Failure
FOL - Failed on Loading

Table XXXIII Cadmium Plated Round Notched Tensile Specimen Data (Continued)

Alloy	Heat Number	Specimen Number	Notch Diameter (inches)	Root Radius (inches)	Stress Concentration (K_t)	Notch Strength (ksi)	Sustained Stress Level (ksi)	Time at Stress (hour)
9Ni-4Co-0.30C	3931144	C104	.2346	.004	4.9	+338.0	---	---
		C101	.2363	.005	4.4		* 84.8	7.9 NF
							*109.8	8.1 NF
							*134.8	8 NF
							*159.8	7.9 NF
							*184.8	8.1 NF
							*209.8	8 NF
							*234.8	7.8 NF
							*259.8	8.5 NF
							*284.8	123 NF
							*309.8	35.4 NF
							334.8	FOL
		C102	.2126	.005	4.4		284.8	300 NF
		C103	.2348	.002	6.6		330.0	FOL
		C105	.2336	.002	6.6		325.0	0.05 F
		C106	.2365	.005	4.4		309.0	300 NF
		C107	.2335	.002	6.6		320.0	3.3
		C108	.2107	.002	6.6		315.0	28.9
		C109	.2336	.003	5.5		317.5	31.3

\+ - Not Plated
* - Step Loaded
NF - No Failure
F - Failure
FOL - Failed on Loading

Table XXXIII Cadmium Plated Round Notched Tensile Specimen Data (Continued)

Alloy	Heat Number	Specimen Number	Notch Diameter (inches)	Root Radius (inches)	Stress Concentration (K_t)	Notch Strength (ksi)	Sustained Stress Level (ksi)	Time at Stress (hour)
300 M	3931531	D142	.2440	.007	3.8	+331.0	---	---
		D143	.2346	.004	4.9	+356.5	---	---
		D101	.2370	.004	4.9		103.1	7.1 F
		D103	.2333	.002	6.6		205.0	.9 F
		D104	.2344	.004	4.9		103.1	300 NF
		D105	.2355	.004	4.9		128.1	2 F
		D106	.2344	.004	4.9		153.1	4 F
		D107	.2355	.004	4.9		178.1	300 NF
		D108	.2358	.004	4.9		200.0	4
		D109	.2343	.004	4.9		200.0	29.9

+ - Not Plated
* - Step Loaded
NF - No Failure
F - Failure
FOL - Failed on Loading

Table XXXIII Cadmium Plated Round Notched Tensile Specimen Data (Continued)

Alloy	Heat Number	Specimen Number	Notch Diameter (inches)	Root Radius (inches)	Stress Concentration (K_t)	Notch Strength (ksi)	Sustained Stress Level (ksi)	Time at Stress (hour)
Maraging-250	09148	E142	.2363	.0045	4.7	+357.4		
		E143	.2345	.0025	6.1	+358.3		
		E101	.2351	.005	4.4		*107.3	11.5 NF
							*132.3	35.6 NF
							*157.3	7.9 NF
							*182.3	15 NF
							*207.3	16.1 NF
							*232.3	8.7 NF
							*257.3	8 NF
							*282.3	8.1 NF
							*307.3	8.1 NF
							*332.3	3.3 F
		E102	.2268	.003	5.5		307.4	20.6 F
		E103	.2200	.004	4.9		307.4	300.0 NF
		E104	.2349	.0045	4.7		332.4	300.0 NF
		E105	.2352	.005	4.4		340.0	FOL
		E106	.2359	.0035	5.2		335.0	0.20 F
		E107	.2361	.004	4.9		335.0	FOL
		E108	.2363	.004	4.9		333.5	300 NF
		E109	.2350	.0035	5.2		334.0	1.3 NF

\+ - Not Plated
* - Step Loaded
NF - No Failure
F - Failure
FOL - Failed on Loading

Table XXXIII Cadmium Plated Round Notched Tensile Specimen Data (Concluded)

Alloy	Heat Number	Specimen Number	Notch Diameter (inches)	Root Radius (inches)	Stress Concentration (K_t)	Notch Strength (ksi)	Sustained Stress Level (ksi)	Time at Stress (hour)
9Ni-4Co-0.45C (Quench-Temper)	3931120	F142	.2354	.004	4.9	+310.3	---	---
		F143	.2357	.004	4.9	+321.1	---	---
		F101	.2347	.004	4.9		* 94.7	35.5 NF
							*119.7	1.8 F
		F102	.2342	.004	4.9		119.7	1.0 F
		F103	.2350	.004	4.9		69.7	300 NF
		F104	.2347	.003	5.5		94.7	300 NF
		F105	.2342	.005	4.4		119.7	42.2 F
		F106	.2352	.004	4.9		125.0	11.5 F
		F107	.2357	.004	4.9		120.0	2.0 F
		F108	.2342	.004	4.9		125.0	20.0 F
		F109	.2342	.004	4.9		120.0	285.6 F
9Ni-4Co-0.45C (Bainitic)	3931120	G142	.2337	.004	4.9	+363.6		
		G143	.2347	.004	4.9	+347.7		
		G101	.2345	.004	4.9		106.7	4.3 F
		G102	.2352	.004	4.9		106.7	300 NF
		G103	.2336	.005	4.4		131.7	300 NF
		G104	.2350	.0035	5.2		156.7	26.6 F
		G105	.2355	.004	4.9		181.7	6.7 F
		G106	.2351	.004	4.9		200.0	20.1 F
		G107	.2343	.005	4.4		200.0	19.6 F
		G108	.2351	.004	4.9		210.0	8.8 F
		G109	.2357	.004	4.9		140.0	11.0 F

+ - Not Plated
* - Step Loaded
NF - No Failure
F - Failure
FOL - Failed on Loading

10.0 NOTCHED FATIGUE TESTING

Much of the previous testing in this program has been designed to determine the reliability of high strength steel alloys to insure a fail-safe structure. However, fatigue S-N curves for each alloy are desirable for determination of the cycles to originate cracks. Once cracks have originated they may propagate by stress corrosion cracking without a cycling load.

10.1 PROCEDURE

Notched fatigue specimens with a stress concentration factor of 2.5 were selected for this study as being representative of aircraft structure. The specimen and description of test equipment are included in Sec. 3.0. All specimens were cycled at 1800 cycles/min. using a stress ratio of 0.06.

10.2 RESULTS AND DISCUSSION

It was intended to test three specimens at each of three stress levels to develop a stress-level versus cycles-to-failure curve. However, since there is generally better reproducibility at higher stress levels, in some cases more specimens were tested at lower stress levels to better define the endurance limit. The fatigue data for the six alloys are included in Table XXXIV and the individual S-N curve for each alloy are shown in Figs. 101 through 107.

The curves were drawn through the log average of the higher data points and were somewhat conservative at the endurance limit because of the limited number of data points to define the endurance limit. A comparison of the seven curves (Figs. 108 and 109) indicates very little difference in endurance limit. All steels tested in this program had endurance limits which fell between 50 and 60 ksi gross area fatigue stress even though the ultimate strengths varied from 219 to 284 ksi. Because the number of specimens were limited it is difficult to determine those alloys with the highest endurance limit, however, the 9Ni-4Co alloys in the quenched and tempered condition appear to be highest. The general conclusion from this somewhat limited data is that the endurance limits of these high strength steels are similar and other variations such as specimen geometry, environment, grain direction, and stress ratio would have considerably greater effects on results.

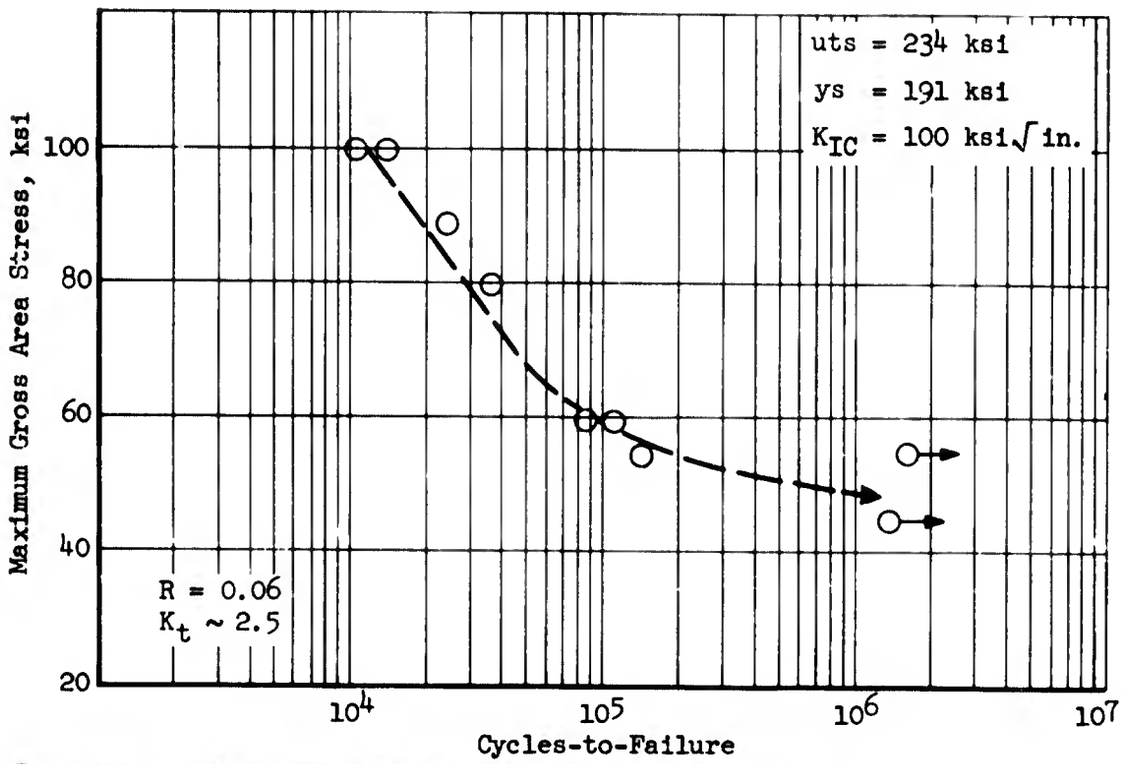

Figure 101. 4330 V-Modified Fatigue Data, Transverse Grain Direction

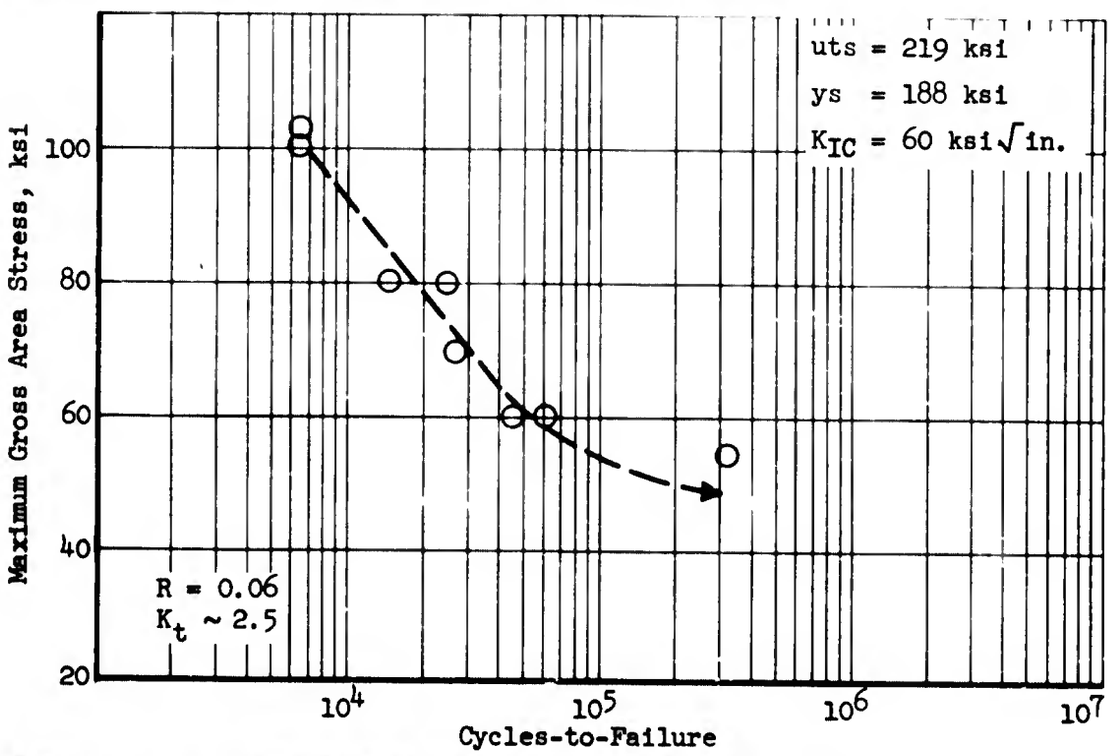

Figure 102. H-11 Modified Fatigue Data, Transverse Grain Direction

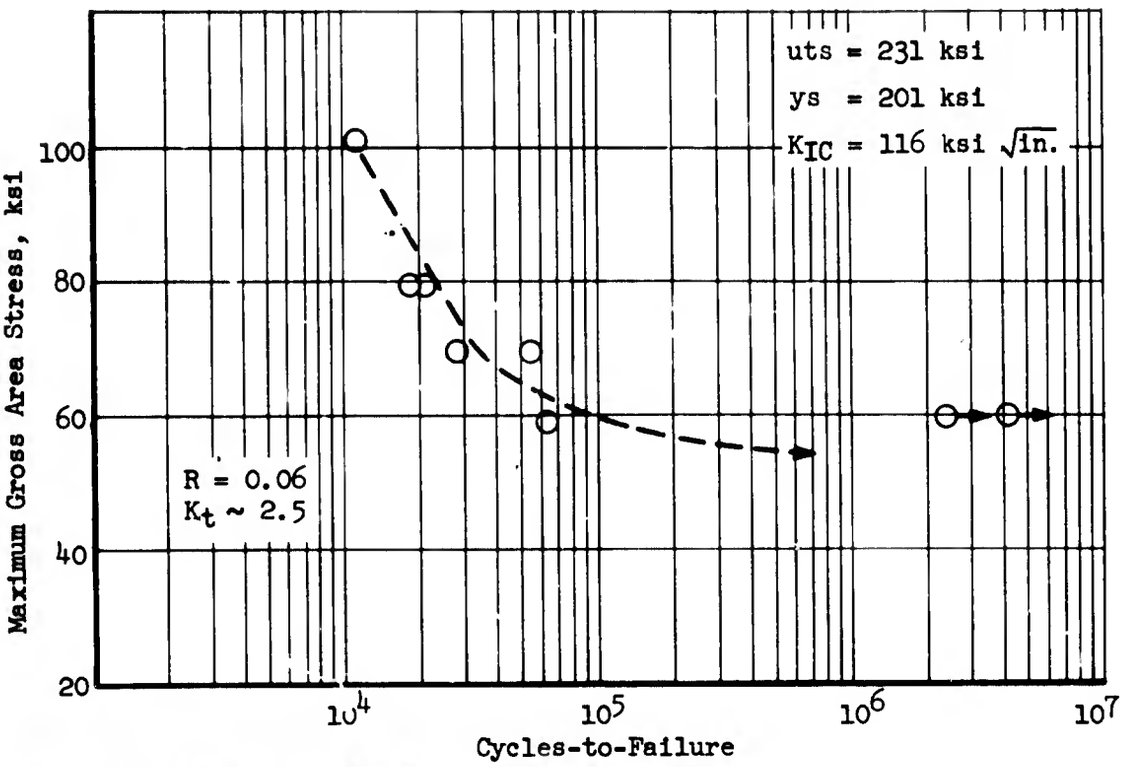

Figure 103. 9Ni-4Co-0.30C Fatigue Data, Transverse Grain Direction

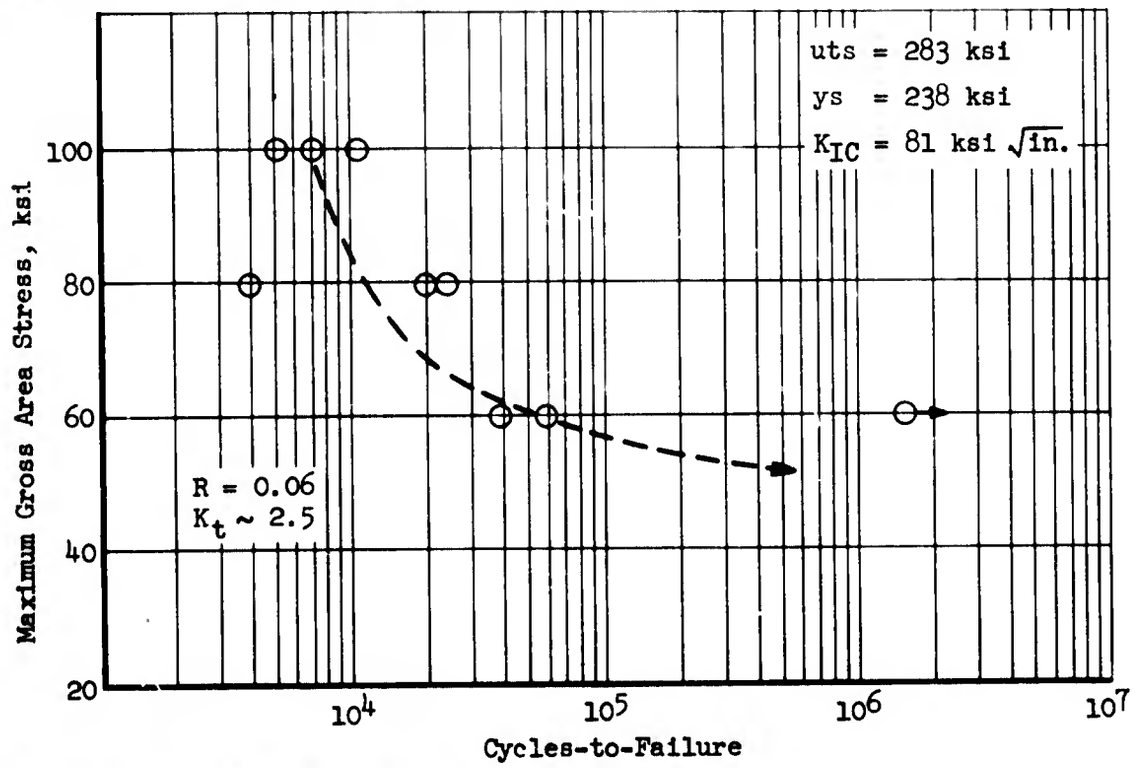

Figure 104. 300M Fatigue Data, Transverse Grain Direction

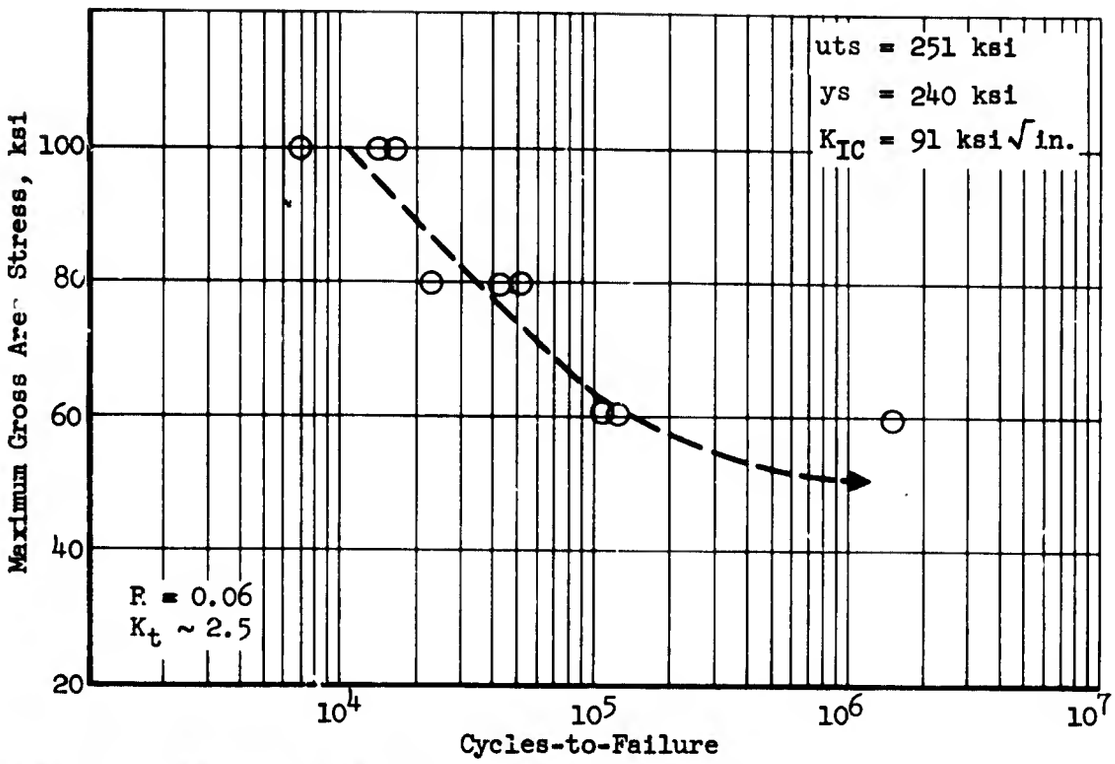

Figure 105. Maraging 250 Fatigue Data, Transverse Grain Direction

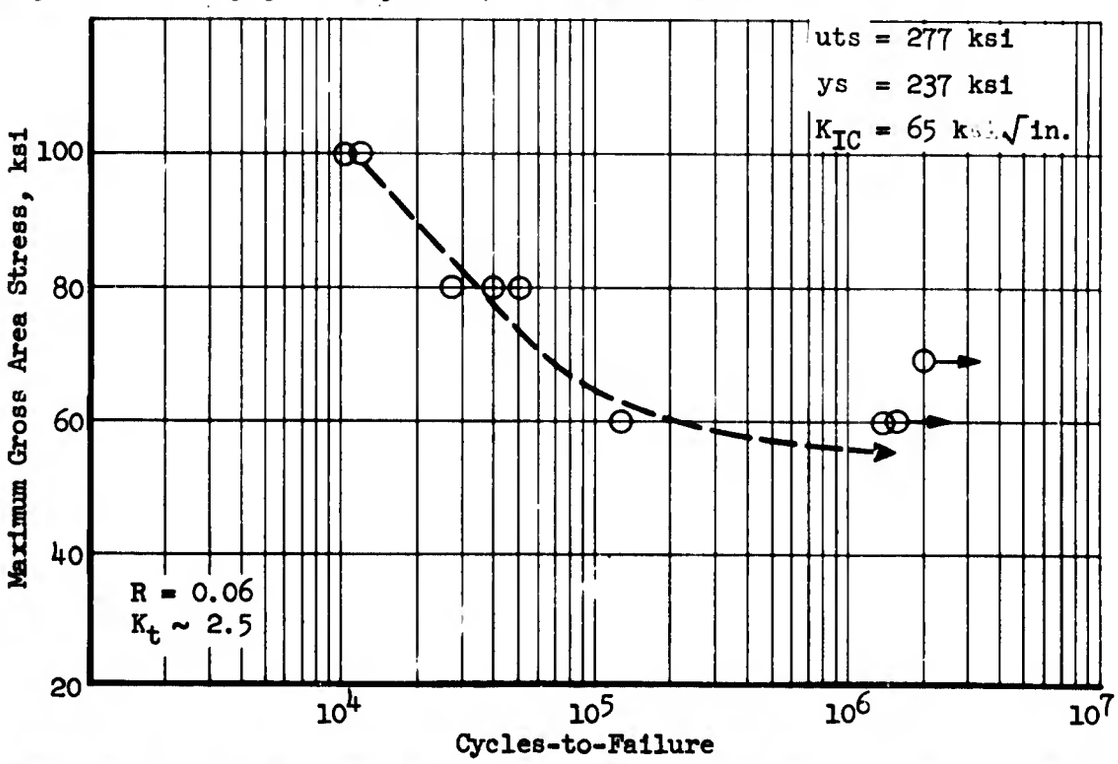

Figure 106. Quench-and-Tempered 9Ni-4Co-0.45C Fatigue Data, Transverse Grain Direction

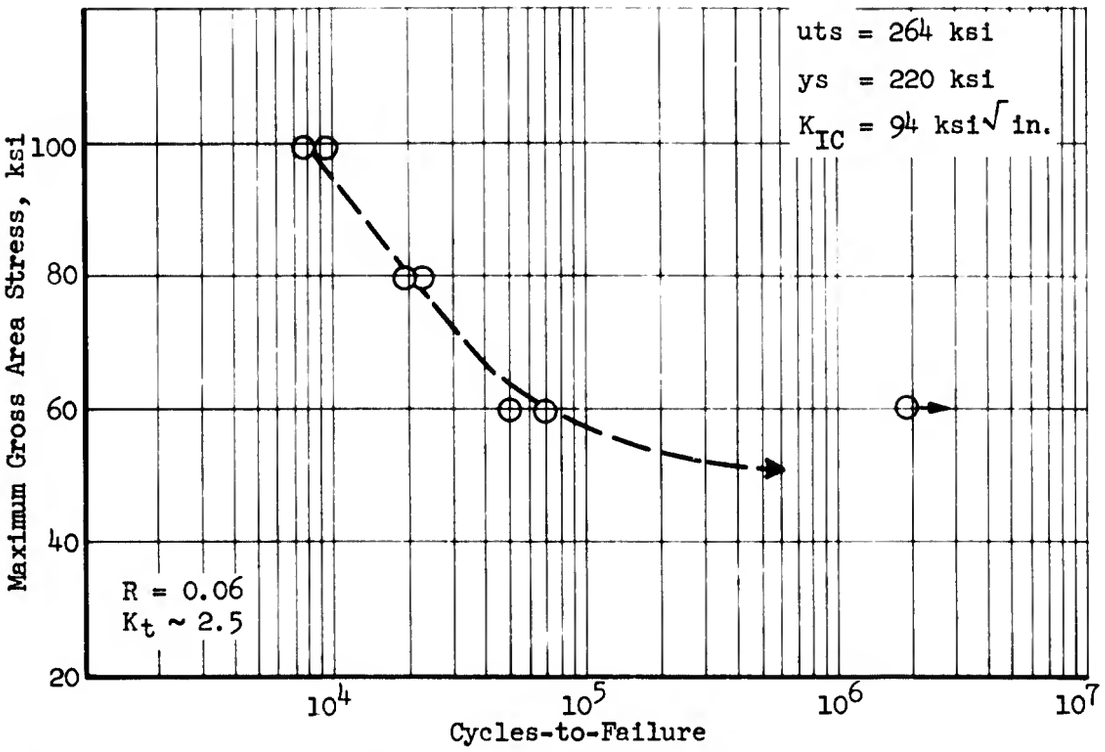

Figure 107. Bainitically Treated 9Ni-4Co-0.45C Fatigue Data, Transverse Grain Direction

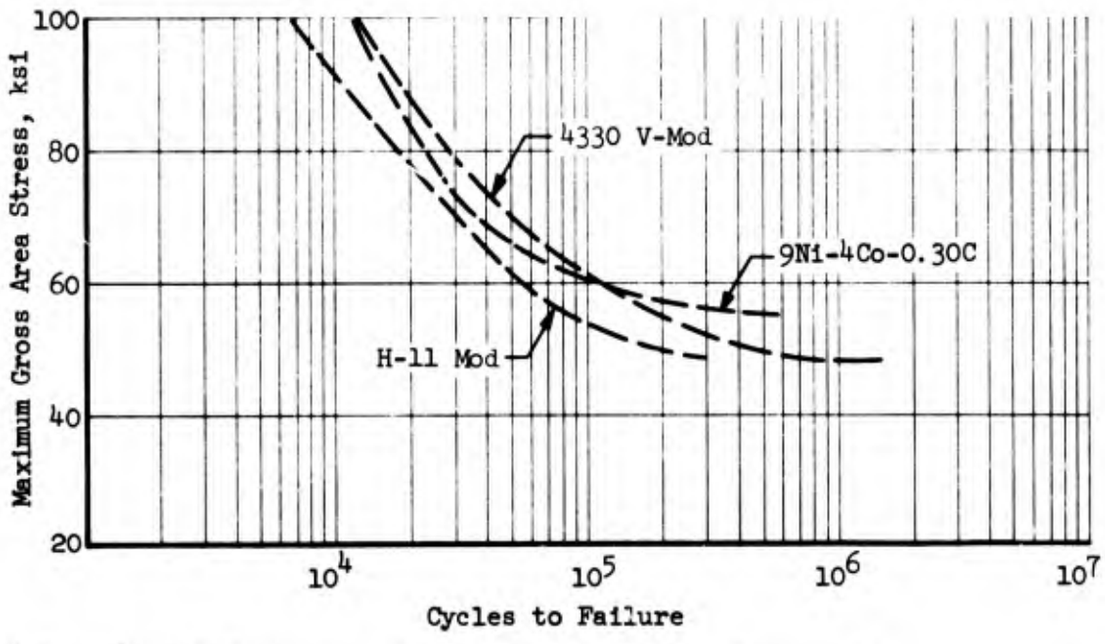

Figure 108. Fatigue Properties of Alloys Heat-Treated to Ultimate Strength Strength of 220-240 KSI

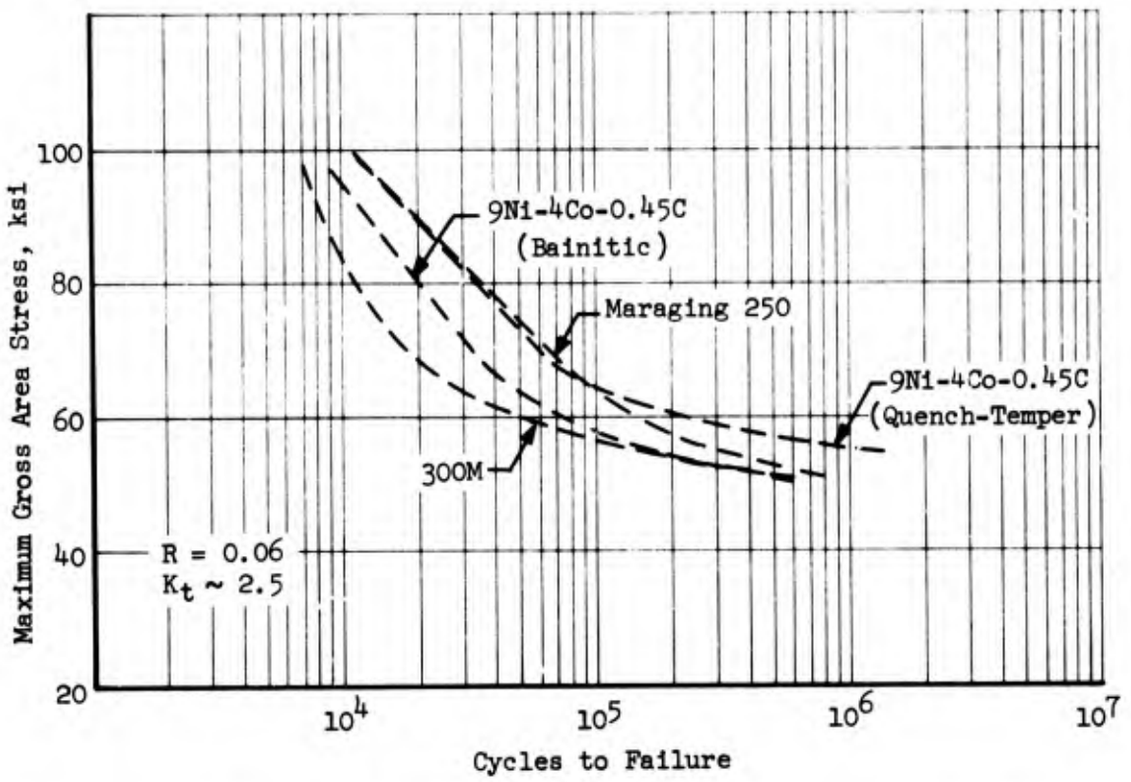

Figure 109. Fatigue Properties of Alloys Heat-Treated to Ultimate Strengths Greater than 250 KSI

Table XXXIV Room Temperature Fatigue Data

Alloy (Showing comparative strength and toughness)	Heat Number	Specimen Number	Gross Area (sq. inch)	Maximum Gross Area Stress (ksi)	Cycles to Failure
4330 V-Modified UTS - 234 ksi YS - 191 ksi K_{IC} - 100 ksi$\sqrt{in.}$	C10157	A115	.1516	100	11,000
		A110	.1513	100	15,000
		A111	.1498	90	24,000
		A116	.1486	80	36,000
		A112	.1510	60	84,000
		A118	.1524	60	119,000
		A114	.1498	55	154,000
		A117	.1519	55	1,775,000 NF
		A113	.1528	45	1,407,000 NF
H-11 Mod UTS - 219 ksi YS - 188 ksi K_{IC} - 60 ksi$\sqrt{in.}$	09099	B110	.1561	100	7,000
		B111	.1519	100	7,000
		B116	.1576	80	16,000
		B113	.1505	80	17,000
		B112	.1508	80	26,000
		B117	.1523	70	29,000
		B114	.1482	60	48,000
		B115	.1504	60	61,000
		B118	.1522	55	301,000
9Ni-4Co-0.30C UTS - 231 YS - 201 K_{IC} - 116 ksi$\sqrt{in.}$	3931144	C110	.1582	100	12,000
		C111	.1567	100	12,000
		C112	.1532	80	19,000
		C113	.1573	80	21,000
		C117	.1535	70	28,000
		C116	.1577	70	59,000
		C115	.1522	60	64,000
		C114	.1543	60	2,343,000 NF
		C118	.1574	60	4,028,000 NF

NF - No Failure

Table XXXIV Room Temperature Fatigue Data (Continued)

Alloy (Showing comparative strength and toughness)	Heat Number	Specimen Number	Gross Area (sq. inch)	Maximum Gross Area Stress (ksi)	Cycles to Failure
300 M UTS - 283 ksi YS - 238 ksi K_{IC} - 81 ksi$\sqrt{in.}$	3951531(R)	D111	.1471	100	5,000
		D116	.1501	100	7,000
		D110	.1507	100	11,000
		D113	.1495	80	4,000
		D112	.1506	80	20,000
		D117	.1511	80	24,000
		D118	.1457	60	38,000
		D115	.1485	60	59,000
		D114	.1513	60	1,544,000 NF
Maraging 250 UTS - 251 ksi YS - 240 KSI K_{IC} - 91 ksi$\sqrt{in.}$	09148	E110	.1524	100	7,000
		E111	.1578	100	15,000
		E117	.1567	100	16,000
		E113	.1587	80	23,000
		E112	.1547	80	42,000
		E116	.1580	80	50,000
		E118	.1566	60	105,000
		E114	.1614	60	112,000
		E115	.1580	60	1,706,000
9Ni-4Co-0.45C (Quench and Temper) UTS - 277 ksi YS - 237 ksi K_{IC} - 65 ksi$\sqrt{in.}$	3931120	F111	.1561	100	11,000
		F110	.1539	100	12,000
		F112	.1583	80	29,000
		F116	.1555	80	41,000
		F113	.1515	80	50,000
		F118	.1556	70	1,967,000 NF
		F115	.1558	60	132,000
		F114	.1545	60	1,502,000 NF
		F117	.1546	60	1,533,000 NF

NF - No Failure

Table XXXIV Room Temperature Fatigue Data (Concluded)

Alloy (Showing comparative strength and toughness)	Heat Number	Specimen Number	Gross Area (sq. inch)	Maximum Gross Area Stress (ksi)	Cycles to Failure
9Ni-4Co-0.45C (Bainitic) UTS - 264 ksi YS - 220 ksi K_{IC} - 94 ksi$\sqrt{in.}$	3931120	G111	.1514	100	8,000
		G110	.1551	100	10,000
		G113	.1539	80	20,000
		G112	.1549	80	22,000
		G117	.1538	70	51,000
		G116	.1522	70	52,000
		G118	.1527	60	52,000
		G115	.1530	60	71,000
		G114	.1534	60	1,979,000 NF

NF - No Failure

11.0 CONCLUSIONS

The purpose of this program was to provide data for a comparison of high strength steels for applications on the supersonic transport. To make a meaningful comparison, measurement of a number of material properties was considered necessary. In addition, the alloys fell in two general strength ranges; 220 to 240 ksi and 250 to 290 ksi. Because of the large number of materials, heat treatments & types of tests, it is clearer and more relevant to summarize the conclusions in the form of a table for each strength level.

Table XXXV Summary of Evaluation, 220-240 KSI Ultimate Strength

PROPERTY	RATING		
	FIRST	SECOND	THIRD
RT Fracture Toughness	9Ni-4Co-0.30C	4330 V-Mod	H-11 Mod
-65°F Fracture Toughness	9Ni-4Co-0.30C	4330 V-Mod	H-11 Mod
-65°F Impact Strength	9Ni-4Co-0.30C	4330 V-Mod	H-11 Mod
Stress Corrosion Resistance	9Ni-4Co-0.30C	4330 V-Mod H-11 Mod	
Ductility (RA)	4330 V-Mod 9Ni-4Co-0.30C H-11 Mod		
Fatigue (Limited Data)	9Ni-4Co-0.30C	4330 V-Mod	H-11 Mod
H_2 Embrittlement	9Ni-4Co-0.30C H-11 Mod 4330 V-Mod		
Potential for Elevated Temperature Applications	H-11 Mod	9Ni-4Co-0.30C	4330 V-Mod

Table XXXVI Summary of Evaluation, 250-290 KSI Ultimate Strength Range

Property	Rating		
	First	Second	Third
Ultimate Strength	300M	9Ni-4Co-0.45C (Q+T)	9Ni-4Co-0.45C (B) Maraging 250
RT Fracture Toughness	Maraging 250 9Ni-4Co-0.45C (B)	300M	9Ni-4Co-0.45C (Q+T)
-65°F Fracture Toughness	Maraging 250 9Ni-4Co-0.45C (B)	300M 9Ni-4Co-0.45C (Q+T)	
-65°F Inpact Strength	Maraging 250 9Ni-4Co-0.45C (B)	9Ni-4Co-0.45C (Q+T)	300M
Stress Corrosion Resistances	Maraging 250 9Ni-4Co-0.45C (B)	9Ni-4Co-0.45C (Q+T) 300M	
Ductility (RA)	300M 9Ni-4Co-0.45C (B) 9Ni-4Co-0.45C (Q+T)	Maraging 250	
Fatigue (Limited Data)	9Ni-4Co-0.45 (Q+T)	9Ni-4Co-0.45C (B) Maraging 250 300M	
H_2 Embrittlement	Maraging 250	9Ni-4Co-0.45C (Q+T) 9Ni-4Co-0.45C (B) 300M	
Potential for Elevated Temperature Applications	Maraging 250 300M	9Ni-4Co-0.45C (Q+T) 9Ni-4Co-0.45C (B)	

12.0 FUTURE WORK

The original proposal for this work included the forging and testing of six Boeing Model 720 landing gear torsion links from the 9Ni-4Co-0.45C alloy. Three forgings were sectioned for microscopic examination and for tensile strength and fracture toughness testing. The remaining three forgings were fabricated into finished parts, one of which is presently being fatigue tested under simulated 720 aircraft service conditions. Further, microstructural investigations are also planned to study the controlling mechanism of some of the more interesting effects on the fracture toughness versus tempering temperature curves. These microstructures will be studied with carbide extraction replica and transmission electron microscopy.

The supplemental report covering the above work will be submitted at the end of June 1967.

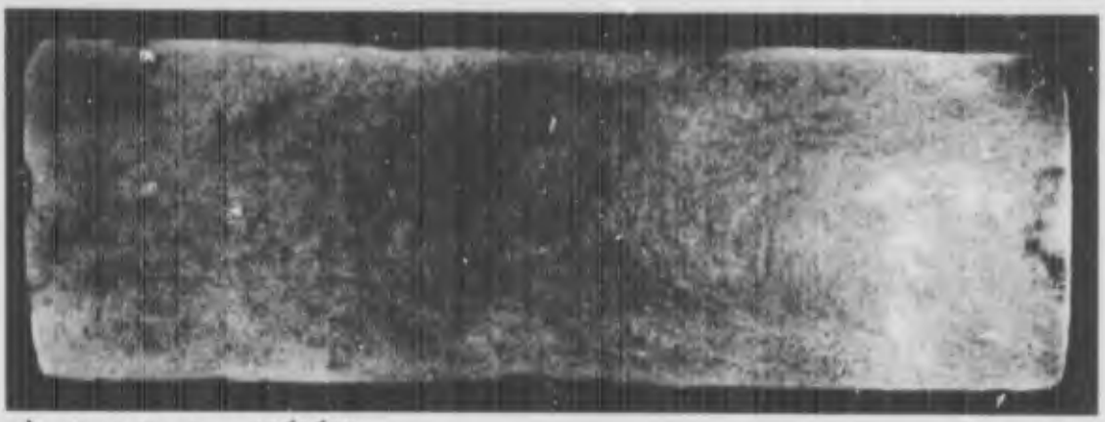

a) Heat Number 3960633

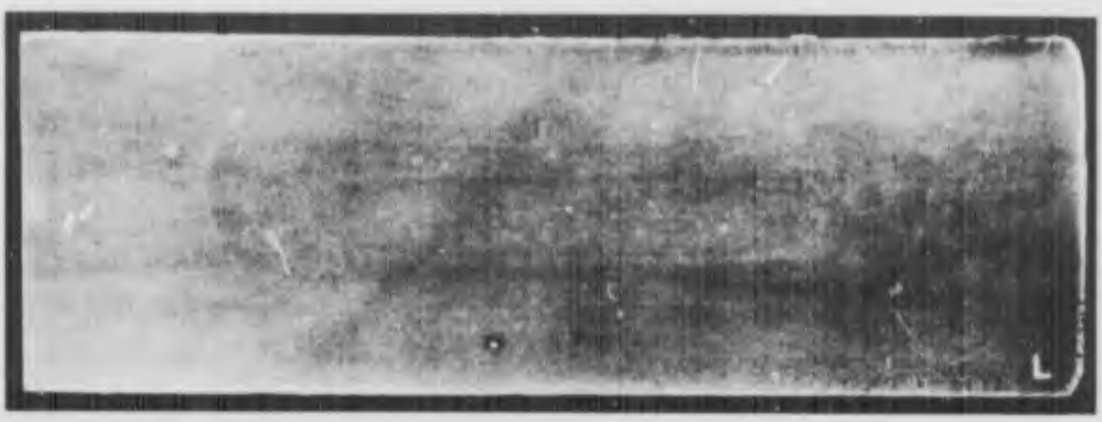

b) Heat Number C10151

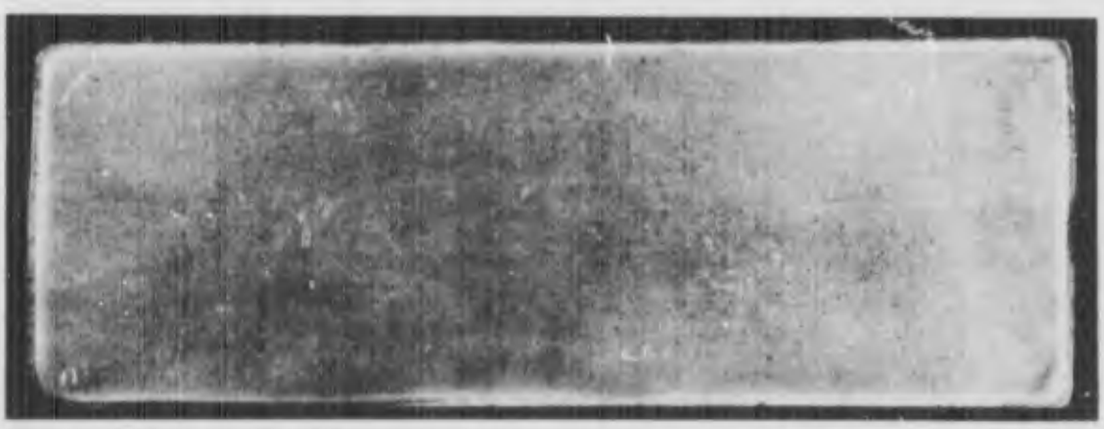

c) Heat Number C57046

Figure A-1. Macroetched Section from Ends of 4330 V-Mod Billets

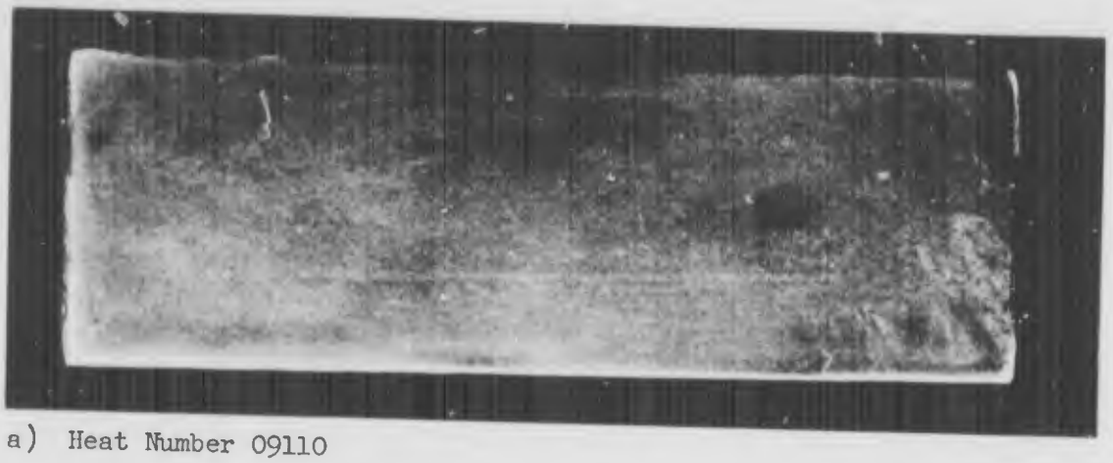

a) Heat Number 09110

b) Heat Number 09099

c) Heat Number 08990

Figure A-2. Macroetched Sections from Ends of H-11 Mod Billets

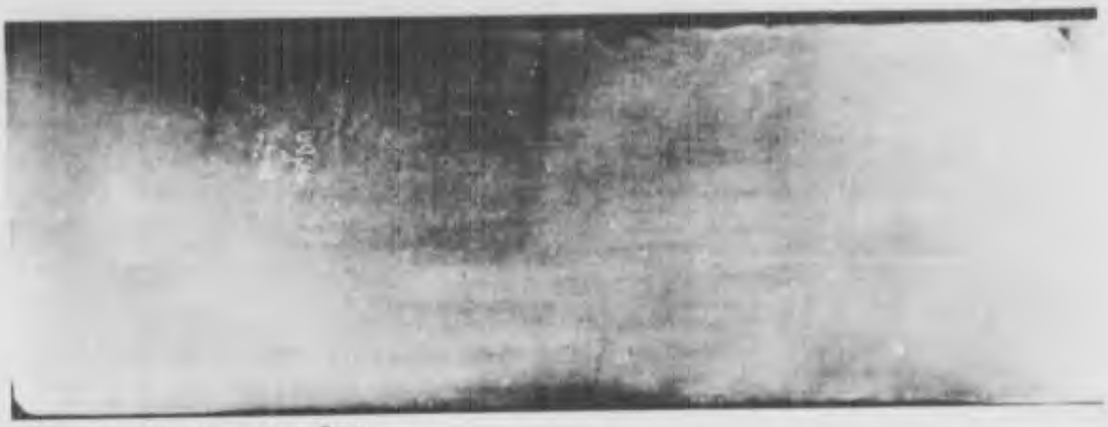

a) Heat Number 3930852

b) Heat Number 3931144

c) Heat Number 3931145

Figure A-3. Macroetched Section from Ends of 9Ni-4Co-0.30C Billets

a) Heat Number 09715

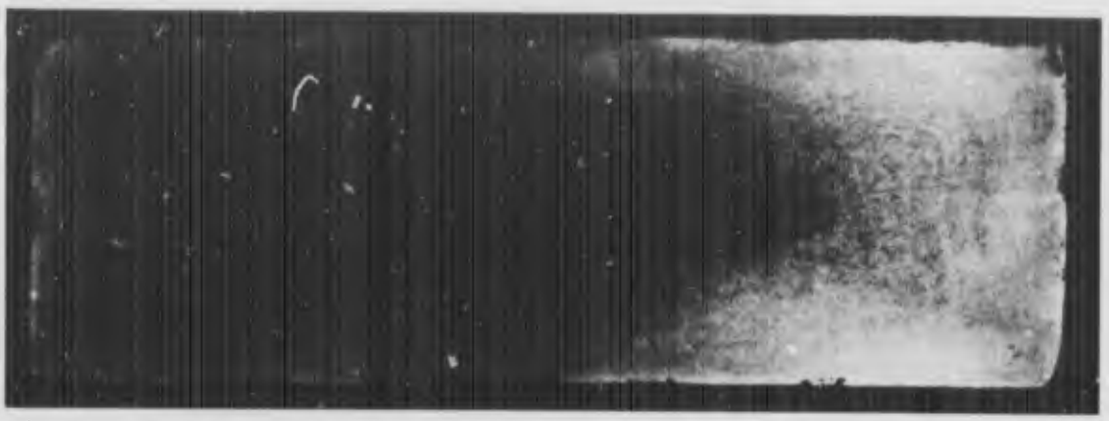

b) Heat Number 3951531 (Billet P)

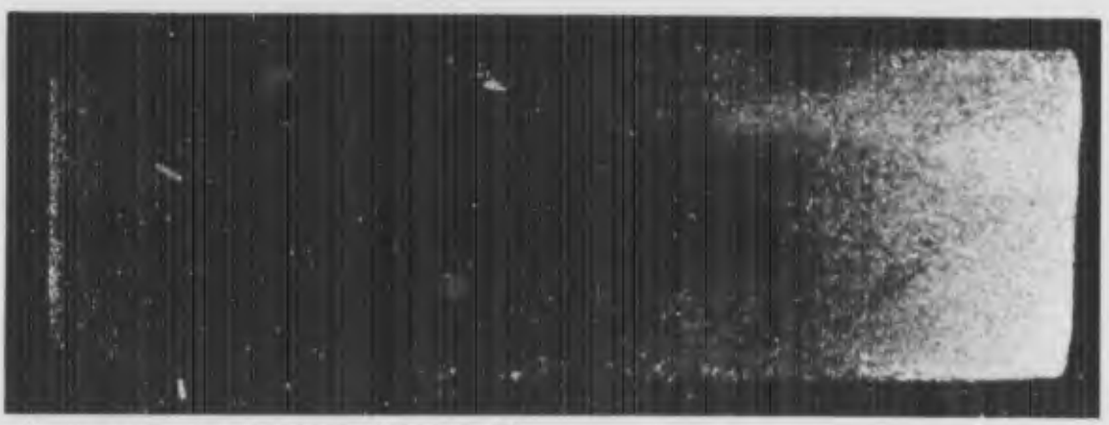

c) Heat Number 3951531 (Billet R)

Figure A-4. Macroetched Sections from the Ends of 300M Billets

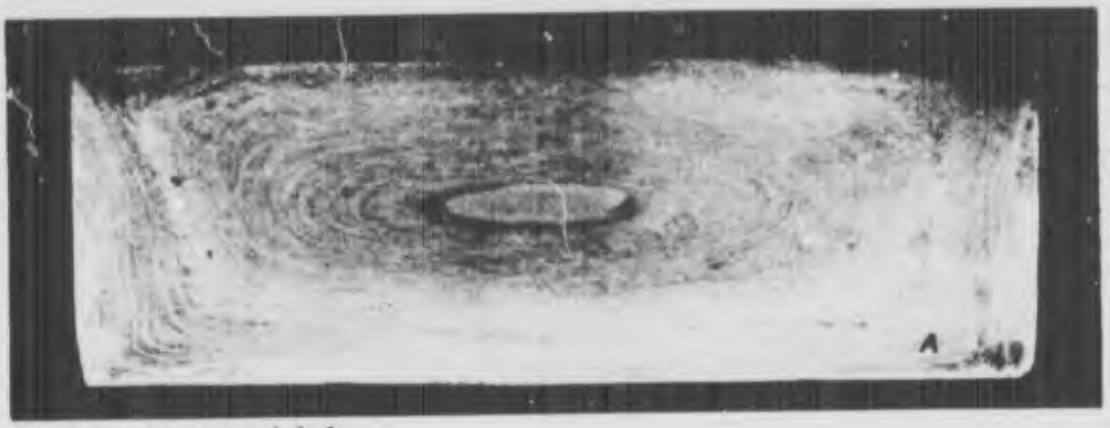

a) Heat Number 24676

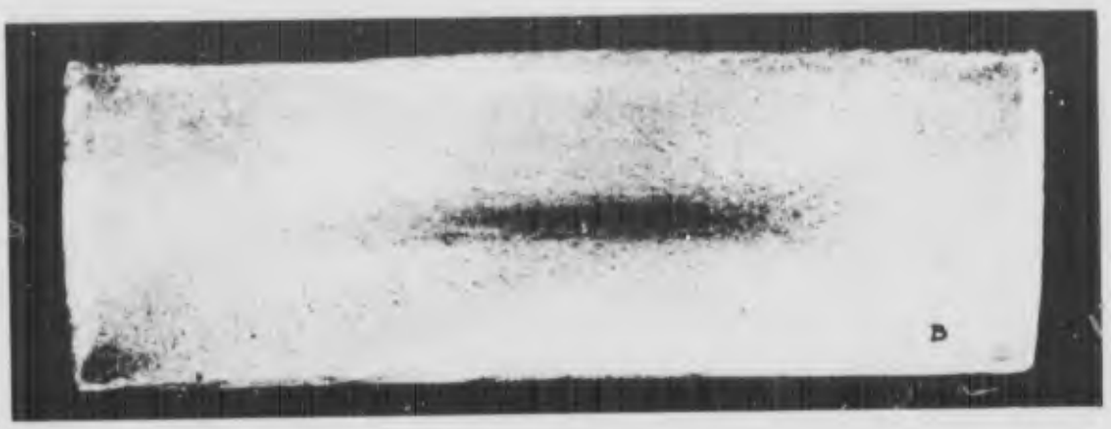

b) Heat Number 09148

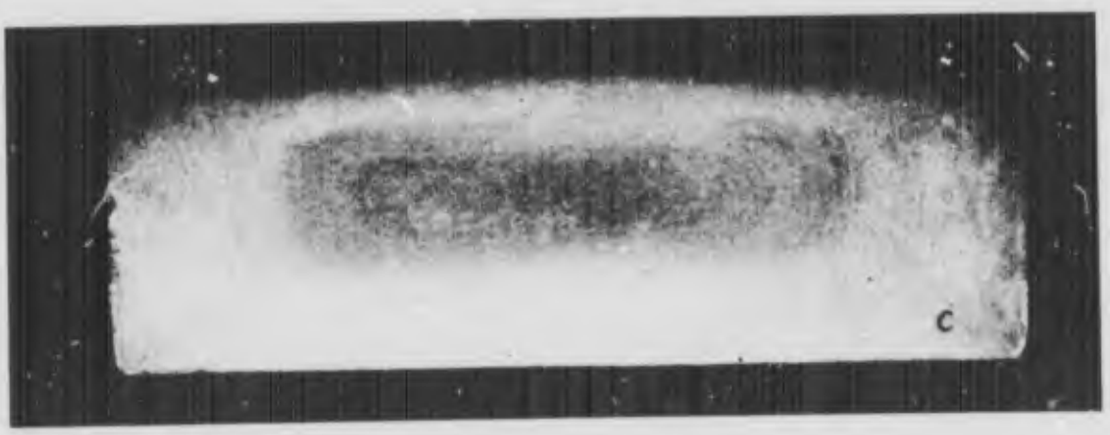

c) Heat Number 3930879

Figure A-5. Macroetched Sections from Ends of Maraging-250 Billets

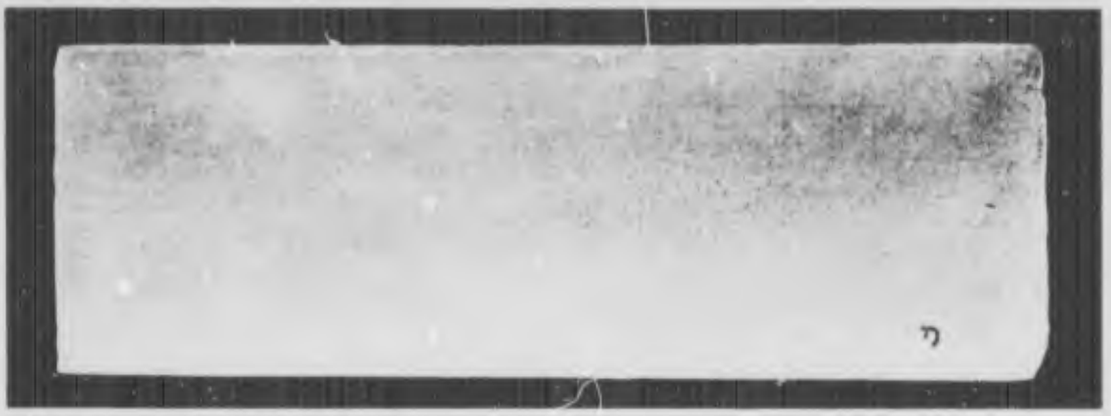

a) Heat Number 3882720

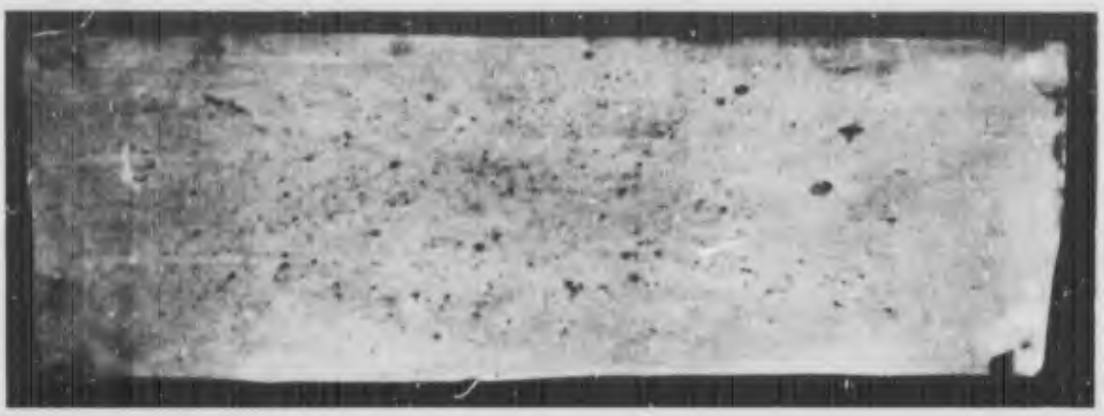

b) Heat Number 3931120

c) Heat Number 3931141

Figure A-6. Macroetched Section from Ends of 9Ni-4Co-0.45C Billets

Longitudinal Grain Direction

Transverse Grain Direction

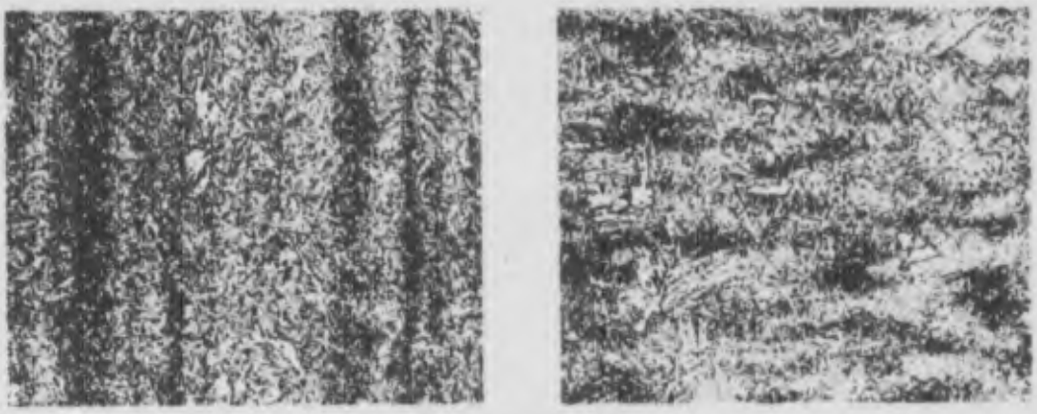

a) Heat 3960633

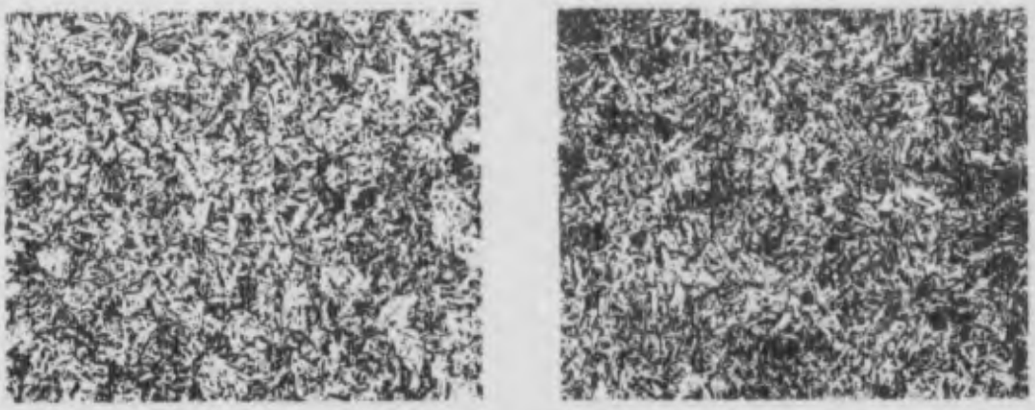

b) Heat C10157

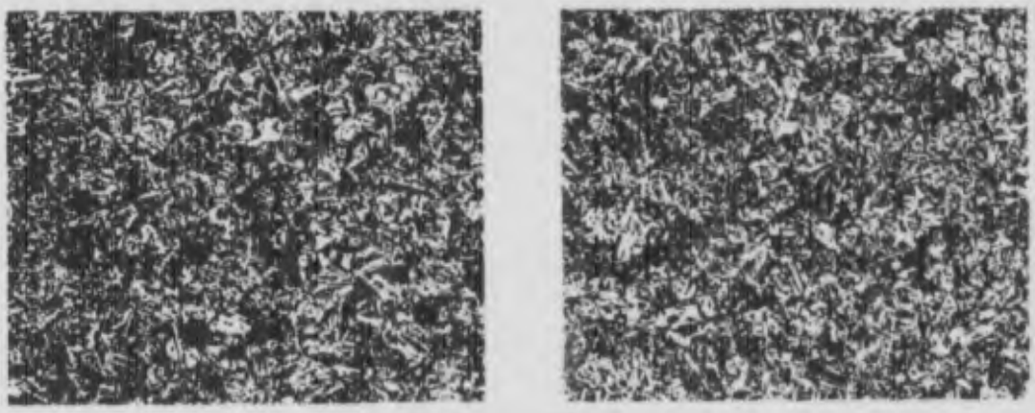

c) Heat C57046

Figure A-7, As Received Microstructure of 4330 V-Mod, Mag: 100X, Etchant: 2% Nital

Longitudinal Grain Direction

Transverse Grain Direction

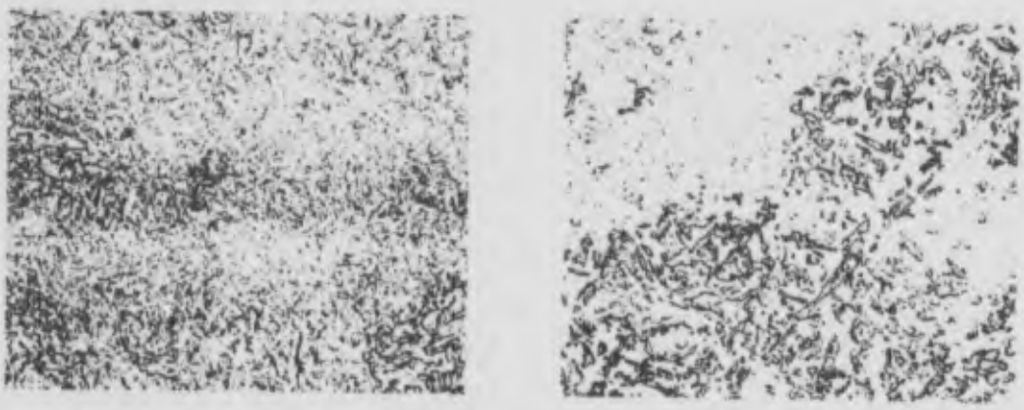

a) Heat 09110

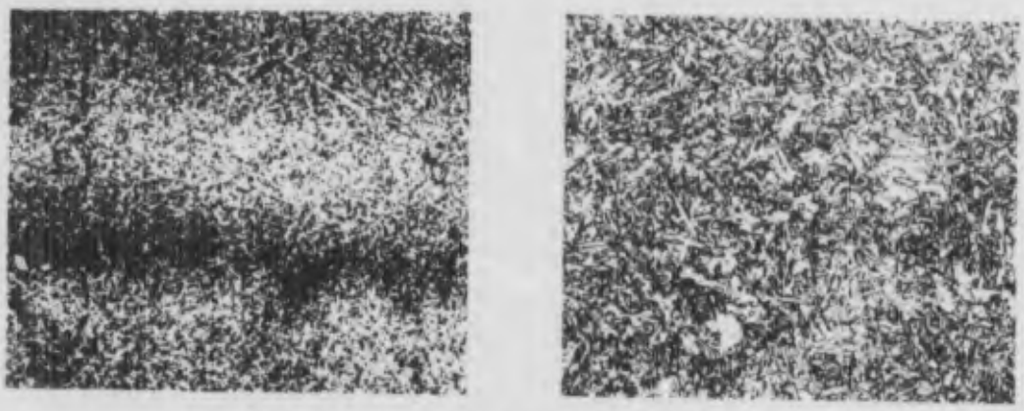

b) Heat 09099

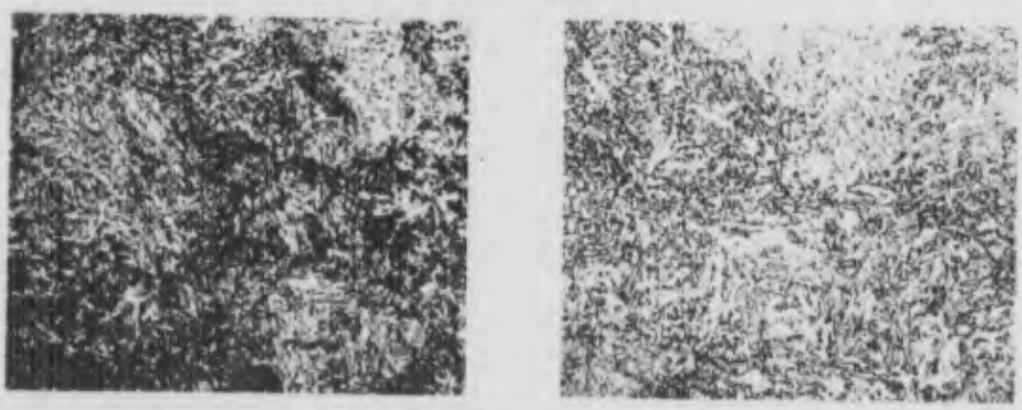

c) Heat 08990

Figure A-8. As Received Microstructure of the H-11 Mod, Mag: 100X, Etchant: 2% Mital, Villela's

Longitudinal Grain Direction

Transverse Grain Direction

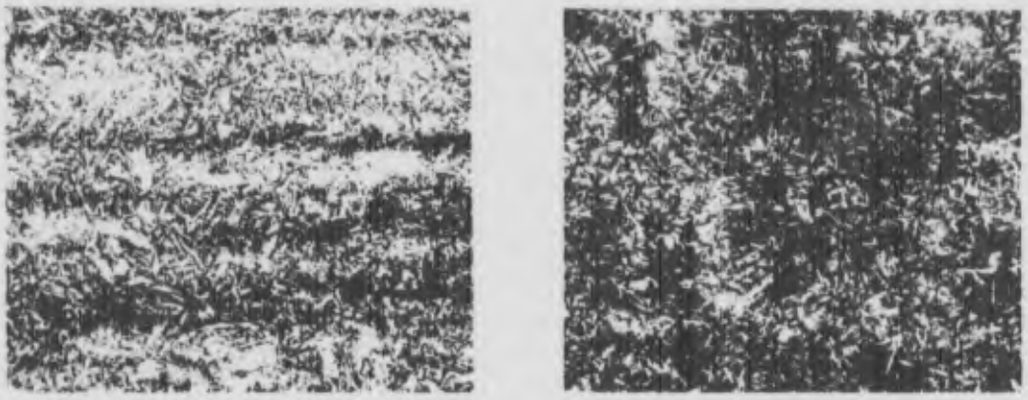

a) Heat 3931144

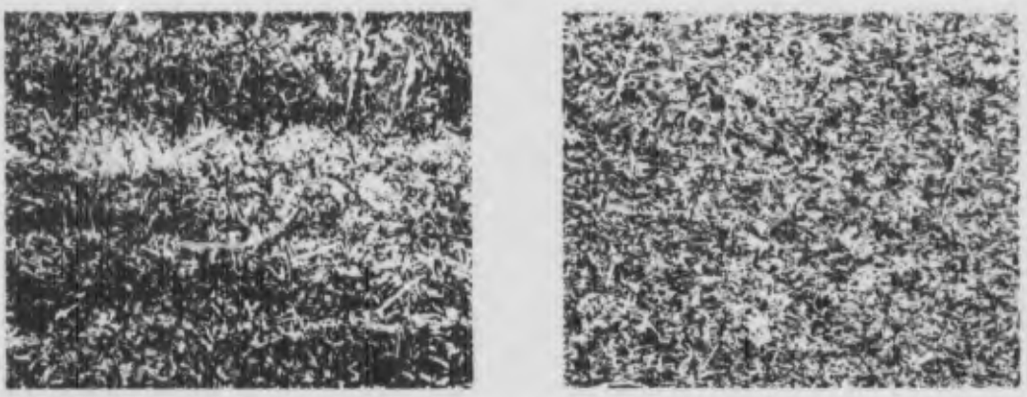

b) Heat 3930852

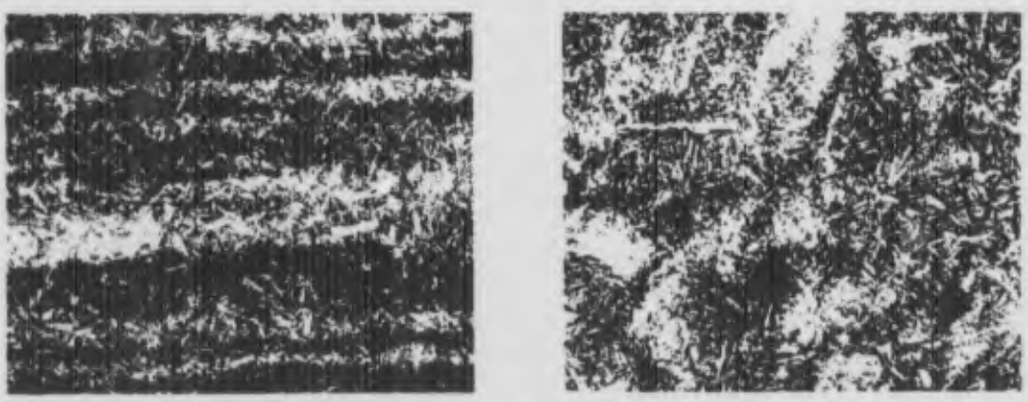

c) Heat 3931145

Figure A-9. As Received Microstructures of 9Ni-4Co-0.30C, Mag: 100X, Etchant: 2% Nital

Longitudinal Grain Direction

Transverse Grain Direction

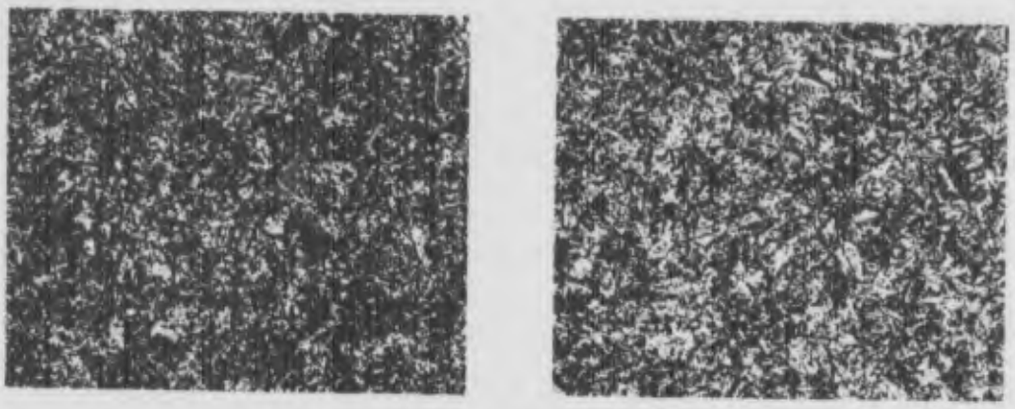

a) Heat 3951531

b) Heat 3951531

c) Heat 09715

Figure A-10. As Received Microstructure 300 M , Mag: 100X, Etchant: 2% Nital

Longitudinal Grain Direction

Transverse Grain Direction

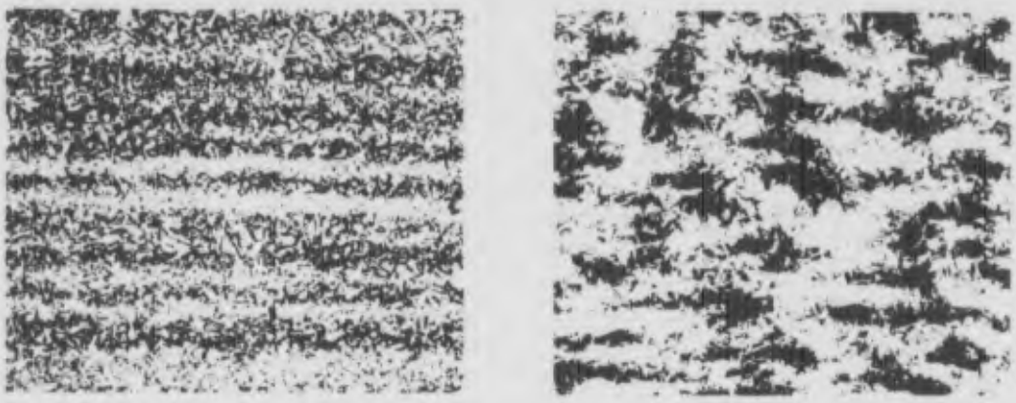

a) Heat 24676

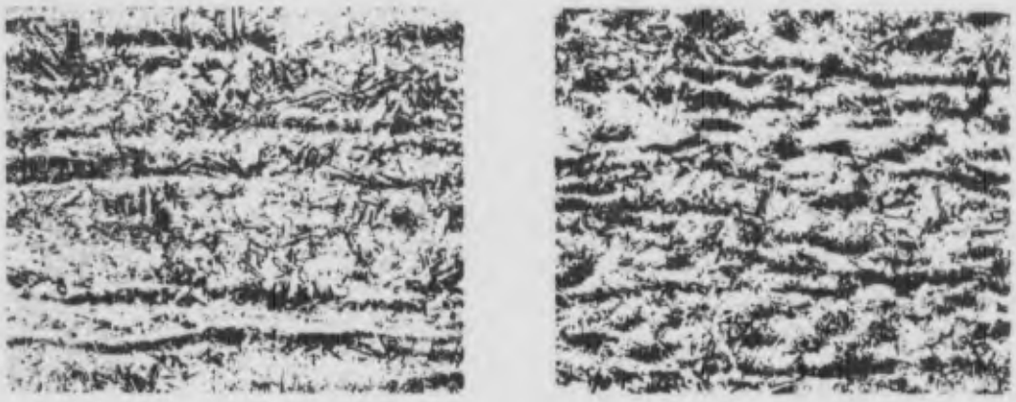

b) Heat 09148

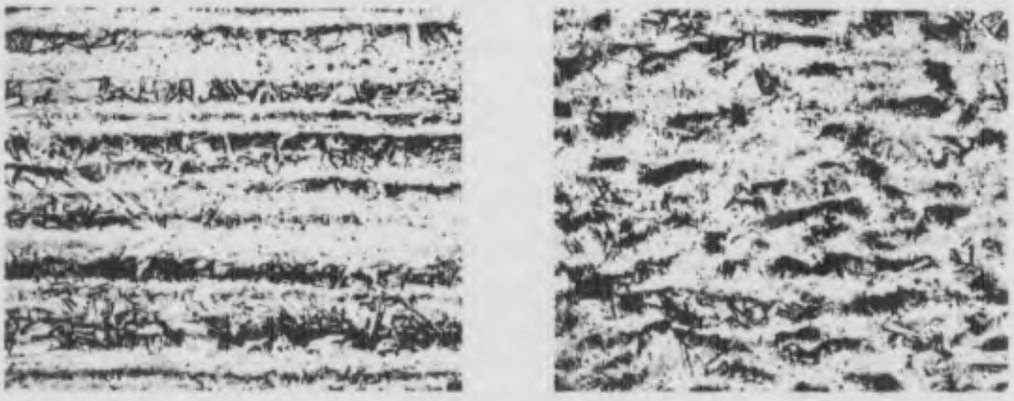

c) Heat 3930879

Figure A-11. As Received Microstructure of Maragine-250, Mag: 100X, Etchant: Nitric-Hydroflouric

Longitudinal Grain Direction

Transverse Grain Direction

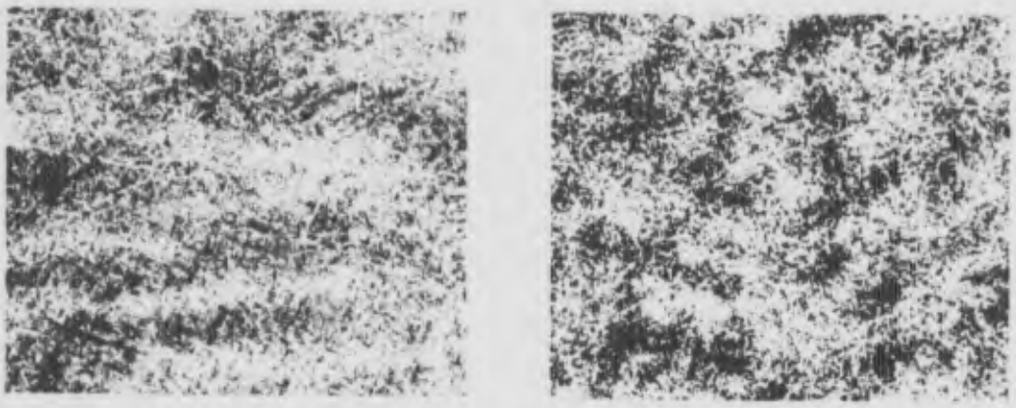

a) Heat 388270

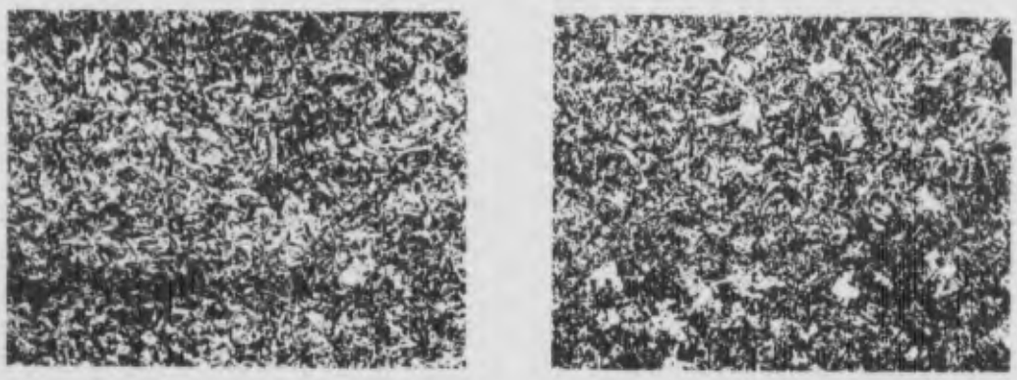

b) Heat 3931141

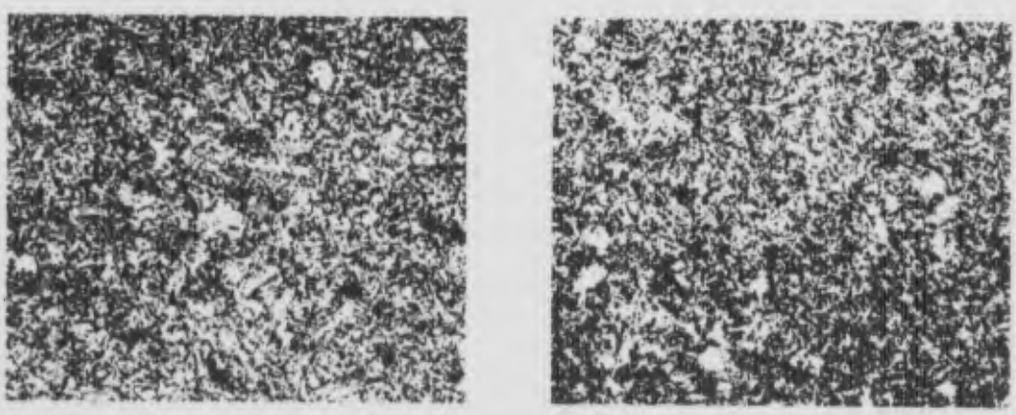

c) Heat 3931120

Figure A-12. As Received Microstructure of 9Ni-4Co-.45C, Mag: 100X, Etchant: 2% Nital

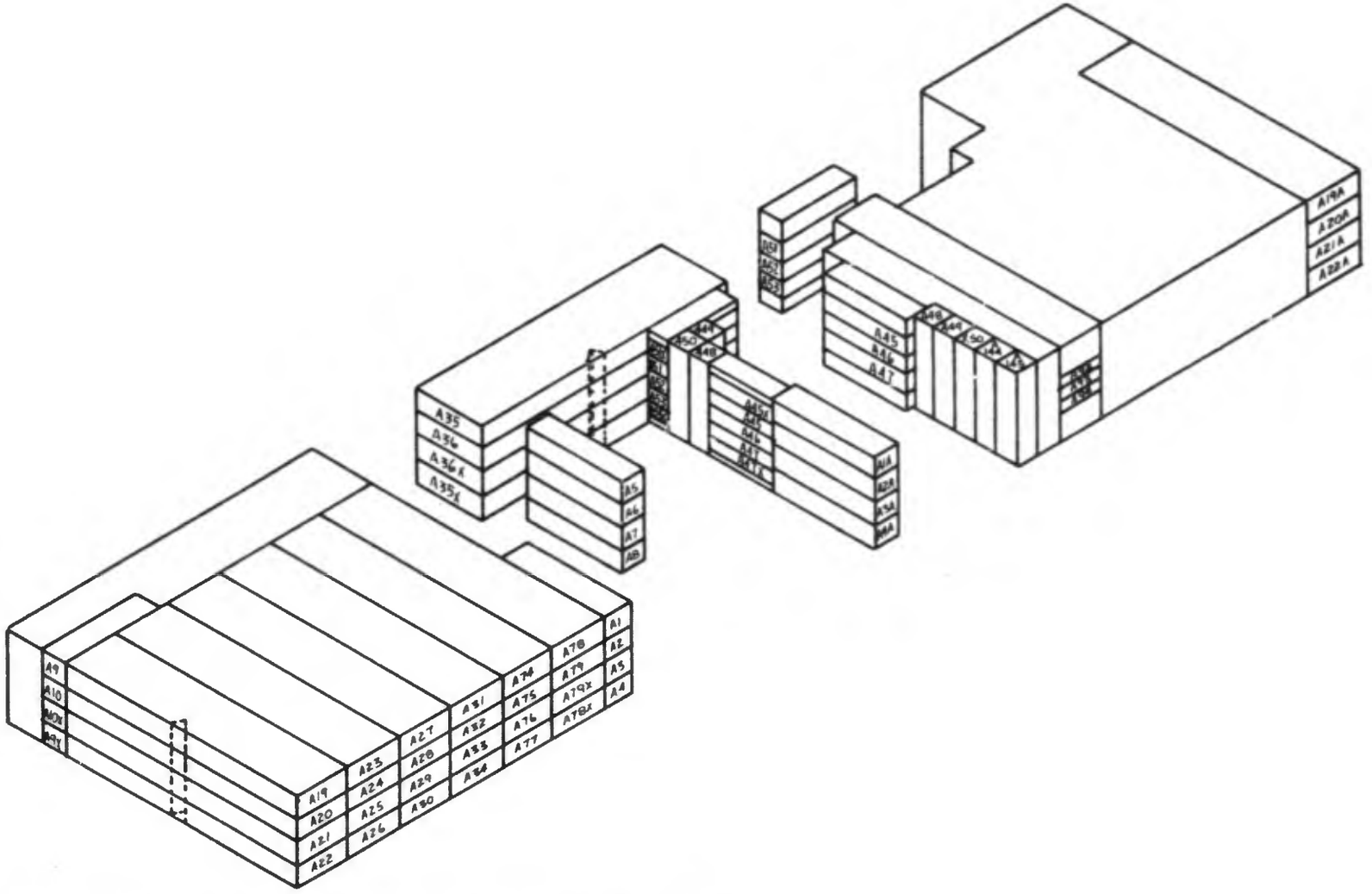

Figure A-13. 4330 V-Modified Billet Cutting Diagram, Heat No. C57046

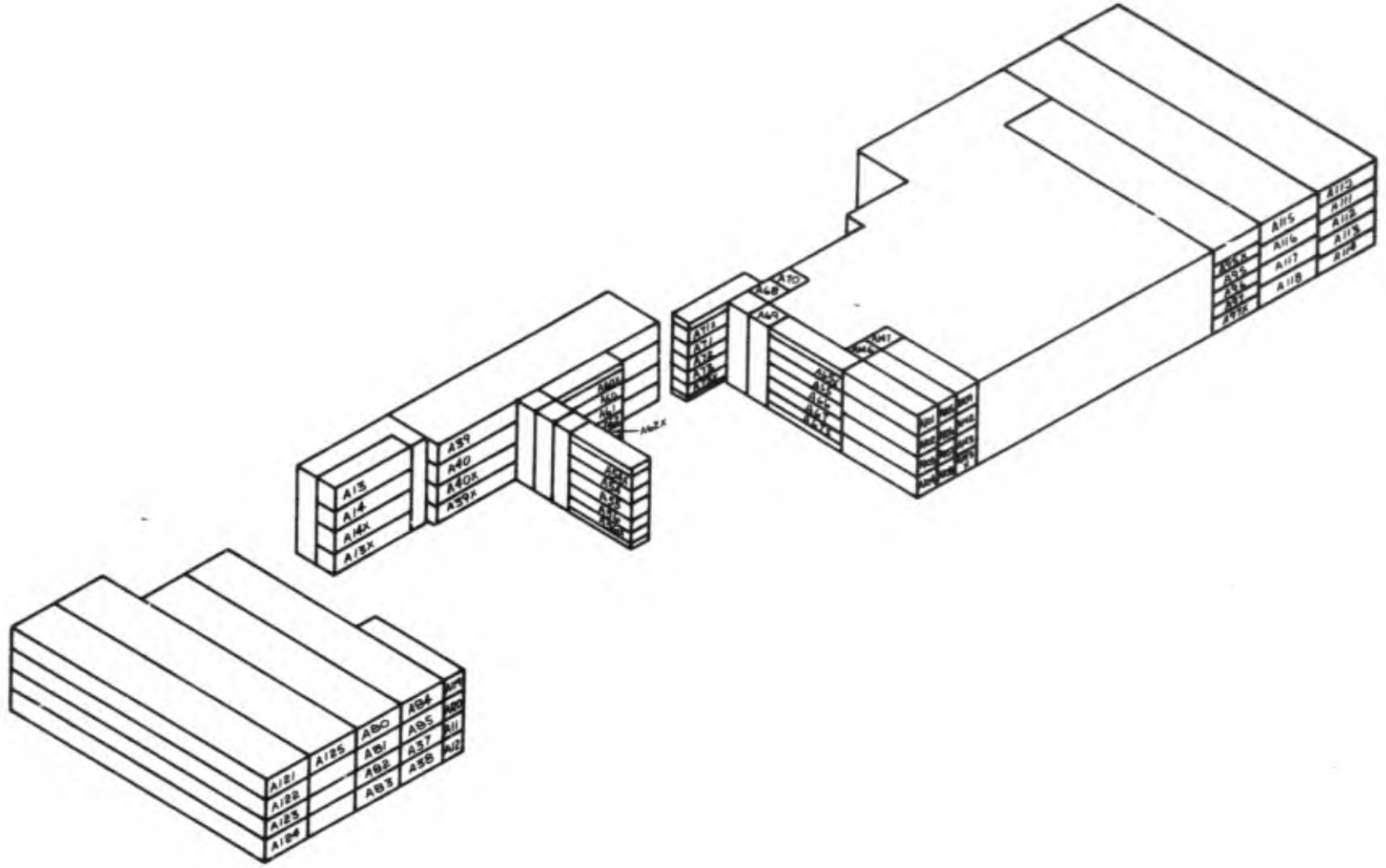

Figure A-14. 4330 V-Modified Billet Cutting Diagram, Heat No. C10157

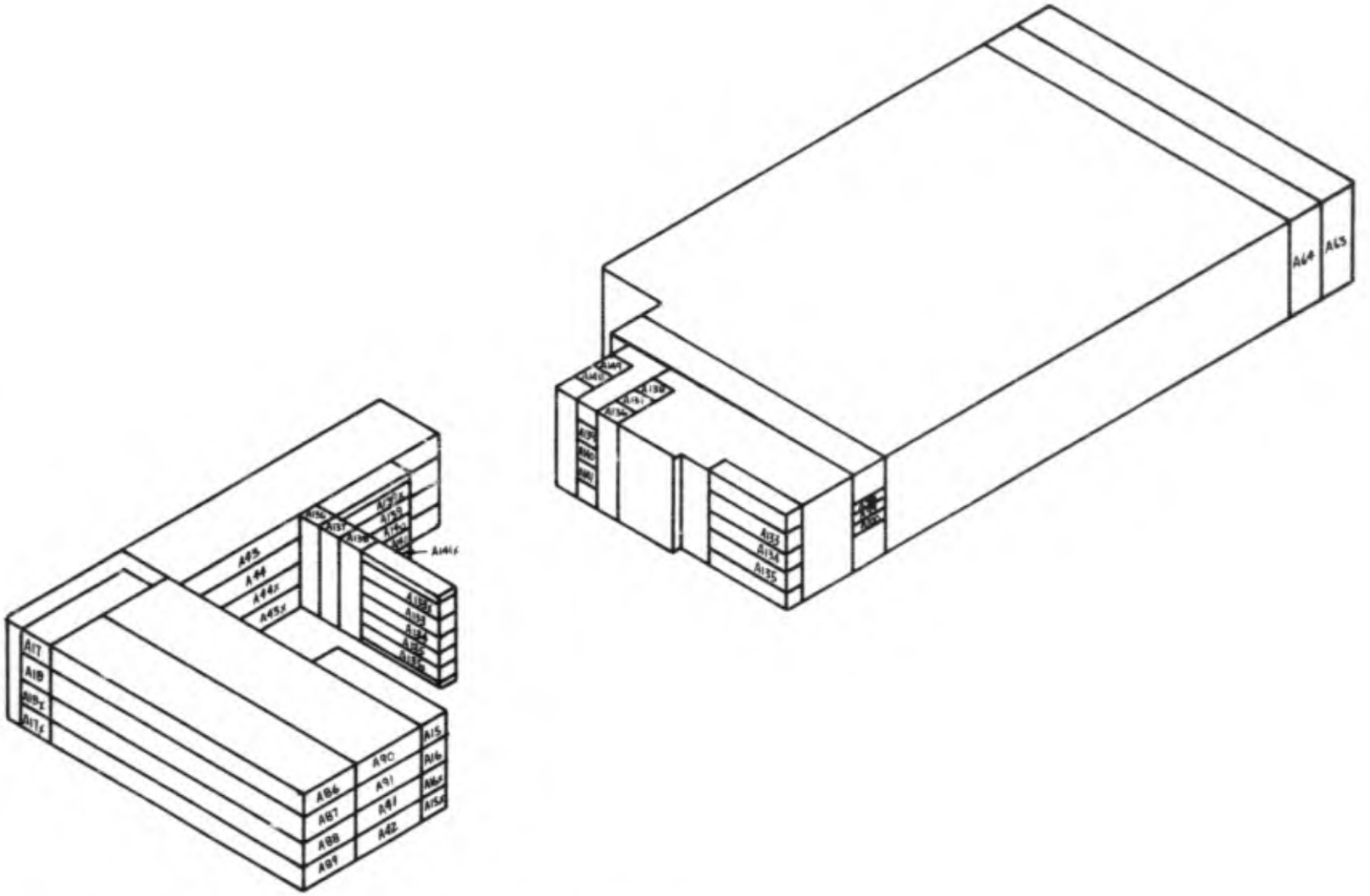

Figure A-15. 4330 V-Modified Billet Cutting Diagram, Heat No. 3960633

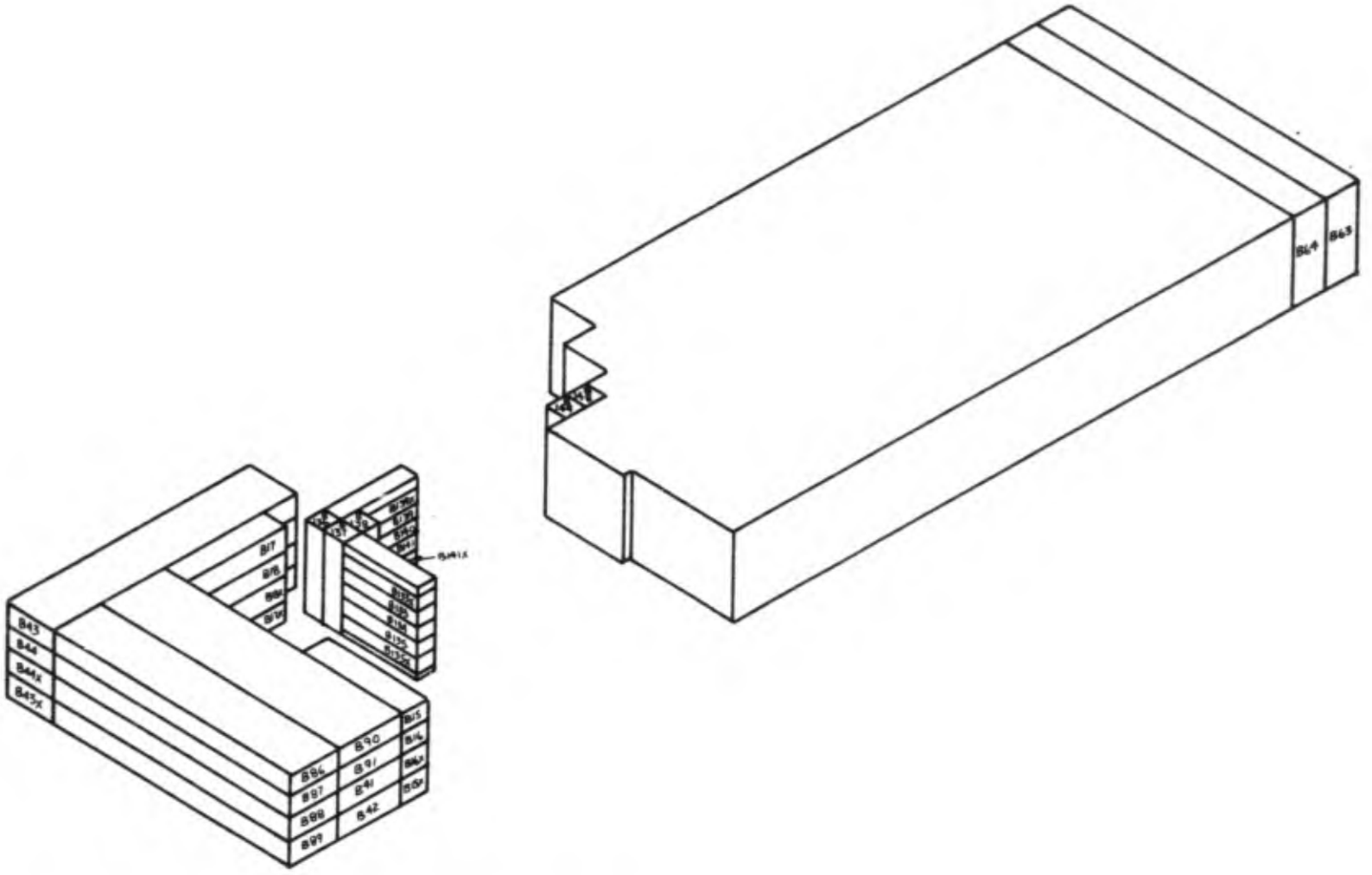

Figure A-16. H-11 Modified Billet Cutting Diagram, Heat No. 08990

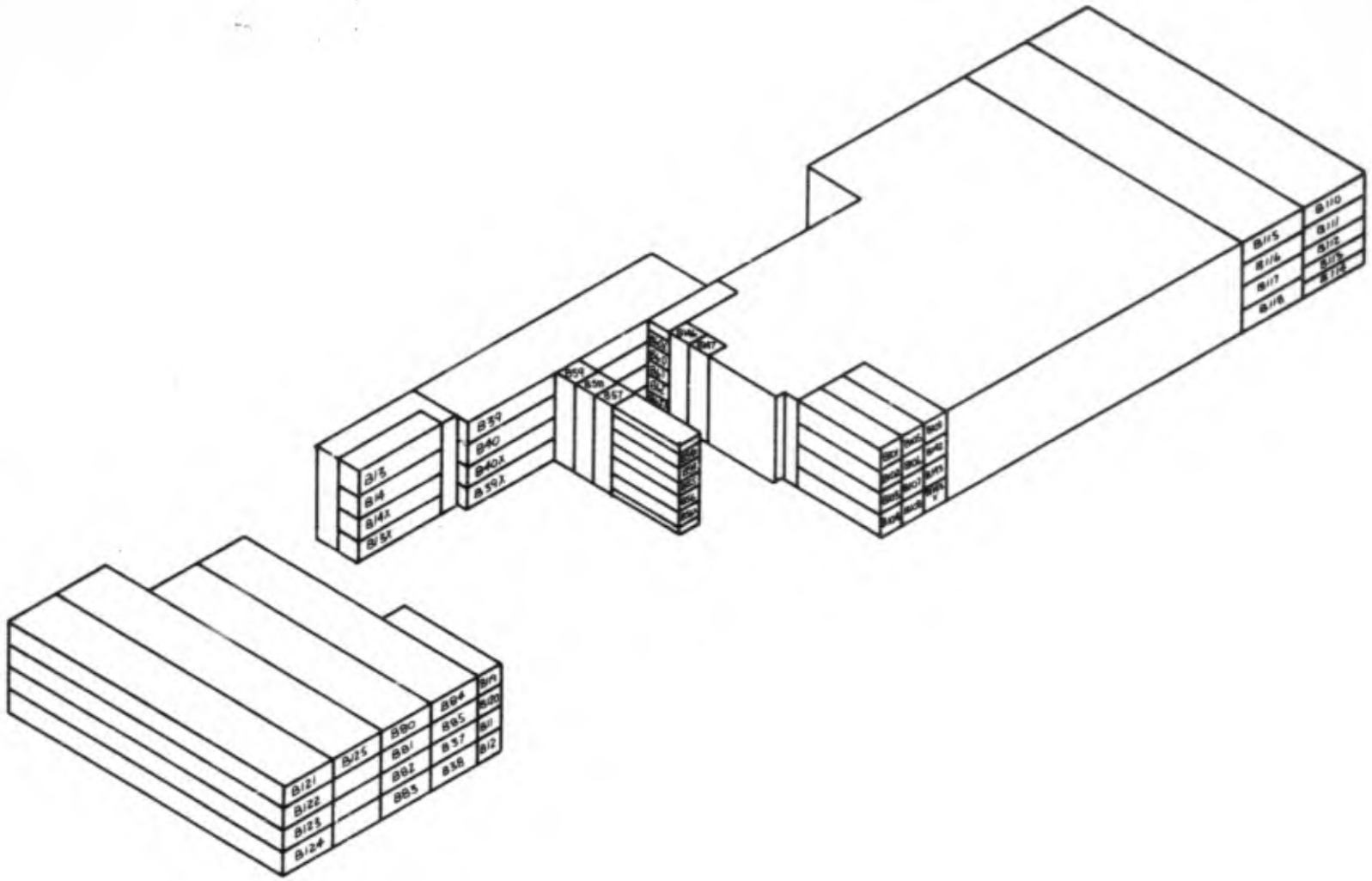

Figure A-17. H-11 Modified Billet Cutting Diagram, Heat No. 09099

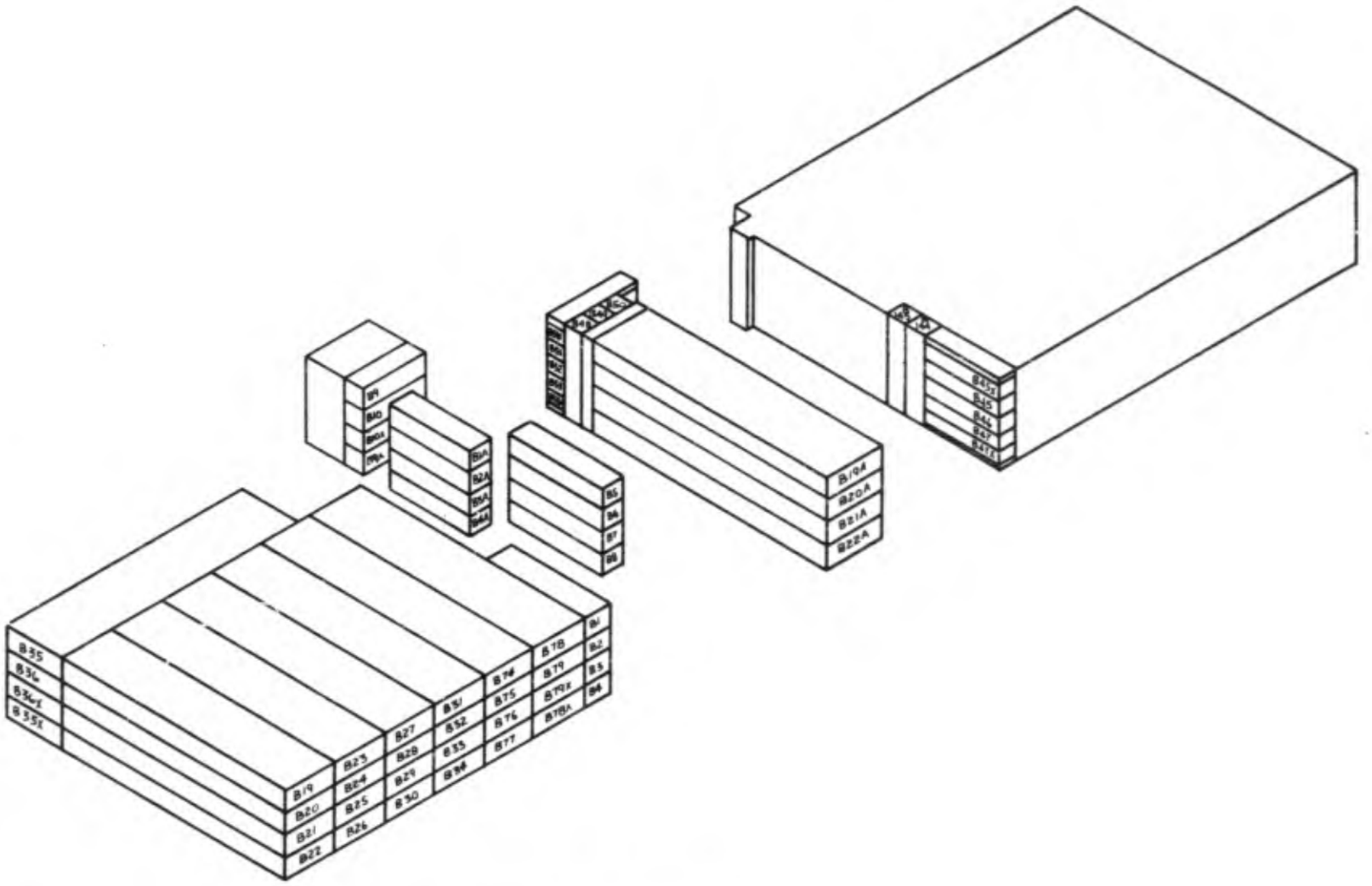

Figure A-18. H-11 Modified Billet Cutting Diagram, Heat No. 09110

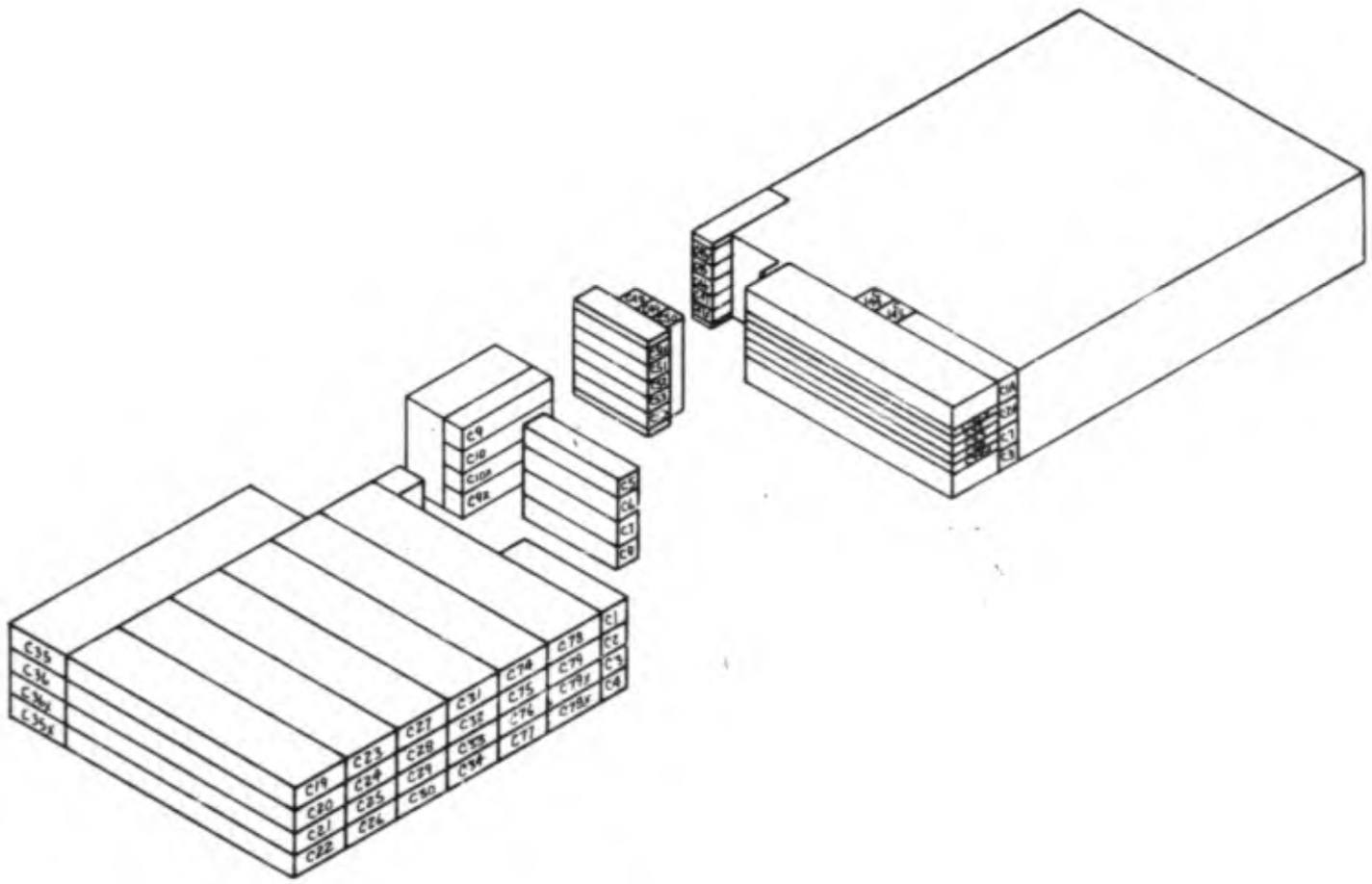

Figure A-19. 9Ni-4Co-0.45C Billet Cutting Diagram, Heat No. 3882720

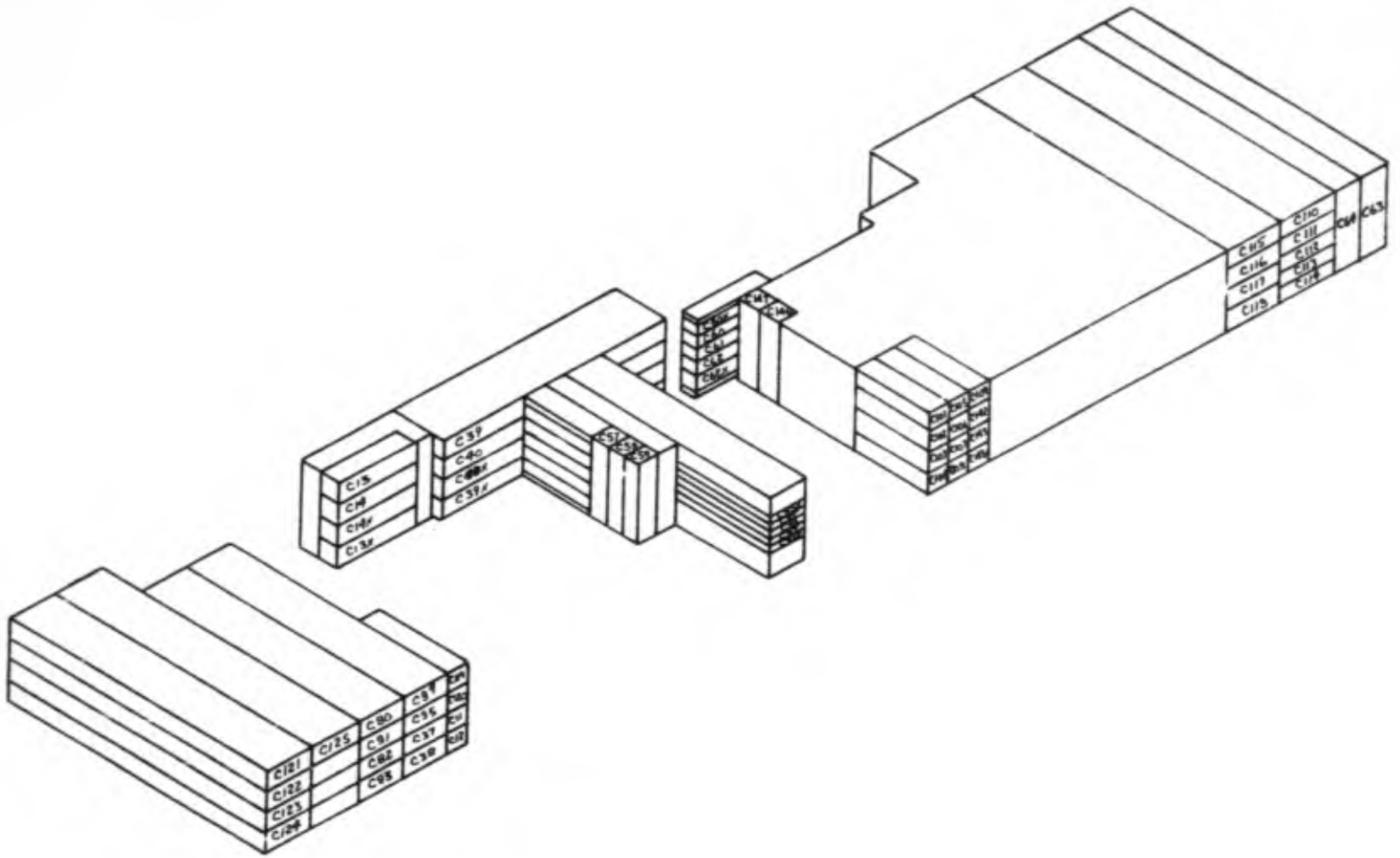

Figure A-20. 9Ni-4Co-0.30C Billet Cutting Diagram, Heat No. 3931144

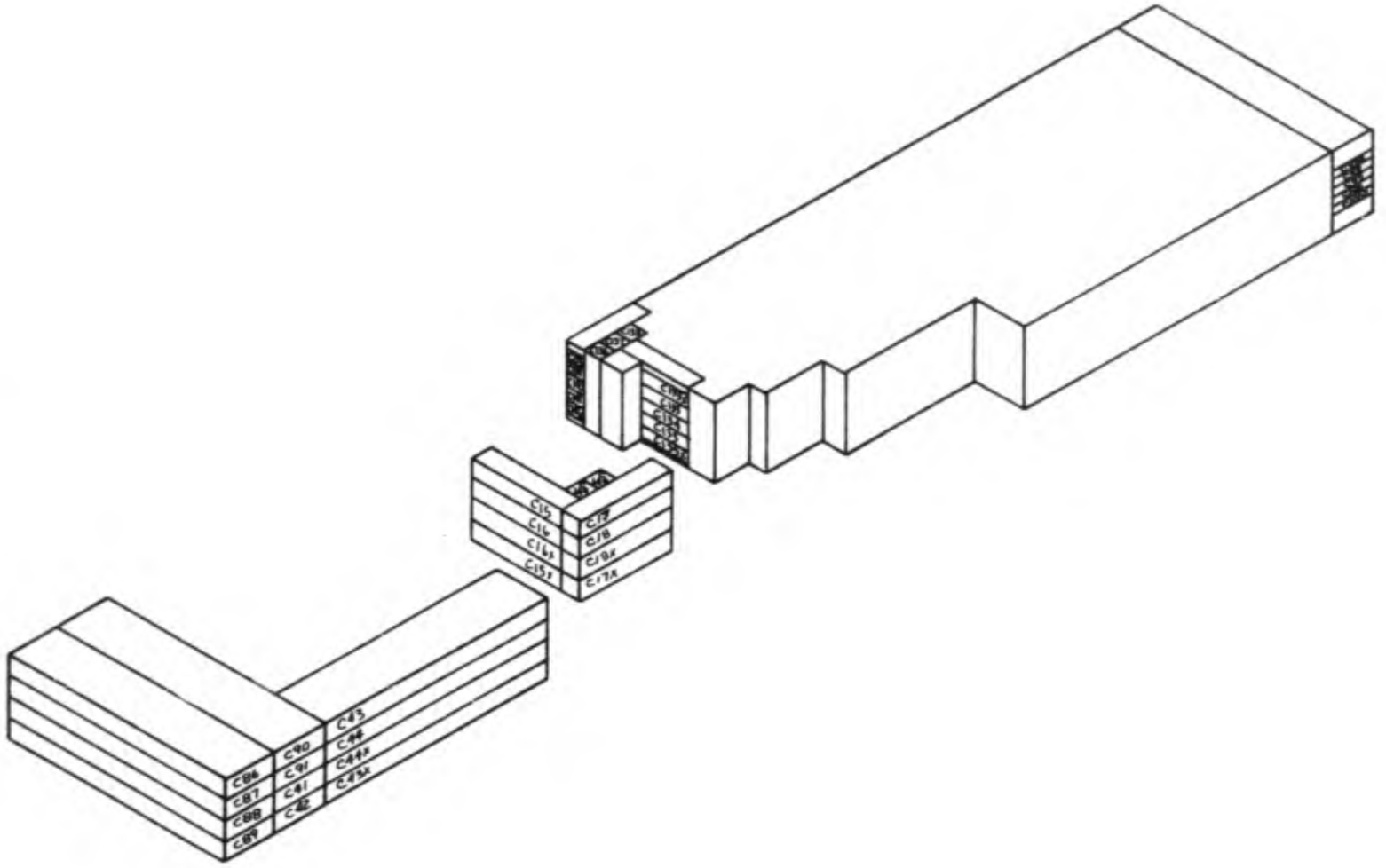

Figure A-21. 9Ni-4Co-0.30C Billet Cutting Diagram, Heat No. 3931145

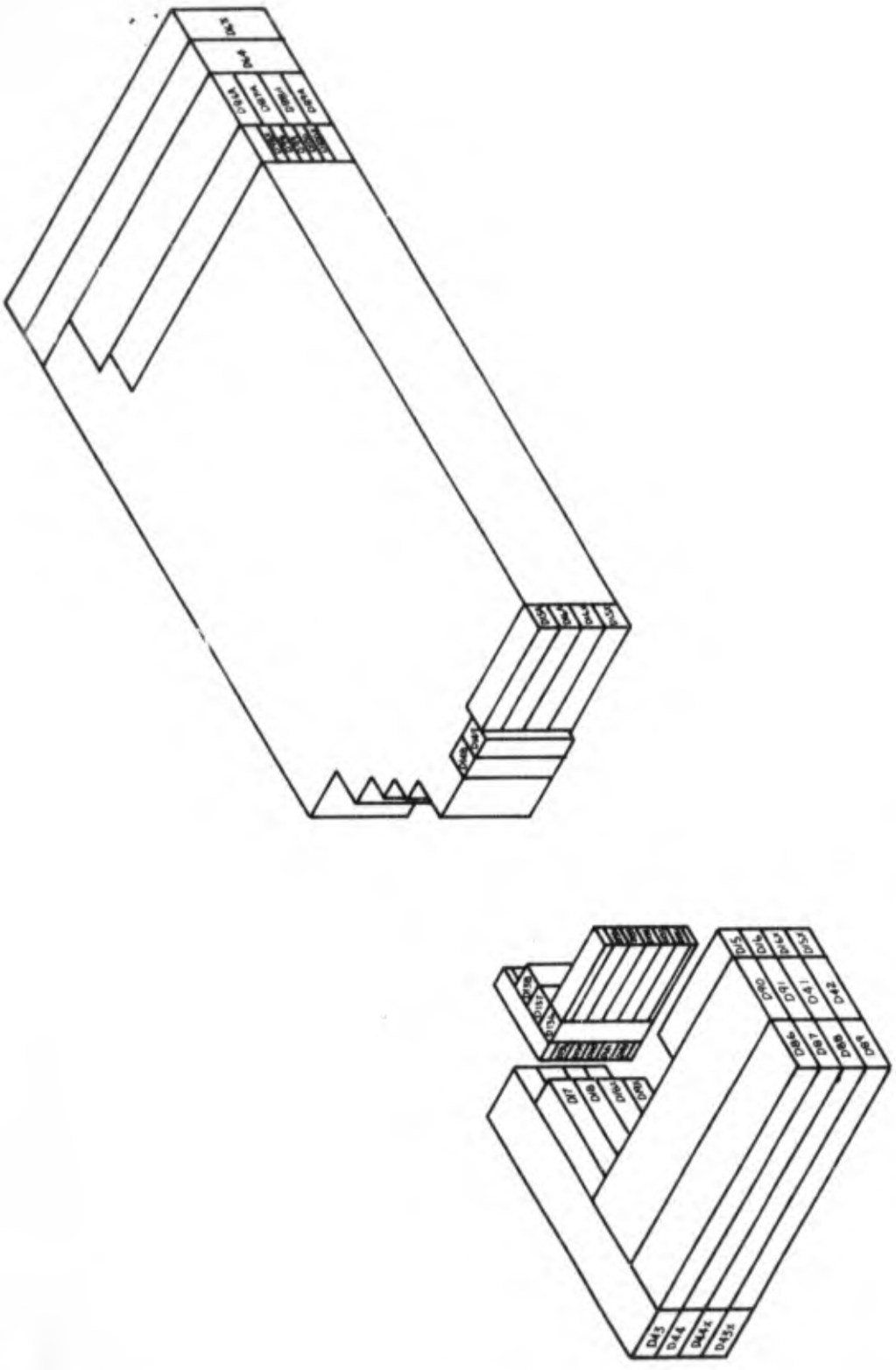

Figure A-22. 300M Billet Cutting Diagram, Heat No. 09715

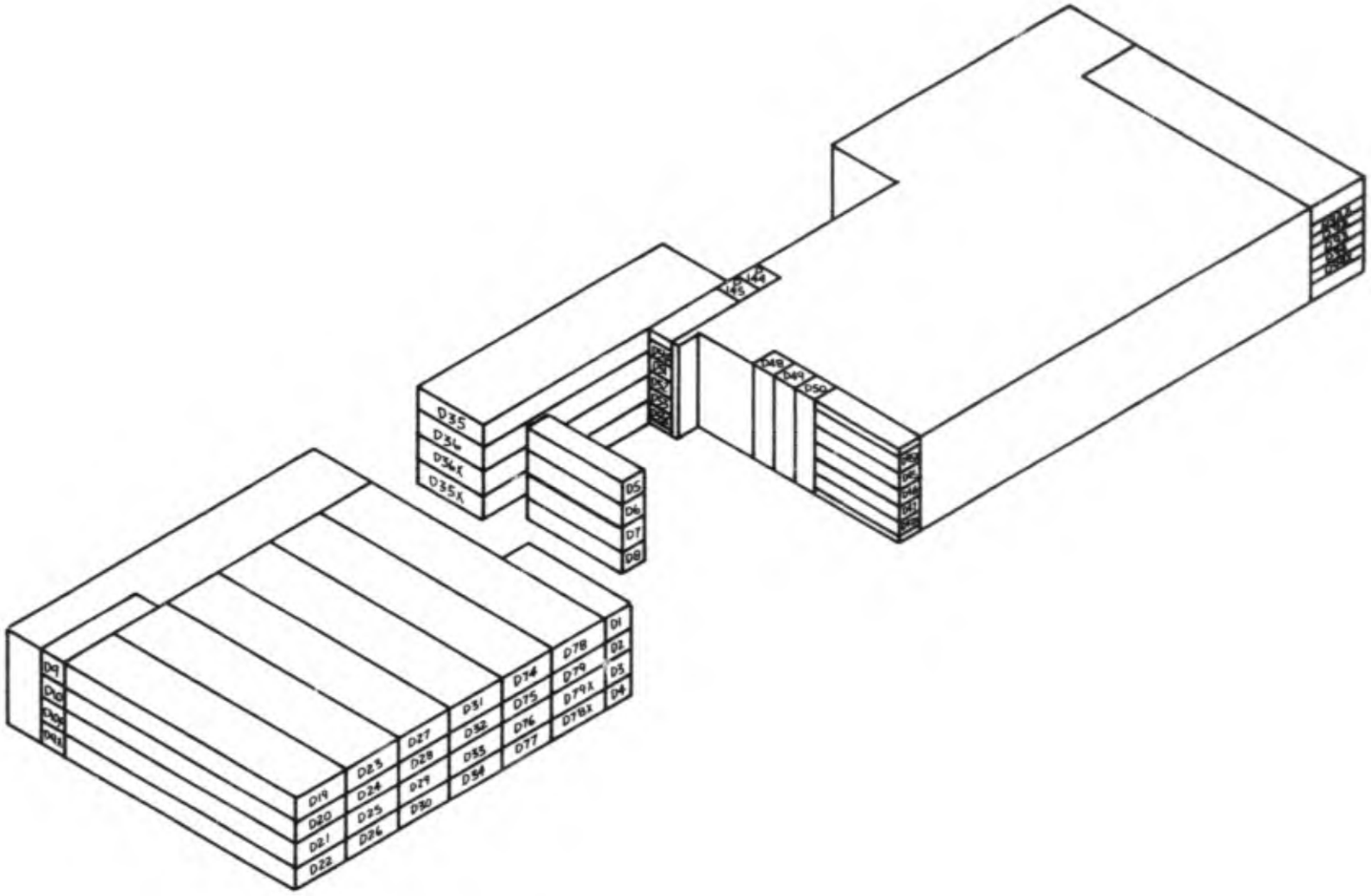

Figure A-23. 300M Billet Cutting Diagram, Heat No. 3951531, Billet P

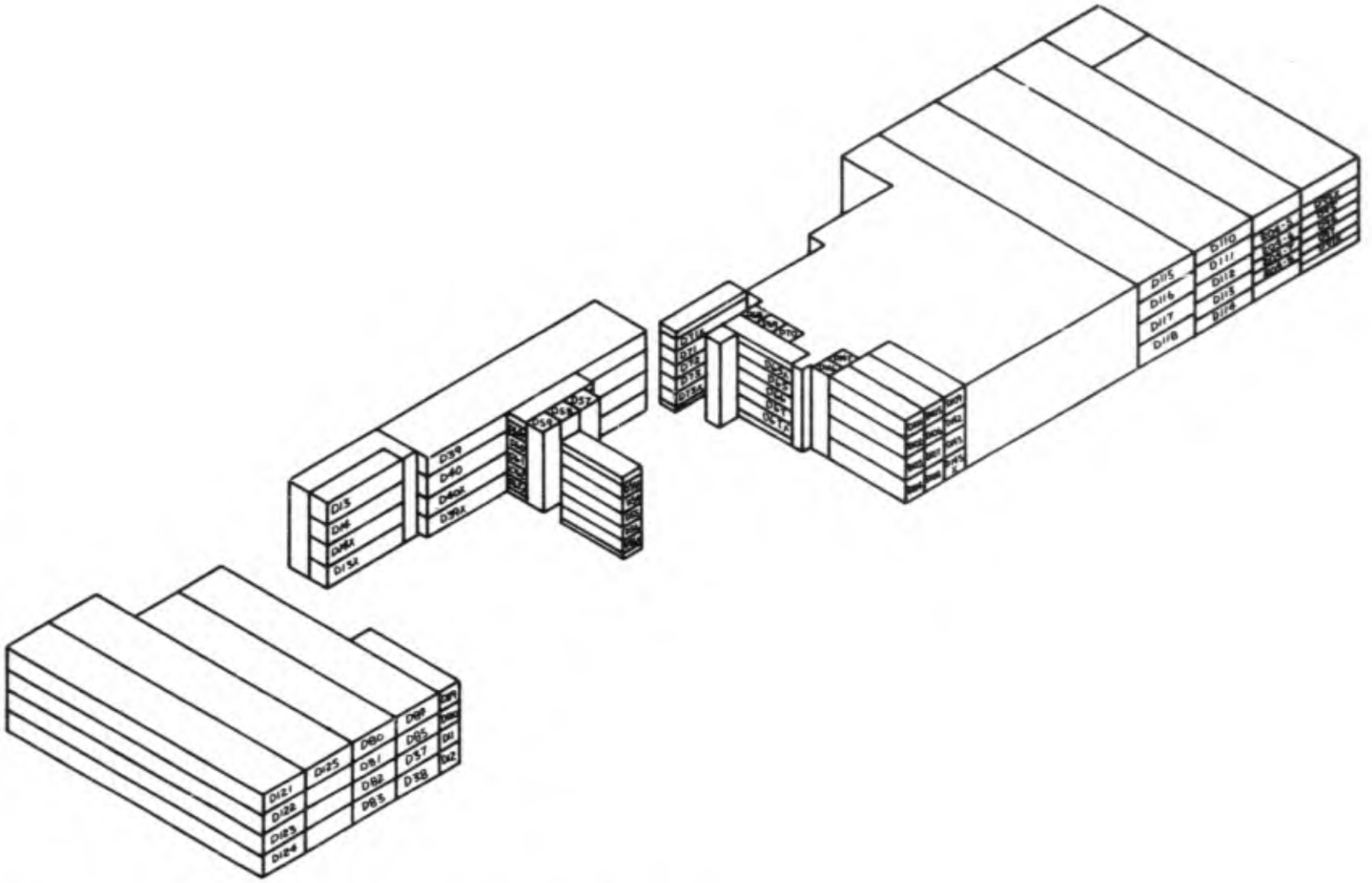

Figure A-24. 300M Billet Cutting Diagram, Heat No. 3951531, Billet R

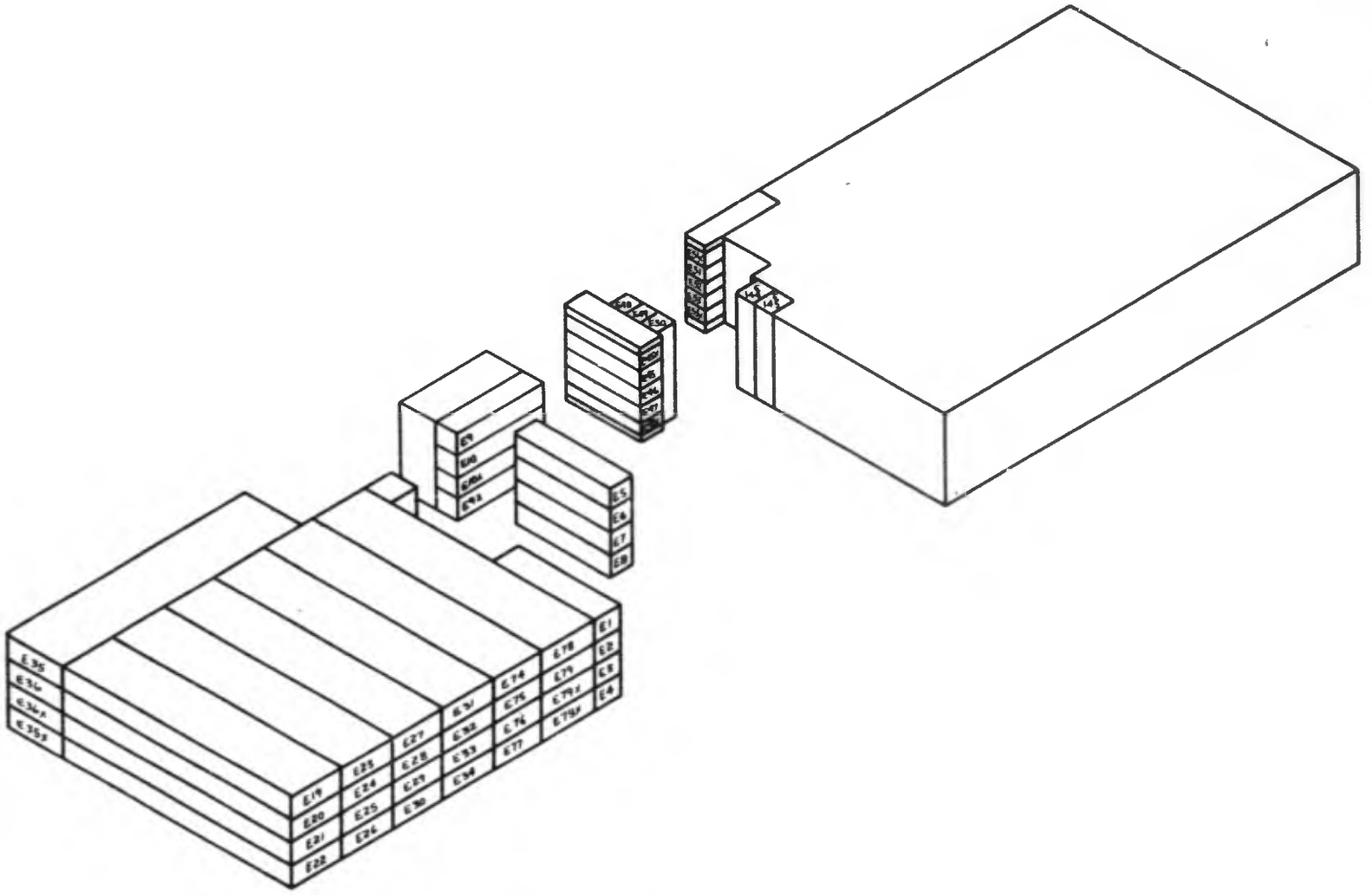

Figure A-25. Maraging 250 Billet Cutting Diagram, Heat No. 24676

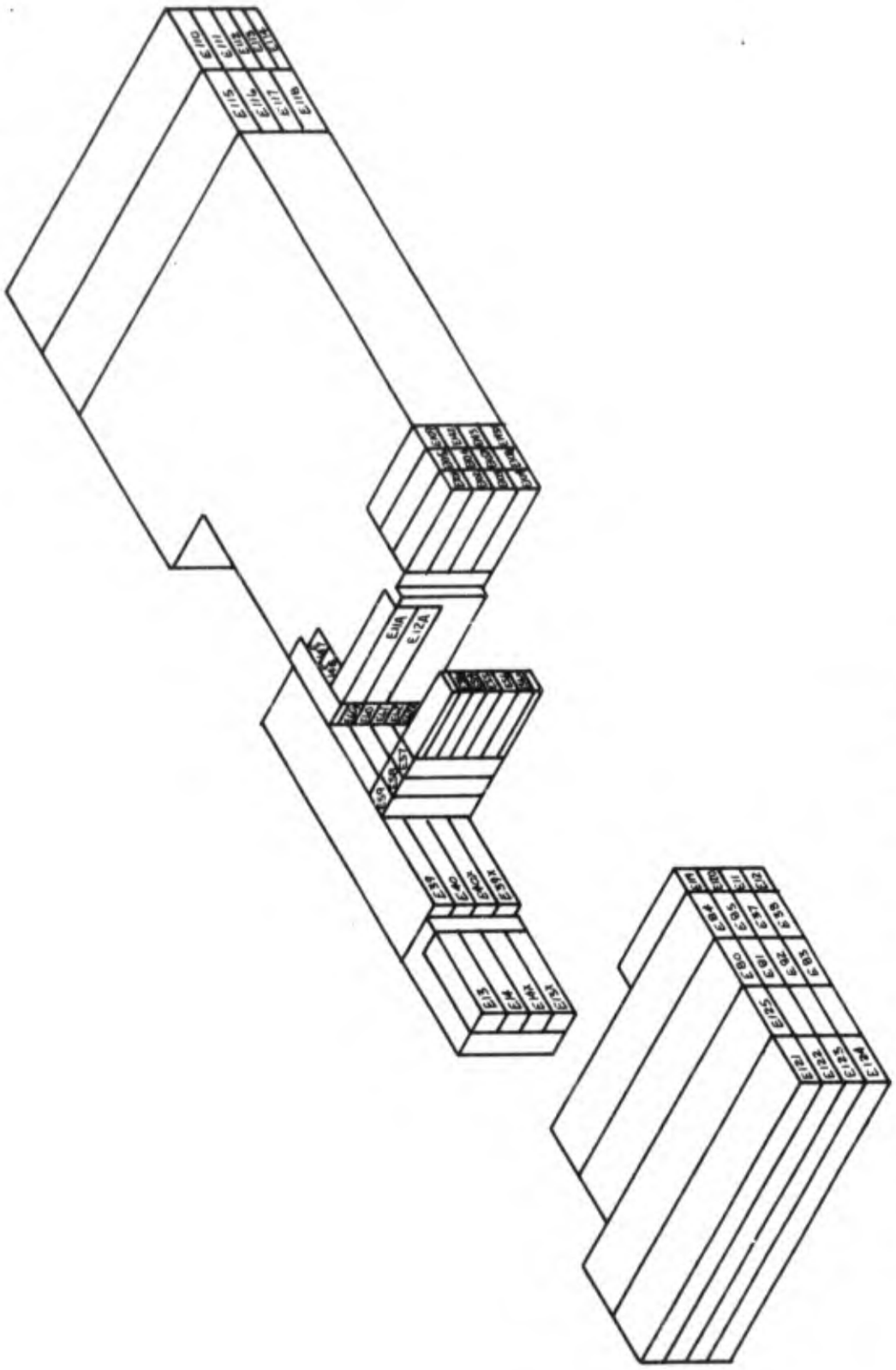

Figure A-26. Maraging 250 Billet Cutting Diagram, Heat No. 09148

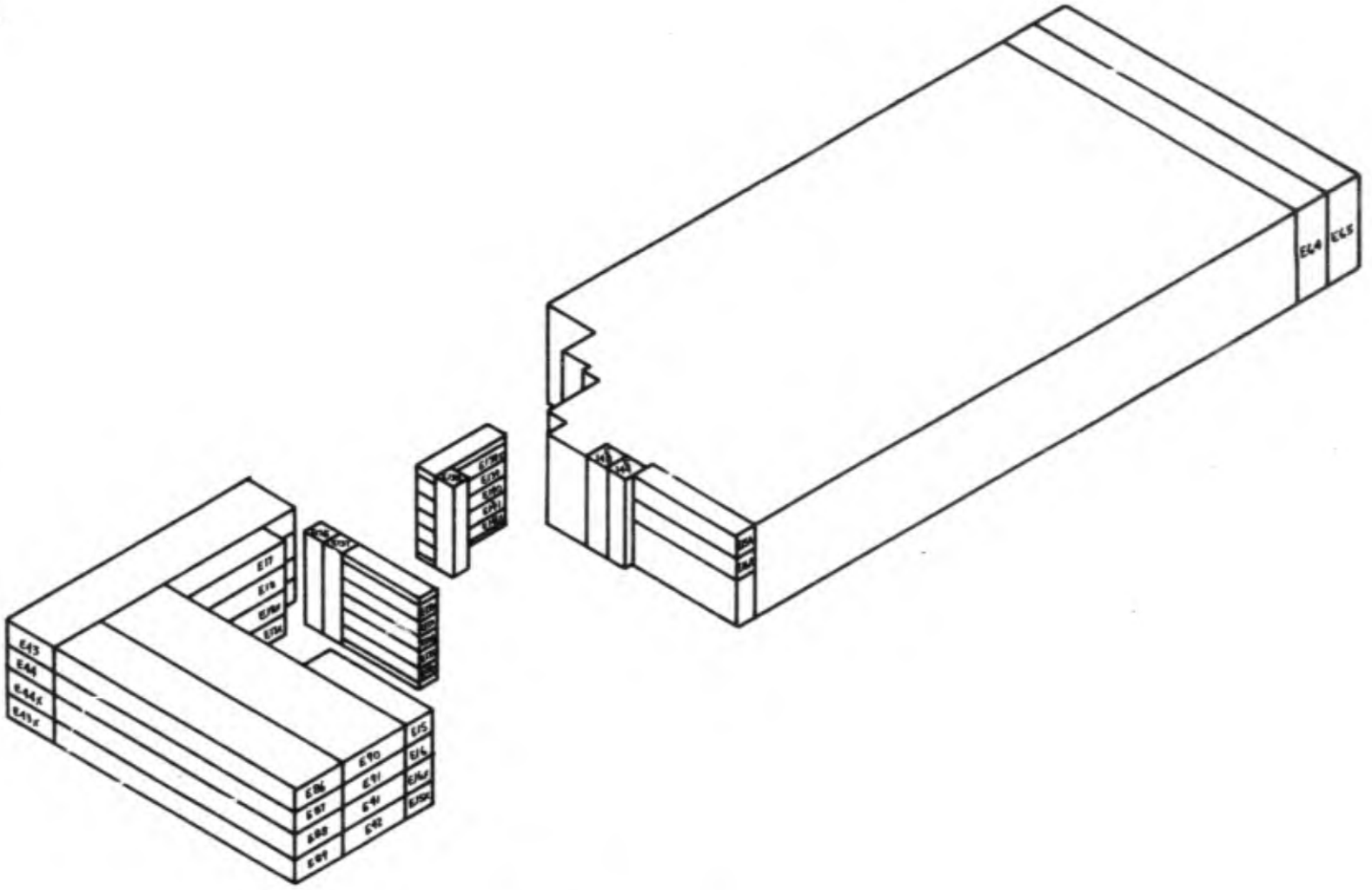

Figure A-27. Maraging 250 Billet Cutting Diagram, Heat No. 3930879

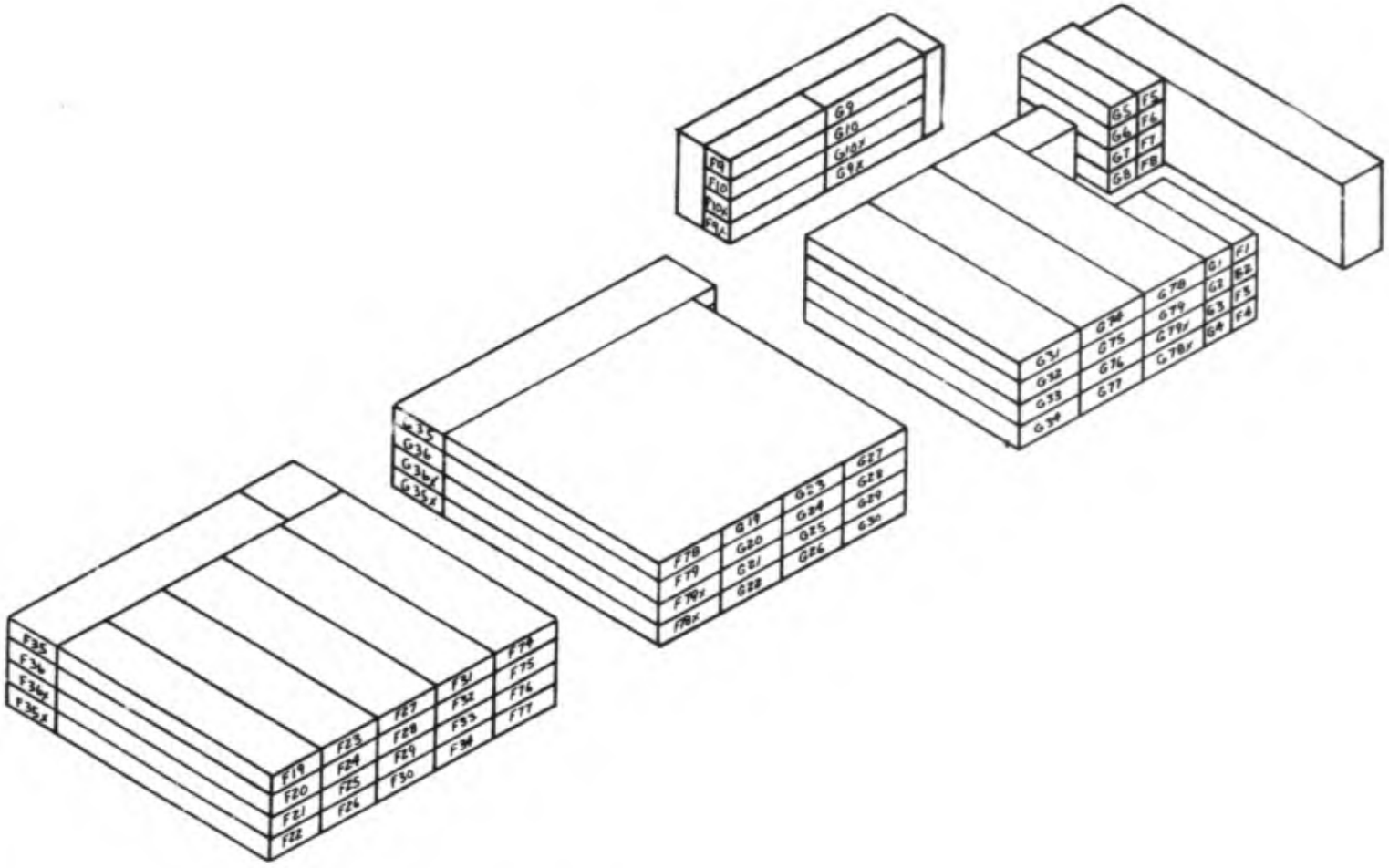

Figure A-28. 9Ni-4Co-0.45C Billet Cutting Diagram, Heat No. 3931141

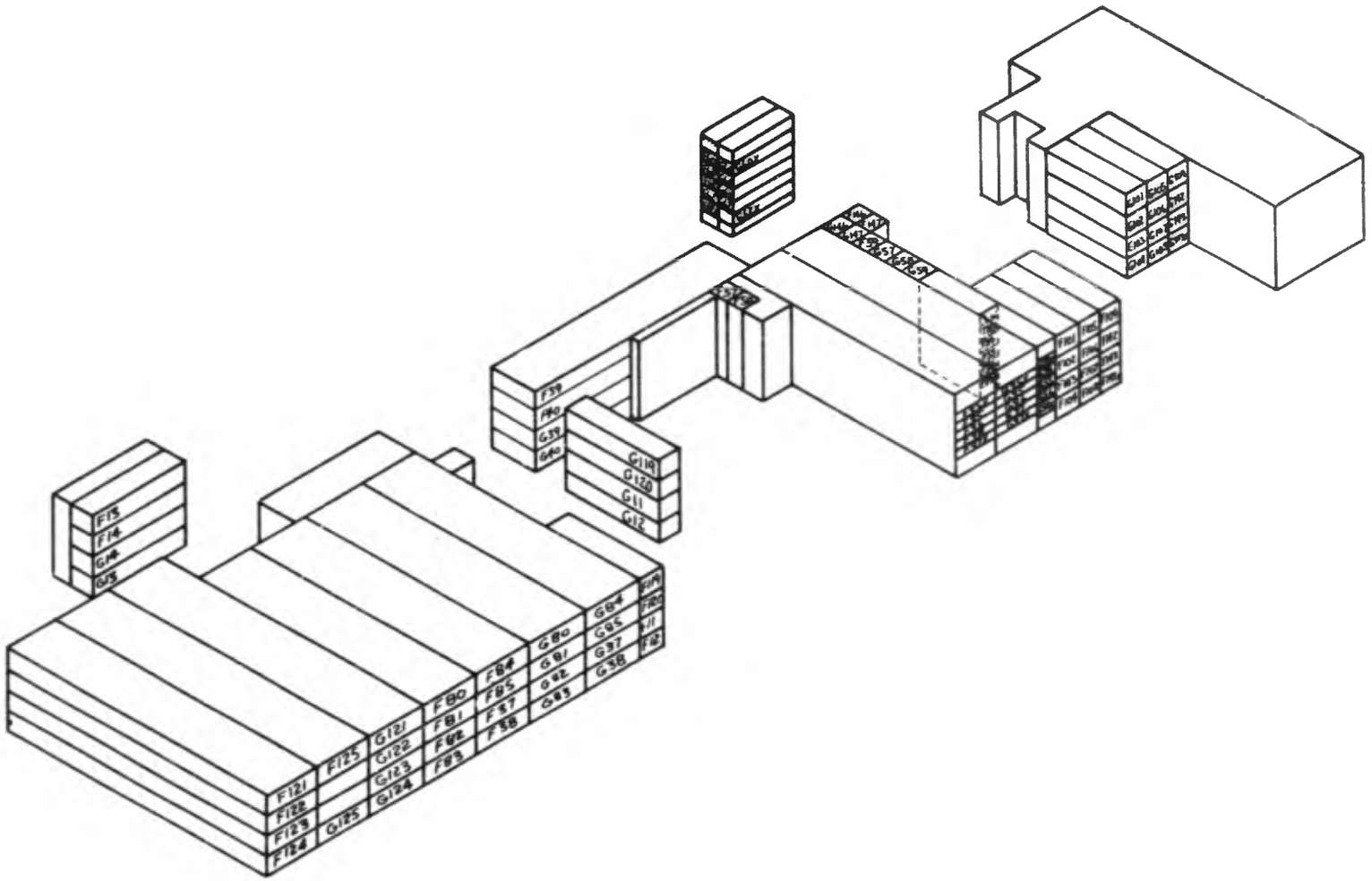

Figure A-29. 9Ni-4Co-0.45C Billet Cutting Diagram, Heat No. 3931120

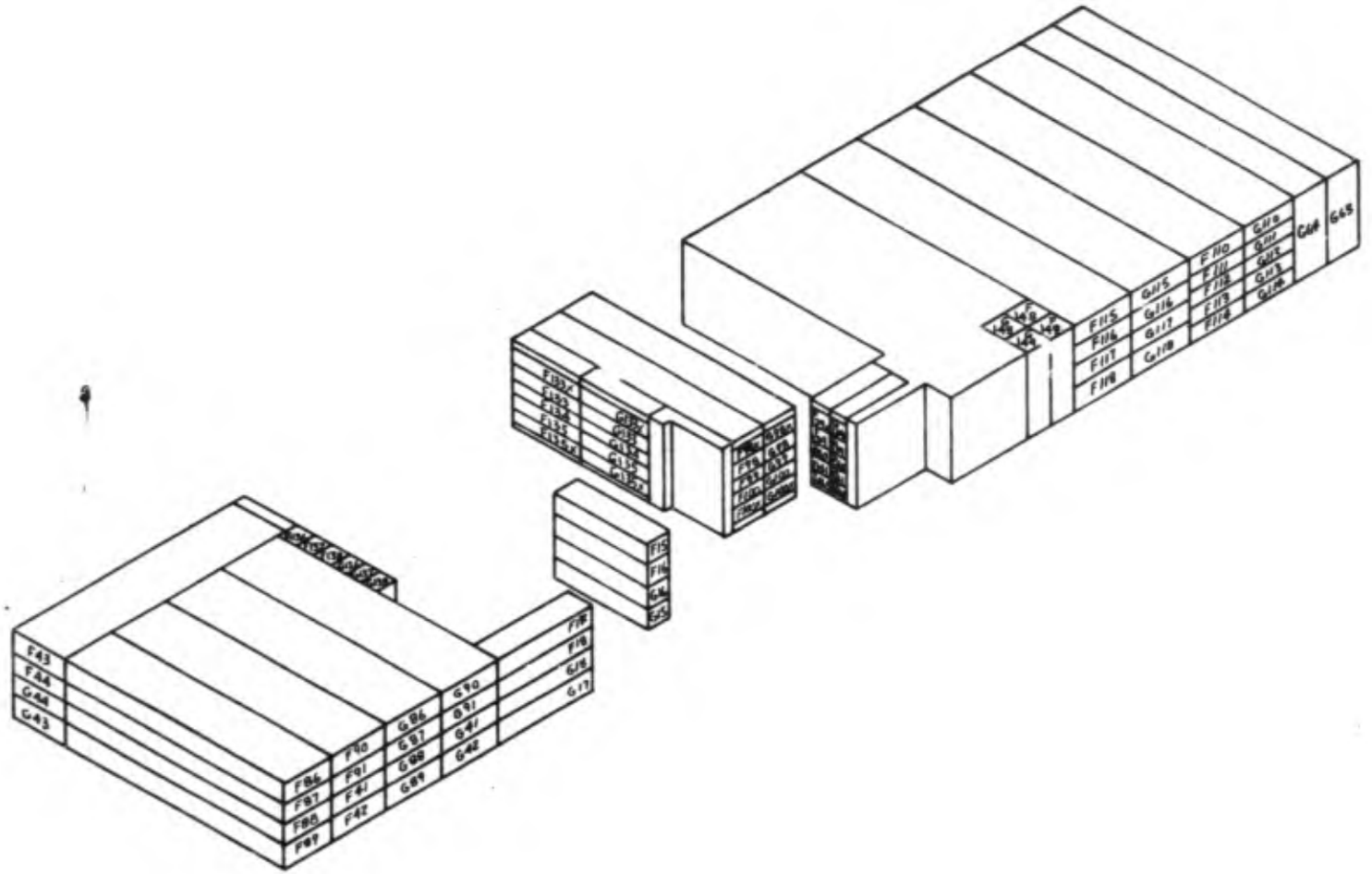

Figure A-30. 9Ni-4Co-0.30C Billet Cutting Diagram, Heat No. 3930852

REFERENCES

1. "The Use of High Strength 4340M for SST Landing Gear," Boeing Document No. D6-17640.
2. D. C. Ludwigson and F. R. Morral, "A Summary of Comparative Properties of Air-Melted and Vacuum-Melted Steels and Superalloys," DMIC Report 128, March 28, 1960. Battelle Memorial Institute, Columbus, Ohio.
3. F. R. Larson, "Impact Properties of Air and Vacuum Melted AISI 4340 Steel," U.S. Army Materials Research Agency, Watertown, Mass., September 1965.
4. A. R. Johnson and J. C. Hamaker, "Vacuum Melted Steels, Their Properties and Uses," Materials In Design Engineering, January 1965.
5. "Ultrasonic Inspection," Boeing Process Specification BAC 5439.
6. "Machining of Steels," Boeing Process Specification BAC 5440.
7. G. L. Hanna and E. W. Steigerwald, "Development of Standard Test Methods to Determine Plane Strain Fracture Toughness," Technical Report AFML-TR-65-213, Materials Research and Equipment Development Laboratories, TRW, Inc.
8. "Fracture Toughness Testing and Its Applications," ASTM Special Technical Publication No. 381, American Society for Testing Materials, Philadelphia, Pa., April 1965.
9. G. A. Dreyer, "Investigation of Susceptibility of High Strength Martensitic Steel Alloys to Stress Corrosion," Technical Documentary Report No. ASD-TDR-62-876, September 1962.
10. "Magnetic Particle Inspection," Boeing Process Specification BAC 5424.
11. "Bright Cadmium Plating," Boeing Process Specification BAC 5701.
12. B. S. Lement, B. L. Averback, and M. Cohen, "Microstructural Changes on Tempering Iron Carbon Alloys," Trns. ASM 46 (1954).
13. Vasco Jet 1000, Latrobe, Pa.: Vanadium Alloys Steel Co. (1959) 25 pp.
14. Y. H. Liu, J. H. Bucher, G. W. Powell, J. W. Spretnak, "The Relationship of Microstructure to Strength and Toughness in High Strength Steel," Technical Documentary Report ASD-TDR-62-1064, April 1963.
15. C. J. Alstetter, M. Cohen, and B. L. Averback, "Effect of Silicon on the Tempering of AISI 43XX Steels, Trans. ASM 55 (June 1962).

REFERENCES (Continued)

16. B. G. Resisdorf and A. J. Baker, "The Kinetics and Mechanisms of the Strengthening of Maraging Steels," Technical Report AFML-TR-64-390.
17. J. J. Shimnior, "Manufacturing Process Development for High Strength Steels." Report IR-157(II), Manufacturing Technology Laboratory, Wright-Patterson Air Force Base, Ohio, Contract AF 33(657)-11277 by Republic Steel Corporation, November 1963.
18. R. L. Jones and F. C. Nordquist, "An Evaluation of High Strength Steel Forgings." Technical Documentary Report No. RTD-TDR-63-4050, Air Force Materials Laboratory, Wright-Patterson Air Force Base, Ohio, Contract No. AF 33(600)-41891 by General Dynamics, May 1964.
19. C. W. Marshall, "The Factors Influencing the Fracture Characteristics of High-Strength Steel." DMIC Report 147, Defense Metals Information Center, Battelle Memorial Institute, Columbus, Ohio., February 1961.
20. G. A. Dreyer and W. C. Gallaugher, "Investigation of the Effects of Stress Corrosion on High-Strength Steel Alloys." Technical Documentary Report No. ML-TDR-64-3, Wright-Patterson Air Force Base, Ohio, Contract No. AF 33(657)-8705 by The Boeing Company, February 1964.
21. G. L. Hana and E. A. Stiegerwald, "Stress Corrosion Cracking Mechanisms in Martensitic High Strength Steels - First Quarterly Progress Report," Report No. ER 6877-1, Contract AF 33-615-3651 by Thompson Ramo and Wooldridge, Inc., June 1966.
22. L. J. Klingler, W. J. Barnett, R. P. Frohmberg, and A. R. Troniano, "The Embrittlement of Alloy Steels at High Strength Levels," Transactions ASM, Volume 46, 1954.
23. R. E. Peterson, "Stress Concentration Design Factors," John Wiley and Sons, Inc., New York 1953.
24. E. P. Klier, B. B. Murdi, G. Sachs, "Design Properties of High Strength Steels in the Presence of Stress Concentrations and Hydrogen Embrittlement," WADC Technical Report 56-395 Part 3, Wright-Patterson Air Force Base, Ohio, Contract No. AF 33(616)-2362, S/A 4(56-445) by Syracuse University, March 1957.